AD-A021 948

PROCEEDINGS OF THE ANNUAL SYMPOSIUM 'TRACE ANALYSIS AND DETECTION IN THE ENVIRONMENT' (6TH) HELD AT EDGEWOOD ARSENAL ON 29 APRIL-1 MAY 1975 AND SPONSORED BY THE AMERICAN DEFENSE PREPAREDNESS ASSOCIATION

John A. Brown

Edgewood Arsenal
Aberdeen Proving Ground, Maryland

January 1976

EDGEWOOD ARSENAL SPECIAL PUBLICATION

EO-SP-76001

PROCEEDINGS OF THE SIXTH ANNUAL SYMPOSIUM "TRACE ANALYSIS AND DETECTION IN THE ENVIRONMENT"

29 APRIL–1 MAY 1975

SPONSORED BY THE AMERICAN DEFENSE PREPAREDNESS ASSOCIATION

Compiled by

Dr. John A. Brown
R&D Consultant

Office of the Technical Director

January 1976

DEPARTMENT OF THE ARMY
Headquarters, Edgewood Arsenal
Aberdeen Proving Ground, Maryland 21010

Disclaimer

The findings in this report are not to be construed as an official Department of the Army position unless so designated by other authorized documents.

Disposition

Destroy this report when no longer needed. Do not return it to the originator.

UNCLASSIFIED

SECURITY CLASSIFICATION OF THIS PAGE *(When Data Entered)*

REPORT DOCUMENTATION PAGE

READ INSTRUCTIONS BEFORE COMPLETING FORM

1. REPORT NUMBER: EO-SP-76001
2. GOVT ACCESSION NO.:
3. RECIPIENT'S CATALOG NUMBER:

4. TITLE *(and Subtitle)*: PROCEEDINGS OF THE SIXTH ANNUAL SYMPOSIUM "TRACE ANALYSIS AND DETECTION IN THE ENVIRONMENT" 29 APRIL-1 MAY 1975 SPONSORED BY THE AMERICAN DEFENSE PREPAREDNESS ASSOCIATION

5. TYPE OF REPORT & PERIOD COVERED: Special Publication

6. PERFORMING ORG. REPORT NUMBER:

7. AUTHOR(s): Dr. John A. Brown (Compiler)

8. CONTRACT OR GRANT NUMBER(s): NA

9. PERFORMING ORGANIZATION NAME AND ADDRESS:
Commander, Edgewood Arsenal
Office of the Technical Director
Aberdeen Proving Ground, Maryland 21010

10. PROGRAM ELEMENT, PROJECT, TASK AREA & WORK UNIT NUMBERS:

11. CONTROLLING OFFICE NAME AND ADDRESS:
Commander, Edgewood Arsenal
Attn: SAREA-TS-R
Aberdeen Proving Ground, Maryland 21010

12. REPORT DATE: January 1976

13. NUMBER OF PAGES: 318

14. MONITORING AGENCY NAME & ADDRESS *(if different from Controlling Office)*:

15. SECURITY CLASS. *(of this report)*: UNCLASSIFIED

15a. DECLASSIFICATION/DOWNGRADING SCHEDULE: NA

16. DISTRIBUTION STATEMENT *(of this Report)*:
Approved for public release; distribution unlimited.

17. DISTRIBUTION STATEMENT *(of the abstract entered in Block 20, if different from Report)*:

18. SUPPLEMENTARY NOTES:

19. KEY WORDS *(Continue on reverse side if necessary and identify by block number)*

EPA policies	Tropical organics	Liver cancer	Optical microscopy
EPA program	Organic film	JP-4 fuel	Ppb ranges
Cryogenic sampling	Canal Zone	JP-4 exhaust	Noise-equivalent concentration
Smog spectroscopy	Laser intracavity cell	Vinyl chloride	

(CONTINUED ON REVERSE SIDE)

20. ABSTRACT *(Continue on reverse side if necessary and identify by block number)*

Papers on concentration, detection and sampling of trace gases in the air were given. Techniques using cryogenic sampling, infrared spectroscopy, Isotope-Zeeman Atomic Absorption Mercury Detector, multipass Raman instrument, ultramicroscopy, plasma chromatography, ultrasensitive flame photometer, data-A pattern recognition, isotope dilution enzymatic systems, chemical agent decision technology, liquid crystal technology, microwave emission spectroscopy polarography and other methods are described.

DD FORM 1 JAN 73 1473 EDITION OF 1 NOV 65 IS OBSOLETE

UNCLASSIFIED

SECURITY CLASSIFICATION OF THIS PAGE *(When Data Entered)*

19. KEY WORDS (Continued)

Air sampling
Chemiluminescence
Transmission electron microscopy
Hashish vapors
Marihuana vapors
Cocaine vapors
Conditional probability
CAM-1
Terpenes
Adsorption rate
Chemical-reagent kits
Carbamates
Plasma chromatography
Single-ion monitoring
Positive-ion clusters
Radiocarbon dioxide laser
Absorbents
Dinitrocresol
Laser elastic backscatter
Raman-shifted radiation
Flame-photometric detector
Plume characteristics
Plume concentrations
Plume tracing
Carbon dioxide
Polarography, dc
Gas adsorption
Triaryltetrazolium salt
Semiconducting elements
EBBA
Photoconducting effects
4-Pyridinecarboxylic acid
Impregnated films
Lyotropic mesophases
Gas discharges
Coulombic PE
Nematic liquid crystals
Iridescence
Electron acceptors
Diindolylpyridyl methanes
Raman cell
Unsaturated hydrocarbons
Biosensor dog
Teflon plug
Limonene
Marihuana resin
Maximum likelihood
Bayesian classification
Point sampling alarms
Myrcene
Desorption
M8 alarm
Caryophyllene
Multiple-ion monitoring
Field ionization spectrum
XM256 kit
Ion-molecule reactions
Drift gases
Crude oils
Remote Raman
DIMP
Pattern recognition
PETN
Plume meander
Air quality
Nitrogen dioxide
Fluorescence omission
Sea water
Lead
Transducer alarms
Infrared-emitting diodes
Ultratrace determinations
Argon matrix
Liquid crystals
Liquid-crystal detectors
Smectic liquid crystals
Atomic emission
Dielectric constant
Cholesteric liquid crystals
Differential thermal analysis
DB-3
Jet exhaust
Trace analysis
Mechanical sensor
Morphine vapors
Absorbents
Opium vapors
Isotope dilution
Enzymatic system
Remote-sensing alarms
Δ^3-Carene
Rate of diffusion
Cyanide
Beta VII instrument
Mass spectrometry
Ethyl centralite
LAD paper
Catalytic oxidation
Molecular sieve traps
Low volatilities
Back scattering
Nitrotoluenes
Tetracosene
Continuous aqueous monitor
Methane
Nitric oxide
Transition temperatures
Adsorption kinetics
Cadmium
Transducer dosimeters
MBBA
Matrix-isolated donors
Tetracyanoethylene
Transparency
Thermotropic mesophases
Microwave-induced emission
Electron affinity
Trace gases
Birefringence
Differential scanning colorimetry
Activated carbon
Exhaust analysis
Ultramicroanalysis
Narcotic vapors
Terpeneol
Negative-ion plasma chromatography
Joint probability
Electrochemical enzyme cell
Heroin
Carrier molecules
Hydrogen sulfide
Electron donors
Diphenylamine
Methyl centralite
Passive LOPAIR
Carrier gases
Dibutyl phthalate
Smokeless powders
Kerosene
2,4-DNT
2,4,6-TNT
Trapped ChE ase
Structure walker
Carbon monoxide
Oxygen
Film thickness
Zinc
Air monitoring
Nondispersive optical absorption
Matrix-isolated acceptors
Microporous polypropylene
Emission spectrometer
Ionization potential
M.A.C.
Circular dichroism
Diatomic emission
Mercury
Adsorption bed series

1a

PREFACE

The sixth Annual Symposium on Environmental Research, jointly sponsored by the CB Division and the Chesapeake Chapter of the Americal Defense Preparedness Association, was held at Edgewood Arsenal on 29 April–1 May 1975. The meeting was planned and conducted under the guidance of COL Norman I. Shapira, USA(Ret.), Chairman of the CB Division. The Meeting Chairman was Dr. John A. Brown, Chairman of the Environmental Research Section, assisted by Mr. R. Bruce Young, President of the Chesapeake Chapter, and by Mr. John Garber of Edgewood Arsenal. The assistance of the members of the Program Committee, listed elsewhere, is gratefully acknowledged, as is the hospitality of COL Kenneth Stahl, Commander of Edgewood Arsenal.

This collection of the papers presented constitutes the Proceedings of the meeting, and it is being distributed to the attendees. This document is a US Government Special Report with a limited distribution,* and it does not constitute publication of the papers it contains. Most of the papers will be offered for publication in the regular scientific literature or have already been published as noted.

This report is sponsored by COL Kenneth Stahl, Commander, Edgewood Arsenal and Dr. Benjamin L. Harris, Technical Director of Edgewood Arsenal.

SPECIAL NOTE

Unfortunately Dr. James A. Hodgeson's paper, Evaluation of the Isotope-Zeeman Atomic Adsorption Mercury Detector (Session I), a paper by Dr. William Sarver, Problems in Analysis in Land Reclamation (Session II), another by Dr. T. O. Tiernan, Measurements of Tetrachlorodibenzo-p-Dioxins in USAF Herbicide Stocks and in Environmental Samples, and yet another by Charles S. Harden, Detection and Identification of Trace Quantities of Organic Vapors in the Atmosphere by Ion Cluster Mass Spectrometry and the Ionization Detector System (Session IV), could not be obtained for inclusion in this special publication.

A paper by Leonard A. Jonas, Joseph Rehrmann and Jacqueline M. Eskow, Kinetics of Trace Gas Adsorption from Contaminated Air was given instead of Dr. Sarver's paper, but the other papers were presented verbally.

* Although the publication will be *available* to the public through Defense Documentation Center and the National Technical Information Service.

CONTENTS

Page

KEYNOTE ADDRESS 7
TRACE ANALYSIS AND DETECTION IN THE ENVIRONMENT
Dr. Wilson K. Talley
Assistant Administrator, Office of Research and Development
US Environmental Protection Agency

SESSION I 12
Chairman: Mr. Charles Brunot
Office of Monitoring Systems
US Army Environmental Protection Agency

CRYOGENIC SAMPLING OF AMBIENT ATMOSPHERES AS A MEANS OF CONCENTRATING TRACE ORGANIC COMPOUNDS FOR CHEMICAL ANALYSIS 13
James P. Conkle, Ph.D. *et al.*

A SPECTROSCOPIC STUDY OF CALIFORNIA SMOG 17
Philip L. Hanst *et al.*

NEW SAMPLING TECHNIQUE FOR IDENTIFYING ORGANIC FILM ACCUMULATION ON ARMY MATERIEL IN THE TROPICS 71
James F. Sprouse

SESSION II 83
Chairman: Dr. George J. Rotariu
US Energy Research & Development Administration

LASER INTRACAVITY RAMAN CELL 84
Philip J. Miller *et al.*

KINETICS OF TRACE GAS ADSORPTION FROM CONTAMINATED AIR 88
Leonard A. Jonas *et al.*

DEVELOPMENT AND EVALUATION OF A SAMPLING AND HYDROCARBON CLASSIFICATION SYSTEM FOR JET ENGINE EXHAUST ANALYSIS 89
Joseph J. Brooks *et al.*

CHEMILUMINESCENT MEASUREMENT OF SUB-PPM CONCENTRATIONS OF VINYL CHLORIDE AND CERTAIN LOW-MOLECULAR-WEIGHT UNSATURATED HYDROCARBONS 104
Ralph Baumgardner *et al.*

NEEDLE IN THE HAYSTACK ANALYSIS 111
Walter C. McCrone

CONTENTS (Contd)

Page

SESSION III 117
Chairman: Mr. Joseph Hirata
US Drug Enforcement Administration

A DAY IN THE LIFE OF "CHOPPER" 118
Guy T. Barry, Ph.D.

DETECTION OF VAPOR PHASE COMPOUNDS OF ILLICIT NARCOTICS . . 119
D. Hagel *et al.*

DETECTION OF NITROAROMATICS WITH PLASMA CHROMATOGRAPHY/ PRECONCENTRATION 141
Glenn E. Spangler

AN ULTRASENSITIVE FLAME PHOTOMETRIC DETECTOR FOR SULFUR DIOXIDE AND HYDROGEN SULFIDE 149
R. K. Stevens *et al.*

ANALYSIS OF TRACE CONSTITUENT DATA – A PATTERN RECOGNITION APPROACH 154
H. T. McAdams *et al.*

DETERMINATION OF CONCENTRATION OF EXPLOSIVES IN AIR BY ISOTOPE DILUTION 180
Gilbert A. St. John *et al.*

SESSION IV 196
Chairman: Mr. Robert Moll
Edgewood Arsenal, Aberdeen Proving Ground, Maryland 21010

RECENTLY DEVELOPED ENZYMATIC SYSTEM FOR ENVIRONMENTAL MONITORING 197
Louis H. Goodson *et al.*

DETECTION OF POLLUTANTS BY CHEMICAL AGENT DETECTION TECHNOLOGY 203
Harvey Tannenbaum

CONCENTRATIONS FOR DILUTE PLUMES RELEASED AT GROUND LEVEL AND DISPERSING UNDER DIFFERENT SURFACE AND ATMOSPHERIC CONDITIONS 208
P. B. S. Lissaman *et al.*

CONTENTS (Contd)

Page

SESSION V. 241
Chairman: Dr. Erskine Harton
US Department of Transportation

BUREAU OF MINES GAS DETECTION SENSOR RESEARCH 242
George H. Schnakenberg

RESEARCH IN THE USE OF LIQUID CRYSTALS IN CHEMICAL DETECTION 253
Edward J. Poziomek *et al.*

MICROWAVE-INDUCED EMISSION SPECTROSCOPY: A NEW ANALYTICAL TOOL FOR ULTRATRACE ELEMENT DETERMINATION OF INDUSTRIAL, CLINICAL AND ENVIRONMENTAL INTEREST 268
G. W. Wooten

SIMULTANEOUS DETERMINATION OF ZINC, LEAD AND CADMIUM ION CONCENTRATION IN CONTAMINATED SEA WATER USING DIRECT CURRENT POLAROGRAPHY 292
Joseph H. Klein *et al.*

A NEW HIGHLY SENSITIVE DETECTION TECHNIQUE BASED ON THE PHOTOELECTRIC PROPERTIES OF MATRIX ISOLATED DONOR AND ACCEPTOR COMPLEXES 302
A. Snelson

STUDIES ON THE FORMATION OF DYES FROM DIINDOLYPYRIDYL-METHANES 316
David N. Kramer *et al*

DISTRIBUTION LIST 320

KEYNOTE ADDRESS

TRACE ANALYSIS AND DETECTION THE THE ENVIRONMENT

by

Dr. Wilson K. Talley
Assistant Administrator, Office of Research and Development
US Environmental Protection Agency

As the recently appointed Assistant Administrator of Research and Development for Environmental Protection Agency (EPA), I am in the enviable position of being able to implement recommendations which I like to think I was instrumental in developing. As some of you may know, I participated as a staff member of the "Ash" Council, which was created in April of 1969 to act as the President's Advisory Council on Executive Organization. One of the major recommendations of that Council was the formation of a single agency responsible for developing an integrated standard setting, regulatory, and assistance program relative to the protection and enhancement of the environment. This recommendation, in a rare stroke of bureaucratic positiveness, was accepted and EPA was created. I am now an insider in EPA, and I have found that the old saying that planners never have to implement their plans is, at least in this instance, "inoperative."

Perhaps it would be proper to review the original concepts, charges and impressions as they were interpreted during the period of the Ash Council and, in hindsight, comment briefly.

At that time, as it is now, there was a plethora of environmental protection programs within the Federal community, and categorizing these programs was difficult indeed. It seemed that everyone was wearing a white hat, and the word "environment" crept into program objective statements regardless of the tack taken in previous years. In spite of this confusion, a package of programs having to do with pollution control, standard setting and research was assembled to form a lean or rawboned regulatory agency. That agency was not to perform all ancillary environmental functions. For example, in research the intent was that in addition to its own programs it had only to be cognizant of the many other environmental research programs and be able to interpret and utilize their results. EPA research and development was designed to respond to problems associated with the regulatory mission of the Agency; not to conduct research independent of that mission. It was not envisioned that a heavily funded program would result, and that in fact has not been the case. The major effort within EPA has been, and continues to be centered in the technical assistance and grant programs associated with municipal and state pollution control efforts.

It is not premature to assess the results of the implementation of the Ash Council recommendations: Does EPA work? What progress has been made toward agency and national goals? Is EPA research adequate?

The questions surrounding the achievement of the National Air Quality Goals present an interesting history and perhaps provide one framework in which to assess EPA's research efforts.

By the end of December of 1971, states were required to have adopted ambient air quality standards and to have submitted implementation plans indicating their ability and course of action to meet these goals. These were subject to the approval of the EPA Administrator and they

were to include the six criteria pollutants: carbon monoxide; sulfur dioxide; nitrogen dioxide; ozone; hydrocarbons; and particulate matter. The standards (or goals) were to be designed to protect the health and welfare of the citizens.

Plans for controlling these contaminants normally fit into two categories: (1) controlling stationary sources for sulfur oxides and particulates and (2) controlling automobile or mobile sources for carbon monoxide, nitrogen dioxide, hydrocarbons and the subsequent formation of ozone. This appears to be straightforward; however, the implementation of control plans has revealed conditions and situations unforeseen by the Federal and state drafters. Obviously if one limits the sulfur content of fuel, the sulfur dioxide in the ambient air will be reduced by some amount. And which environmentalist could predict the force of the current energy and economic situation that has resulted in an emphasis on available high-sulfur coal?

Further as research on health effects continues, there may be indications that the culprit is not sulfur dioxide alone but its photolytic product, sulfate, as well. And, further, we suspect that the size and chemical composition of the sulfate/particulate complexes are the important determinants in health effects. Now we have crossed from gas to particulate, and not just particulate, but a particle small enough to possibly elude collection on the standard particulate-matter collection filter. In other words, what started as a straightforward control of a gas and particulate has, it seems, merged into a new problem.

How has the research capability of EPA responded to these much more complex problems? Obviously there is a need for new detailed research information on the generation, transformation, transport, health effects and ultimate fate of these chemical and physical phenomena. Research is also needed in the measurement of, and the effects of these newly defined species prior to the implementation of effective control plans.

The second suspension of the automotive emission standards is another instance in which there is an urgent need for research to yield new technology. The automotive catalyst cauldron continues to boil. The combination of EPA and Detroit research and development appears to have left many old questions unanswered and has generated new issues. Obviously something more must be done in this area.

While on the subject of automotive emissions, I should mention the status of the nitrogen oxides-hydrocarbon-ozone relationship. The state-of-the-art regarding modeling has been altered somewhat by research into the nature of this chemical-physical triangle. The air quality standards imply that if one controls the morning rush-hour hydrocarbons, the afternoon ozone will be reduced. Recent ozone monitoring has provided additional information resulting in reconsideration of this premise. The presence of inordinately high levels of photochemical pollution in rural or remote areas (far removed from automotive traffic) is at this time a subject of intense investigation by EPA research and other offices. As in the case of the sulfur oxides, information on generation, transformation, transport and sinks is urgently needed.

We are meeting here to discuss trace analysis and detection of contaminants in the environment. This is another area in which the nature of our research activity seems to be changing. We are monitoring parts per trillion; we are getting less and less of more and more. What does this mean? That is, are these small amounts important? Our ability to detect has momentarily outstripped our ability to interpret. Further, we continue to need archival capability. But we have new problems in preserving samples, and acquiring the ability to avoid contamination of samples of such small concentrations. The interpretation of these data is critical. What does the pressure to

abandon the concept of a threshold level of a contaminant do to our standards? The burden is on the scientist now, as he has an increased responsibility, as less of more is found, to identify the significance of these trace substances. He must inform not inflame, the public.

There are other frameworks in which to assess the research role in this regulatory agency. The taconite-Duluth situation involving the contamination of drinking water with asbestos raises further questions about what kind of research EPA can or should do. The case was placed in the hands of the courts, and partly because of the paucity of health effects information, the results have been, I feel, less than satisfactory. The stark realities of unfavorable economics played a strong role in this litigation. Perhaps it is time to dwell for a moment on the changing role of environmental research. The cry "damn the environment, I want a job" is being heard with increasing frequency. Ten years ago, in the mid 60's, it was considered somewhat chic to march in favor of environmental control. The pendulum was swinging with great amplitude in favor of the environmentalist. The clean-life wave continued to build until somewhere around 1972-73 when the legislative mandates and the myriad of ramifications associated with them came home to industry and the consumer. Large industries with marginal operations were faced with the realities of "clean up or shut down." The consumer too was to feel the bite. Clean air is expensive. He noticed his new '73 auto was not as easy to operate nor as inexpensive to run as the old 1970 model. Then came the oil embargo. The heavy artillery of industry had been turned toward EPA. Thus we have yet another aspect to environmental research unforeseen in its complexity by the original planners of EPA. We must abate pollution, but within the constraint that the abatement not unnecessarily injure the Nation's economic environment. We are, as a society, facing hard decisions concerning how much environmental enhancement we want or are willing to pay for. Further, how badly we want environmental improvement is a moving target, dependent upon the day's crises, the economic situation, and many other factors. The Agency, and consequently its research effort, must be in phase with this target.

I spoke earlier of having to implement the plans I helped establish for EPA s R&D effort. Are the original intentions for an environmental research program still valid in light of these new demands? I think they are. In fact, the new and broader needs point again to EPA's research role as being cognizant of other agencies' and industry's efforts. We do not so much need more money or manpower as we need the R&D products of other agencies and industry. We have received this help in the past, I hasten to add. But we need much more, of a higher sophistication; we need to know about products of others' research, which, with minor modifications introduced early into their designs, may be applicable to our needs. We need to be informed of other agencies' planning at a yet earlier stage, instead of learning of the products of research after the fact. Reading the literature, which reports completed research, is not enough; it's often years too late.

More specifically, in view of all this philosophy and history, it may be time to return to some of the hard facts surrounding EPA R&D. As nearly as can be determined, the Federal community managed to dispense approximately 18.8 billion dollars for R&D in FY 75. Of this, Department of Defense (DOD), National Aeronautics and Space Administration (NASA), Energy Research and Development Agency (ERDA), Health, Education and Welfare (HEW) and National Science Foundation (NSF) budgeted nearly 90%. EPA R&D spend approximately 1.5% or about 285 million. This does not seem to be much when we consider the charges placed on EPA R&D. Indeed, the recommendations of the Ash Council have been adhered to – ours is a lean operation. The projected FY 76 budget is 258 million an approximate 10% reduction. The following table provides a breakdown by media of these funds for FY 74, 75 and 76. As can be seen, about one-half of the FY 76 decrease occurs within the energy R&D program. Also, I should call to your attention that this program constitutes nearly 45% of the total and that it is basically an extramural effort that was not part of the FY 74 budget.

Table. Environmental Protection Agency, Office of Research and Development
Comparison of Resource Levels in FY-74, FY-75, and FY-76 By Media

Media	FY-74	FY-75	FY-76
	$(M)	$ (M)	$(M)
Air	46.8	53.9	45.9
Water quality	42.2	46.1	44.6
Water supply	2.5	5.2	12.8
Solid wastes	2.2	5.8	4.0
Pesticides	5.1	8.5	8.5
Radiation	2.2	2.6	1.6
Noise	0.5	0.6	0.1
Interdisciplinary	14.8	18.6	20.6
Toxic substances	0.2	1.2	1.2
Energy	17.4	134.0	112.0
Program management & support	7.8	7.9	6.6
OR&D program total	141.7	284.4	257.9

The FY-74 base program (energy exclusive) breakdown indicates a 57.5 million dollar in-house effort with 25.5 million in grants, 44.0 million in contracts and 15.0 million interagency. During FY-76, excepting the energy R&D, I would not expect these ratios to change dramatically. And as I mentioned previously, the energy R&D will be basically extramural.

So EPA R&D should and must rely on R&D contributions from outside the agency. For instance, NSF plans to spend about 29 million on ecology and population biology and about 15 million on atmospheric sciences in FY-76; NASA plans to spend 175 million on space applications in FY-76; ERDA plans to allocate 156 million for biomedical and environmental research. The total for these selected examples is 375 million. It seems quite possible that the EPA, NSF, NASA and ERDA programs can be designed to complement each other with a minimum of duplication and a maximum of information for all agency objectives. It is imperative that closer interagency coordination be achieved at the project-planning stage and that there be much less parochialism within agencies if we are to reach our goals. This was the original idea for EPA research, that is, to not do all the environmental research but, rather, to be cognizant that it *is* being done and to benefit from it where possible in the achievement of their R&D goals that are associated with standard setting and regulatory mandates.

In conclusion, I would like to commend the organizers of this symposium and those government, industrial and academic components who have supported it. This appears to be an excellent forum for the transfer of R&D findings. This of course is one of the best ways to accomplish some of the objectives of the Federal environmental effort and as a result of this symposium perhaps we will have chipped away a bit more of the interagency parochial facade that continues to be a barrier to the transfer of technology and the completion of closely allied objectives.

SESSION I

Chairman: Mr. Charles Brunot
Office of Monitoring Systems
US Army Environmental Protection Agency

CRYOGENIC SAMPLING OF AMBIENT ATMOSPHERES AS A MEANS OF CONCENTRATING TRACE ORGANIC COMPOUNDS FOR CHEMICAL ANALYSIS

by

James P. Conkle, Ph.D and Richard L. Miller, Ph.D.
Environmental Sciences Division, USAF School of Aerospace Medicine
Aerospace Medical Division (AFSC)
Brooks Air Force Base, TX 78235

This paper describes a cryogenic sampler that permits concentration of common organic air pollutants. The sampler employs a 3-stage condensation series, at 0°C (ice water), -78°C (dry ice), and -175°C (liquid nitrogen). Liquid oxygen formation is prevented by maintaining the final trap at -175°C with a gaseous nitrogen flush. The sampler in field configuration is 44 X 51 X 51 cm and weighs about 48 kilograms. Liquid nitrogen, gaseous nitrogen, dry ice, ice and 110-volt power are required for its operation. The sampler provides for the identification and quantitation of trace organic compounds in the ambient atmosphere when analyzed with a gas chromatograph-mass spectrometer-data acquisition system.

The system has been used in environmental pollution applications. The identification of the contaminant which made the contents of Armed Forces subsistence vans usable was a dramatic demonstration of the usefulness of the system. The system has also been used in the identification of the gaseous organic compounds contained in the exhaust of turbine engines.

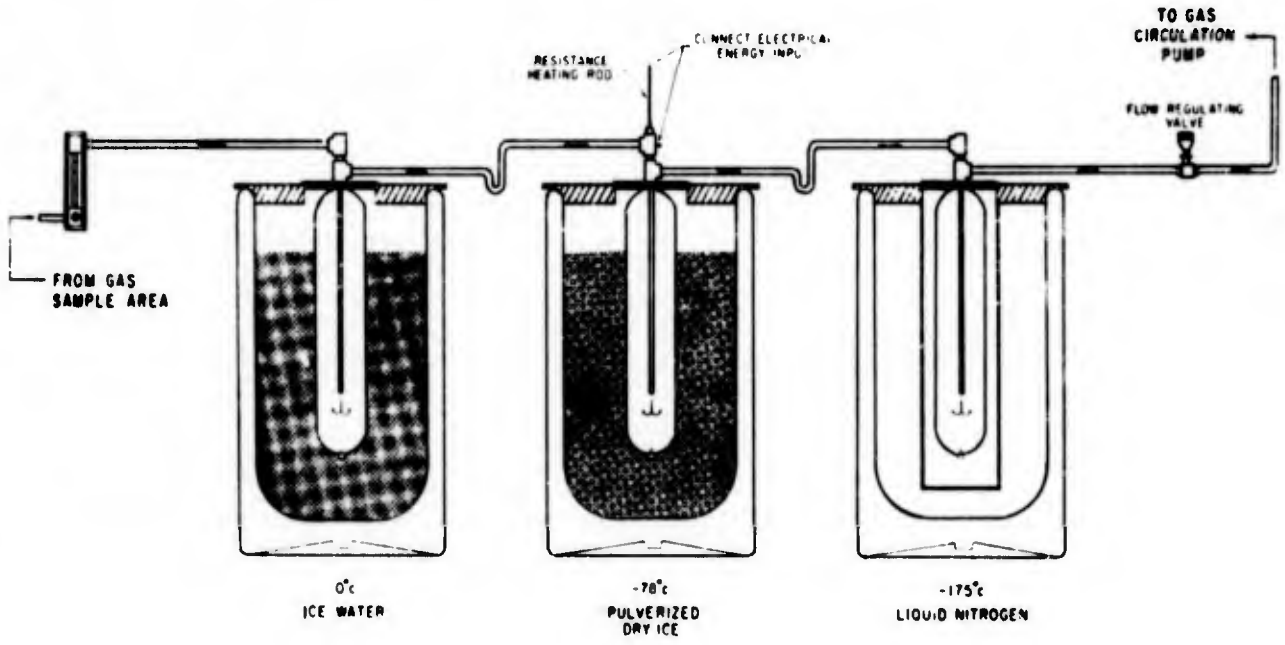

Figure 1. Gas Flow Path for Multistage Cryogenic Trapping System

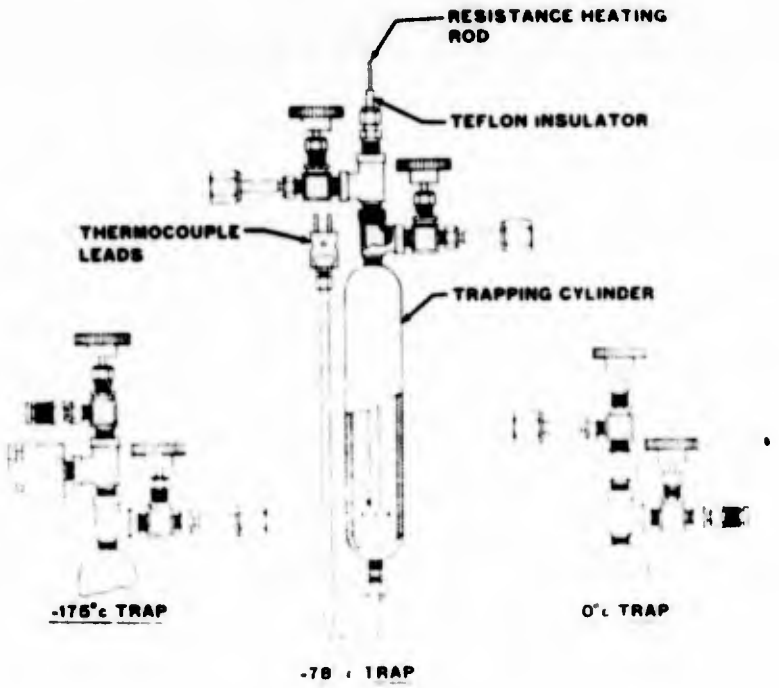

Figure 2. Valve Connections

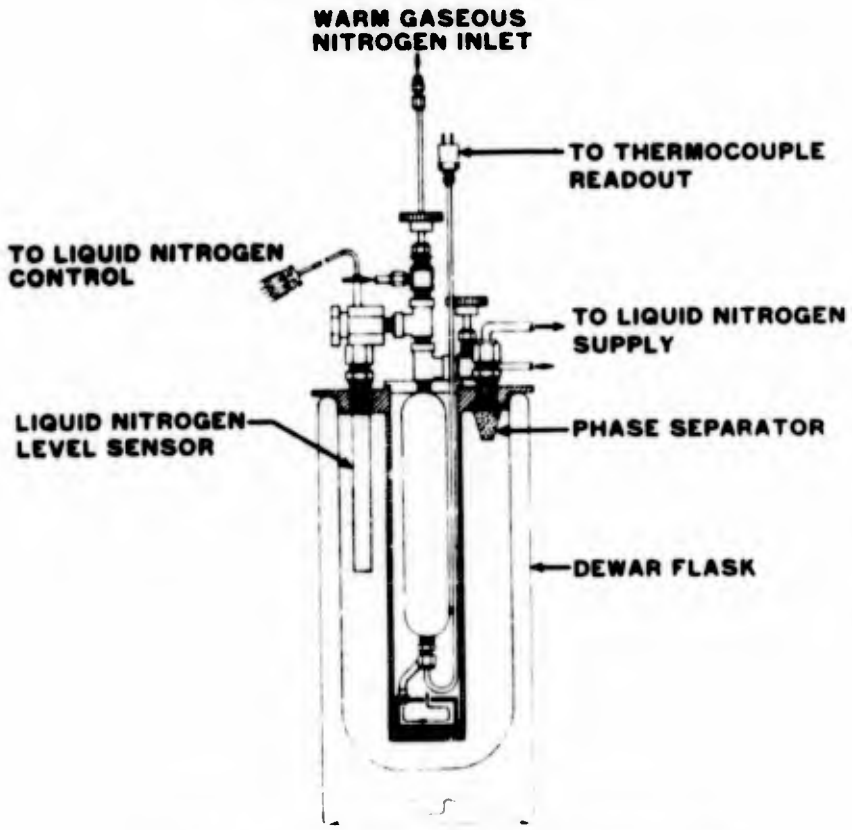

Figure 3. Liquid Nitrogen Trap Cross-Section

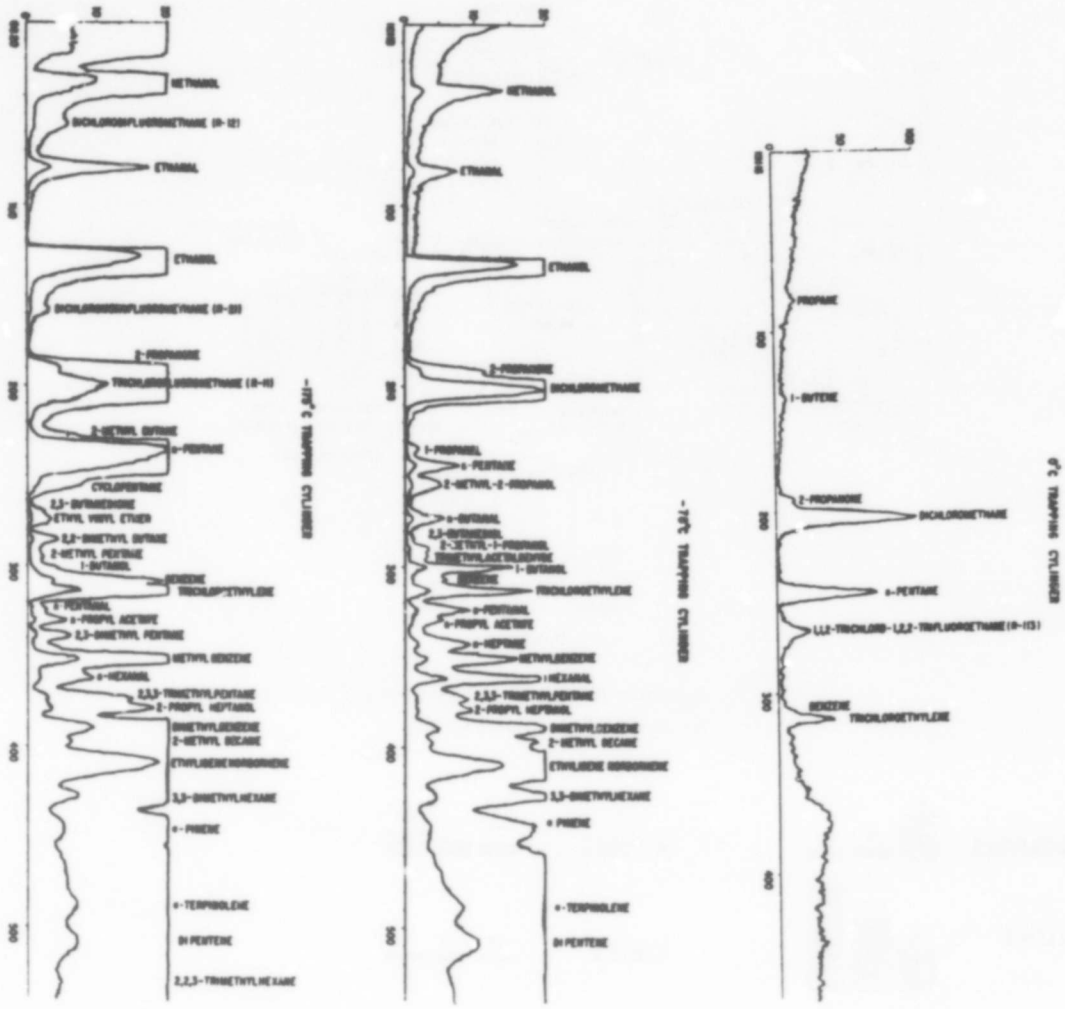

Figure 4. Fractionation of Liquids Obtained in Each of the Traps

Table. Major Compounds in Contaminated Trailers

Trichloroethane	Cumene
Tetrachloroethylene	Acetaldehyde
Toluene	Crotonaldehyde
Methanol	Limonene
Ethanol	Ethylidene Norbornene

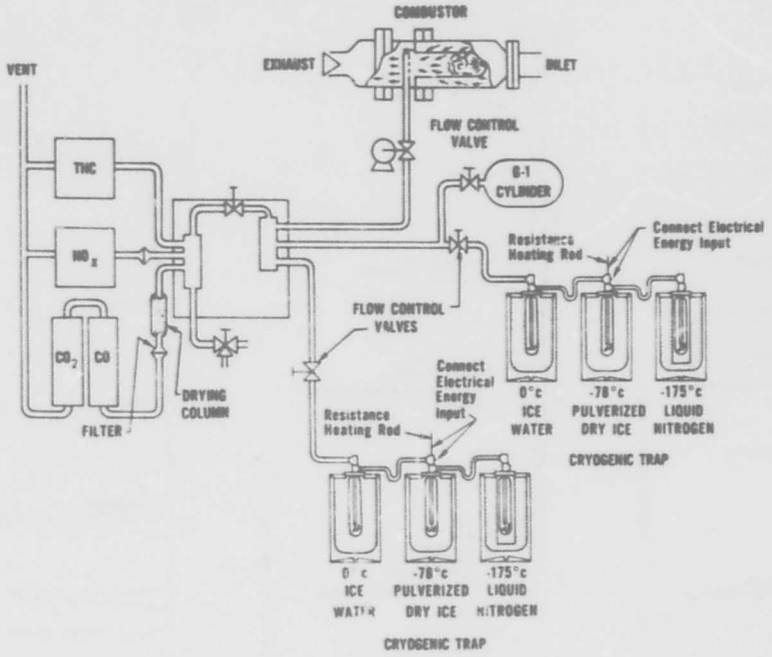

Figure 5. Another Example of Cryogenic Technique Analysis of Oxidized Gases

Figure 6. Exhaust Hydrocarbon Concentration (ppm) as Benzene with Various Fuels at 33 psig Inlet Pressure

A SPECTROSCOPIC STUDY OF CALIFORNIA SMOG

by

Philip L. Hanst, William E. Wilson, Ronald K. Patterson,
Bruce W. Gay and Lucian W. Chaney
Chemistry and Physics Laboratory, National Environmental Research Center

and

Charles S. Burton
Rockwell International, Thousand Oaks, CA

INTRODUCTION

BACKGROUND

The composition of the polluted Los Angeles air has been studied for many years with a variety of measurement methods. The main purpose of direct atmospheric analysis is to determine what people are exposed to, but in addition it can indicate the sources of the pollution, the transformations of the compounds, and the pollution removal paths. The main prior application of long-path infrared absorption to atmospheric analysis was the work of the Franklin Institute group between 1953 and 1957.[1-4] Among the results of that earlier infrared work were the discovery of the peroxyacyl nitrate family of pollutants, the proof of the presence of peroxyacyl nitrates in the Los Angeles atmosphere, and spectroscopic confirmation that ozone is a major product of atmospheric photooxidations.

Infrared techniques were exploited in those earlier studies as fully as the equipment allowed. A prism spectrometer was used, with a thermocouple detector. The folded path was about 240 meters long. Atmospheric spectra were compared to reference spectra by inspection, and point-by-point ratio plots were made through slide-rule calculations. These techniques yielded a limit of pollutant detectability of about 0.05 ppm for peroxyacetyl nitrate, ozone, ethylene, and acetylene. This was sufficient for detection in the ambient air under some conditions, but not all. The limit of detectability for nitric acid, formic acid, and formaldehyde fell in the vicinity of 0.2 ppm--too high for detection. Most of the compounds that were detected by infrared can also be measured with simpler equipment, and therefore long-path infrared studies were relegated to a minor role for the following 15 years.

In the laboratory, the infrared method has continued to be successful. Infrared studies of pollutant reactions at parts-per-million levels have been carried on at the General Motors laboratories and in several university laboratories. These studies have been a major source of progress in air pollution chemistry.[5,6]

Ambient air analysis has been carried out mainly by the gas chromatographic method. In hydrocarbon analysis, this method easily exceeds the capability of long-path infrared. The infrared method can give a fairly sensitive measure of total hydrocarbons in the air, and a highly sensitive measure of individual hydrocarbon species with one, two, and three carbons, but it cannot resolve the heavier hydrocarbons. Gas chromatography, in contrast, cleanly separates and identifies nearly all components of a mixture of hydrocarbon pollutants, down to parts-per-billion (ppb) levels.

The main value of the infrared method is in identifying and measuring all the assorted nonhydrocarbon species in the air, especially the oxygenated and nitrogenated compounds. This is just the aspect of air analysis in which the chromatographic method is weakest. Thus, the two methods are complementary, and long-path infrared methodology still has a vital role to fill in atmospheric studies.

Improved optical components of many different types have been developed in the past 20 years. These include the solid-state detectors, the laser, the scanning Michelson interferometer, and the dedicated minicomputer for processing interferograms and spectra. The Fourier transform spectrometer systems now commercially available bring all of these components together in a package that yields higher resolution and higher signal-to-noise ratios than conventional grating or prism spectrometers. Furthermore, the new spectrometer data systems permit the automatic plotting of ratio spectra when a single absorption cell is used.

Since new instrumental improvements were capable of yielding a 10-fold or even 100-fold increase in measurement sensitivity in an atmospheric long-path infrared experiment, a new long-path absorption cell has been built especially for use with a Fourier transform spectrometer. It was soon demonstrated that the combination was yielding a parts-per-billion detection sensitivity for many of the important air pollutant species. These results were described in a recently published article, which should be consulted for additional details.[7]

EQUIPMENT AND METHOD

In 1972, as part of a study of particulate and gaseous pollution, the Fourier transform spectrometer and long-path cell were set up in Pasadena on the roof of the Keck Engineering Building at the California Institute of Technology. A folded-path White cell with a base path of 8.7 meters was used.[8] The path was enclosed in a glass tube 9.2 meters long and 0.3 meter in diameter. The tube is shown in Figure 1. Either 44 or 48 passes

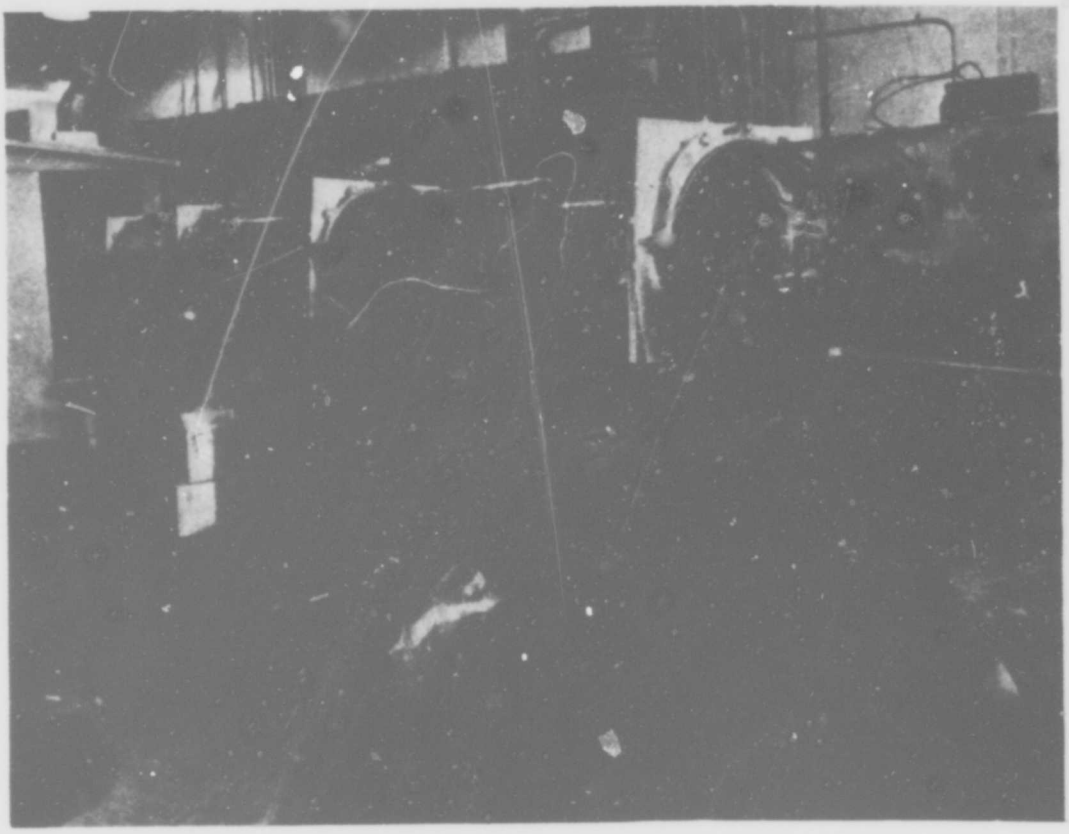

Figure 1. Glass tube in penthouse.

were used, yielding path lengths of 383 and 417 meters. The only place available to locate the system was inside the penthouse for the air conditioning and heating machinery of the building. Although this proved to be a shaky and noisy environment, most of the vibration was eliminated by shock mounts placed under the tube and the spectrometer. The spectrometer and its data system were housed in a small air-conditioned shed, as shown in Figure 2. Two detectors were used, each at liquid nitrogen temperature:

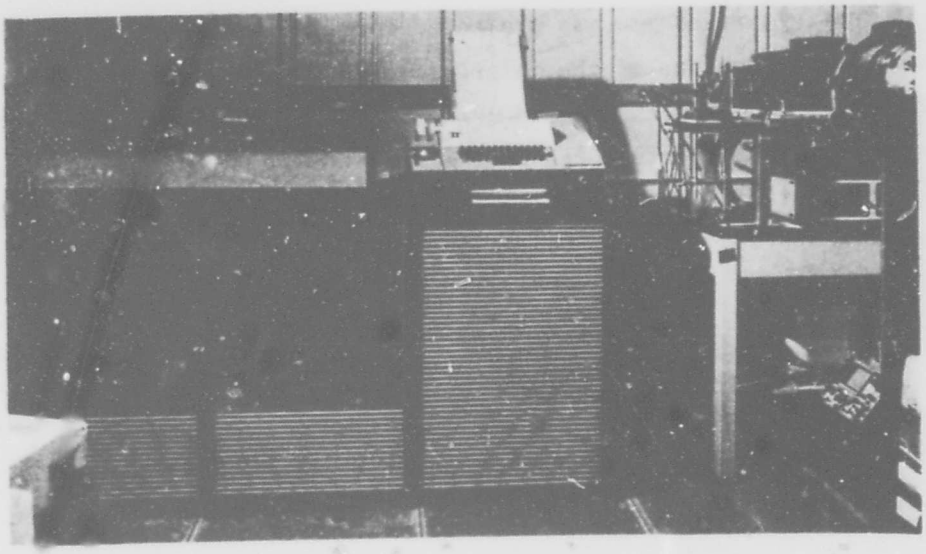

Figure 2. Spectrometer and data system in shed.

indium antimonide for the frequency region 2000 to 3300 cm^{-1}, and mercury-cadmium-telluride for the region 700 to 1360 cm^{-1}. The region 1360 to 2000 cm^{-1} was not recorded because of water vapor interference.

The system components are diagrammed in Figure 3. Infrared radiation

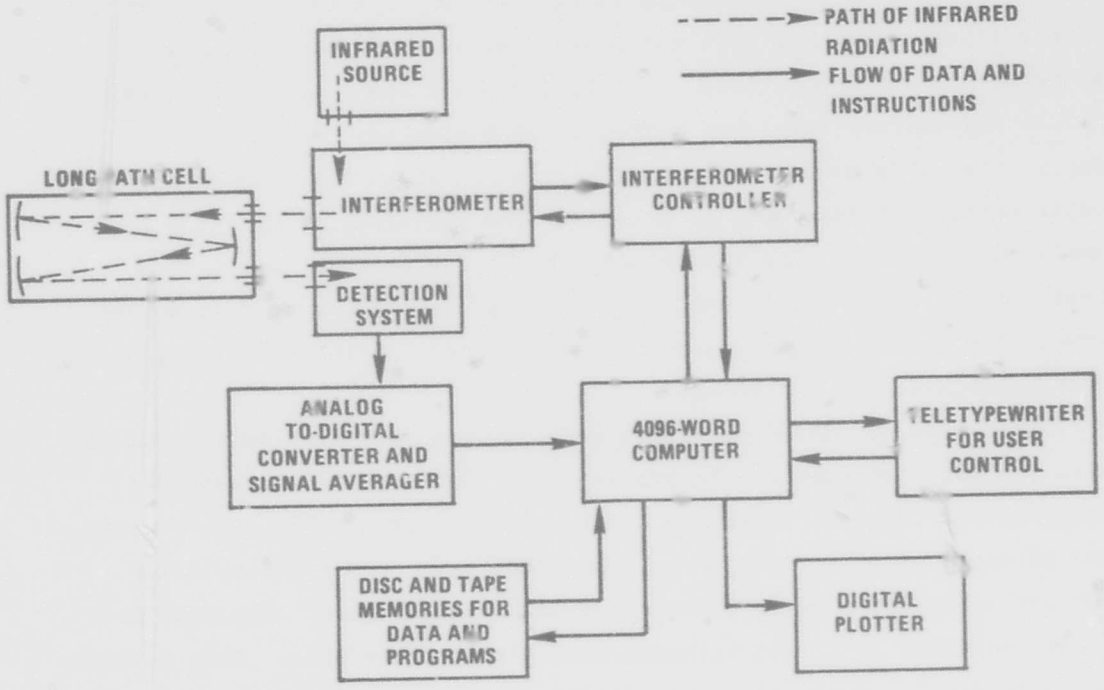

Figure 3. Pollutant measuring system.

from a Nernst glower source was projected into the interferometer. The modulated optical output of the interferometer (the interferogram) was passed through the long absorption cell to the detector. Forty digitized recordings of each interferogram were added together in the data system in order to increase the signal-to-noise ratio. The summed interferogram was then transformed to yield the spectrum. (Spectral resolution was approximately 2 cm^{-1}.) The digitized spectrum could be displayed, or it could be stored in the computer memory for future access. Generally, the ratio between the air spectrum and a stored reference spectrum was computed and plotted.

The air sample was taken in through a 0.1-meter-diameter plastic pipe, which ran out the door of the penthouse and up into the air about 9 meters above the roof on the fourth floor. This placed the intake point about 27 meters above the street. A blower kept the air moving through the intake pipe at all times. The glass long-path cell was evacuable down to less than 1 torr pressure. The manner of collecting a sample was as follows: (1) The long-path cell was evacuated. (2) By opening a valve, the flow of outside air was directed into the long-path cell so that the cell was filled to a pressure sufficient to cancel the water vapor lines against those in a reference spectrum. Generally, the pressure was between 500 and 600 torrs. (3) Recording of the spectrum was begun immediately and was completed within about 5 minutes. It is hard to imagine that this manner of sampling could result in the loss of any labile species of molecules in the air. The residence time of the air sample in the intake pipe was no more than a few seconds, and in the glass cell it was no more than a few minutes. There was good agreement between the values of ozone measured by infrared and the values measured by chemiluminescence instruments.

The reference air samples were made up from tank air, humidified to match the water content of the ambient air. Humidity was adjusted by mixing two portions of reference air in the long-path cell. One portion came straight from the tank, dry. The other came from a reservoir of tank air stored in a large plastic bag with liquid water. The work done in late November 1972 used Matheson Zero Air for reference. This turned out to be nearly devoid of carbon dioxide but to contain about 1 ppm of carbon monoxide. The absence of carbon dioxide was a disadvantage

because it allowed atmospheric carbon dioxide to show in the ratio plots. The presence of carbon monoxide was also a disadvantage because it cancelled some of the absorption by ambient carbon monoxide pollution, thus requiring a correction factor. The 1973 work used Scott reference air to which 300 ppm of carbon dioxide had been added. This cancelled most of the carbon dioxide in the ratio plots, but not all. The Scott air also turned out to include about 1 ppm of carbon monoxide. It did not prove feasible to obtain an exact water balance in all cases; but, generally, at least 90 percent of the water interference was removed.

CALIBRATION SPECTRA

Incorrect absorption coefficients are the most likely source of error in atmospheric infrared studies. Many of the molecular species detected and measured in this work do not have well-documented reference spectra. Published absorption coefficients must be used with caution because of the many possible sources of error in handling the gas and in recording and interpreting the spectra. Whenever possible, absorption coefficients to be used were rechecked by running new reference spectra on samples at parts-per-million concentrations in a laboratory long-path cell. The simplest and safest cases of absorption coefficient measurement involve the large polyatomic molecules, which are thermally stable. This includes, for example, paraffinic hydrocarbons, alkyl nitrates, ketones, alcohols, and alkyl halides with two or more carbons. The spectra in these cases have so many overlapping lines that there is no inherent fine structure in the bands at atmospheric pressure. The absorption coefficient is therefore independent of pressure and instrumental resolution; the absorption equation is obeyed at all absorptivities. The most difficult cases involve the molecules with a small number of lines in their spectra, such as carbon monoxide, nitric oxide, and hydrogen chloride. The apparent absorption coefficients in these cases are dependent on total pressure, concentration of the absorbing species (because of self-broadening), and instrumental resolution. The absorption equation is only obeyed at small absorptivities. Thermally unstable species, such as ozone and hydrogen peroxide, and species that adsorb or polymerize, such as formic acid and formaldehyde, have their own

characteristic measurement difficulties. For these reasons, a listing of absorption coefficients and the conditions under which they were obtained is given in Table 1.[7, 9-12] Reference spectra with sharp bands or lines were measured with resolution similar to that used in recording the atmospheric spectra. The values of the absorption coefficient, κ, are those used in the absorption equation:

$$\ln (I_o/I) = \kappa PL$$

where:

$\ln$ = natural logarithm

I_o = incident intensity of infrared frequency specified

I = transmitted intensity

P = partial pressure of component, atm

L = optical path length, cm

κ = absorption coefficient, cm^{-1} atm^{-1}

For proper calibration of carbon monoxide measurements, it was necessary to measure the absorption coefficient as a function of the apparent energy ratio at the chosen point in the spectrum. A range of concentration of carbon monoxide between 9 and 0.5 ppm was used. The results are plotted in Figure 4. The absorption coefficient values for carbon monoxide were found to be about one-half as great as they were found to be in a similar measurement made at torr-level concentrations in a 10-cm absorption cell.[9] The difference is probably due to self-broadening of the lines.

Table 1. ABSORPTION COEFFICIENTS

Pollutant	Measurement frequency, cm^{-1}	Absorption coefficient, cm^{-1} atm^{-1}	References and comments
Acetylene (C_2H_2)	720	180	Present work; measured at parts-per-million concentration in air
Ammonia (NH_3)	930 967	27 35	Present work
Carbon monoxide (CO)	2170	See curve in Figure 4	Present work; spectra of parts-per-million concentrations of CO in 600-torr air were recorded in the long-path cell at a resolution similar to that used in Pasadena
Carbon tetrachloride (CCl_4)	793	210	Reference 10
Ethylene (C_2H_4)	950	20	Present work; measured at parts-per-million concentrations in air
Formaldehyde (H_2CO)	2780	10	Present work
Formic acid (HCOOH)	1105	13	Applies to central peak only; measured at parts-per-million concentration in long-path cell
Freon 12 (CCl_2F_2)	921	45	Reference 10
Hydrogen peroxide (H_2O_2)	1250	9 ± 3	Present work
Methane (CH_4)	3017 1307	12 11	Reference 9; rechecked in present work with 1.7 ppm CH_4 in atm of air
Methanol (CH_3OH)	1033	25	Present work
Methyl nitrate (CH_3ONO_2)	853 1018 1290	30 18 35	Present work
Nitric acid (HNO_3)	896	20	Reference 7
Nitrogen pentoxide (N_2O_5)	740 1248	40 40	Present work
Ozone (O_3)	1053	8.6	Reference 11
Nonmethane paraffinic carbon (CH_x)[a]	2970	4.0	An average of the absorption coefficient values, per carbon, calculated for propane, butane, pentane, and hexane from Reference 9
Peroxyacetyl nitrate (PAN)	1162	32	Reference 12
Trichloroethylene (C_2HCl_3)	852	22	Reference 10

[a]Does not include methane or the ring carbons in aromatics; thus, the subscript x indicates two or three hydrogens, but not one or four.

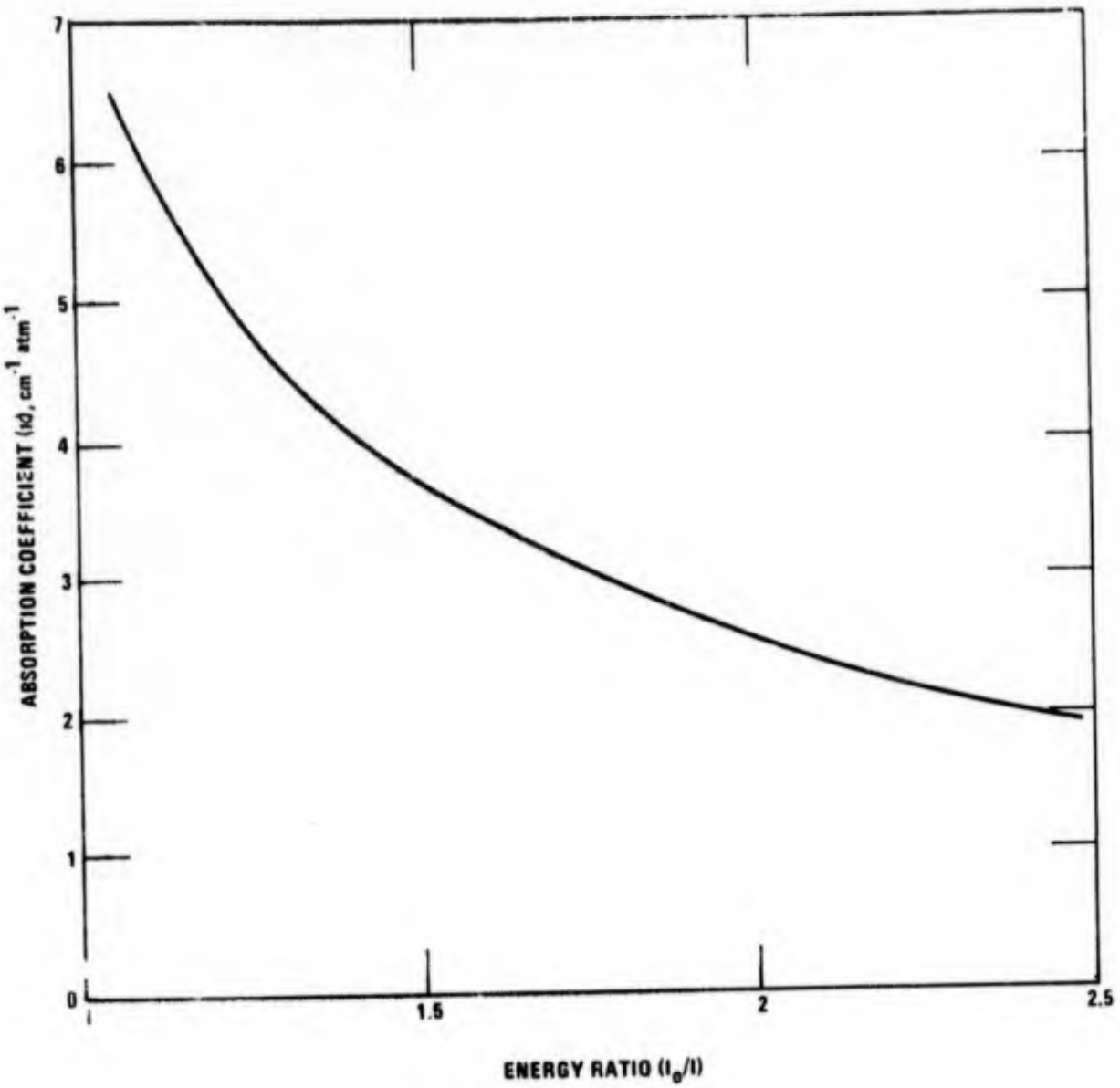

Figure 4. Carbon monoxide absorption coefficient as a function of apparent energy ratio at 2700 cm^{-1}.

RESULTS AND DISCUSSION

RESULTS

There were two periods of data taking: (1) late November 1972 and (2) July and August 1973. The 1972 period did not include any smoggy days, but it did include mornings and evenings of stationary air that, although visually clear, showed an accumulation of gaseous pollution. The 1973 summer period included the smog attack of July 24 and 25, which yielded the highest ozone concentrations Pasadena had seen for several years.

A sample spectrum from the late November period is shown in Figure 5. This spectrum was obtained on Thursday evening, November 30, 1972, at 5:15 p.m. Sample pressure was 760 torr, and the path length was 383 meters. Only the higher frequency end of the spectrum recorded with the indium antimonide detector is shown. In interpreting this spectrum, it should be recognized that approximately 10 percent of the signal was due to stray radiation that travelled only a few tens of meters in the cell, rather than the full path. This condition could have been corrected but was not recognized in time. When properly allowed for, the stray radiation does not invalidate any of the results. The single-beam atmospheric absorption spectrum appears in the lower part of the figure, and the ratio plot of that spectrum over the spectrum of humidified reference air appears in the upper part. The single-beam plot shows the many water vapor lines, which are removed in the ratio plot. In proceeding from lower frequency to higher, the single-beam spectrum shows a gradual decrease in signal due to the response characteristics of the detection system. The ripples

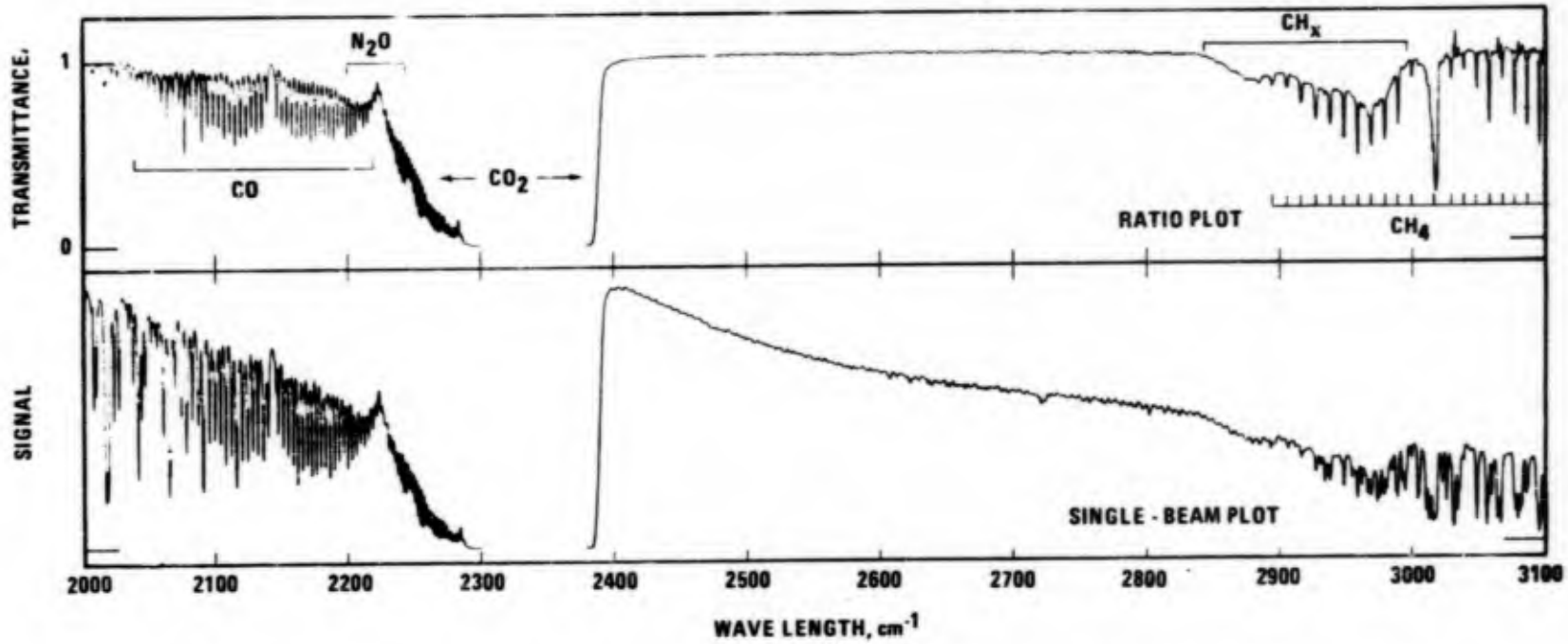

Figure 5. Atmospheric spectrum, November 30, 1972, 5:15 p.m. Path, 383 meters; pressure, 760 torr; detector, indium antimonide.

in the single-beam plot, which are especially evident between 2400 and 2500 cm^{-1}, are the result of interference phenomena in the train of optical components. The ripples are cancelled out in the ratio plot. A slight overcompensation of the water vapor absorption has driven some of the strong water lines above unity in the ratio plot. The Matheson Zero Air used for reference contained about 1 ppm of carbon monoxide, but no carbon dioxide, nitrous oxide, or methane. The carbon monoxide band in the ratio plot is therefore smaller than it should be, but the other bands appear at full strength. Concentrations of pollutants calculated from the spectrum are carbon monoxide, 11.5 ppm; methane, 2.8 ppm; non-methane paraffinic carbon atoms (CH_x), 2.2 ppm. Nitrous oxide was at its normal value of 0.25 ppm.[13] Carbon dioxide was not calculated from the spectrum. There was no indication of formaldehyde.

Spectra from July 25, 1973, covering the region 700 to 1360 cm^{-1} are shown in Figures 6 and 7. Stray light in these cases was probably less than 5 percent. For these spectra, the mercury-cadmium-telluride detector was used. In the 9:30 a.m. spectrum, Figure 6, the sample pressure was 600 torr, and the path length 417 meters. The lower spectrum is the single-beam plot, showing mainly water and carbon dioxide bands. The middle spectrum is a ratio plot using a reference spectrum of Scott tank air properly humidified to cancel nearly all of the water vapor absorption. This air also contained about 300 ppm of carbon dioxide, which cancelled about 90 percent of the carbon dioxide absorption. The reference air did not contain methane or other hydrocarbons. The upper spectrum in the figure is a scale-expanded plot of the spectral region 800 to 1200 cm^{-1} in which the ordinate scale is 19 times larger than in the center spectrum. Marked on the spectra are absorption bands for the following compounds and concentrations: ozone, 0.09 ppm; peroxyacetyl nitrate, 0.016 ppm; methanol, 0.015 ppm; Freon 12, 0.008 ppm; trichloroethylene, 0.015 ppm (perhaps underlaid with some absorption by Freon 11); formic acid, 0.020 ppm (underlaid with some absorption by Freon 12); acetylene, 0.028 ppm; ethylene, 0.015 ppm (distorted by a noise spike); and methane, 2.0 ppm.

In the 1:00 p.m. spectra, Figure 7, we see that the photochemical reaction products--ozone, formic acid, and peroxyacetyl nitrate---have increased substantially. In Figure 7, the expansion factor of the upper

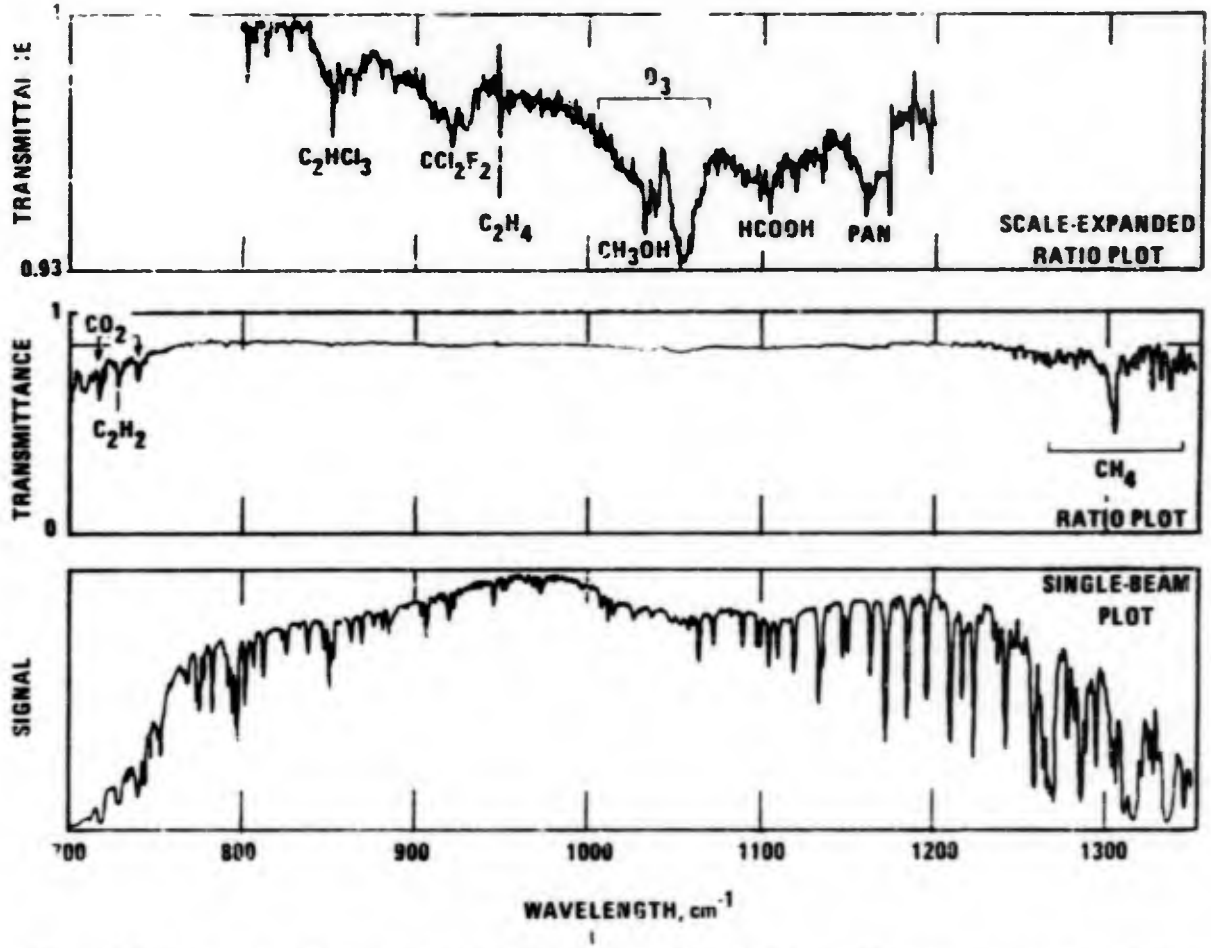

Figure 6. Atmospheric spectrum, July 25, 1973, 9:30 a.m. Path, 417 meters; pressure, 600 torr; detector, mercury-cadmium-telluride.

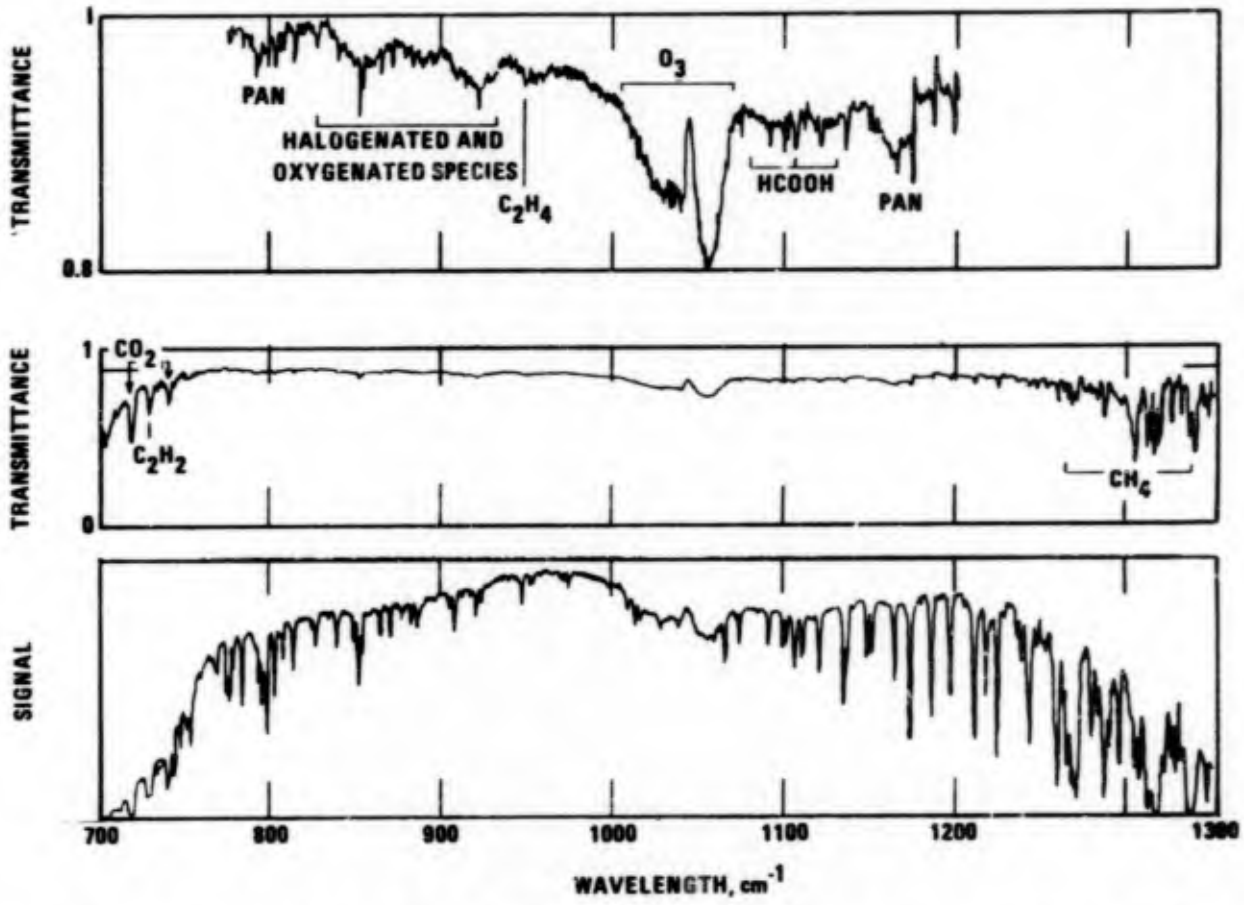

Figure 7. Atmospheric spectrum, July 25, 1973, 1:00 p.m. Path, 417 meters; pressure, 535 torr; detector, mercury-cadmium-telluride.

spectrum is only 7-fold. The 1:00 p.m. values were ozone, 0.60 ppm; formic acid, 0.063 ppm; and peroxyacetyl nitrate, 0.051 ppm. By 1:00 p.m. the acetylene and methane had increased slightly to values of 0.030 ppm and 2.4 ppm, respectively. The ethylene concentration had decreased to approximately 0.009 ppm.

Pollutant concentrations measured between November 20, 1972, and December 1, 1972, are listed in Table 2. In general, this was a time of air stagnation morning and evening, ventilation and clean air in the middle of the day, and no smog.

Concentrations measured on selected days in the summer of 1973 are listed in Table 3. July 24 and 25 were days of very high ozone concentration, and all values calculated from the spectra of those days are listed. July 26 was also expected to be a day of very high oxidant, and in fact, Federal employees in the Los Angeles area were excused from work. However, the atmospheric conditions changed--perhaps beginning in the late afternoon of the 25th--and very little smog developed. Other days of high ozone showed a pattern of concentrations and variations with time generally similar to those observed on the smoggy days of July 24 and 25. Since the ratio of nonmethane paraffinic hydrocarbon to carbon monoxide can indicate pollutant sources, the values for those two pollutants measured on 5 days in August are also listed. The gaps in the table result from the choice of detectors and spectral regions for recording. The bulk of the July 24 data was obtained in the 700- to 1400-cm^{-1} region, using the mercury-cadmium-telluride detector; hence, they do not show carbon monoxide or paraffinic carbon. On July 25 and 26, the data obtained with the mercury-cadmium-telluride detector were recorded out to 2300 cm^{-1} and hence include carbon monoxide. The various measurements that show paraffinic carbon and carbon monoxide were obtained with the indium antimonide detector. Some additional details from the spectra will be included in the following discussions.

DATA ANALYSIS AND DISCUSSION

Analysis of the results yields information on the sources and sinks of the pollutants and on the pollutant transformations in the air. The

Table 2. POLLUTANT CONCENTRATIONS (ppm), PASADENA, 27 meters ABOVE GROUND, NOVEMBER 20-DECEMBER 1, 1972[a]

Date and time	Carbon monoxide	Methane	Nonmethane paraffinic carbon	Acetylene	Ethylene
Nov. 20-11:30 a.m.	1.2	2.1	0.16	0.011	0.010
20- 4:45 p.m.	3.4	2.2	0.45		
21-11:00 a.m.	1.2	1.9	0.11	0.017	0.010
21- 4:10 p.m.	2.7	2.3	0.29	0.030	0.025
22- 8:10 a.m.	7.5	2.8	1.23	0.083	0.098
22-12:00 a.m.	3.1	2.3	0.34	0.022	0.026
27- 8:10 a.m.	9.5	2.7	1.42	0.090	0.071
27- 3:10 p.m.	4.8	2.5	0.89	0.041	0.030
27- 5:00 p.m.	6.0	2.6	1.34	0.043	0.042
28- 9:00 a.m.	4.0	2.4	0.45	0.030	0.030
28- 3:30 p.m.	3.6	2.6	0.63	0.039	0.020
28- 5:00 p.m.				0.058	0.046
29-10:00 a.m.	2.6	2.2	0.30	0.019	0.015
29- 3:15 p.m.	0.9	2.0	0.16	0.006	0.005
30- 8:10 a.m.	6.1	2.2	1.2	0.044	0.045
30- 1:10 p.m.	1.8	2.2	0.42	0.022	0.015
30- 5:15 p.m.	11.5	2.8	2.2	0.071	0.065
Dec. 1- 8:15 a.m.	11.2	2.7	2.0	0.090	0.092
1- 4:00 p.m.	5.6	2.6	1.25	0.041	0.031

[a]Blanks indicate no measurement.

Table 3. POLLUTANT CONCENTRATIONS (ppm), PASADENA, 27 meters ABOVE THE GROUND, SUMMER 1973[a]

Date and time	Carbon monoxide	Methane	Nonmethane paraffinic carbon	Acetylene	Ethylene	Ozone	Formic acid	Peroxy acetyl nitrate
July 24-10:00 a.m.		2.0		0.022	0.014	0.07	0.017	0.011
10:30 a.m.		1.9		0.025	0.012	0.10	0.020	0.013
11:00 a.m.		1.9		0.024	0.012	0.13	0.027	0.016
11:30 a.m.		1.9		0.021	0.005	0.22	0.031	0.026
12:00 noon		1.9		0.019	0.005	0.25	0.030	0.025
12:30 p.m.		2.2		0.019	0.005	0.26	0.031	0.038
1:00 p.m.		2.3		0.026	0.004	0.35	0.033	0.029
1:30 p.m.		2.3		0.029	0.004	0.41	0.038	0.035
2:00 p.m.		2.2		0.024	0.005	0.57	0.048	0.041
2:30 p.m.		2.1		0.033	0.005	0.59	0.057	0.047
3:00 p.m.		2.1		0.036	0.005	0.57	0.053	0.047
3:30 p.m.		1.9		0.033	0.005	0.46	0.047	0.036
4:10 p.m.	3.3		0.71					
July 25- 7:10 a.m.	2.2		0.78					
8:00 a.m.	2.4	2.0	1.05	0.023	0.018	--	0.013	0.004
9:30 a.m.	2.1	2.0		0.028	0.015	0.09	0.020	0.016
10:00 a.m.	2.1	2.0		0.026	0.015	0.19	0.038	0.019
10:30 a.m.	2.6	2.0		0.026	0.009	0.25	0.043	0.022
11:00 a.m.	2.8	2.1		0.022	0.009	0.32	0.060	0.037
11:30 a.m.	2.8	2.2		0.025	0.007	0.37	0.064	0.034
12:00 noon	2.6	2.2		0.024	0.006	0.39	0.054	0.033
12:30 p.m.	2.9	2.2		0.024	0.007	0.42	0.057	0.040
1:00 p.m.	3.9	2.4		0.030	0.009	0.60	0.063	0.051
1:30 p.m.	3.9	2.4		0.032	0.010	0.68	0.072	0.051
2:00 p.m.	3.5	2.4		0.036	0.011	0.66	0.068	0.053
2:30 p.m.	2.9	2.3		0.031	0.009	0.59	0.063	0.044
3:00 p.m.	2.8	2.3		0.025	0.006	0.53	0.064	0.046
3:30 p.m.	2.5	2.2		0.019	0.005	0.45	0.057	0.043
4:00 p.m.	2.1	2.0		0.014	0.004	0.35	0.055	0.034
4:30 p.m.	2.2		0.49					
July 26- 8:10 a.m.	2.5		1.1					
9:30 a.m.	2.0	2.0		0.022	0.015	0.06	0.010	0.009
10:00 a.m.	1.5	2.0		0.020	0.016	0.12	0.010	0.010
10:30 a.m.	1.8	2.1		0.022	0.015	--	--	--
11:00 a.m.	1.9	2.1		0.024	0.013	0.05	0.005	0.005
11:30 a.m.	1.8	2.0		0.020	0.010	0.04	--	--
12:00 noon	1.5	1.8		0.017	0.006	0.05	--	--
12:30 p.m.	1.5	1.8		0.013	0.004	0.05	--	--
3:05 p.m.	1.6		0.67					
Aug. 8 - 4:30 p.m.	1.7		0.44					
9 - 8:00 a.m.	2.5		0.75					
3:00 p.m.	2.2		0.61					
22 - 3:00 p.m.	2.1		0.60					
23 -10:00 a.m.	1.5		0.36					
24 -11:30 a.m.	1.3		0.51					

[a]Blanks indicate no measurement. Dashes indicate not detected.

data will be discussed in terms of (1) the ratios of pollutant concentrations, (2) the time variations of the concentrations, (3) the amounts of the pollutants seen or not seen, and finally, (4) the material balance (or unbalance) in the photochemically reacted air.

Ratios of Pollutant Concentrations

Plots have been made of the pairs of acetylene and carbon monoxide values for the separate fall and summer periods. These are shown in Figure 8. The fall data are from Table 2 for 8 days between November

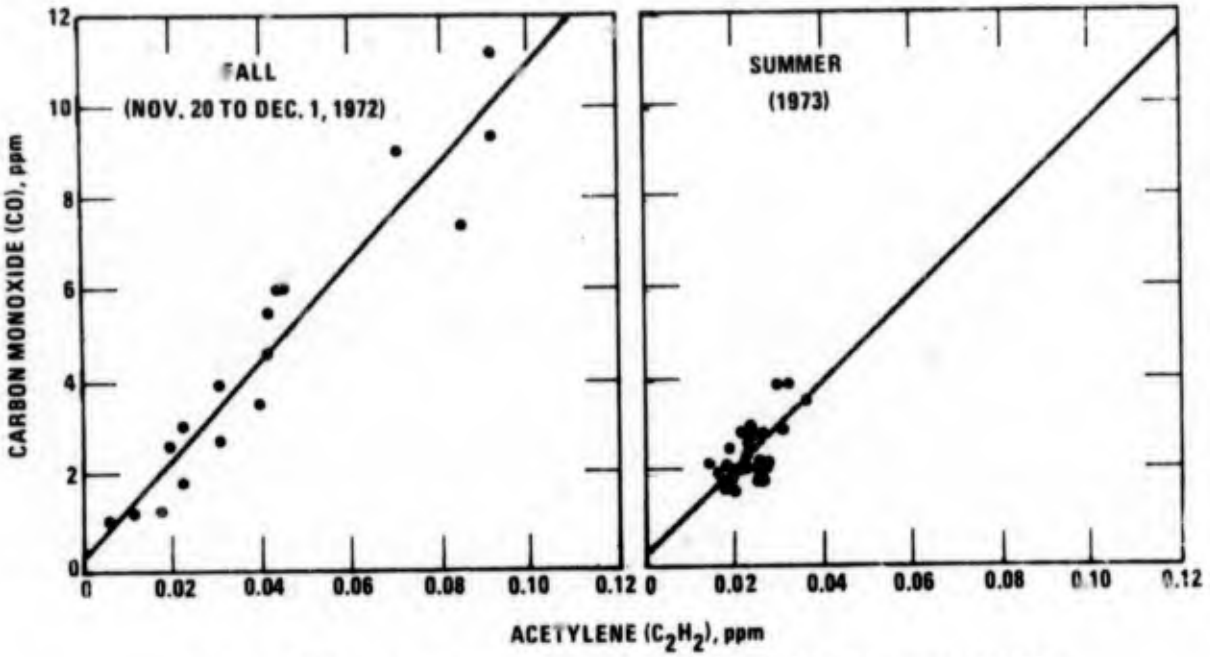

Figure 8. Acetylene versus carbon monoxide, fall and summer periods.

20 and December 1, 1972. The summer data, from Table 3, apply to July 25 and 26 and August 9, 1973. The ratios indicated by the lines drawn through the points are about 0.009 in each case. This ratio is typical of auto exhaust, which is thus indicated as the principal source of both pollutants during both periods. Acetylene and carbon monoxide each are low in photochemical reactivity, and it can be assumed that they did not undergo oxidation between the time of emission into the air and the time of the measurements.

Plots of carbon monoxide concentrations against the concentrations

of nonmethane paraffinic hydrocarbons, as indicated by the C-H absorption band at 2970 cm^{-1}, are given in Figure 9. These plots show ratios that

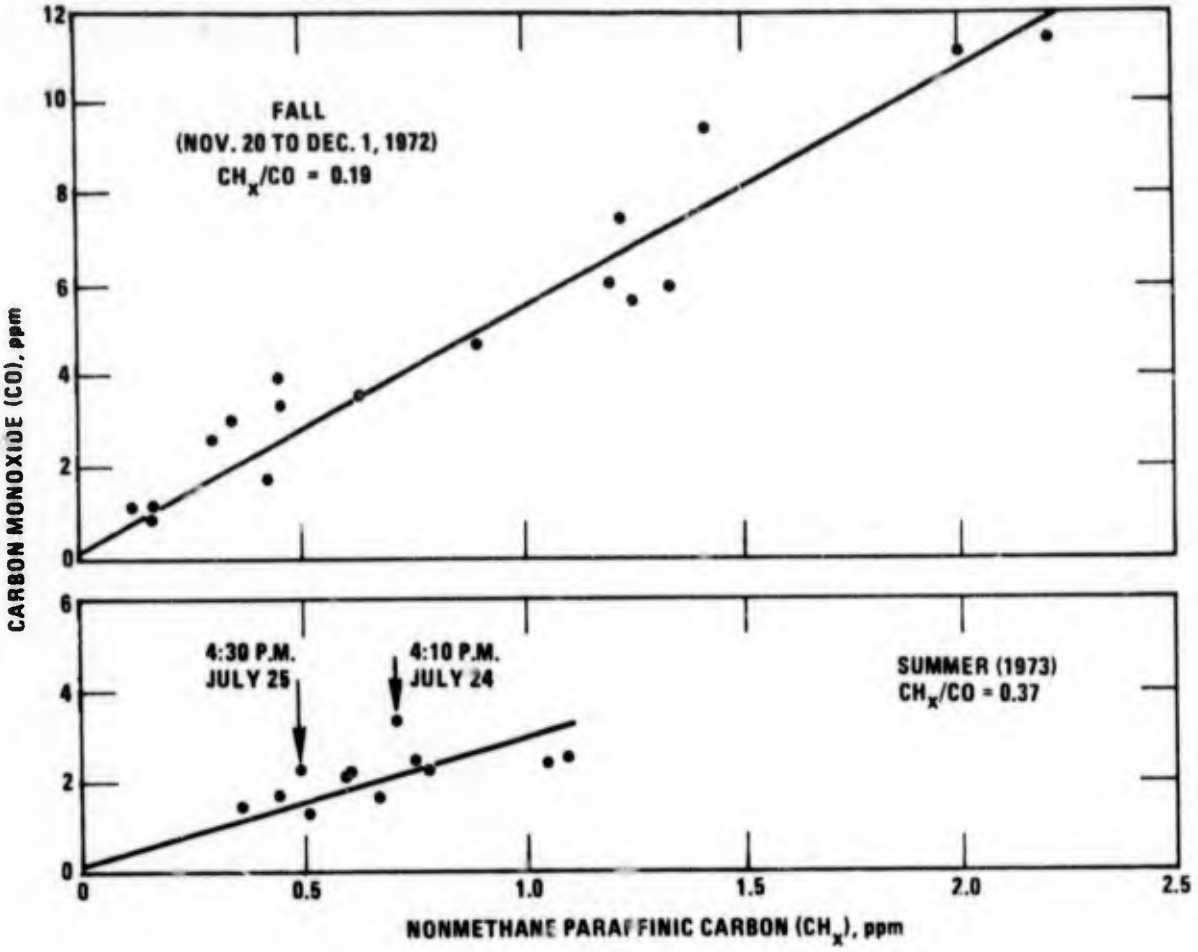

Figure 9. Nonmethane paraffinic carbon versus carbon monoxide, fall and summer periods.

differ almost by a factor of 2 between the fall and summer periods. These ratios can be interpreted as indicating two different mixes of pollutant sources.

The difference might possibly be a result of atmospheric oxidation of the hydrocarbons. That explanation seems unlikely, however, because of the direction of the differences. Hydrocarbon oxidation occurs more in the summer, which is a time of stagnant midday air, rather than in the fall, which is a time of midday ventilation and air movement. If oxidation were a major factor, the hydrocarbon-to-carbon monoxide ratio would be lower in the summer--the reverse of what has been observed.

A more likely explanation of the difference in ratios can be derived from differences in atmospheric physical properties and atmospheric movements. It is to be noted that the fall measurements taken in the morning and evening showed pollutant concentrations averaging about twice as high as in the summer. This was the result of the air being trapped under a very low-altitude temperature inversion. In the summer, the temperature inversion occurred at a higher altitude, with a resulting larger mixing volume. In the fall, the shallowness of the polluted air layer would restrict the lateral pollution transport. In this case, the pollution at the campus of the California Institute of Technology would be largely auto exhaust from the cars in the nearby streets, and there would be little influence from distant industrial sources or natural sources.

In the summer, the larger mixing volume gives a smaller pollutant concentration than in the fall, but at the same time allows more pollutant transport from a distance. Thus, the summer air at the site could contain, in addition to auto exhaust, evaporated organic materials from sources farther out, including industrial operations, solvent evaporation, and petroleum leaks.

Another factor to be considered is temperature differences, as pointed out recently by Stephens.[14] Midday heat will vaporize organic materials. In the summer, the air is not only warmer and the sun more intense than in the fall, but the air is trapped under a temperature inversion in midday, thus allowing accumulation of the organic vapors. In the fall, the sun and warmth of midday release vapors into a mobile atmosphere that dissipates them quickly.

In summary, this interpretation of the data indicates that in the summer a substantial portion of the organic pollutants comes from sources other than auto exhaust. These infrared data do not give a sufficiently detailed analysis of the hydrocarbon portion of the pollution to identify specific nonautomotive sources of hydrocarbons. Chromatographic analyses are much more informative in that regard.[15,16]

The ratio between ethylene and acetylene is a measure of the degree of photolysis of the polluted air mass. Both pollutants come almost ex-

clusively from auto exhaust and have a fixed ratio if there are no atmospheric transformations. Measurements have shown the average ethylene-to-acetylene ratio in auto exhaust to be approximately one-to-one.[17] A ratio fairly close to this was obtained in the measurements of November 20 to December 1, as shown in Table 2. However, Table 3 illustrates that in the summer, the ratio was frequently much smaller. The ethylene is much more reactive photochemically than the acetylene, with a disappearance rate in smog-chamber experiments many times greater. Thus, the "photochemical age" of the air mass can be judged from this ratio, as discussed, for example, by Stephens and Burleson.[18]

Data from the tables, plotted in Figures 10 and 11, show the variations of pollutant concentrations during the day. The data for July 24 and 25 show an ethylene-to-acetylene ratio about half of the auto exhaust value by midmorning and a ratio in the afternoon only about one-fifth of the auto exhaust value. The indicated high degree of photochemical activity is confirmed by the high values of ozone obtained on those days.

The observation that by noon the ethylene concentration had already fallen as low as one-fifth of the acetylene concentration indicates that fresh ethylene was not coming into the air mass at a high rate. Laboratory measurements with simulated atmospheric conditions have shown the ethylene to have a half-life of several hours. If a large continuous influx of ethylene existed, the steady-state ethylene-to-acetylene ratio should therefore remain much higher than observed. Instead, it appears that the reactive components were transformed early in the day, and they were not replaced.

For comparison, data are shown in Figure 12 for August 9, a summer day on which only a moderate amount of ozone was formed. On this day, the ethylene-to-acetylene ratio remained near one-to-one in the morning and evening and dropped only to about three-to-four in the middle of the day when the photochemical oxidation was at its height. There was also a variation in concentrations during the day.

Pollutant Concentrations as Functions of Time

Carbon monoxide and acetylene, both indicators of auto exhaust, did not vary markedly with time during the smoggy days of July 24 and

25. Nor did they vary markedly during other summer days of moderately high oxidant, such as August 9. The relatively steady value of these pollutants is at variance with a concept of morning and evening auto exhaust peaks. If there was any peaking of the traffic count, it was obscured by the integrating effect of the well-mixed trapped air mass. Probably, the frequently observed morning and evening peaking phenomenon is a result of morning and evening periods of air stagnation separated by a midday period of ventilation. This is the pattern we observed in the fall, when there was no smog. In contrast, on the heavy smog day of July 25, the acetylene and carbon monoxide concentrations peaked at 2:00 p.m. The amounts of carbon monoxide and acetylene on July 24 and 25 were low compared with the amounts frequently reported for urban locations.[16] This emphasizes the important role that the meteorological factors play in the Southern California smog. It is the trapping of the midday air that allows the photochemical reaction products to accumulate.

Three principal reaction products were observed--ozone, formic acid, and peroxyacetyl nitrate. The variations of these with time during the July smog attack are shown in Figure 11. The increase of reaction product concentrations during the morning and early afternoon followed by a falling off in the late afternoon, as seen on July 24 and 25, is typical smog season behavior. This pattern is also shown in the August 9 plots. July 26 seemed to start out as a smoggy day, but by noon the air had gotten moving and cleared out the pollution.

The figures show that on the smoggy days the ethylene concentration went down quickly in the morning. It can be assumed that propylene, butadiene, isobutene, formaldehyde, and other components of the auto exhaust that are more reactive than ethylene decreased in the morning even faster than the ethylene. It is these highly reactive components that are mainly responsible for the morning conversion of nitric oxide to nitrogen dioxide and the start of the ozone buildup. However, there was much more total ozone formed than can be accounted for by the action of the reactive species. It is clear that the less reactive hydrocarbons must

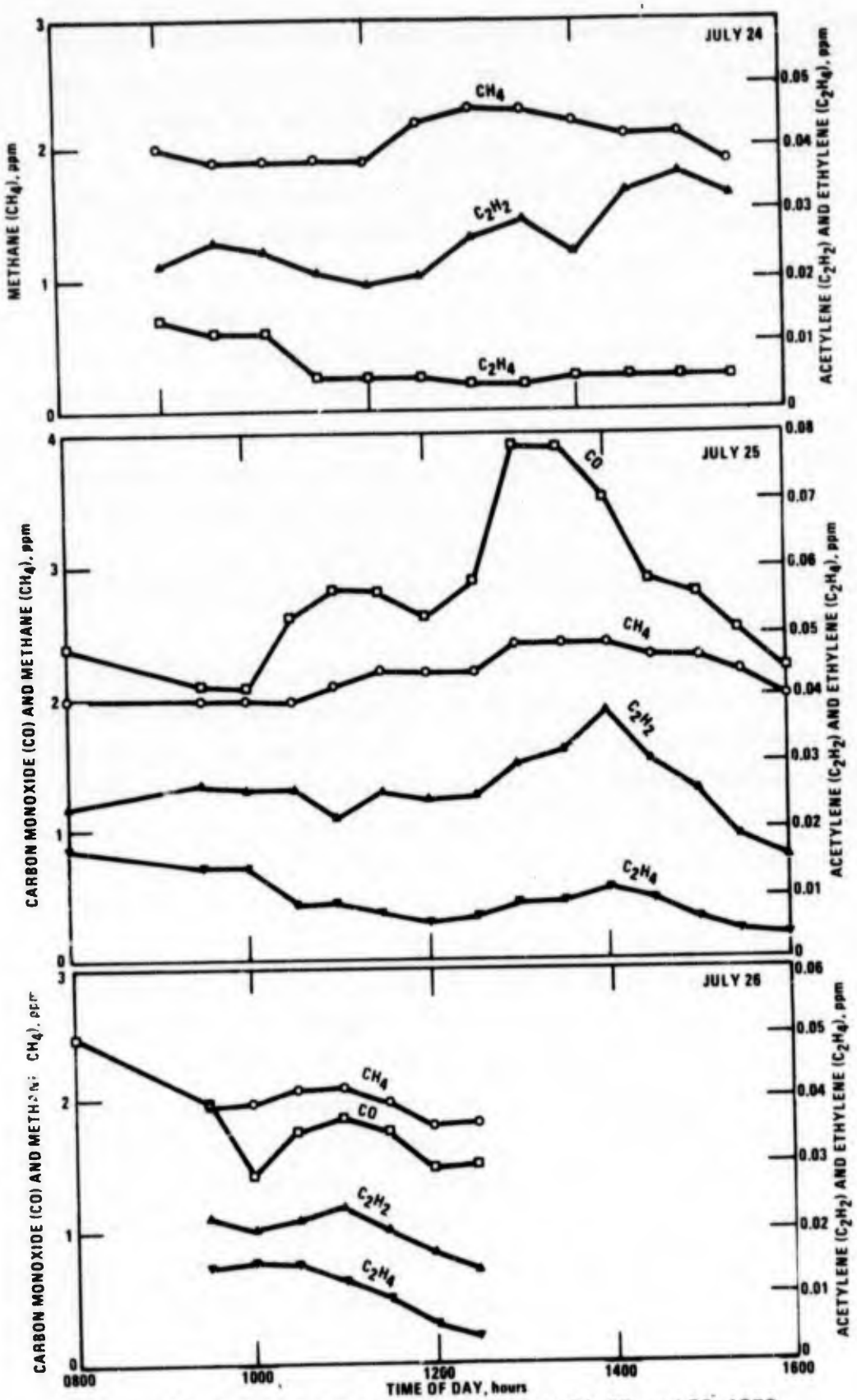

Figure 10. Pollutant concentration plots, July 24, 25, and 26, 1973.

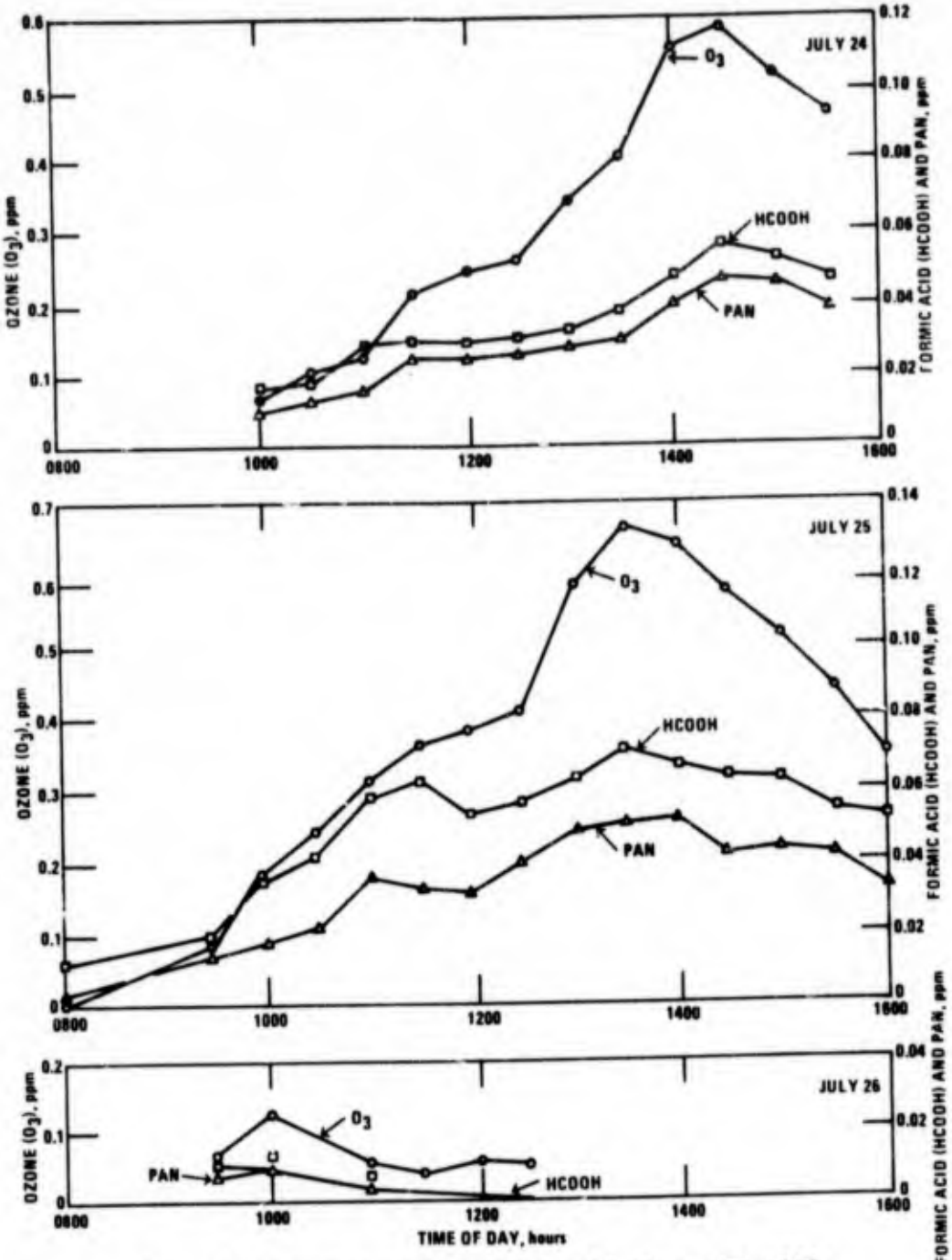

Figure 11. Reaction product plots July 24, 25, and 26, 1973.

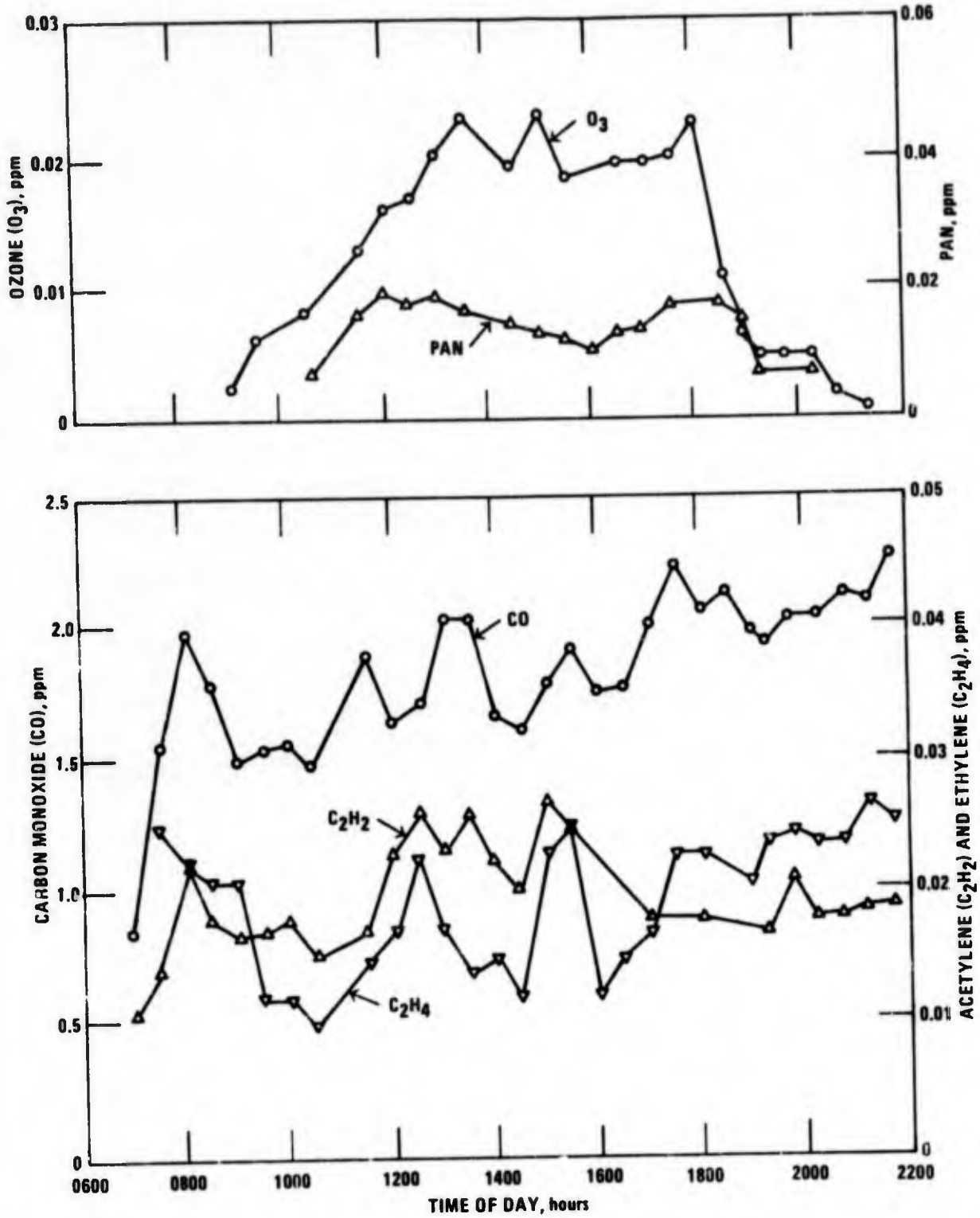

Figure 12. Pollutant and product plots for August 9, 1973.

also be contributing to the ozone buildup. This will be further discussed in connection with the material balance.

Individual Compounds

Acetylene--Acetylene is probably the best indicator compound for the presence of auto exhaust pollution in the atmosphere. No major sources of acetylene other than the internal combustion engine are normally present. Laboratory studies have shown acetylene to be highly resistant to atmospheric oxidation. Its half-life in the atmosphere is probably many days. The compound thus serves as a reference against which to measure the extent of reaction of other species.

The acetylene absorption band at 730 cm^{-1} (Figures 6 and 7) is one of the strongest known, so that small amounts can be measured reliably.

Ammonia--Ammonia is assigned a prominent role in fine particle formation in the atmosphere. Ammonium sulfates and nitrates are major constituents of atmospheric aerosol, as shown, for example, in the reports by Gordon and Bryan and by Charleson et al.[19,20] Decaying vegetation is regarded as the principal source of atmospheric ammonia. Georgii reported about 20 ppb of ammonia in the air at Frankfurt, Germany, but only about 6 ppb in air coming into Europe from the Atlantic Ocean.[21]

The infrared absorption spectrum of ammonia is undoubtedly one of the best indicators of the presence or absence of the compound. The ammonia bands at 930 and 967 cm^{-1} are strong and distinctive. Furthermore, there is very little interference at these wavelengths from water vapor or from other pollutants. We have seen these infrared bands in the spectrum of air at Durham, North Carolina, indicating an ammonia level of about 20 ppb.

Figure 13 shows the 1:00 p.m. spectrum from July 25 as it actually appeared and as it would have appeared if ammonia were present at concentrations of 10 or 40 ppb. Even at 10 ppb, the expected absorption features are several times larger than the noise level in the spectrum. Examination of all of the several hundred spectra recorded in the fall and summer observation periods has failed to show any indication of absorption at the principal ammonia band at 967 cm^{-1}. For many of the spectra, the noise level corresponds to about 5 ppb of ammonia. The indicated low

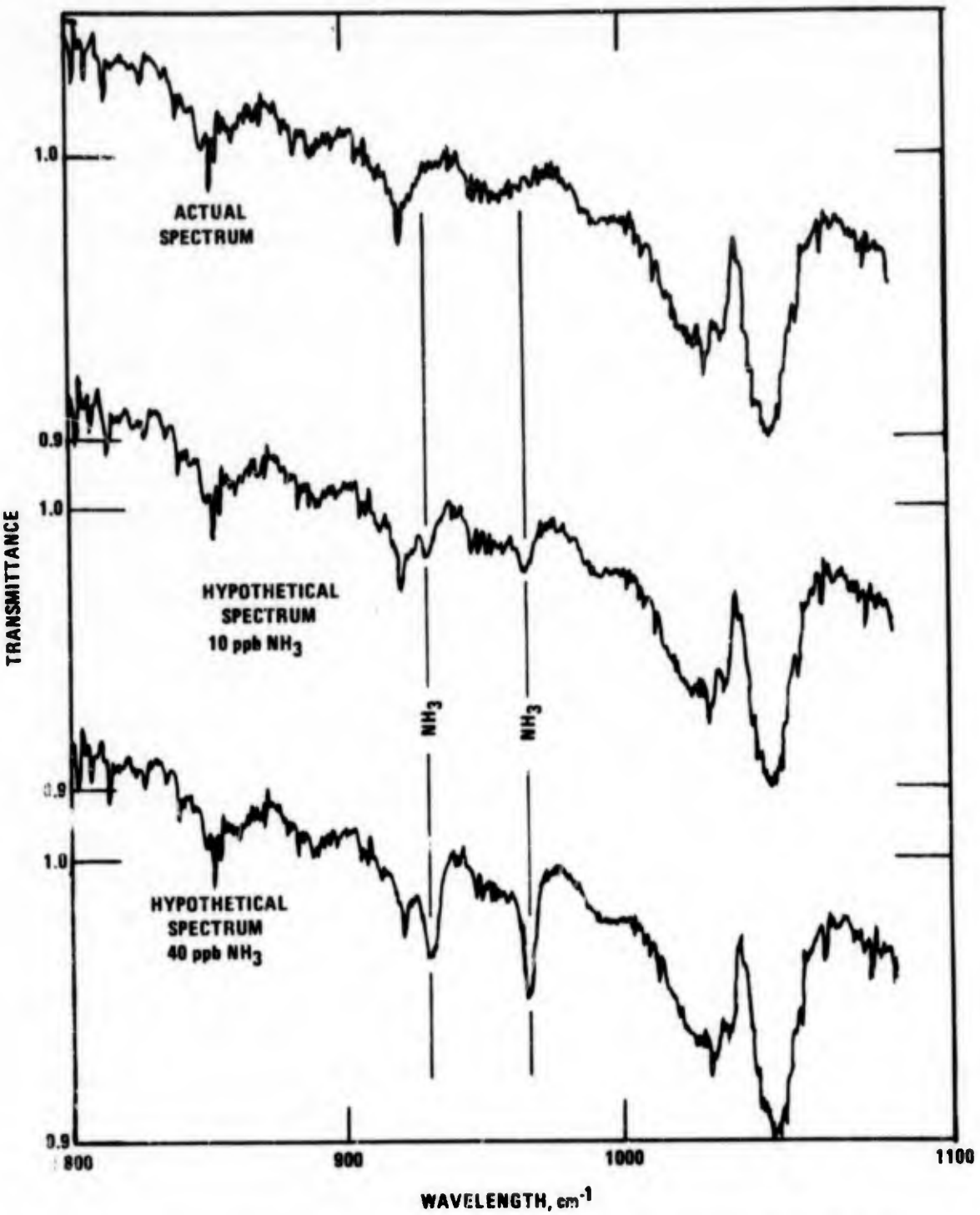

Figure 13. Atmospheric spectrum, July 24, 1973, 1:00 p.m., showing absence of ammonia (NH_3) by comparison with hypothetical spectra for atmospheres containing ammonia.

concentration of gaseous ammonia is understandable in the light of several factors: (1) The amount of decaying vegetation and other organic matter per square kilometer in the Los Angeles area is smaller than in most places where ammonia has been detected. (2) Air coming in from the Pacific Ocean would be expected to be relatively low in ammonia content. (3) Nitrate and sulfate formation in the Los Angeles atmosphere will consume gaseous ammonia.

Carbon Monoxide--The carbon monoxide spectrum occurs with little interference from other compounds. The principal uncertainties of the carbon monoxide measurement come from variations in its apparent absorption coefficient, as previously discussed. The amounts of carbon monoxide detected were smaller than customarily seen in center-city monitoring stations, but were comparable to the amounts measured in outlying areas, such as Riverside.[22] The use of carbon monoxide as an indicator of the air stagnation has been discussed. Carbon monoxide is a comparatively inert compound in the air, with a half-life of several months. Recent studies of carbon monoxide oxidation have outlined the removal paths for carbon monoxide in the air and are important to an understanding of overall atmospheric chemistry.[23] However, it is still generally concluded that carbon monoxide does not significantly influence the short-term atmospheric photochemistry of urban areas.

Ethylene--Much emphasis has been placed on the detection or nondetection of ethylene, and our conclusions as to the low rate of air turnover and high degree of hydrocarbon reaction on smoggy days have largely been based on ethylene measurements. The compound is easily enough measured in the spectrum. Its band at 950 cm^{-1} is strong and sharp, and its spectrum does not suffer serious interference from other atmospheric constituents. Figure 7 shows an ethylene value of 0.009 ppm. Spectra obtained earlier in the summer mornings and in the fall mornings and evenings showed the ethylene band stronger, with a maximum of 0.098 ppm.

Formaldehyde--Formaldehyde is detectable by its characteristic spectral structure in the region 2700 to 2900 cm^{-1}. All the spectra obtained in this study were examined carefully for these spectral lines,

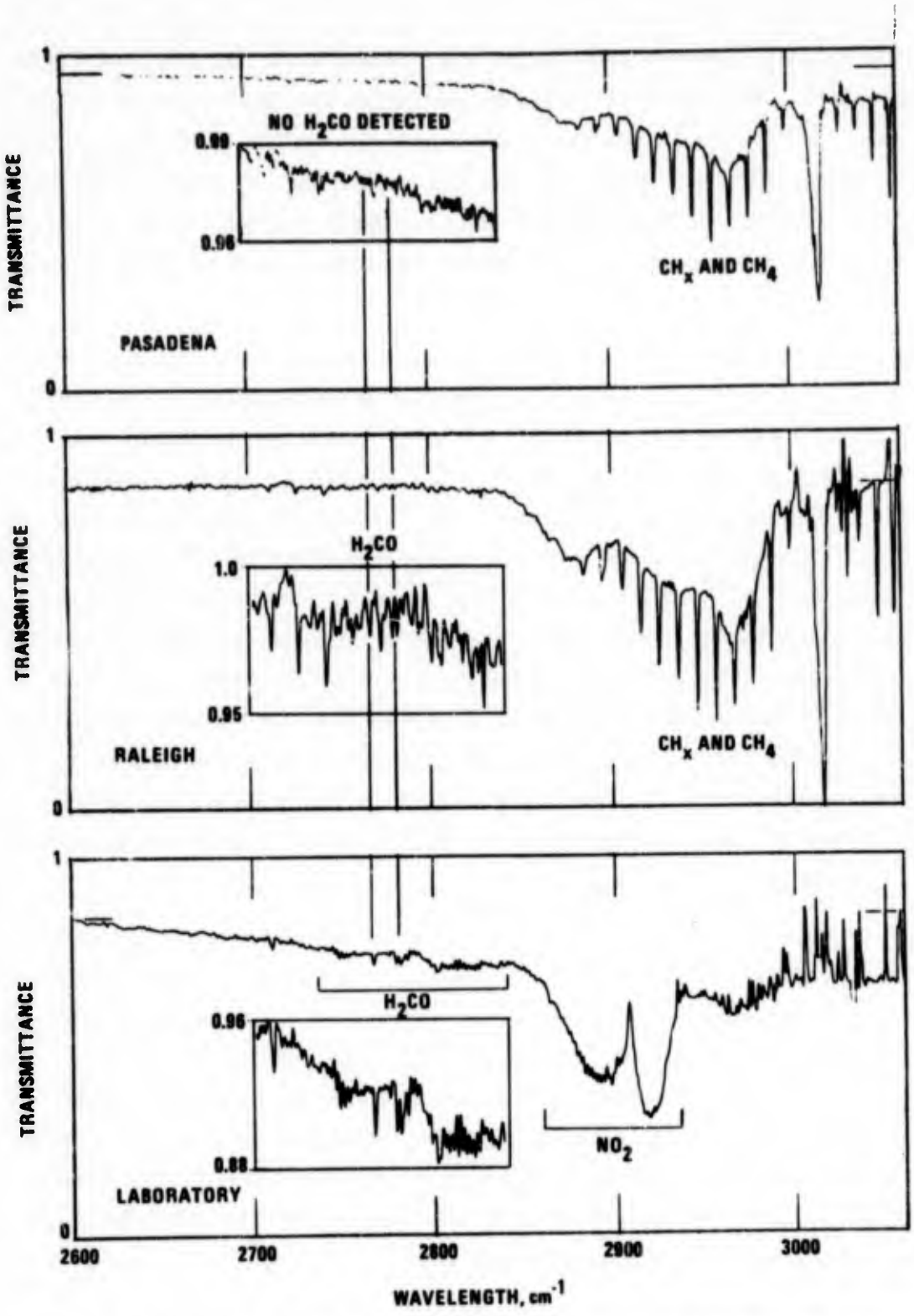

Figure 14. Formaldehyde (H_2CO) response: contrast between Pasadena site, where formaldehyde was not detected, ambient air in Raleigh, N.C., and auto exhaust in laboratory air.

but no lines were found. The detection limit for formaldehyde was approximately 15 ppb in the fall 1972 period and about 30 ppb in the summer 1973 period. The difference is attributed to a somewhat better optical alignment in the fall measurements, which gave a better signal-to-noise ratio.

Although we were surprised at not seeing formaldehyde, we do not believe this to be an anomalous aspect of our results. In the fall period of observation, there was little photochemical activity, so that the only significant source of formaldehyde was its direct emission in auto exhaust. For comparison, we have obtained the absorption spectrum of Raleigh, North Carolina, morning air in the midst of rush-hour traffic. That spectrum did show a trace of formaldehyde vapor but also showed carbon monoxide and hydrocarbon levels two or three times greater than the maximum seen at the Pasadena site. We also obtained the spectrum of air containing a small amount of auto exhaust from a laboratory-operated car equipped with a catalytic muffler. The latter spectrum clearly showed formaldehyde bands along with a large absorption due to nitrogen dioxide. The Raleigh spectrum and the laboratory spectrum are compared in Figure 14 with one of the best of the Pasadena spectra. The formaldehyde is clearly detectable in the laboratory sample at 80 ppb. In the Raleigh air, it is detectable at about 40 ppb. In the Pasadena sample, it is not detectable. It should be noted that the scale-expanded fine structure is similar in the Pasadena and Raleigh samples, except for the formaldehyde bands. This nonformaldehyde fine structure is mainly due to weak lines of methane. If the aldehyde had the same ratio to hydrocarbon in both the Raleigh and Pasadena air samples, it probably was present in the Pasadena air at about 0.015 ppb.

In the summer, more formaldehyde is produced by the photochemical oxidation of hydrocarbons than is emitted directly into the air. Ethylene oxidation is probably the largest single source. However, the aldehyde formed in the air would be further oxidized to formic acid, carbon monoxide, carbon dioxide, and water. In view of the indicated advanced state of oxidation of the polluted air samples on the smoggy days, it is understandable that formaldehyde was not detected.

Formic Acid--The presence of formic acid is revealed by its absorption band centered at 1105 cm^{-1}. This is a fairly strong band that has a distinctive shape and falls in a spectral region where water vapor interference is not great. This band has allowed the infrared detection of formic acid at levels between 10 and 70 ppb.

The detection of formic acid is illustrated in Figure 15. The top curve is a laboratory spectrum of the formic acid and ozone produced by 30 minutes of ultraviolet irradiation of 20 ppm of formaldehyde and 0.5 ppm of nitrogen dioxide in air. The infrared path was 170 meters. Below are seven spectra of the Pasadena air recorded on July 25, 1973, and one recorded on July 26. The spectra show the appearance, growth, and decay of three bands: the ozone band at 1050 cm^{-1}, the formic acid band with absorption peak at 1105 cm^{-1}, and the peroxyacetyl nitrate band at 1165 cm^{-1}. In the 9:30 spectrum at the top, the water bands have been fully cancelled and a very small amount of formic acid appears. The 10:30 spectrum shows more formic acid and a slight undercompensation of the water lines. The 11:30 and 12:30 spectra show an overcompensation of the water lines, which drives them upwards in the ratio plot and clearly reveals the downward-directed formic acid peak. The 1:30 and 2:30 spectra show undercompensation of water, with formic acid still present. The July 26 9:30 a.m. spectrum shows a good water balance, a trace of ozone, and no obvious absorption due to formic acid or peroxyacetyl nitrate. From a scale-expanded plot of this same spectrum, we estimated 8 ppb of formic acid and peroxyacetyl nitrate and 60 ppb of ozone.

The formic acid band appears to lie on top of a weak background of absorption by other species. This caused some difficulty in determining the amount of formic acid, but an attempt was made to minimize the error by measuring only the depth of sharp downward peak.

As Figure 11 has shown, the formic acid concentrations were sightly higher than the peroxyacetyl nitrate concentrations. This means that except for ozone, formic acid is present in the highest concentration of any reaction product seen in these samples of polluted air. Carbon dioxide, carbon monoxide, and water are also products, but they meld into the background and are not measurable.

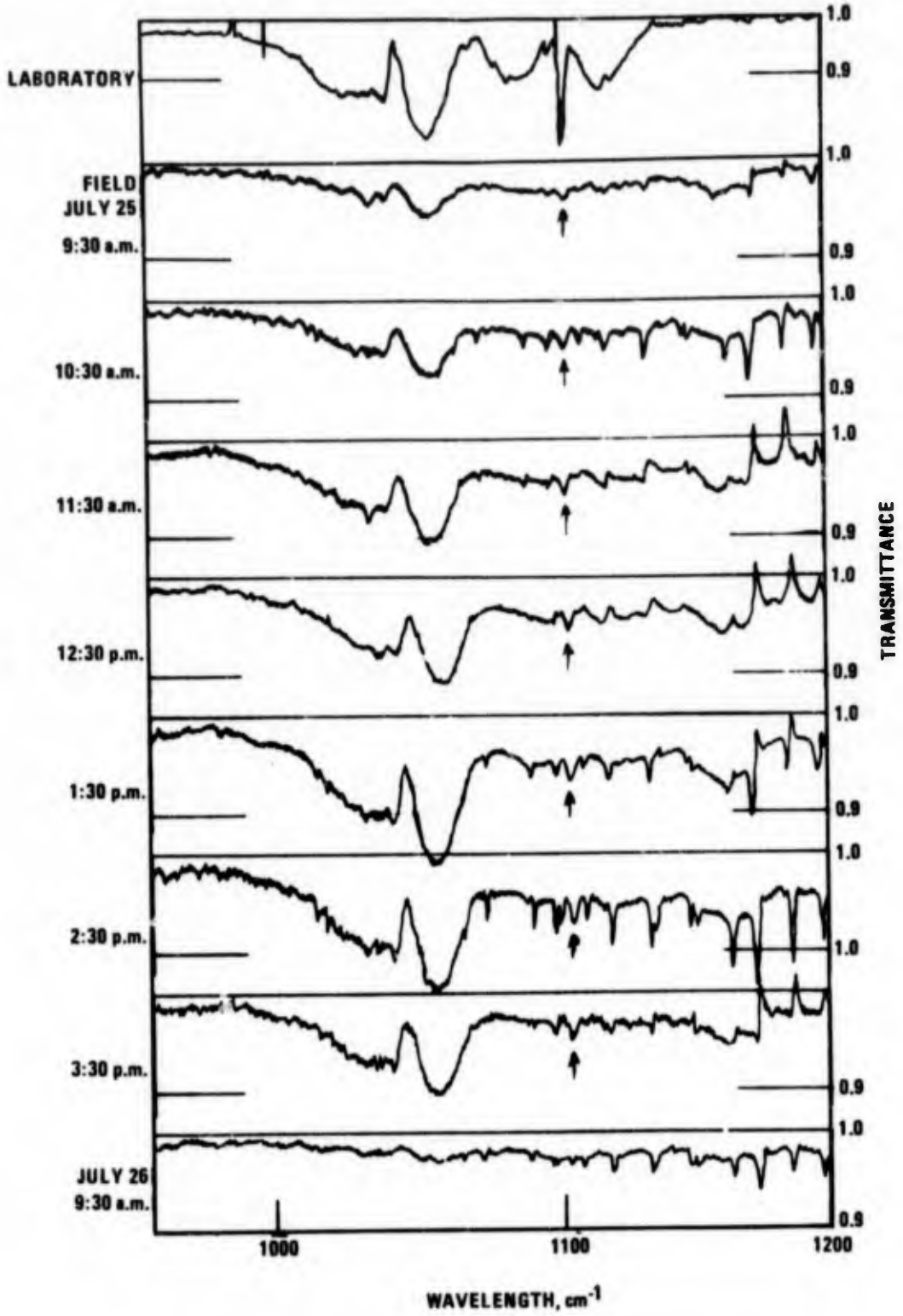

Figure 15. Detection of formic acid (band indicated by arrow).

Laboratory photooxidation studies using the infrared technique for analysis have many times shown the formation of formic acid.[1,2] The acid is a major product of the photooxidation of formaldehyde.[24] Thus, there has always been reason to suspect the acid to be present in the polluted air. However, we believe this to be the first time it has been conclusively identified and measured. In 1955, it was reported that formic acid had been measured in the Los Angeles air at concentrations up to 0.41 ppm.[25] The method used involved the reduction of formic acid to formaldehyde, followed by the reaction of the formaldehyde with chromatropic acid to yield a colored complex. We suspect the method to have been subject to error because the amounts of formic acid reported were about a factor of 5 or 10 greater than the amounts now detected by the infrared method. There is no reason to assume that the composition of the atmosphere is Los Angeles has changed so substantially in the past 20 years. Other indexes of pollution, such as carbon monoxide, ozone, and total hydrocarbons, have not shown such substantial changes. It is interesting to note that Leighton's 1961 summary of the state of knowledge of atmospheric photochemistry[26] did not give any significant consideration to formic acid as a product.

Stability is the reason that there is more acid than aldehyde in the air. The aldehydes are precursors of the acids and have a relatively short lifetime in the smog atmosphere. The acids, especially formic acid, represent a stopping place in the sequences of photochemical reactions. Thus, our observations are consonant with the current measurements that are showing organic acids to be constituents of the fine particles in the air.

Halogenated Compounds--The fluorinated and chlorinated hydrocarbons all have strong absorption bands in the frequency region of 700 to 1360 cm^{-1}. The greater the molecular symmetry, the more likely that the bands will have a characteristic shape, and the more sensitive the infrared detection. Thus, we identify carbon tetrachloride by its strong band at 792 cm^{-1} and Freon 12 by its strong band at 921 cm^{-1}. Trichloroethylene and Freon 11 both absorb near 850 cm^{-1} and are undoubtedly contributors to the persistent absorption band at that frequency. In no cases were the de-

tected amounts of a halogenated compound greater than a few parts per billion. The concentrations did not appear to change in any regular pattern. Because of their inertness, the compounds will accumulate in a sluggish urban atmosphere, just as they are accumulating in the atmosphere on the global scale.

Hydrocarbons--In addition to the selected bands of individual light hydrocarbons such as methane, acetylene, and ethylene, the spectra show the combined band at 2970 cm^{-1} due to C-H stretching vibrations in many hydrocarbons. As noted earlier, the band does not include methane or the ring carbons in aromatics. Thus in designating the band as CH_x, the subscript x means two or three hydrogens, but not one or four. The band is useful as a general indicator of the level of hydrocarbon pollution, as has been previously discussed.

Hydrogen Peroxide--It is logical to expect some hydrogen peroxide to be present in the smog along with the other oxidants. The peroxide has been seen as a product in laboratory photooxidations. In addition, it has been measured by Gay and Bufalini in the air in New York City and in Riverside, California. They used the chemical method developed by Cohen and Purcell, in which titanium IV and 8-quinolinol react with the hydrogen peroxide to form a colored complex. They observed that hydrogen peroxide increased in the afternoon in a pattern similar to the ozone build-up, but at concentrations only about one-fifth as great.[26] If the hydrogen peroxide were present at one-fifth the ozone concentration in the Pasadena air on July 24 and 25, it should appear in the spectra.

A reference spectrum of hydrogen peroxide obtained under low resolution is shown in Figure 16. Water bands are seen on the high-frequency side. In the laboratory, we have measured the maximum absorption coefficient of this hydrogen peroxide band to be 9 ± 3 atm^{-1} cm^{-1}, indicating a fairly strong band, similar to the accessible bands of ozone and formaldehyde (Table 1). When the atmospheric spectrum is recorded over a 417-meter path, water and methane both absorb strongly in the same region as the peroxide, and it is difficult to detect the peroxide absorption if it is only at a few percent. One can say from

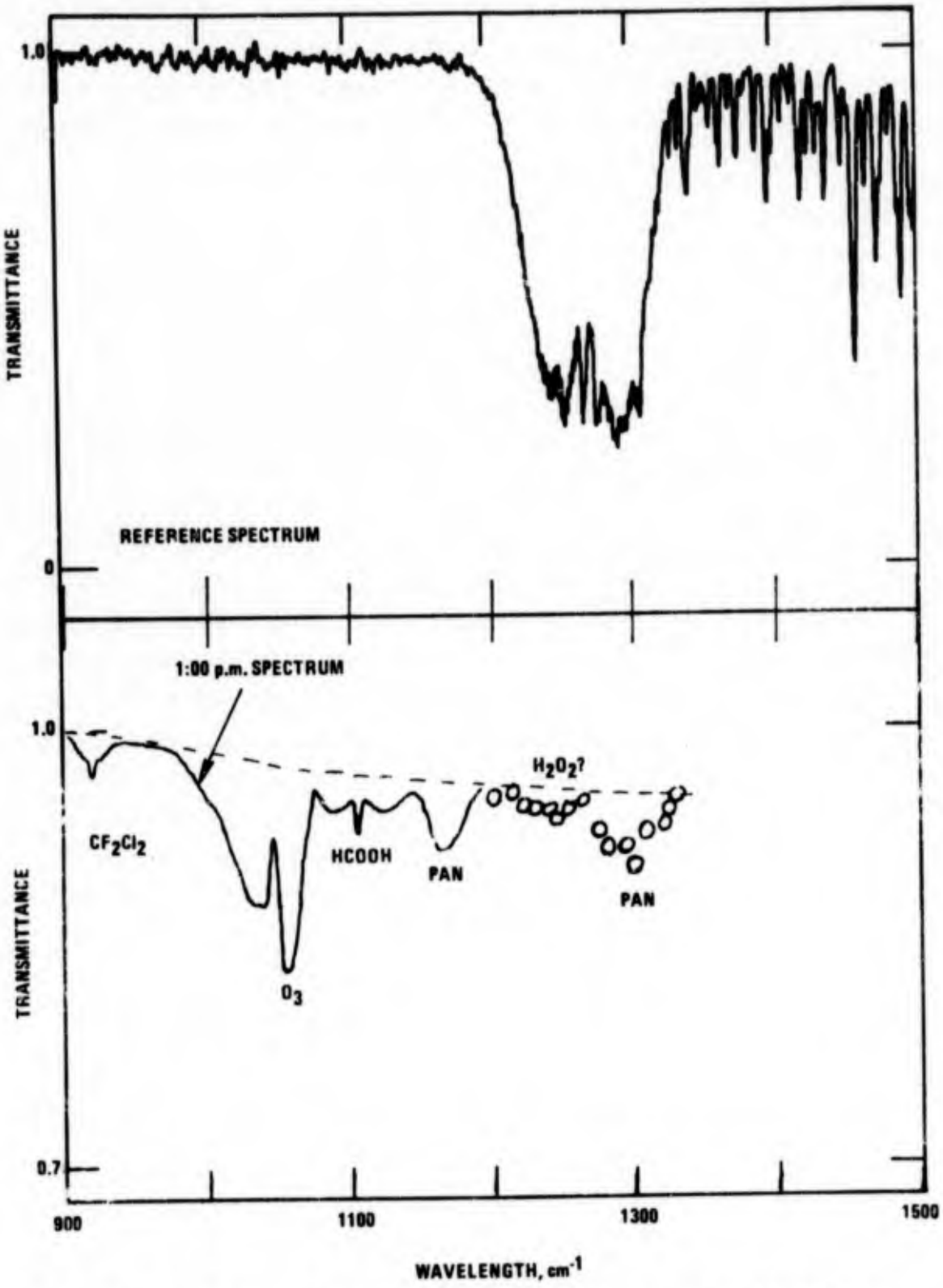

Figure 16. Ratio spectrum showing possible presence of hydrogen peroxide (H_2O_2). Reference spectrum shows 5 ppm H_2O_2 in 1-atm tank air at a path length of 295 meters.

inspection of the ratio spectra, such as in Figure 7, that the peroxide was not present at concentrations of 100 ppb or higher; we wish to go to a lower detection limit than this.

In order to extract any possible hydrogen peroxide absorption from the data, we have carefully compared the single-beam plot of 9:30 a.m. on July 25 with each of the single-beam plots of 1:00 p.m. and 1:30 p.m. on the same day. The spectra were superimposed so that they matched at about 1200 cm^{-1}, and then the ordinates were compared at all the points between the water lines, from 1200 to 1360 cm^{-1}. In each case, this gave us 17 points on a low-resolution ratio plot, showing changes in absorption that occurred between morning and afternoon. The average of the resultant two ratio plots is shown in Figure 16, lower half. The appearance of the peroxyacetyl nitrate absorption band, which we know must be present at about 1300 cm^{-1}, assures us that the ordinate comparison technique is giving a valid answer. From the strength of the 1160-cm^{-1} peroxyacetyl nitrate band, we know that nearly all of the 1300-cm^{-1} band must be due to peroxyacetyl nitrate. The remaining absorption in the figure may be ascribed to hydrogen peroxide. The absorption band depth appears to be about 2 percent, corresponding to about 0.070 ppm hydrogen peroxide. This identification is by no means totally convincing, but at least one might say that the spectrum indicates the possible presence of hydrogen peroxide, not at one-fifth the concentration of the ozone, but perhaps at one-tenth.

Methane--Methane shows in both the high-frequency and low-frequency portions of the spectrum. It was always present at concentrations between 1.8 and 2.8 ppm. The methane is not primarily automotive in origin, and as shown in Figure 10, it does not closely follow the concentration variations of carbon monoxide and acetylene. The most probable source of methane is natural gas.[18,22] It should be noted that the Raleigh air spectrum of Figure 14 shows a higher methane concentration than the Pasadena spectrum.

Methanol--Methanol, revealed by its band centered at 1032 cm^{-1}, appeared in the spectrum occasionally and apparently at random. The maximum amount

detected was about 0.10 ppm, but usually the amount was near or below our detection limit of 0.008 ppm. Consider, for example, the spectra in Figure 15. The 9:30 a.m. spectrum shows 0.013 ppm; the 10:30 spectrum shows none, and the 11:30 a.m. spectrum shows 0.017 ppm; then for the rest of the day the methanol was again below the detection limit. One of the clearest methanol spectra is reproduced in Figure 17. In this

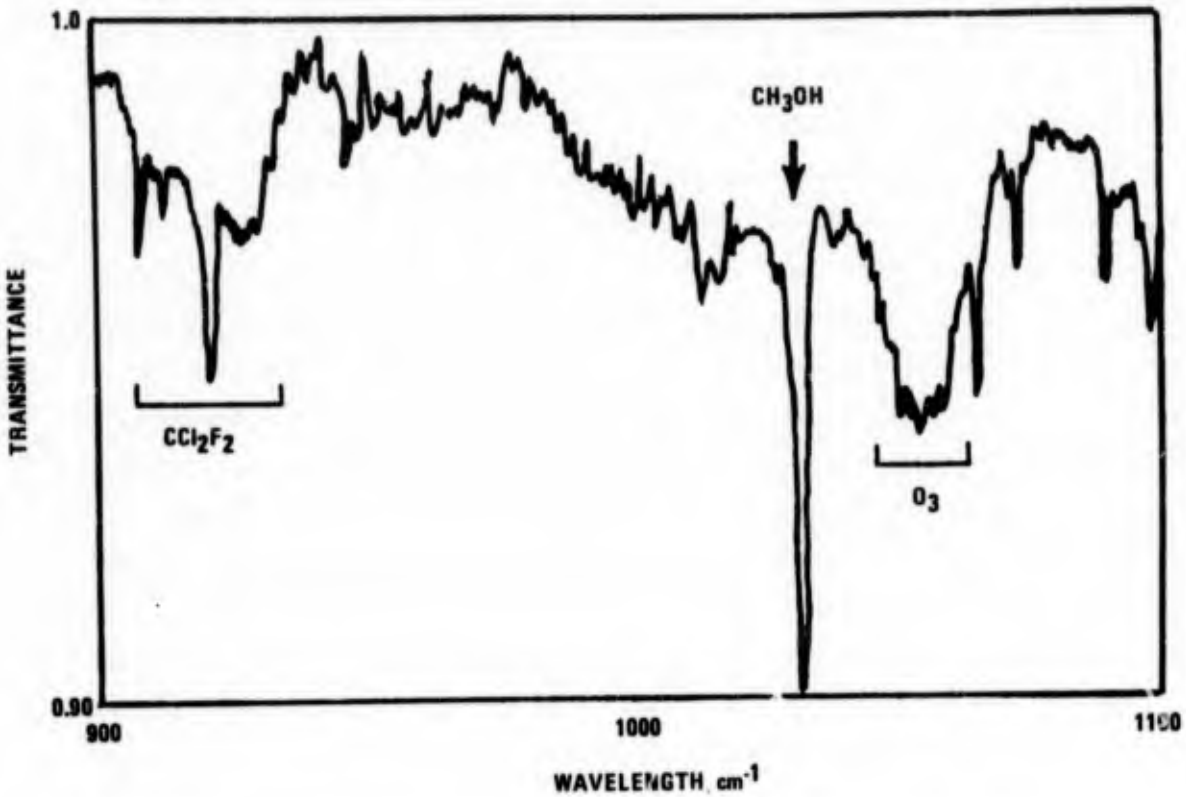

Figure 17. Detection of 0.10 ppm methanol (CH_3OH) and 0.021 ppm Freon 12 (CCl_2F_2); 11:00 a.m., August 23, 1973. Methanol band superimposed on A band due to 0.075 ppm ozone.

case, the amount was 0.10 ppm. The band is somewhat distorted by an overlapping band of 0.075 ppm of ozone. Also shown in the figure is a band due to 0.021 ppm of Freon 12. The random appearances of methanol in our spectra could have resulted from dumping of this solvent somewhere, either in industrial operations, or in some type of activity on the campus. Clearly, methanol is not a photochemical reaction product.

Methyl Nitrate--A laboratory photooxidation of hydrocarbon and nitrogen oxides in air carried out with reactant concentration of one

part per thousand will yield alkyl nitrate as the major nitrogen-containing product. When the reaction is conducted with concentrations of 10 ppm, a mixture of alkyl nitrate and peroxyacetyl nitrate will be formed. At concentrations of 1 ppm, the product is nearly all peroxyactyl nitrate. Thus, we do not expect to find alkyl nitrates in the smog, and the spectra confirm this expectation. The strong methyl nitrate bands at 853, 1018, and 1290 cm^{-1} do not show in any of the spectra. We estimate our detectability limit to have been 0.010 ppm.

Nitric Acid--Evidence of the presence of nitric acid vapor in the air was searched for, but none was found. The spectra place an upper limit of approximately 10 ppb on the level of nitric acid vapor that might have been present but not detected during the period of observation.

The acid has been detected in the upper atmosphere by means of its spectrum, but it has never been detected near the earth's surface. Knowledge of the level of nitric acid present in the lower atmosphere is necessary for understanding the fate of the nitrogen oxides and the mechanics of formation of the nitrate found in the aerosols.

It is known that the acid is formed by the interaction of nitrogen dioxide and ozone:

$$NO_2 + O_3 \rightarrow NO_3 + O_2$$

$$NO_3 + NO_2 \rightarrow N_2O_5$$

$$N_2O_5 + H_2O \rightarrow 2HNO_3$$

We have followed these reactions in the laboratory by observing the infrared spectra of the reactants and products. The rate of conversion of N_2O_5 to HNO_3 depends on the amount of water vapor in the system. It appears that the conversion takes place not in the gas phase but at the surface of droplets or on the vessel walls. Nitric acid appears as a gas, but not with the uniform rate that would indicate a homogeneous gas-phase reaction. After an induction time, the acid appears in a surge that is accompanied by the formation of many fine particles in the mixture.

After being formed in the condensed phase, the nitric acid evaporates.

Other possible nitric acid-forming reactions may include nitrogen trioxide abstracting hydrogen from water or hydrocarbons, and nitrogen dioxide combining with hydroxyl radicals. The NO_2--OH combination may be the source of nitric acid vapor in the upper atmosphere, but at ground level such free radical reactions would appear to be a minor source of HNO_3 compared to the NO_2--O_3 interaction.

The nitric acid absorption band most sensitive for atmospheric analysis is centered at about 880 cm^{-1}. At this frequency, water vapor interference is not serious. There are two distinctive "spikes" in the band, located at 879 and 896 cm^{-1}. These features would have revealed the presence of nitric acid with a sensitivity down to approximately 10 ppb.

Figure 18 shows the spectrum from July 25, 1973, 12 noon. The actual spectrum is drawn in the upper part of the figure. Many trace molecules were detected, as indicated, but there is no evidence of nitric acid. The calculated concentrations of detected species illustrate the detection sensitivity: carbon tetrachloride, 3 ppb; Freon 12, 8 ppb; ethylene, 6 ppb; methanol, 14 ppb; formic acid, 55 ppb; and peroxyacetyl nitrate, 35 ppb. The middle and lower spectra in the figure show the upper spectrum redrawn with added bands of 20 and 100 ppb of nitric acid. We believe the absorption peaks would have been discernible even at nitric acid concentrations as low as 10 ppb. No peaks were seen in any of the several hundred spectra recorded.

Nitrogen Pentoxide--Nitrogen pentoxide is formed in the reaction of nitrogen dioxide and ozone. It hydrolyzes to yield nitric acid. We expect this hydrolysis to take place primarily at the surface of aqueous fine particles, but no measurements or other experimental data on which to base predictions of the rate of hydrolysis were available. All we can say is that a hydrolysis half-life on the order of an hour or more should allow the nitrogen pentoxide to remain in the gaseous state long enough to develop a detectable concentration. Actually, none of the spectra shows the strong nitrogen pentoxide bands at 745 and 1245 cm^{-1}.

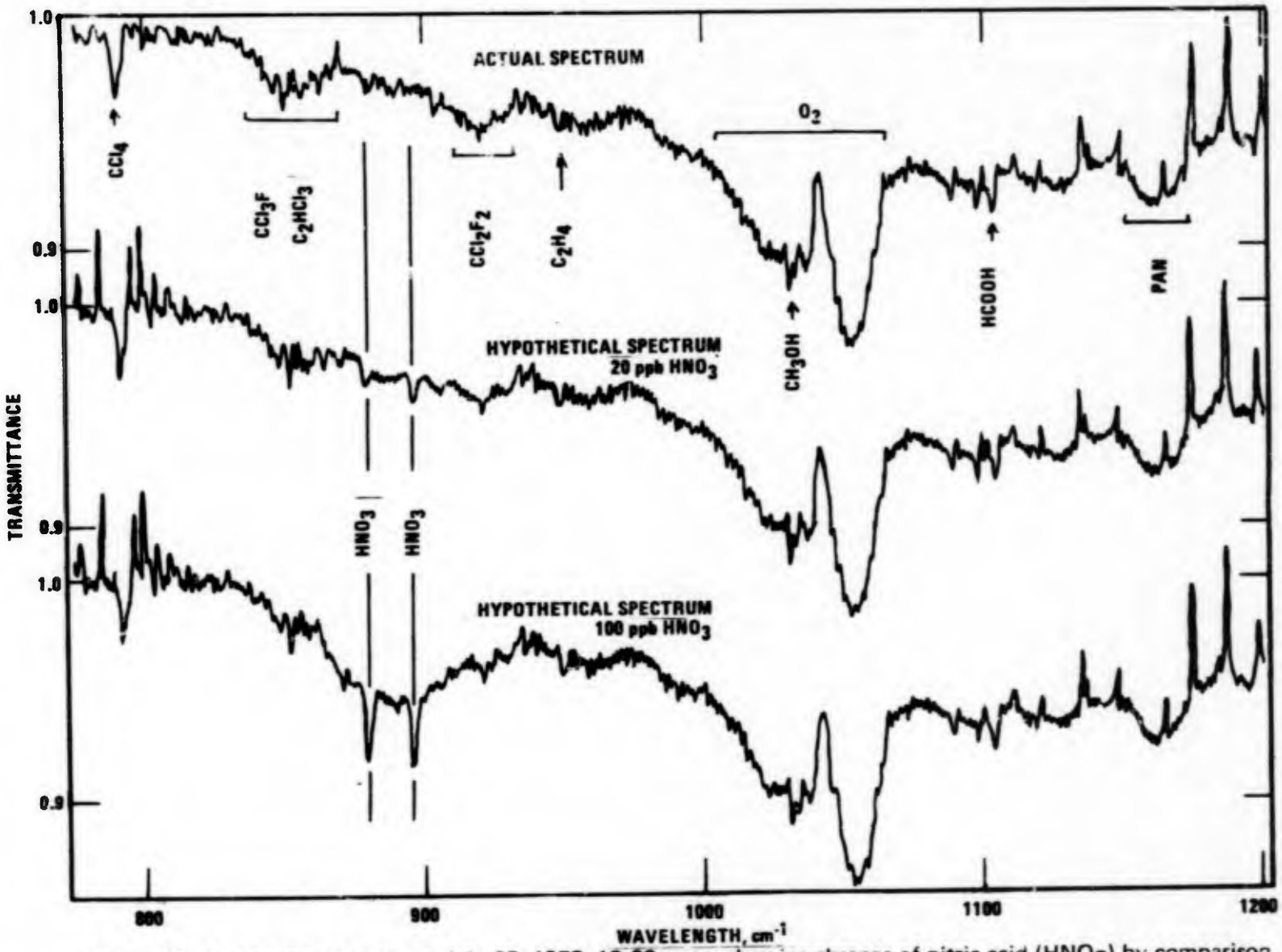

Figure 18. Atmospheric spectrum, July 25, 1973, 12:00 noon, showing absence of nitric acid (HNO_3) by comparison with hypothetical spectra for atmospheres containing nitric acid.

We estimate the detection limit to have been 0.010 ppm.

Nitrous Oxide--Nitrous oxide is an inert constituent of the atmosphere, uniformly distributed. Although it is an oxide of nitrogen, it takes no part in the atmospheric chemistry. The only reason that it is mentioned is that it does appear in the spectra at about 2200 cm^{-1}. The atmospheric concentration of the nitrous oxide is a constant 0.25 ppm, and its bands, along with the bands of carbon dioxide and water, are a permanent part of the infrared background.

Ozone--The prominent band centered at 1050 cm^{-1} gives an accurate measure of ozone, as shown in the figures. Occasionally, a small amount of methanol absorption was seen superimposed on the ozone band, but the amount of methanol could be judged from the band at 1033 cm^{-1}, and a correction could be made. The ozone went through the typical photochemical cycle, as shown in Figure 11, with the highest value being the 680 ppb observed at 1:30 p.m. on July 25, 1973. This unusually high level of photochemical oxidant will be discussed further in the section on material balance.

Peroxyacetyl Nitrate--Peroxyacetyl nitrate is seen most easily by its band at 1165 cm^{-1}, as shown in many of the spectra. Its concentration was very low at night and in the early morning. During the day, it built up to a maximum and then declined in a pattern similar to the pattern of ozone and formic acid concentrations, as shown in Figure 11. Peroxyacetyl nitrate is a strong oxidizing agent, and it is thermally stable in the gaseous state. It readily reacts at surfaces, damaging plants and irritating the eyes. Its reactions with other gaseous pollutants have not been studied extensively, but it is reasonable to assume that such reactions do take place, especially in the case of nitric oxide. Details on the properties and occurrence of peroxyacetyl nitrate in the atmosphere have been given by Stephens.[27]

Material Balance Considerations

The high acetylene-to-ethylene ratio observed on July 24 and 25 leads one to suspect that the average irradiation time for pollutants in the air mass was at least several hours. A more accurate estimate of the rate of air exchange on those days can be made by considering the acetylene and ethylene

to be components in a well-stirred flow reactor. The following assumptions are made: acetylene is nonreactive; ethylene, (E), has a first-order reaction rate: $-d(E)/dt = k(E)$; and, for daytime conditions of high ozone and high photochemical activity, the ethylene half-life is 2 hours. This half-life was derived from the slopes of the ethylene plots of Figure 10 for July 24 and 25 between the hours of 10 and 11 a.m. and is supported by laboratory smog-chamber data. It corresponds to a rate constant, k, of 0.35 hr^{-1}.

Consider the air to be well mixed at the sampling point, with an influx of unreacted polluted air at the ground level, and an outflow of photochemically reacted air at the top of the inversion. Assume the entering ethylene to be at 30 ppb (equal to acetylene), and the outflowing ethylene to be at 6 ppb, as given by our afternoon measurements. At the steady state we have

$$\text{Flow in} - \text{flow out} = \frac{-d(E)}{dt} = k(E)$$

Taking x as the fractional turnover of the air per hour yields:

$$(30x - 6x) = 0.35\ (6)$$

$$x = 0.087\ hr^{-1}$$

The reciprocal of x gives about 11 hours as the time required for one air mass to pass through the reactor.

In view of the low air turnover, it is of interest to estimate the total degree of photochemical oxidation of the air sample. The amounts of acetylene, carbon monoxide, methane, and nonmethane paraffinic hydrocarbons have been given by the infrared measurements. Details of the initial atmospheric composition can be filled in by reference to other work. From measurements at Riverside by Stephens and Burleson[18] and at Los Angeles by Kopczynski et al.,[28] the concentrations of hydrocarbon species were estimated and are given in Table 4. Likewise, the amount of nitric oxide introduced into the air mass was estimated through reference to the profile of air contaminant emissions issued by the Los Angeles Air Pollution Control District in January 1971.[29]

The requirement for peroxy radicals, RO_2, is derived from the following considerations. It is firmly established that the O_3 is

Table 4. MATERIALS IN THE PHOTOOXIDATION PROCESS, AVERAGED FOR JULY 24 and 25, 1973

Pollutant	Product maxima	Reactant availability[a]	RO_2 requirement	Maximum RO_2 availability
Ozone	640		640	
Nitric Oxide		350	450	
Peroxy acetyl nitrate	50		100	
			(1190 Total)	
Formic acid	62			
Acetylene		35		
Methyl Acetylene		1		
Olefins				
Ethylene		35		140
Propylene		10		60
1,3-butadiene		1.8		14
1-butene		1.3		10
Isobutene		2.6		21
Trans-2-butene		0.7		6
Cis-2-butene		0.7		6
2-methyl butene-1		1.2		12
Cyclopentene		2.2		22
Trans-2-pentene		1.2		12
2-methyl butene-2		1.3		13
				(316 Total)
Total aromatics, assuming eight carbons per molecule		63		1000
Total nonmethane paraffins, assuming six carbons per molecule		170		2000

[a] Composition of olefin fraction from the September 24, 1968, data of Stephens and Burleson[18]; nitric oxide estimate from Los Angeles Air Pollution Control District Emissions Profile; aromatics and paraffins estimates from Kopczynski et al.[29]

formed from the photolysis of NO_2:

$$NO_2 + NO \rightarrow NO + O$$

$$O + O_2 + M \rightarrow O_3 + M$$

It is also known that the O_3 reacts very rapidly with the NO to

regenerate NO_2:

$$O_3 + NO \rightarrow O_2 + NO_2$$

The principal role of hydrocarbons in the O_3 buildup is to supply an alternate path for oxidation of NO to NO_2 via peroxy radicals:

$$RO_2 + NO \rightarrow RO + NO_2$$

R may be a saturated or unsaturated hydrocarbon radical and may be partially oxygenated. The RO radical can continue in subsequent reactions. If R is large, the RO radicals can be oxidized to some kind of RO_2 radical one or more additional times.

The O_3 reacts with NO coming into the system, and then with the resulting NO_2 to remove it from the system:

$$O_3 + NO \rightarrow O_2 + NO_2$$

$$O_3 + NO_2 \rightarrow O_2 + NO_3$$

$$NO_3 + NO_2 \rightarrow N_2O_5$$

$$N_2O_5 + H_2O \text{ (at surface)} \rightarrow 2\ HNO_3$$

For each two NO molecules converted to HNO_3, three O_3 molecules are removed, using up to three RO_2 radicals. Formation of a peroxyactyl nitrate molecule uses two RO_2 radicals:

$$NO + RO_2 = NO_2 + RO$$

$$CH_3C(O)OO + NO_2 = CH_3C(O)OONO_2$$

It is assumed that all the NO ends up as HNO_3, nitrate salts, or peroxyacetyl nitrate. Overall, the number of reacted RO_2 radicals equals the total of: (1) the number of O_3 molecules accumulated; (2) 1-1/2 times the number of NO molecules that do not go into peroxyacetyl nitrate but disappear from the system, presumably into HNO_3 or nitrate salts; and (3) 2 times the number of peroxyacetyl nitrate molecules formed. Loss of O_3 in reaction with hydrocarbons is not counted because that reaction probably regenerates RO_2 radicals.

The number of RO_2 radicals available from each organic molecule can be estimated. The number actually generated will depend on how

far the oxidation proceeds. Without considering the detailed oxidation mechanism, it can be stated that the number of RO_2 radicals to be derived from each carbon is probably not more than two. A carbon atom that begins as a $-CH_2-$ group and ends as a CO molecule probably serves as the oxygenated carbon in an RO_2 group only once. If the carbon atom ends up as CO_2 or as HCOOH, it may have been through the RO_2 phase twice. Hydroperoxy radicals (HO_2) may also form, but it is not easy to say how frequently. Only a weakly bound hydrogen will be abstracted by O_2 to yield HO_2. The more strongly bound hydrogens can be abstracted by OH, O, and RO, which do not yield HO_2. In summary, therefore, if each carbon atom is assumed to be able to serve twice as the oxygenated carbon in an RO_2 radical, then some CO, HO_2, aliphatic acid, peroxyacetyl nitrate, and CO_2 can be formed. The figures listed in the table under "Maximum RO_2 availability" are just twice the number of carbons for each molecule listed.

The low measured values of ethylene indicate that olefins were nearly all reacted. Let it be assumed, as shown in Table 4, that 316 ppb of the required 1190 ppb of RO_2 came from olefin oxidation. The aromatics as a class are somewhat more reactive than the paraffins, as shown by Kopczynski et al.[28] Since there probably was about twice as much paraffinic materials as aromatic, it seems fair to estimate that the remaining 874 ppb of required RO_2 came half from aromatics and half from paraffins. Overall, a 20 to 30 percent depletion of carbon by oxidation is estimated. This is borne out by the two measurements of C-H absorption in the late afternoon on July 24 and 25. These points, marked on Figure 9, both have slightly higher CO/CH_x ratios than the average.

In summary, the data show a substantial degree of oxidation of the nonmethane hydrocarbon matter in the air on July 24 and 25. Olefins and aldehydes can be assumed to have been nearly completely reacted. The degree of oxidation of other compounds undoubtedly followed their photochemical reactivities. Highly substituted aromatics and branched-chain paraffins were probably fairly well oxidized, and straight chain paraffins, benzene, methane, and

acetylene were probably only slightly oxidized.

The high level of photochemical oxidation at the sampling location in the July 24 and 25 period is demonstrated by a comparison of the ozone-to-hydrocarbon ratios with those shown in the Environmental Protection Agency document Air Quality Criteria for Hydrocarbons, Figure 5-3.[30] That figure shows the measured maximum 1-hour ozone concentrations plotted against average nonmethane hydrocarbon concentrations for the period 6 to 9 a.m. From our measurements on July 24 and 25, we get a 6 to 9 a.m. total nonmethane hydrocarbon concentration of 1.25 ppm. This is derived from our measured nonmethane paraffinic carbon values with a 30 percent increment to correct for the low absorption coefficient of aromatics and small olefins. From Figure 11, we get 0.57 and 0.66 as the maximum 1-hour average ozone concentration. This yields ozone-to-hydrocarbon ratios of 0.45 and 0.53. Each of these ratios is several times higher than the ones shown in the criteria document. There, the three highest ozone values are shown to have been achieved with ozone-to-hydrocarbon ratios of 0.12, 0.11, and 0.13. Two reasons are seen for the abnormally high ratios in the present work: (1) our sampling point was well above the street, in contrast with the street-level measuring points of many monitoring stations; and (2) the 24th and 25th were days of unusually high photochemical activity.

We now consider the fate of the 350 ppb of nitric oxide which must have entered the air mass along with the measured inert pollutants. Since peroxyacetyl nitrate, at 50 ppb, was the only nitrogen-containing compound detected, the remaining 300 ppb of nitric oxide must have ended up either (1) in the particulate matter and gaseous species that were below the detection threshold, or (2) in the vegetation, soil, and other surfaces.

The nitric oxide equivalents of the measured or allowed compounds are easily enough totaled: 50 ppb are in peroxyacetyl nitrate, 10 ppb

might be in nitric acid, 5 ppb might be in alkyl nitrates, and 20 ppb might be in nitrogen pentoxide. Practically no free nitric oxide would exist because of its fast reaction with ozone. If nitric oxide must be absent, then its equilibrium partner, nitrous acid, must also be absent. Let us estimate a 2 ppb maximum for each.

High levels of nitrogen dioxide are also disallowed because of reaction with ozone. An NO_2 level can be calculated from the stirred-flow reactor approximation with the aid of published rate data.

$$\text{Flow in - flow out} = \frac{-d(NO_2)}{dt}$$

The NO_2 is oxidized to N_2O_5 in two steps:

$$NO_2 + O_3 = NO_3 + O_2$$

$$NO_3 + NO_2 = N_2O_5$$

According to data quoted by Leighton,[31] the first reaction determines the rate by being the slower of the two, with a bimolecular rate constant at 25° C somewhere between 0.010 and 0.002 $ppb^{-1}\ hr^{-1}$. Considering that two NO_2 molecules are removed for each O_3 reacted and using an average O_3 concentration of 400 ppb, we have:

$$\text{Flow in - flow out} = 2 \times \begin{Bmatrix} 0.010 \\ \text{to} \\ 0.002 \end{Bmatrix} \times 400 \times (NO_2) = \begin{Bmatrix} 8 \\ \text{to} \\ 16 \end{Bmatrix} \times (NO_2)$$

We now get the flow in and flow out by using the fractional air turnover of 0.087 hr^{-1} previously calculated from the ethylene-to-acetylene ratio:

$$0.087 \times 350 - 0.087 \times (NO_2) = \begin{Bmatrix} 8 \\ \text{to} \\ 16 \end{Bmatrix} \times (NO_2)$$

Hence: Lower estimate of NO_2 = 3.8 ppb

Upper estimate of NO_2 = 19 ppb

The above estimates consider only the reaction of nitrogen dioxide with ozone; reactions with radicals and molecules other than ozone would further reduce the nitrogen dioxide level.

We believe that there is no point in attempting to compare this estimate with measurements of nitrogen dioxide in the July 24 and 25 afternoon air mass, because the measurement methods in use do not give believable answers under afternoon smog conditions. One method which, in our opinion, would give believable answers is the recently developed laser fluorescence method, in which blue laser light is absorbed by the nitrogen dioxide and emitted as red light. This method has been shown to be highly sensitive, proportional to nitrogen dioxide, and free from interference. In an afternoon smog at El Segundo, California, Tucker et al. showed the nitrogen dioxide concentration to be not more than a few parts per billion.[32] We believe that their measurement method would have given a similar answer if applied to the air at our sampling site.

The amount of nitrate in the atmospheric fine particles can only be roughly estimated, but even a liberal estimate cannot account for more than a small part of the total nitric oxide that entered the air. In an intense smog, there might be 200 micrograms of particulate matter per cubic meter. If this were as much as 30 percent nitrate, by weight, it would only be equivalent to about 20 ppb of nitric oxide.

The sum of all the possible amounts of combined nitrogen is equivalent to only about 130 ppb of nitric oxide. Thus, about 220 ppb are not accounted for, and may have been removed at the surface. These conclusions are summarized in Table 5.

If the estimate of 350 ppb of nitrogen oxides (NO_x) obtained from the Los Angeles emission profile was too high, then the missing fraction of nitrogen oxides would be correspondingly smaller. However, even if the estimate was 100 percent too high, we would still have a substantial fraction of nitric oxide not accounted for.

If the nitrogeneous compounds are not present in the air either in gaseous or particulate form, then they must have been removed at the surface. Such removal processes need to be studied further both in the field and in the laboratory.

Table 5. NITROGEN-CONTAINING COMPOUNDS[a]

Compound	Amount detected, ppb	Maximum allowed, ppb nitrogen
Peroxyacetyl nitrate	50	
Alkyl nitrate		5
Nitric oxide		2
Nitrous acid		2
Nitric acid		10
Nitrogen pentoxide		20
Nitrogen dioxide		20
Particulate nitrate		20
Totals	50	79

[a]Nitric oxide entering air mass: 350 ppb.
Nitric oxide not accounted for: 221 ppb.

Future Work

A few improvements in the infrared detection technique used in this work should yield substantial further progress. Although the detection threshold for many pollutants has been reduced to a level near 10 ppb, this is still about a factor of 10 higher than the limits of detection claimed for the method in a previous paper.[7]

One major source of difficulty in this work was the unsatisfactory working environment, which was too shaky, too cramped, and too subject to temperature fluctuations. The remedy for this is simply to set up the optical system in a fully air-conditioned room away from machinery, with ample space for the optical components. This will allow maintenance of proper optical alignment for maximum throughput, minimum spectral

noise, and less shifting of interference fringes. These environmental improvements alone should double or triple the sensitivity.

Another limitation of the present work was the use of imperfect reference air. Carbon dioxide interference was never fully removed in the ratio plots, and nitrous oxide interference was not removed at all. Furthermore, the balance of the water lines in the ratio spectra was not always ideal because of the temperature fluctuations in the working environment. These errors can be significantly reduced in future studies. We recommend that vaporized liquid nitrogen be used in place of tank "zero air." Measured amounts of carbon dioxide and nitrous oxide gases should be carried into the long-path cell with the nitrogen. Humidification can be achieved by the "wet bag" method already developed in the present work.

Finally, it appears that there is still much to be gained in more fully utilizing the capabilities of the Fourier transform spectrometer system. Tape storage of the ratio spectra will allow retrieval and processing at a later time. The plotting of one ratio spectrum against another will reveal small increases or decreases in pollutant concentrations. A much greater number of scans should be added together in recording the spectra, thus raising the signal-to-noise ratio. The use of a copper-doped germanium detector at liquid helium temperature promises two benefits: it will cover the whole spectral region from 300 to 3500 cm^{-1} on each scan, and it will have higher detectivity than the detectors previously used.

REFERENCES

1. Stephens, E.R., P.L. Hanst, R.C. Doerr, and W.E. Scott. Reactions of Nitrogen Dioxide and Organic Compounds in Air. Ind. Eng. Chem. 48:1948, 1956.

2. Stephens, E.R., W.E. Scott, P.L. Hanst, and R.C. Doerr. Recent Developments in the Study of the Organic Chemistry of the Atmosphere. J. Air Pollut. Contr. Assoc. 6:159, 1956.

3. Scott, W. E., E. R. Stephens, P. L. Hanst, and R. C. Doerr. Further Developments in the Chemistry of the Atmosphere. Proc. Amer. Petroleum Inst. 37(III):171, 1957.

4. Stephens, E.R., P.L. Hanst, R.C. Doerr, and W.E. Scott. Auto Exhaust: Composition and Photolysis Products. J. Air Pollut. Contr. Assoc. 8:333, 1959.

5. Tuesday, C.A. The Atmospheric Photooxidation of Trans-Butene-2 and Nitric Oxide. In: Chemical Reactions in the Lower and Upper Atmosphere. New York, Interscience, 1961. p. 15.

6. Huess, J.M. and W.A. Glasson. Hydrocarbon Reactivity and Eye Irritation. Environ. Sci. Technol. 2:1109, 1968.

7. Hanst, P.L., A.S. Lefohn, and B.W. Gay, Jr. Detection of Atmospheric Pollutants at Parts-per-billion Levels by Infrared Spectroscopy. Appl. Spectroscopy. 27:188, 1973.

8. White, J.U. Long Optical Paths of Large Aperture. J. Opt. Soc. Amer. 32:285, 1942.

9. Hanst, P.L. Spectroscopic Methods for Air Pollution Measurement. In: Advances in Environmental Science and Technology, Pitts, J.N. and R.L. Metcalf (ed.). New York, John Wiley and Sons, Inc., 1971. p. 91.

10. Erley, D.S. and B.H. Blake. Infrared Spectra of Gases and Vapors (Vol. II). Dow Chemical Company. Midland, Mich. 1965.

11. Hanst, P.L., E.R. Stephens, W.E. Scott, and R.C. Doerr. Absorptivities for the Infrared Determination of Trace Amounts of Ozone. Anal. Chem. 33:1113, 1961.

12. Stephens, E.R. Absorptivities for the Infrared Determination of Peroxy Acyl Nitrates. Anal. Chem. 36:928, 1964.

13. Junge, C. and J. Hahn. N_2O Measurements in the North Atlantic. J. Geophys. Res. 76:8143, 1971.

14. Stephens, E.R. Hydrocarbons in Polluted Air. University of California. Riverside, California. Summary Report, Project CAPA-5. June 1973.

15. Stephens, E.R. and F.R. Burleson. Analysis of the Atmosphere for Light Hydrocarbons. J. Air Pollut. Contr. Assoc. 17:147, 1967.

16. Lonneman, W.A., S.L. Kopczynski, P. Darley, and D. Sutterfield. Hydrocarbon Composition in Urban Areas. Environ. Sci. Technol. 8:229, 1974.

17. Neligan, R.E., P.L. Mader, and L.A. Chambers. Exhaust Composition in Relation to Fuel Composition. J. Air Pollut. Contr. Assoc. 11:178, 1961.

18. Stephens, E.R. and F.R. Burleson. Distribution of Light Hydrocarbons in Ambient Air. J. Air Pollut. Contr. Assoc. 19:929, 1969.

19. Gordon, R.J. and R.J. Bryan. Annonium Nitrate in Airborne Particles in Los Angeles. Environ. Sci. Technol. 7:645, 1973.

20. Charleson, R.J., A.H. Vanderpol, D.S. Conert, A.P. Waggoner, and N.C. Alquist. Sulfuric Acid-Ammonium Sulfate Aerosol: Optical Detection in the St. Louis Region. Science. 184:156, 1974.

21. Georgii, H.W. Oxides of Nitrogen and Ammonia in the Atmosphere. J. Geophys. Res. 68:3963, 1963.

22. Stephens, E.R., E.F. Darley, and F.R. Burleson. Sources and Reactivity of Light Hydrocarbons in Ambient Air. Proc. Amer. Petroleum Inst. Division of Refining. 47:466, 1967.

23. Weinstock, B. and H. Niki. Carbon Monoxide Balance in Nature. Science. 176:290, 1972.

24. Hanst, P.L. and J.G. Calvert. The Oxidation of Methyl Radicals at Room Temperature. J. Phys. Chem. 68:71, 1959.

25. Mader, P.P., G. Cann, and L. Palmer. Effects of Polluted Atmospheres on Organic Acid Composition in Plant Tissues. Plant Physiol. 30:318, 1955.

26. Gay, B.W., Jr., and J. J. Bufalini. Hydrogen Peroxide in the Urban Atmosphere. In: Advances in Chemistry Series, No. 113. Washington, D. C. American Chemical Society, 1972. p. 225.

27. Stephens, E.R. The Formation, Reactions, and Properties of Peroxyacyl Nitrates (PANS) in Photochemical Air Pollution. In: Advances in Environmental Science and Technology Vol. 1, Pitts, J.N. and R.L. Metcalf, (ed.). New York, Wiley Interscience, 1969. p. 119.

28. Kopczynski, S.L., W.A. Lonneman, F.D. Sutterfield, and P. E. Darley. Photochemistry of Atmospheric Samples in Los Angeles. Environ. Sci. Technol. 2:132, 1968.

29. Air Quality Profile of Air Contaminant Emissions. Los Angeles County Air Pollution Control District. Los Angeles, Calif. Jan. 1971.

30. Air Quality Criteria for Hydrocarbons. National Air Pollution Control Administration, U. S. Department of Health, Education, and Welfare. Washington, D. C. Publication No. AP-64. March 1970.

31. Leighton, P.A. Photochemistry of Air Pollution. New York, Academic Press, 1961. p. 157.

32. Tucker, A.W., A.B. Peterson, and M. Birnbaum. Fluorescence Determination of Atmospheric NO and NO_2. Applied Optics. 12:2036, 1973.

NEW SAMPLING TECHNIQUE FOR IDENTIFYING ORGANIC FILM ACCUMULATION ON ARMY MATERIEL IN THE TROPICS

by

James F. Sprouse
US Army Tropic Test Center
Fort Clayton, Canal Zone

A 1-year research project has recently been completed at the US Army Tropic Test Center, Fort Clayton, Canal Zone that sampled the tropic environment for ambient organic compounds. One objective of the investigation was to study test methods for use in assessing environmental damage to military items undergoing prolonged storage in the tropics. Materiel degradation usually occurs from a combination of environmental forces which vary in intensity depending upon the type of tropic test site. Test sites typically consist of open grasslands, coastal areas, dense tropical forests, or man-made structures placed at the sites to help protect test items from the environment. Degrading forces range from ultraviolet radiation, moisture, salt and constantly warm temperatures to microorganisms and environmental chemicals. It is usually a combination of these forces that causes a malfunction in the tropics. This paper will discuss sampling and analysis of ambient organic compounds that enter into the environmental degradation process found in the tropics of Panama. These compounds can enter into environmental deterioration processes in the tropics by serving as a carbon source for sustaining microbiological life, by reacting directly with the substrate or by providing electrical shorts in electronic components.

Sampling for ambient organic compounds was completed by two methods: First, air sampling for volatile organic compounds was carried out to determine whether the majority of compounds originated from natural sources (vegetation) or man-made pollutants. Secondly, a simple new technique was used that involved placing glass plates at field test sites and allowing compounds to naturally accumulate on the surface.

Seven tropic test sites were sampled for both volatile and condensed compounds. Figure 1 shows site locations in the Canal Zone on the Pacific side of the isthmus, the Atlantic or Caribbean side and the geographical mid-isthmus. On the Pacific side and at mid-isthmus, grassland and forest sites were sampled. On the Atlantic side, a mangrove forest site was added to the grassland and forest sites.

Air samples were collected using the system shown in figure 2. The system consists of a filter which eliminates particulate matter, a sampling tube for concentrating organic volatile materials, a flow meter and a vacuum pump. Approximately 50 liters of air are passed through the system at a flow rate of 1 liter/minute. As the air passes through the sampling tube, volatile organic materials are retained by the chromosorb 102 solid adsorbant. Chromosorb 102 is a nonpolar packing which is not adversely affected by high levels of ambient moisture.

After collection of samples in the field they were returned to the laboratory for analysis. Figure 3 shows a gas chromatogram for a sample collected at the Pacific grassland test site in the Canal Zone. Identification of the component peaks is based on retention times, infrared analysis and mass spectrometry.

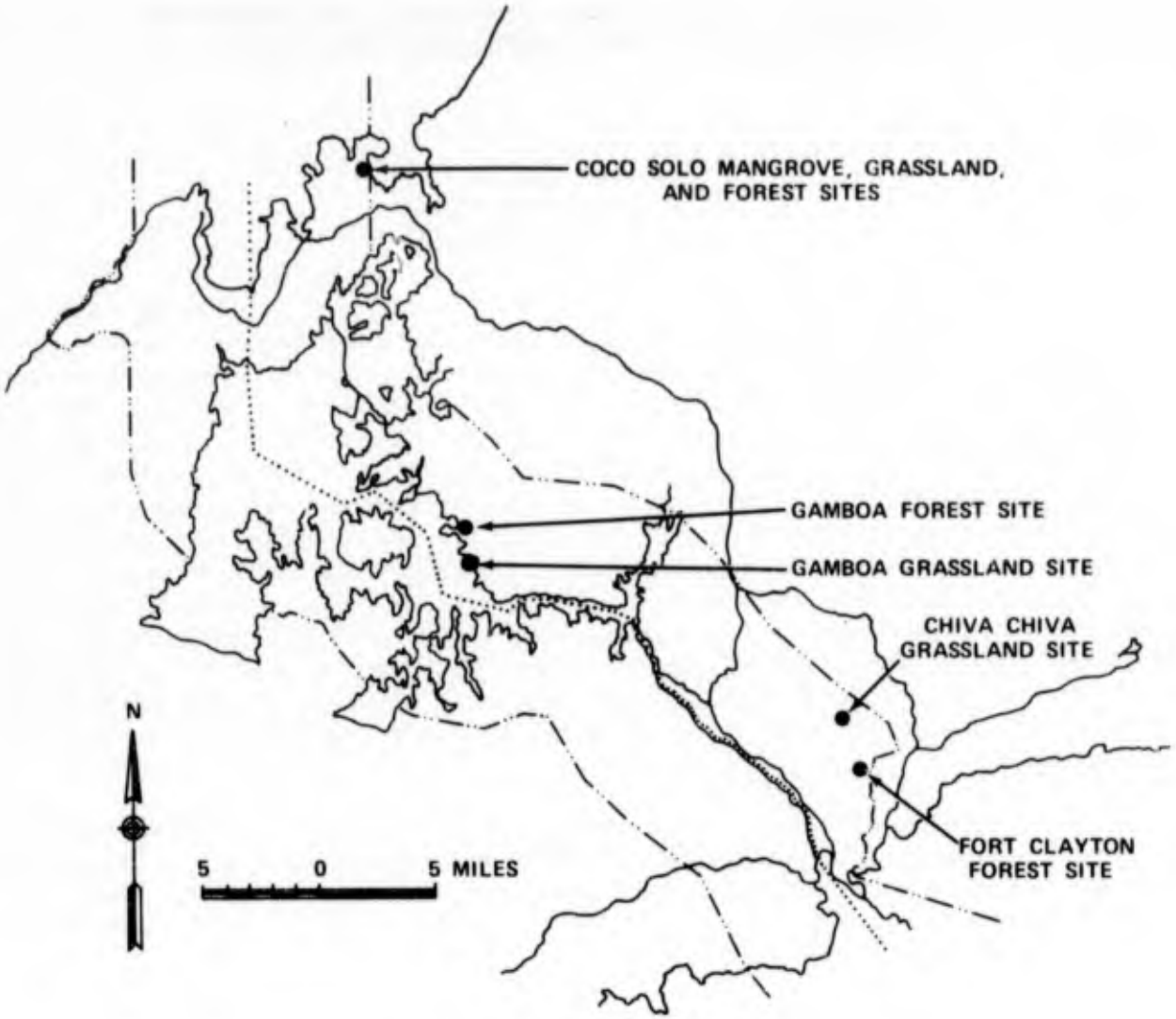

Figure 1. Tropic Test Sites

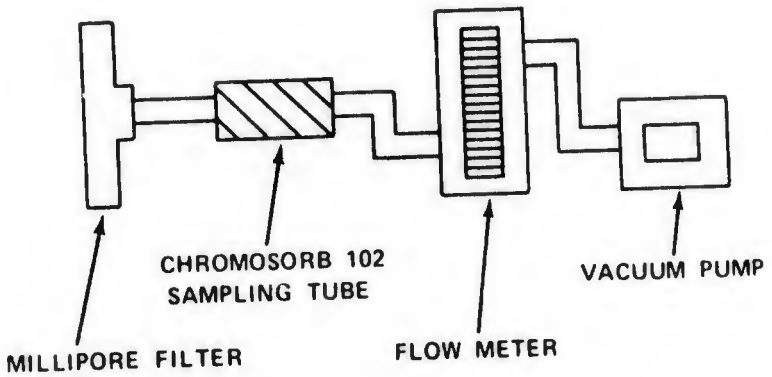

Figure 2. Field Air Sampling System

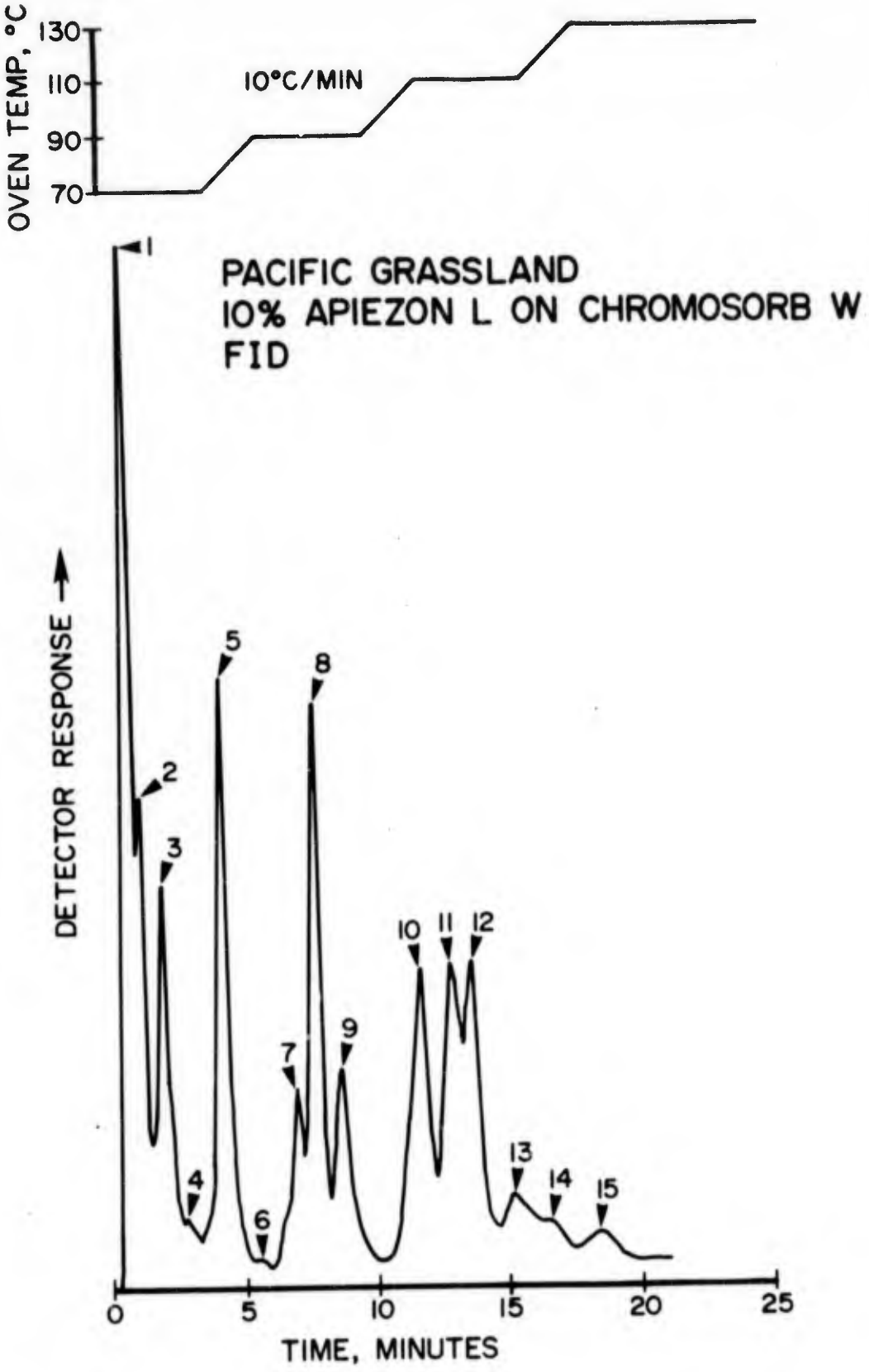

Figure 3. Gas Chromatogram of Air Sample (Pacific Grassland)

Fifteen major components are generally resolved by gas chromatography with flame ionization detection using the temperature program shown in figure 3. Nine of the components have presently been identified. Peak number 1 is mostly hexane but other light hydrocarbons are probably eluted at the same time. Peak 3 is benzene and peak 5 is toluene. Peaks 7, 8 and 9 are p, m and o-xylene, respectively, but ethylbenzene is also eluted with the p-xylene. Peaks 10, 11 and 12 are n-propylbenzene, methylethylbenzene and trimethylbenzene, respectively.

Figure 4 shows a gas chromatogram of an air sample from the Gamboa forest site at mid-isthmus. Note the temperature program is from -70°C to 150°C using a Durapak column as opposed to the previous slide which used a program from 70°C to 130°C using an Apiezon column.

The majority of the components identified are POL combustion and incomplete combustion products. The concentration ranges are generally less than 5 parts-per-billion. Diurnal measurements have shown that ambient concentrations fluctuate throughout the day, but the inventory of materials detected is usually constant regardless of site location.

Figure 5 shows the average total concentration for volatile hydrocarbons for four sampling times in a 24-hour period versus combined site location and site classification, (i.e., grassland, forest and mangrove). The total hydrocarbon measurements are the average of samples collected at 0600, 1200, 1800 and 2400 hours at all sites. Almost identical concentrations are found for the Pacific and Atlantic sides of the isthmus, while the mid-isthmus area contains a concentration only 75 percent as high as the other site locations.

The hydrocarbon concentrations were highest in forest sites, followed by grassland and lowest in mangrove swamps. The total hydrocarbon concentrations on the Pacific and Atlantic sites of the isthmus reflect a greater number of pollution sources available at these locations than those at the geographical mid-isthmus locations.

Figure 6 shows material-sampling plates set under the jungle canopy. The glass plate technique works on the principle of providing a biologically inert substrate for collecting ambient organic materials through natural condensation. The plates were exposed at the seven field sites continuously for 11 months in order to accumulate materials. Plates were returned to the laboratory after 4, 8 and 11 months, chemically extracted, and the extracts analyzed by gas chromatography..

Figure 7 shows a typical chromatogram for analysis of condensed materials. Fifteen to twenty components are usually isolated from a single plate.

As may be seen from the temperature program in figure 7, the condensed materials should have boiling points in the range of 160°C to 240°C. Of the 19 components resolved in this chromatogram, our laboratory has only worked with the higher boiling compounds that are present in the greatest concentrations. Limited mass spectra obtained on these compounds indicate their molecular weights are 208 and 198 respectively.

Figure 8 shows the infrared spectra of peak 19 in the chromatogram in figure 7. Enough sample was concentrated into sufficient quantity for obtaining IR spectra by collecting peak 19 into a microfraction collector during repetitive gas chromatographic analysis. A beam condenser was used for obtaining the spectra.

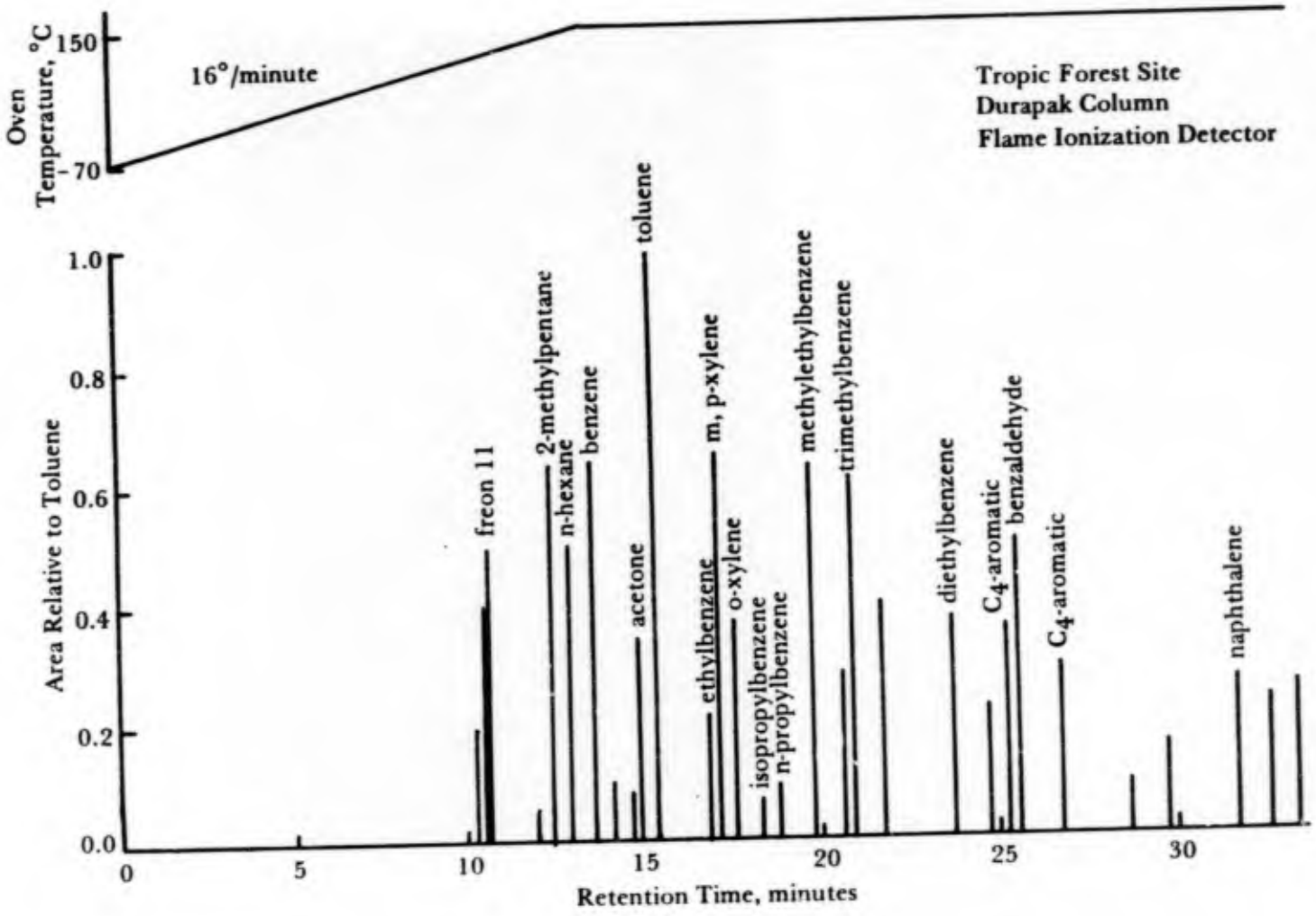

Figure 4. Gas Chromatogram of Air Sample (Tropic Forest Site)

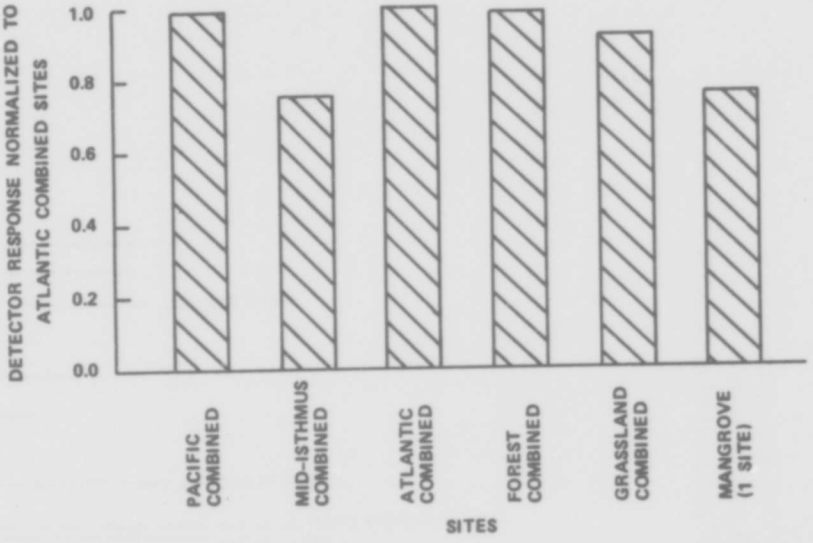

Figure 5. Average Total Hydrocarbon Concentration by Air Sampling for Sites Combined Because of Geographical Proximity and Similar Characteristics over a 24-Hour Period

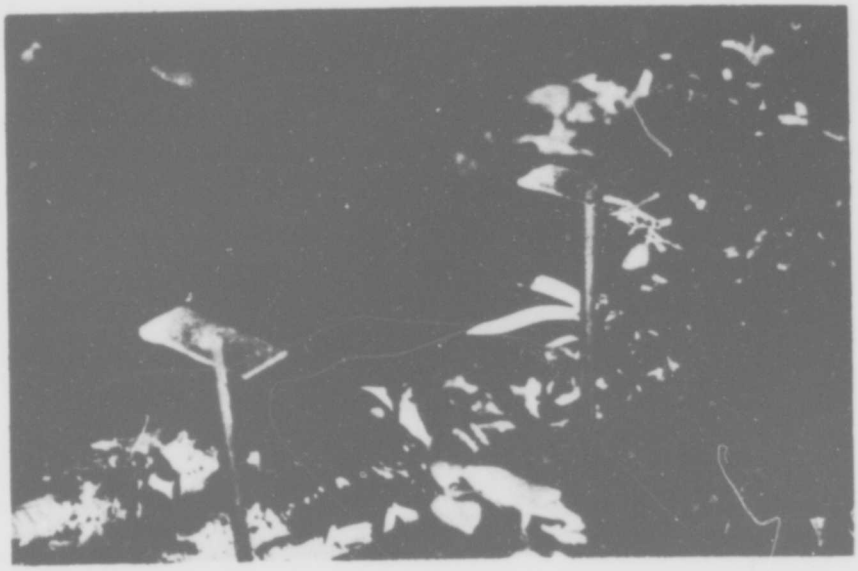

Figure 6. Glass Sampling Plates for Collecting Condensed Material

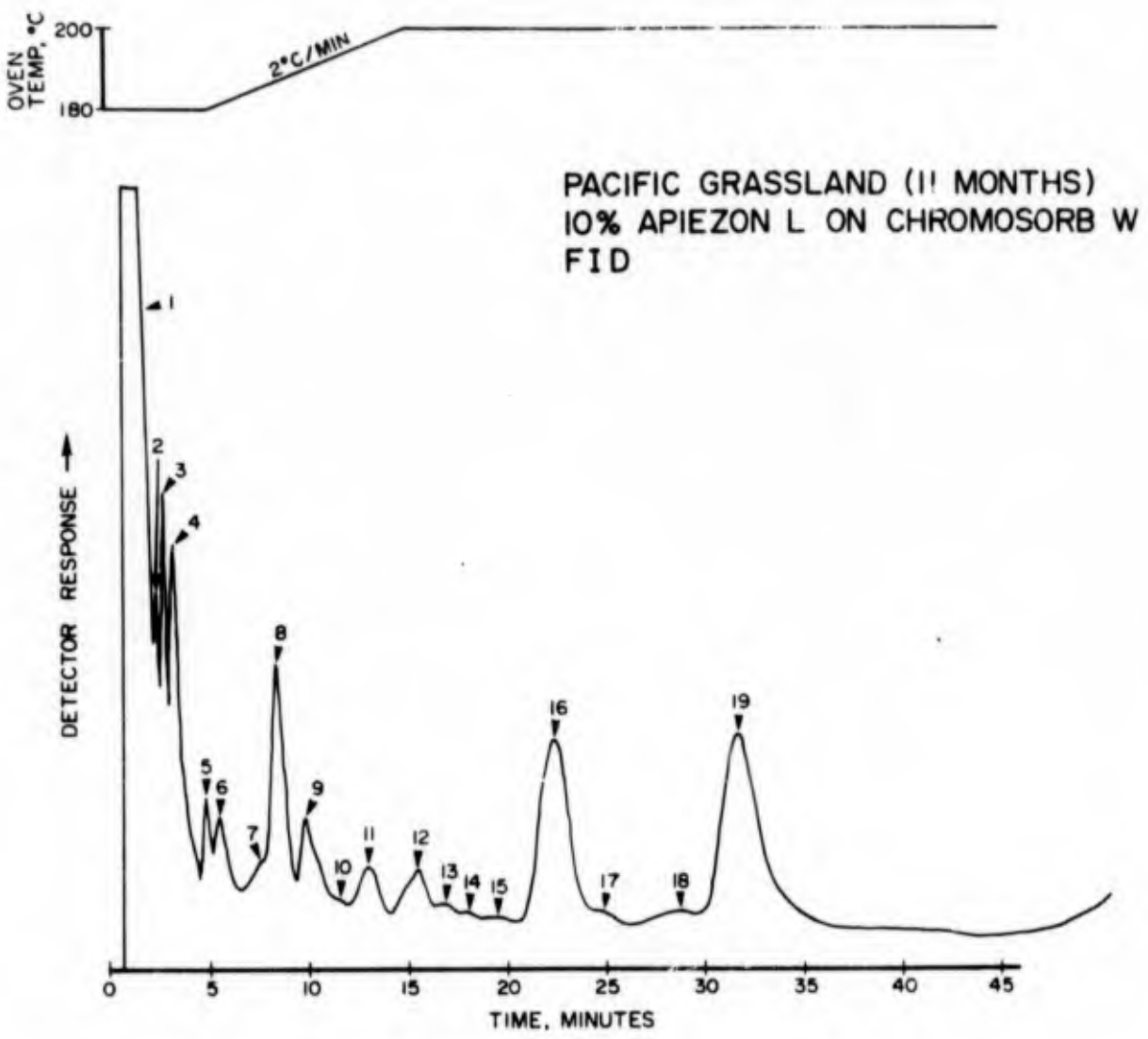

Figure 7. Gas Chromatogram of Condensed Material Extracted from Glass Sampling Plate

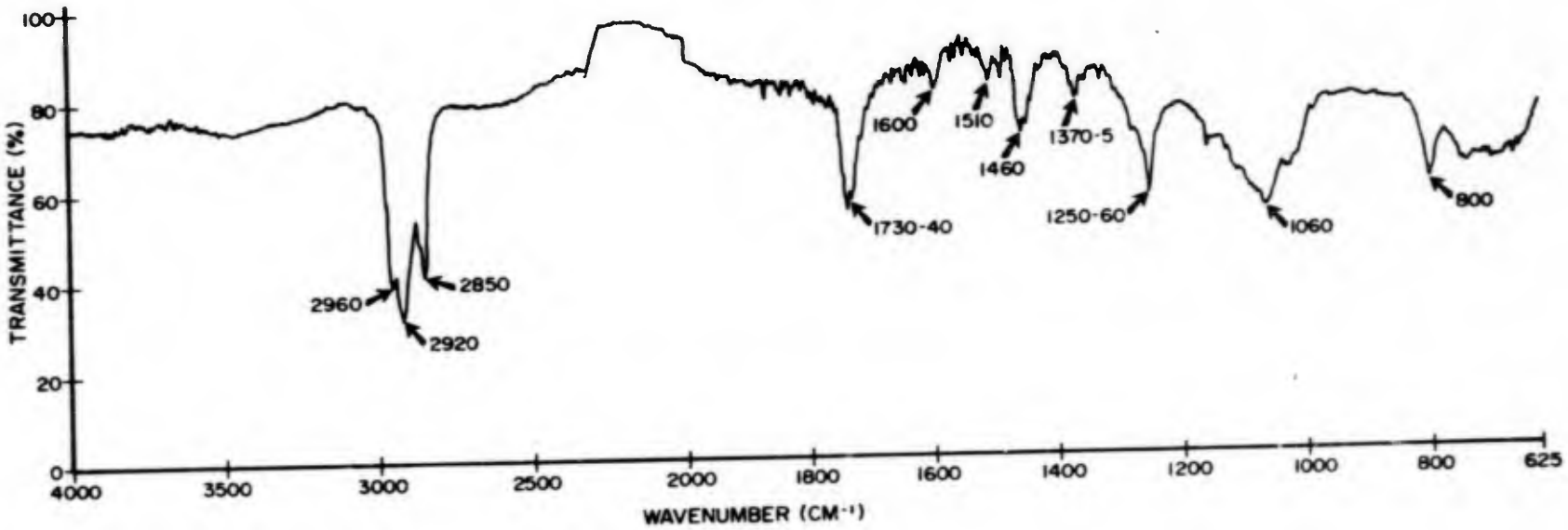

Figure 8. Isolated Component (Peak 19) of Condensed Material on Glass Sampling Plate

The spectra in figure 8 show absorption bands characteristic of alkanes (2800 to 3000 wave numbers and 1370 and 1460 wave numbers). The band at 1730-40 is characteristic of the carbonyl ester stretching vibration and the band at 1250-60 is characteristic of C-O stretching. The doublet shown at 1730-40 is also characteristic of an α-keto ester compound.

The bands at 1600, 1510 and 1060 show the possible presence of an aromatic component. However, the band at 1060 is likely to be a straight chain or cyclic ether (figure 9) which means that the aromatic compound in the plate extract may be trace contamination from a second component eluted at the same retention time. The band at 800 cm^{-1} indicates unsaturation in the aliphatic chain.

Figure 9 shows an IR spectra of a compound extracted from *Gynerium sagittatum* (tropical grass). This grass is found adjacent to nearly all of the test sites. This spectra is nearly identical to the previous spectra of peak 19 (figure 8). The adsorption bands at 1600 and 1510 which are characteristic of aromatic structure are not resolved, but the resolution at 1060-70 and 1110 cm^{-1} is more defined. This strengthens the argument that the band results from a straight chain or cyclic ether. The spectra in figures 8 and 9 offer sound evidence that the accumulation of organic materials on the glass substrates is at least partly of vegetative origin.

Figure 10 shows the average total hydrocarbon accumulation on plates for sites grouped according to geographical proximity and characteristics in common (i.e., forest and grasslands). After 11 months of exposure, the greatest average accumulation of condensed material on the plates was on the Pacific side of the isthmus. The mid-isthmus sites at Gamboa had accumulated approximately 75 percent as much as at Pacific sites; and at Atlantic sites, approximately 55 percent as much material as the Pacific sites. The grassland sites accumulated more condensed material than the forest, and the mangrove site accumulated the least amount.

CONCLUSIONS.

The sampling for hydrocarbon compounds in the tropics has shown that volatile compounds are mainly combustion and incomplete combustion products. Their concentrations are typically 1 to 2 ppb.

The glass-plate-sampling technique has proven to be a simple method for sampling organic films that accumulate on items exposed to the tropic environment. The glass plate can be placed adjacent to a test item stored in the tropics and the effects of environmental chemicals studied without destroying the test item Organic films analyzed to date have components that have been traced to vegetative sources. After isolating these compounds from the glass plates, their characteristics can be evaluated with respect to chemical reactivity, biological effects, optical characteristics and general degrading effects upon Army materiel.

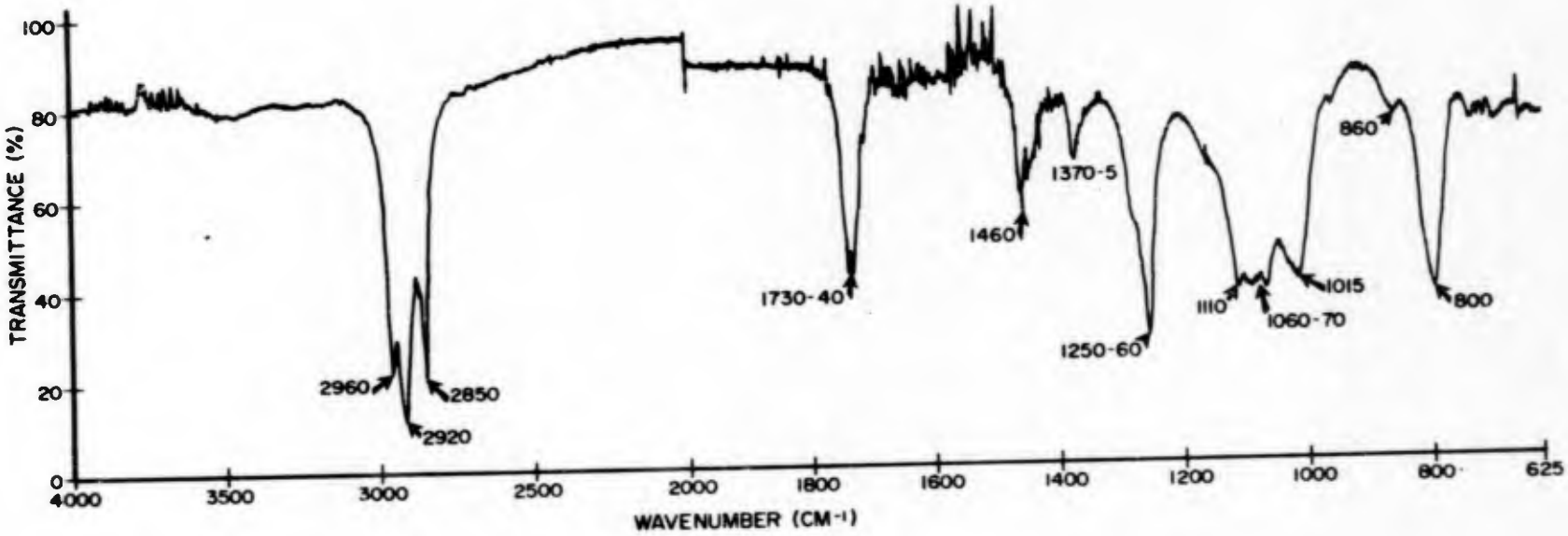

Figure 9. Isolated Component of *Gynerium Sagittatum* (Tropical Grass)

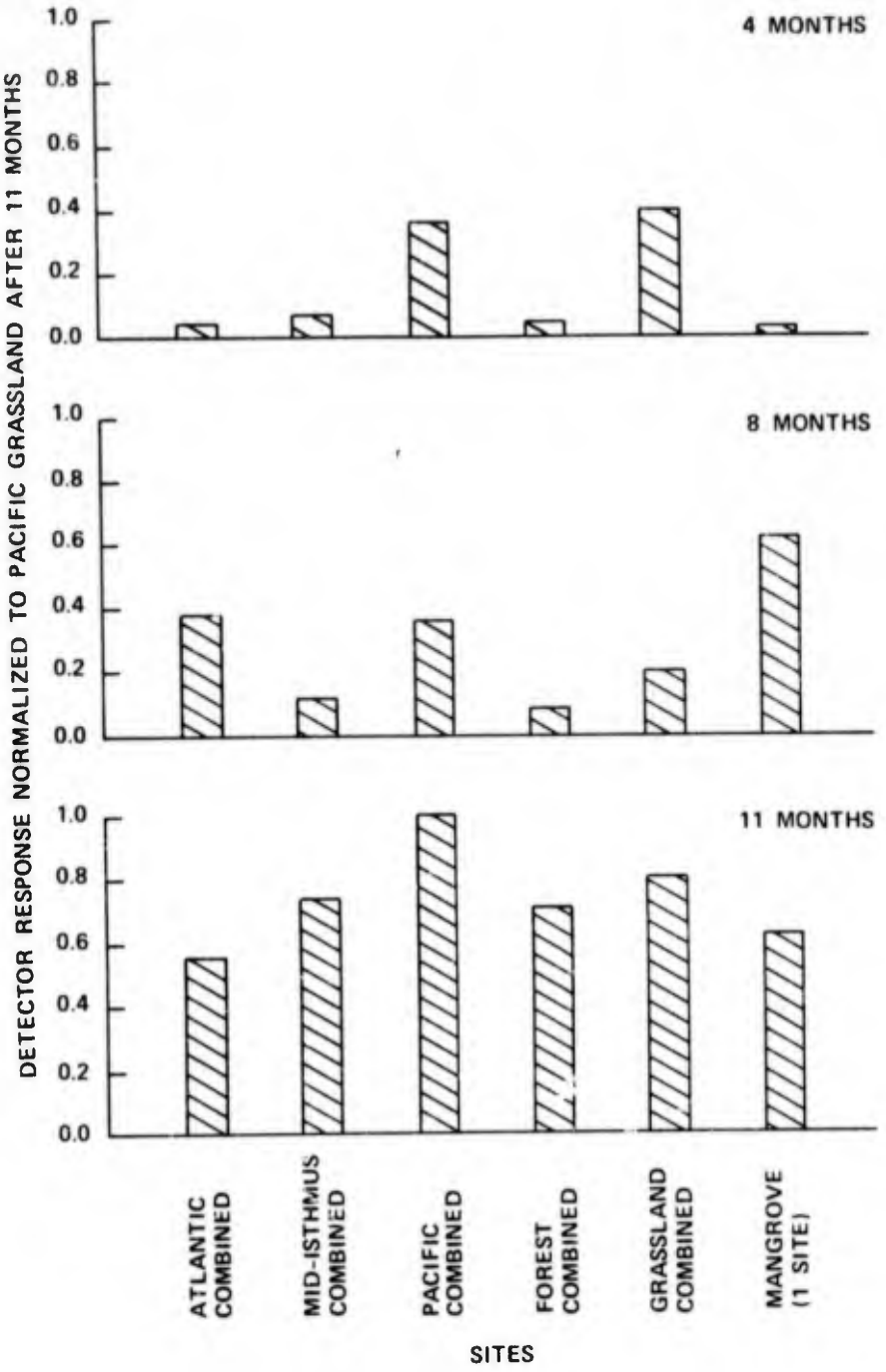

Figure 10. Average Concentration of Organic Condensates after 4, 8 and 11 Months of Exposure

SESSION II

Chairman: Dr. George J. Rotariu
US Energy Research & Development Administration

LASER INTRACAVITY RAMAN CELL

by

Philip J. Miller and Stanley M. Klainer

Presented at the Sixth Annual Symposium on Environmental Research
American Defense Preparedness Association, 29 April 1975

ABSTRACT

Raman scattering of trace gases in the atmosphere is obtained from a laser intracavity sample cell. The design of the sample cell in configuration with optical filters and photo-multiplier tube for frequency discrimination is such that scattering is collected over a large solid angle (F/2.5→3.5) and from a large sample volume (approaching 10 cm^3). The combination of the increase in sample volume, in solid angle of collection, and in laser power gives an effective 10^4 increase in sensitivity over the conventional laboratory Raman spectrometer. The method and apparatus are usable in a variety of applications relating to the real time monitoring of gas in the atmosphere for the 0.1-ppm to 100-ppm concentration range.

INTRODUCTION.

The technique of Raman scattering spectroscopy for analyzing trace quantities is not a sensitive technique. The reason is obvious when the magnitude of the Raman scattering cross-section ($\sim 10^{-30}$ cm^2/molecule) is compared to that of an absorption cross section ($\sim 10^{-17}$ cm^2 /molecule). However, there are circumstances when Raman scattering can and indeed does measure part-per-million concentrations. For example, in remote Raman spectroscopy where one observes scattering from sample volumes of the order cubic meters, the technique is highly sensitive to trace constituents in the atmosphere and is successfully utilized.

The expression for the Raman scattering return signal (in photons per second) is

$$N_R = \frac{E}{h\nu} \rho \frac{V_S}{A} \sigma T\Omega \eta \qquad (1)$$

where

$E/h\nu$ is the number of photons of frequency ν generated by the laser with power E (watts);

ρ is the concentration (molecules/cm^3) of sample;

V_S/A is the effective path length (cm) of sample scattering, where V_S is the total volume of sample and A is the cross-sectional area of the laser beam

σ is the scattering cross-section cm^2-$molecule^{-1}$-st^{-1};

T is the transmission to the detector of the scattered light;

Ω is the effective solid angle of collection of the scattered Raman radiation, ster; and

η is the quantum efficiency of the detector.

As can be seen from this expression, the only way to effectively increase N_R, the Raman signal, for a fixed concentration and scattering cross sections is to increase E, V_s/A, and Ω.

In the typical laboratory Raman experiment using a 1-watt laser and a commercial Raman spectrophotometer, $E\Omega(V_s/A)$ has the value 0.015 (watts·cm·ster) as determined from the scattering volume and light-gathering capabilities of the system. Block Engineering, Inc. has designed a system for analyzing trace components in gases which gives a $>10^4$ times larger value of $E\Omega(V_s/A)$ (>150 watts·cm·ster) and therefore a 10^4 increase in the N_R, the Raman return signal or conversely allows for the observation of a 10^{-4} weaker concentration of the sample.

TECHNICAL DISCUSSION.

The following gives a short description of this system. The exact details of the design are, at this time, proprietary to Block Engineering, Inc. Increasing the term, $E\Omega(V_s/A)$, as defined previously, is accomplished by: (1) Putting the sample intra-cavity with the laser where effectively a 20-fold increase in laser power is obtained; (2) Using interference filters (this allows for the F number of this system to be ~ 3 as compared to 7 for the typical commercial Raman system: the collection solid angle is related to F^{-2}, thus an effective fivefold increase in Ω is obtained): (3) expanding the sample path length. (In the typical laboratory Raman experiment, V_s/A is determined from scattering volume of the laser-exposed sample, which is determined from the cross sectional area of the focused laser beam. This has a value of ~ 2 cm. This corresponds to the slit height which assumes that the optics of the spectrometer are such that all the light of the focused-laser beam is in the optical sample volume. The design of the present sample cell requires an unfocused-laser beam and gives an effective 100-fold increase in the path length over that of the conventional sampling technique.) (4) Finally, one may use a combination of color filters and interference filters for spectral discrimination. (This gives a twofold increase in the transmission efficiency of the system over a double monochromator).

EXPERIMENTAL RESULTS.

Commercial Raman spectrometers have stray light rejection ratios of 10^{-12} to 10^{-14}. That is to say that of the light entering the monochromator, this amount is undispersed. By far the major component of the light that one needs to reject is light with the same frequency as the laser, which includes the reflected laser light and the Rayleigh scattering from the sample. The measured rejection of light at the laser frequency used in our system is less than 10^{-15}. This is accomplished by the use of the color filters and interference filters. However, since we are attempting to measure ppm concentrations of particular species, it is also necessary to have Raman scattered light rejection of 10^{-6} or better. Experimental results have shown thus far, that that with 10Å resolution at least 10^{-7} rejection of unwanted Raman light can be obtained. This arises from the major components in the atmospheric sample such as N_2 and O_2.

Using a 1-watt (4880Å) line of an argon laser the Raman spectrum of water vapor in the air (about 10^4 ppm) shows a signal with maximum intensity of 20 photons/sec. Using the same laser and the intracavity sample cell, a signal of greater than 200,000 cps is observed which verifies the original predictions. At this time, detection of 10^{-6} concentrations have not been observed due to interferences in the background from the laser plasma at the wavelength of interest which gives a background of $\sim$5000 cps. We are attempting to eliminate this effect by introducing a dispersive prism into the laser cavity. The sensitivity of this system using a 4-watt argon ion laser for a variety of molecules is expected to be as follows:

Molecule	Concentration	Expected Raman signal
	ppm	photons/sec
H_2O	0.1	100
H_2	1	400
CO_2	1	750
CH_4	0.1	300
N_2	1	800
SO_2	0.01	125

INDIVIDUAL APPLICATIONS.

The system described was designed and built, using a high-power gas laser, for the determination of trace quantities, less than a ppm of homonuclear diatomic molecules, aerosols, and free radicals by both Raman and fluorescent scattering.

The system has the potential of being made into a battery-operated portable device. It can, in either configuration, be used for both ambient and industrial pollutant detection and quantification. With the right selection of components it can be used for resonant light-scattering measurements.

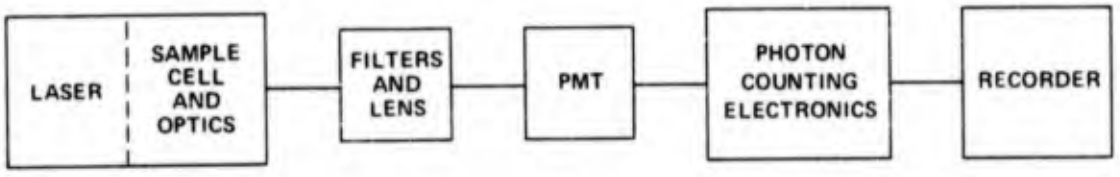

Figure 1. Block Diagram

Intracavity Raman Cell and Spectral Discriminator.

1. 10^{-15} REJECTION RATIO OF LIGHT AT LASER FREQUENCY

2. 10^{-7} REJECTION RATIO OF UNWANTED RAMAN LIGHT OF MAJOR ATMOSPHERIC COMPONENTS

3. 200,000 CPS OBSERVED FOR 10^4 PPM H_2O VAPOR IN ATMOSPHERE

Figure 2. Experimental Results

	E	V_s/A	Ω	$E(V_s/A)\Omega$
COMMERCIAL SYSTEM	1 (WATTS)	2 (CM)	0.015 (STER)	.030
THIS SYSTEM	20	200	0.075	300

Figure 3. Comparison to a Commercial Raman System

KINETICS OF TRACE GAS ADSORPTION FROM CONTAMINATED AIR[1]

by

Leonard A. Jonas, Joseph Rehrmann, and Jacqueline M. Eskow
Edgewood Arsenal, Aberdeen Proving Ground, MD 21010

ABSTRACT

A study was made of the kinetics of trace gas adsorption from contaminated air flowing into beds of activated carbon arranged in series. The purpose of the study was to determine if it were possible to predict the period of time for which the discharge flow emitted to the atmosphere from two carbon filters in series, would not exceed an environmentally imposed limit on concentration which was below the sensitivity of existing monitoring equipment. The results of the study showed that (1) gas adsorption by carbon beds in series was equivalent to adsorption by a single bed with a proportionate increase in depth, (2) the present equations describing gas adsorption kinetics were applicable to carbon beds in series, (3) the gas concentration exiting the first carbon filter, monitored by a relatively insensitive alarm, could serve to predict the subsequent time period during which the concentration emitted from the second filter would never exceed the imposed emission standards.

[1] Paper originally presented at the symposium "Removal of Trace Contaminants from the Air" American Chemical Society meeting in September 1974 at Atlantic City, NJ. This paper, as well as others in that symposium will be published by the ACS in an Advances in Chemistry Series due for publication in 1975.

DEVELOPMENT AND EVALUATION OF A SAMPLING AND HYDROCARBON CLASSIFICATION SYSTEM FOR JET ENGINE EXHAUST ANALYSIS

by

Joseph J. Brooks
Monsanto Research Corp., Dayton, OH

and

Marilyn S. Black, William R. Rehg and Robert E. Sievers
Aerospace Research Laboratories
Wright-Patterson AFB, OH

INTRODUCTION

The incomplete combustion of nonhomogeneous hydrocarbon-based fuels produces an exhaust which contains a complex mixture of organic compounds. As an illustration of the complexity of this mixture, table 1 contains a partial list of compounds identified in the exhaust from the combustion of JP-4 fuel by the Air Force School of Aerospace Medicine (AFSAM). Each of these compounds is of environmental significance depending upon the degree to which it exhibits properties that are detrimental to the environment or harmful or irritating to the public. Toxicity smog-producing capability, odor, and eye irritability are examples of environmentally significant properties. More generally, certain of these properties have been associated with particular reactivity classes of compounds. As examples, olefins are known to be important links in the reaction sequence which produces smog, and oxygenated and aromatic compounds are recognized as being among the more odorous and toxic compounds. By comparison, the paraffins are relatively innocuous.

Since these compounds have different potentials for affecting the envrionment, total hydrocarbon analyses do little to provide useful information concerning the environmental consequences of hydrocarbon exhaust. On the other hand, a quantitative compound-by-compound determination, which is the most complete type of analysis for this purpose, is expensive and time consuming, and requires instrumental sophistication beyond the capability of many analytical laboratories. There is a need for an intermediate analytical capability which provides enough detail to reasonably assess the environmental consequences of the hydrocarbon portion of exhaust, and yet is relatively inexpensive and fast for routine or multiple analyses. This need has spurred several attempts at developing analysis schemes which divide organic exhaust products into various classifications based on reactivity or compound type. The goal of research conducted at the Aerospace Research Laboratories by ARL and MRC personnel has been to investigate methods of accomplishing such an analysis and applying this technology to real-world samples from the combustion of various fuels under selected conditions.

ANALYTICAL SYSTEM

The instrumentation used in the analytical system includes:

(a) A Hewlett-Packard Model 5750B research gas chromatograph equipped with a dual flame ionization detector (FID).

Table 1. Compounds Identified in JP-4 Exhaust by USAF School of Aerospace Medicine

Paraffins	Aromatics
Methane	Ethylbenzene
2,2,3-Trimethylbutane	1,4-Dimethylbenzene
3-Methylhexane	1,2,3-Trimethylbenzene
2,3,4-Trimethylpentane	n-Propylbenzene
3,4-Dimethylhexane	1,2,4-Trimethylbenzene
2,4-Dimethylhexane	1,3-Diethylbenzene
3,4-Dimethylheptane	
n-Octane	Olefins
n-Nonane	
4-Methyloctane	Ethylene
2-Methyl-4-ethylhexane	Acetylene
n-Decane	Propylene
2-Methyl-5-ethylheptane	Propyne
Isopropylcyclopropane	2-Methylpropene
Methylcyclohexane	1-Butene
	2-Butene-cis
Ketones	2-Methyl-1-pentene
	1-Hexene
2-Butanone	3-Heptene-trans
Methyl propyl ketone	Allene
3-Hexanone	
5-Methyl-2-hexanone	Ethers
Propyl benzyl ketone	
3-Heptanone	Furan
	3-Methylfuran
Alcohols	2,3-Epoxybutane
	Isooctyl vinyl ether
Methanol	
Cyclohexanemethanol	Esters
2-Propylheptanol	
	Amyl acetate
Aldehydes	
Acetaldehyde	
Propionaldehyde	
Crotonaldehyde	
Butyraldehyde	

(b) An Autolab System IV computing integrator.

(c) A Hewlett-Packard Model 19021A heated gas-sampling valve modified to accommodate solid sorbent-sampling tubes.

(d) A specially designed tube furnace for desorbing samples from sorption tubes.

The heart of the analytical system is the column arrangement shown in figure 1. The essential components are:

(a) A 1-m analytical column packed with 60/80 mesh Chromosorb P coated 30% by weight with 1,2,3-tris-(2-cyanoethoxy)propane (TCEP).*

(b) A four-port switching valve.

(c) A removable subtractor column consisting of two sections:

(1) Ag_2SO_4/H_2SO_4 on 60/80 mesh Chromosorb W, and

(2) $PdSO_4/H_2SO_4$ on 60/80 mesh Chromosorb W.

(d) An analytical column packed with 13 cm of Chromosorb 105.

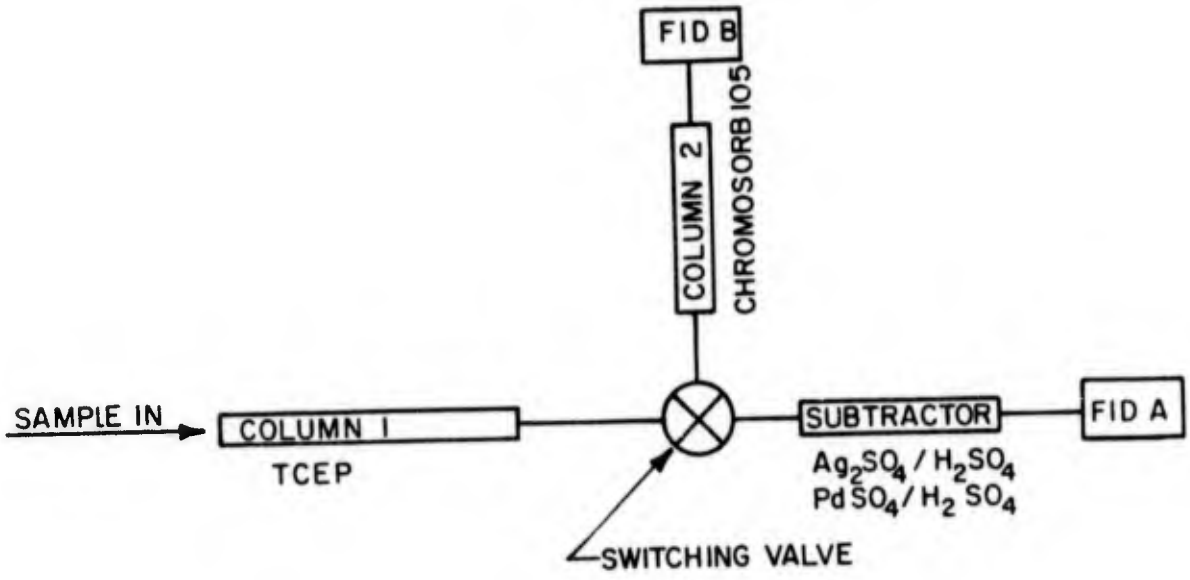

Figure 1. Analytical System

* C. A. Index name (1,2,3-Propanetrioxy)tris(3-propionitrile).

Brief descriptions of the functions of the various components of the column system follow.

A. TCEP Column.

The function of the TCEP column is to retard water and oxygenated and aromatic compounds while allowing paraffinic and olefinic compounds to elute relatively quickly. The column is maintained at 80°C during the analyses. The effectiveness of this column is illustrated by the retention data in table 2. Particular attention should be given to the retention time of n-decane (81 sec.) because previous studies by AFSAM identified this compound as the highest molecular weight saturated compound found in JP-4 exhaust. Consequently, a time corresponding to that required for the elution of n-decane has been chosen for switching the effluent from the TCEP column onto the Chromosorb 105 column. Figure 2 is a chromatogram of a synthetic mixture of representative organic compounds on the TCEP column.

Table 2. Retention Times of Various Compounds on 30% TCEP Column at 80°C (60 ml/min Flow Rate)

Compound	Retention times (sec)	r^{1} *
Methane	14	1.0
Methylcyclopentane	31	2.2
Hexane**	22	1.6
Octane	37	2.6
Decane	81	5.7
Dodecane	222	15.8
Propionaldehyde	128	9.1
Butryaldehyde	196	14.0
Valeraldehyde	323	23.1
Benzaldehyde	375	26.8
Allyl ether	168	12.0
Methylfuran	118	8.4
Methanol	258	18.4
Acetone	187	13.4
Methyl ethyl ketone	273	19.5
Benzene	241	17.2
Acetylene	16	1.1
2,2,4-Trimethyl-1-pentene	30	2.1
1-Nonene	60	4.3
1-Decene	92	6.6

* $r^{1} = RT_{cpd}/RT_{CH_4}$

** These are normal paraffins. The prefix n - is ordinarily understood (C. A. nomenclature).

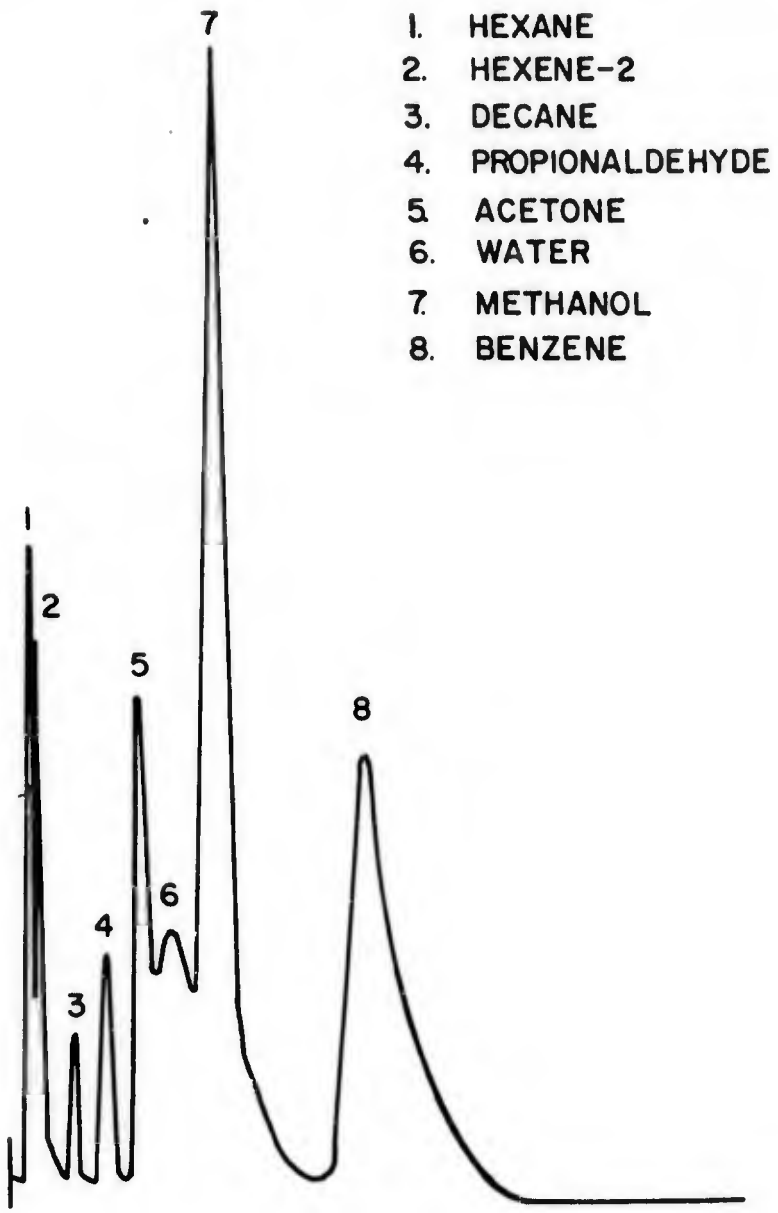

Figure 2. Peak Identification

B. Switching Valve.

The function of the switching valve is to direct the effluent from the TCEP column either into the subtractor (or directly into the FID if the subtractor is not in the system) or into the Chromosorb 105 column. The valve is switched at a predetermined time after injection of a sample. As explained above, this switching time corresponds to total elution of the n-decane peak. In the chromatogram of figure 2, the proper switching time is after peak 3 has passed from the TCEP column. Performing the valve switch in this manner causes olefinic and paraffinic compounds to pass directly into FID A (or into the subtractor if it is in the system), and water, oxygenated and aromatic compounds to pass into the Chromosorb 105 column. Oxygenated compounds which have shorter retention times than propionaldehyde on the TCEP column probably pass through with the olefins and paraffins before the valve switch. Acetaldehyde has been identified by AFSAM in JP-4 exhaust and is probably the only compound which need cause any concern in this respect. Provisions have been made for removing any light oxygenates which may be eluted before the valve is switched (see discussion of subtractor below).

C. Subtractor Column.

The function of the subtractor column is to efficiently remove olefinic and light oxygenated compounds from the effluent coming from the TCEP column before the valve is switched. Ag_2SO_4/H_2SO_4 is an efficient subtractor for the olefinic compounds, and $PdSO_4/H_2SO_4$ serves as a subtractor for any light oxygenated compounds (particularly acetaldehyde). The olefinic subtracting efficiency of the Ag_2SO_4/H_2SO_4 subtractor is illustrated by the data in table 3 and the chromatogram in figure 3. The efficiency of the $PdSO_4/H_2SO_4$ subtractor for removing oxygenated compounds is illustrated by the data in table 4. Of particular importance is the fact that paraffins are essentially unaffected by the subtraction process (see tables 3 and 4).

D. Chromosorb 105 Column.

Chromosorb 105 is a hydrophobic porous polymer which performs the function of allowing the water to pass quickly through the column while retarding the oxygenated and aromatic compounds. This function is considered important since it is feared that water, a major product of the combustion process, might adversely affect the analyses if it is allowed to elute at the same time as the peaks of interest. The Chromosorb 105 column is connected exterior to the oven by passing lines from the switching valve through the oven wall. It is wrapped with heating tape, allowing individual temperature control through a variac. The column is maintained at ambient temperature until the water has eluted, then heated to $\sim$150°C to facilitate the elution of the aromatic and oxygenated compounds. Typical operation of the Chromosorb 105 column is illustrated by the chromatogram in figure 4. The injection sequence used for this chromatogram simulates the order of elution from the TCEP column. Note that the very small response associated with the elution of water is the first to appear in the chromatogram .

E. The Total System.

Figure 5 is a chromatogram illustrating the operation of the complete system on a synthetic mixture of representative compound types. The shift in baseline occurring after peak 2 (decane) corresponds to the switching of the valve. Therefore, hexane and decane pass through the TCEP column and are detected at FID A. Water, propionaldehyde, acetone, methanol, and benzene pass through the TCEP column and the Chromosorb 105 column and are detected at FID B. The data obtainable from this system are divided into the following classifications:

Table 3. Efficiency of Ag_2SO_4/H_2SO_4 Absorbent (80°C)

Compound	Conc.	Efficiency, compound removed
	μg	%
n-Pentane	90	0
n-Heptane	19	1.11
n-Decane	2	3.07
Methylcyclopropane	37	1.41
2,3-Dimethylbutane	56	0.39
Acetylene	5780	100
Ethylene	12/3	99.4
2-Ethyl-1-butene	123	100
4-Methyl-1-pentene	121	100
1-Hexene	47	100
1-Octene	10	100
1-Decene	2	100
Benzene	78	100
Ethylbenzene	48	100

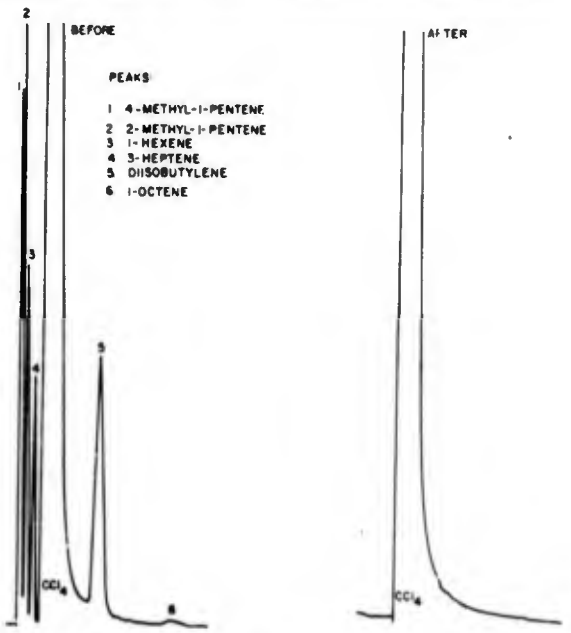

Figure 3. Chromatograms of Olefin Mixture Before and After Subtracting with Ag_2SO_4/H_2SO_4

Table 4. Efficiency of $PdSO_4/H_2SO_4$ Absorbent (80°C)

Compound	Conc.	Efficiency, compound removed
	μg	%
Acetaldehyde	100	99.1
n-Propionaldehyde	67	100
n-Butryaldehyde	22	100
Allyl ether	98	100
2-Methylfuran	125	100
Methyl acetate	53	100
Acetone	25	100
Methanol	19	100
n-Pentane	90	0
n-Heptane	19	0
n-Decane	2	0.1
Methylcyclopropane	37	0.24
2,3-Dimethylbutane	56	0.19

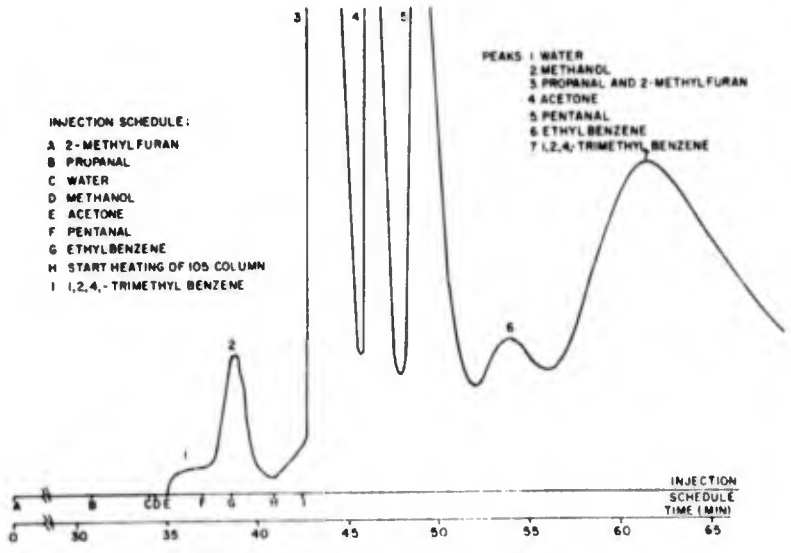

Figure 4. Typical Operation of the Chromosorb 105 Column

(1) total unreactive hydrocarbons (paraffinic compounds)
(2) olefins (+ acetaldehyde)
(3) oxygenates + aromatics
(4) total reactive hydrocarbons (nonparaffinic compounds)
(5) total hydrocarbons (THC)

In order to obtain the complete analysis, it is necessary to have two samples of known sample volumes taken under identical conditions. The first sample is analyzed without the subtractor in the system and yields the following data (see figure 1):

(1) FID A response = paraffins + olefins (+acetaldehyde)
(2) FID B response = oxygenates + aromatics

The second sample is analyzed with the subtractor in the system and yields the following data:

(1) FID A response = paraffins (total unreactive)
(2) FID B response = oxygenates + aromatics

Olefins (+ acetaldehyde) are obtained by difference by subtracting the FID A response of the second sample from the FID A response of the first sample. The total reactive hydrocarbon value is obtained by summing the values for olefins (+ acetaldehyde) and oxygenates + aromatics. A THC value is obtained by combining the total reactive and total unreactive hydrocarbon values. Note that for each analysis (either with or without the subtractor) a value is obtained for the oxygenate + aromatic content. Thus, in general, this value is more precisely determined than other values.

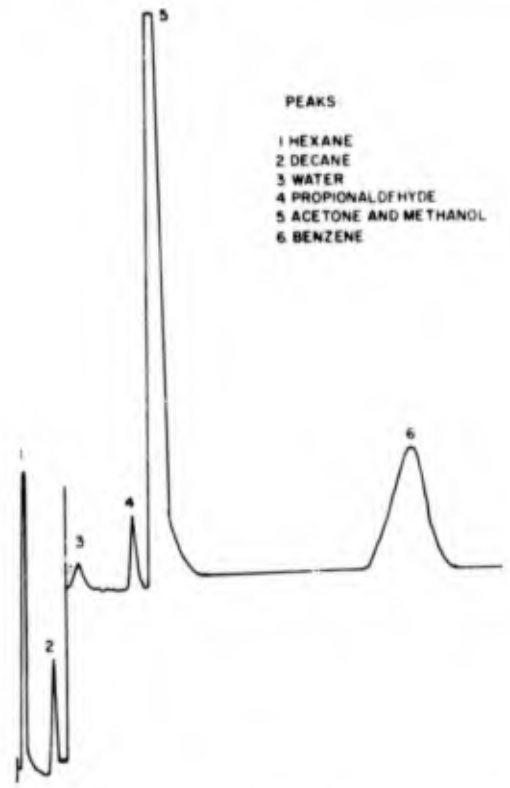

Figure 5. Operation of the Complete System

SAMPLING SYSTEM

Exhaust samples were collected on the combination sorbent trap illustrated in figure 6. The trap is constructed from 1/4-inch OD, 2-mm ID glass tubing and is packed with ∿5 cm of 60/80 mesh Tenax GC and ∿7 cm of 60/80 mesh Carbosieve B. The Tenax GC is used to trap the higher molecular weight organic compounds while the Carbosieve B captures the lower molecular weight compounds not retained by the Tenax GC. The tube is fitted with 1/4-inch Swagelok nuts so that it can be directly connected to the sample line and desorption system. A standard 1/4-inch Swagelok back ferrule is reversed and silicon rubber o-rings are placed on the tube ends to seal the connections of the trap in the sampling and desorption systems. Standard 1/4-inch Swagelok caps are used to seal the tubes during transport and storage.

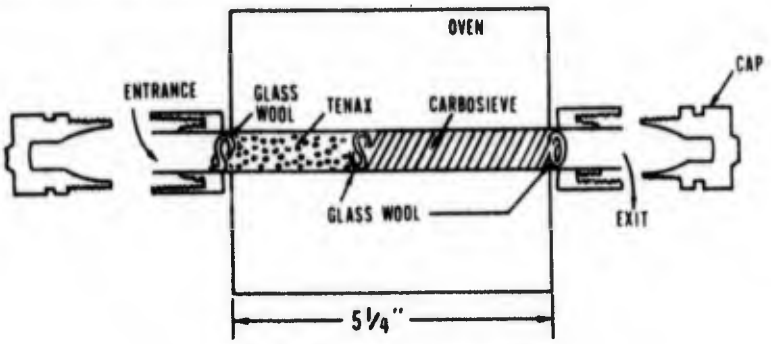

Figure 6. Adsorption Tube in Oven: 1/4-inch OD Glass

The sorbent traps are cooled to -78°C with crushed CO_2 during sampling and storage. Cooling is accomplished by placing modified styrofoam cups around the traps to contain the dry ice. This system has proven to be reasonably effective and inexpensive.

Figure 7 illustrates the actual sampling arrangement used to collect exhaust samples from a T-56 combustor rig at the Air Force Aero Propulsion Laboratory (AFAPL). The valving system makes possible the accomodation of two adsorption tubes. One tube serves as a dummy for regulating the flow rate to 50-100 cc/min. The flow rate is continually monitored so that the total sample volume can be determined. The exhaust sample line is heated to ∿300°F. The adsorption tubes are connected so that the sample passes first through the Tenax GC, then through the Carbosieve B. While the actual samples were being collected, a Beckmann Model 402 total hydrocarbon (THC) analyzer provided continuous on-line THC data.

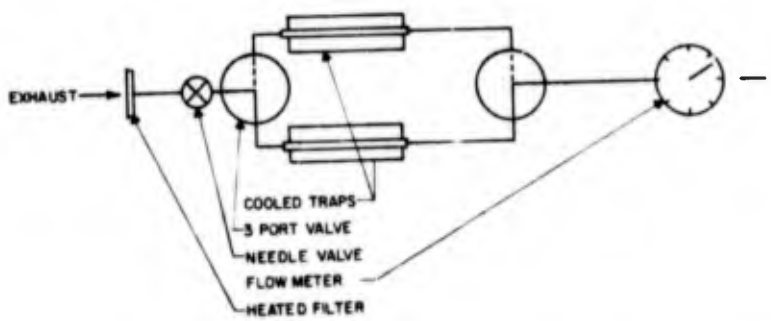

Figure 7. Sampling Arrangement to Collect Exhaust Samples from a T-56 Combuster Rig

The exhaust samples are desorbed into the chromatographic system by means of a modified Hewlett-Packard Model 19021A heated gas-sampling valve. One of the sampling valve loops has been cut and fitted to accomodate the 1/4-inch Swagelok connection of the adsorption traps. This makes possible the switching of the sample trap into the system as shown in figure 8. The desorption is facilitated by means of the specially designed tube furnace. The sorbent traps are heated to 350° to 400°C during the desorption cycle.

Exhaust samples were collected from the T-56 combustor rig at AFAPL using JP-4, JP-5, JP-8, isooctane, and DEL-5 fuels at various inlet pressures.

JP-4, JP-5, and JP-8 are standard military blends used by DOD aircraft. Isooctane was run to compare a pure fuel with the nonhomogeneous fuels. DEL-5 is a specially blended fuel made by adding 1.6 weight percent pyridine to the stock JP-4 fuel and additionally increasing the aromatic content of the fuel from ∼12% to 25%. The DEL-5 was prepared to simulate more closely fuels which may be obtained from alternative sources such as shale oil.

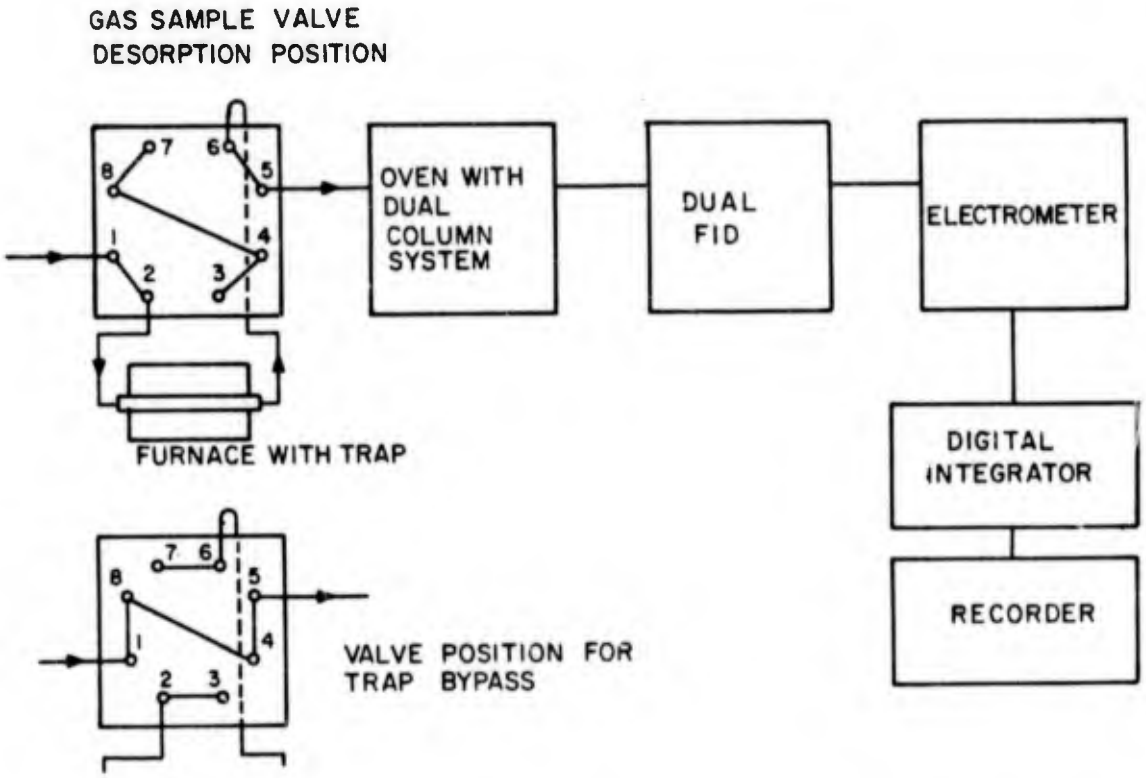

Figure 8. Schematic Diagram Revealing How Sample Trap is Switched into the System

CHROMATOGRAPHIC ANALYSIS

A chromatogram typical of the actual exhaust sample analyses is shown in figure 9. The important events in the analytical sequence are noted on the chromatogram. The first peak is labeled "paraffins" signifying that this particular analysis was performed with the subtractor in the system. The "column switch" designation corresponds to the time at which the effluent from the TCEP column is directed into the Chromosorb 105 column. The area of the chromatogram labeled "reconcentration period" represents the period of time while the Chromosorb 105 column is maintained at ambient temperature to allow the water to pass through. The point at which heating of the Chromosorb 105 column begins is indicated on the chromatogram. After this, the oxygenates and aromatics are eluted as shown by the labeled area of the chromatogram. The final peak of the chromatogram labeled "excess area" is an impurity peak that appears in the baseline when the Chromosorb 105 is heated. This area is routinely discarded from the chromatogram by dropping a perpendicular in the manner indicated.

All samples were subjected to the analytical sequence described above, and the areas corresponding to the different portions of the chromatogram were automatically recorded by the Autolab System IV integrator.

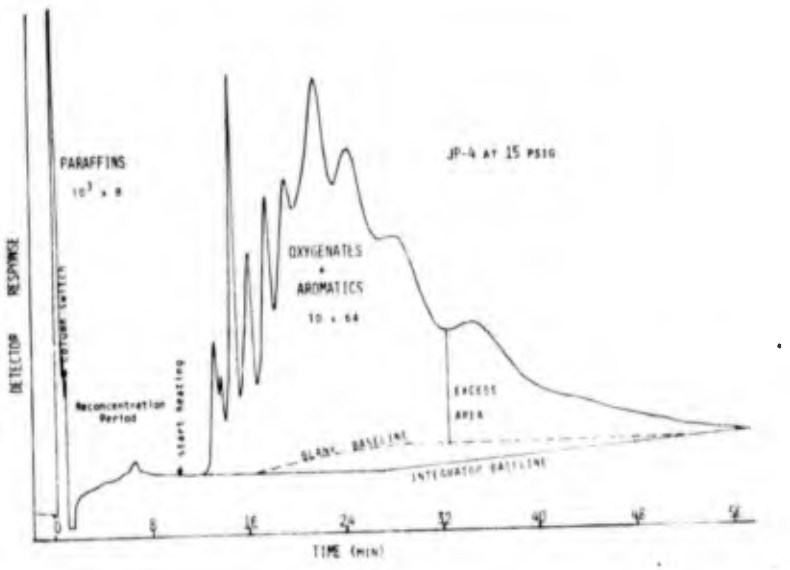

Figure 9. Chromatogram Typical of Actual Exhaust Sample Analysed

SUMMARY OF ANALYTICAL RESULTS

Table 5 lists the average values in terms of ppm C for the various hydrocarbon classifications at the different test points. The percent composition of the exhaust is tabulated in table 6. The term "unreactive" is defined as all paraffinic compounds and "reactive" includes all nonparaffinic compounds. Figure 10 is a graphical representation of JP-4 data at various power settings. The uppermost point at each of the inlet pressure settings is the THC value obtained by the on-line THC analyzer at the time the sample was collected.

Table 5. Hydrocarbon Analyses Summary, ppm C

Fuel (pressure)	Olefins + lt. oxygenates	Oxygenates + aromatics	Total reactive	Total unreactive	THC
JP-4 (15 psig)	54.6	257	312	118	430
JP-4 (33 psig)	22.8	52.5	75.4	13.6	89.0
JP-4 (50 psig)	10.2	17.0	27.3	1.88	29.2
JP-5 (33 psig)	–	77.7	–	–	117
JP-8 (33 psig)	–	81.7	–	–	110
DEL-5 (33 psig)	16.7	50.8	67.5	6.48	74.0
DEL-5 (33 psig)	18.2	62.4	80.6	11.4	92.0
Isooctane (33 psig)	6.82	7.33	14.1	8.70	22.8

Table 6. Composition of the Exhaust

Fuel (pressure)	Percent olefins + lt. oxygenates	Percent oxygenates + aromatics	Percent reactive	Percent unreactive
JP-4 (15 psig)	12.7 (8.6)*	59.8 (40.4)	72.6 (49.1)	27.4
JP-4 (33 psig)	25.6 (13.8)	59.0 (31.8)	84.7 (45.7)	15.3
JP-4 (50 psig)	34.9 (17.9)	58.2 (29.8)	93.5 (47.9)	6.4
JP-5 (33 psig)		66.4 (23.1)		
JP-8 (33 psig)		74.3 (40.2)		
DEL-5 (33 psig)	22.6 (14.8)	68.6 (45.0)	91.2 (59.7)	8.8
DEL-5 (33 psig)	19.8 (11.8)	67.8 (40.5)	87.6 (52.3)	12.4
Isooctane (33 psig)	29.9 (21.3)	32.1 (22.9)	61.8 (44.1)	38.2

* Numbers in parentheses represent percentages compared to APL THC results.

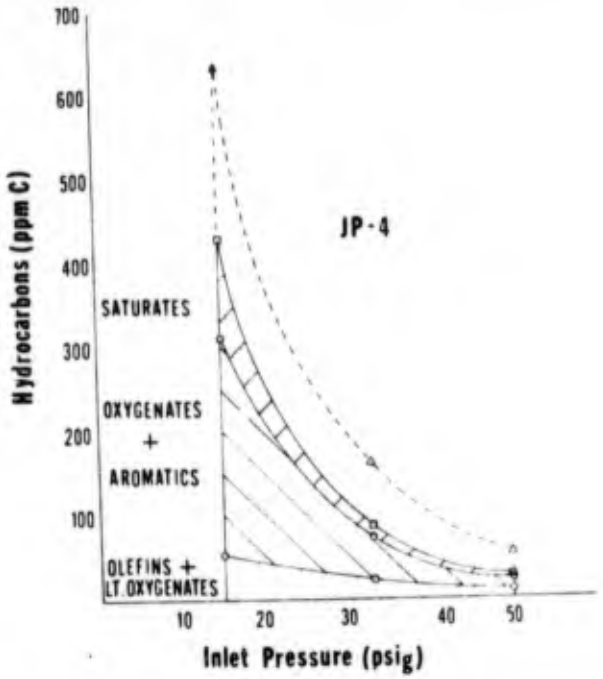

Figure 10. JP-4 Data at Various Power Settings

Some tentative conclusions can be drawn from the data obtained:

(1) The major portion of the hydrocarbon exhaust from all fuels tested is reactive in nature.

(2) For a given fuel, the percentage composition of reactive compounds increases as the power is increased.

(3) There is a general decrease in absolute concentration of all classifications of compounds as the power is increased.

(4) The distribution of hydrocarbon species into the various classifications does not differ appreciable for JP-4 compared to DEL-5 even though DEL-5 is JP-4 with increased aromatic content.

(5) Greater than 55% of the THC sampled from actual jet fuels was classified as either aromatic or oxygenated.

(6) The pure isooctane showed marked reduction in the THC compared with actual jet fuels and had the highest percentage contribution from unreactive compounds.

CHEMILUMINESCENT MEASUREMENT OF SUB-PPM CONCENTRATIONS OF VINYL CHLORIDE AND CERTAIN LOW-MOLECULAR-WEIGHT UNSATURATED HYDROCARBONS

by

Ralph Baumgardner, W. A. McClenny, B. E. Martin and R. K. Stevens
ENVIRONMENTAL PROTECTION AGENCY
National Environmental Research Center
Chemistry and Physics Laboratory

SUMMARY

During the past year with disclosure of a possible relationship between exposure to vinyl chloride and a rare liver cancer, monitoring and analysis of trace concentrations of vinyl chloride have become increasingly important.

Standard exposure limits have been set for employees in the vinyl chloride industry which require monitoring in the ppm and sub-ppm range. EPA is presently monitoring ambient air in the vicinity of vinyl chloride production and processing plants to establish a data base for setting emission standards. More sensitive and specific detection methods will be needed for survey monitoring of residential areas adjacent to sources of vinyl chloride.

Current techniques for field monitoring of vinyl chloride center on a 24-hour integrated sample collected on charcoal with subsequent extraction with carbon disulfide and analysis by gas chromatography (GC) using a flame ionization detector (FID). Direct analysis of air samples by GC-FID is also used. Both methods can be used to detect vinyl chloride concentrations as low as 0.01 ppm. Other continuous and semicontinuous techniques for monitoring vinyl chloride have been sought for greater simplicity, fewer maintenance problems and greater specificity.

A new technique has been developed which allows the detection of sub-ppm concentrations of vinyl chloride plus detection of similar low-molecular-weight unsaturated hydrocarbons. This technique is a combination of chemiluminescence detection and chromatographic separation. The chemiluminescence results from the gas phase reaction of ozone and the unsaturated compound. Specificity for this technique is obtained from the chromatographic separation and from lack of response from compounds which do not chemiluminesce.

In early 1974 experiments were initiated to determine the possibility of detecting vinyl chloride by reacting it with excess ozone and measuring the intensity of the luminescence. A diagram of the reaction chamber used is shown in figure 1. The inside of the chamber is teflon coated with a glass face at one end. The face of the reaction chamber was coupled with a cooled photomultiplier tube. Concentric flow tubes, one of teflon carrying the vinyl chloride sample, the other of stainless steel containing the ozone, allow the reactants to meet near the face of the detector cell. The ozone-vinyl chloride reaction takes place at atmospheric pressure with a spectral intensity centered at 4000°A.

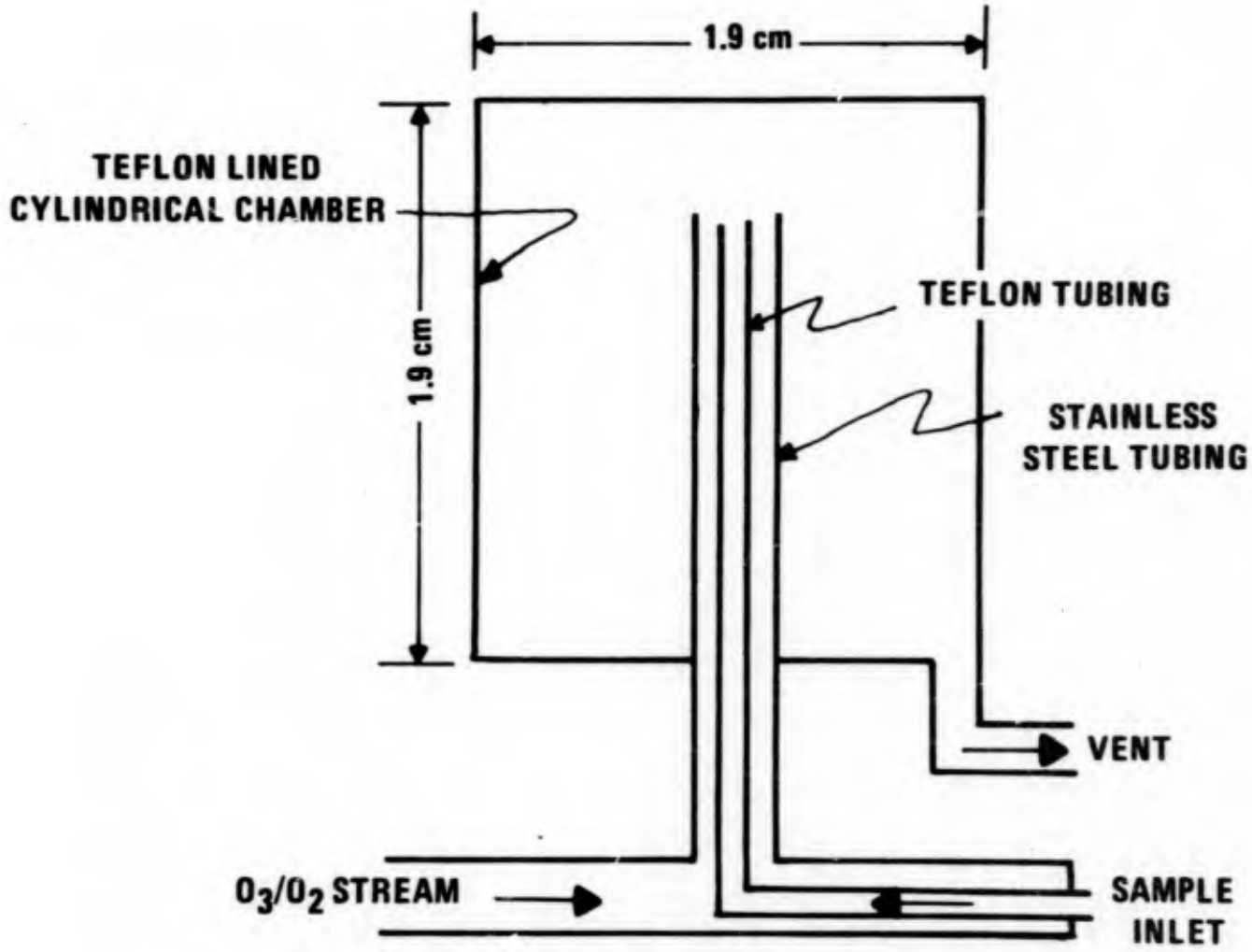

Figure 1. Chemiluminescence Detector

The responses of other unsaturated compounds were also obtained to determine potential interferents and to determine whether other unsaturated compounds could be detected by use of this technique. The response curves are shown in figure 2. A number of other compounds give a response equal to or greater than vinyl chloride; therefore separation of vinyl chloride is necessary for specific detection.

Chromatographic separation of vinyl chloride has been documented and column packing was available commercially. A chromatographic system was constructed which utilized a chemiluminescence detector, a gas-sampling valve and chromatographic column. A chromatronix chemically inert gas-sampling valve was used to bring the vinyl chloride sample into the system. Nitrogen was selected as a carrier gas and the optimum carrier gas flow for the system was found to be 30 cc/min. The chromatographic column which gave the optimum signal and resolution was a 10-ft. teflon tube 3/16-in. OD packed with 0.4% carbowax 1500 on carbopack A. No increase in signal response or resolution was obtained using columns of larger diameters and increased lengths. Column temperature was not controlled and varied from 23 to 25°C. Ozone flow was optimized to 30 cc/min and a concentration of 2%. The reaction chamber was coupled to a RCA 4501 photomultiplier tube which had a peak response at 4500 A°. Signals obtained from the detector were measured using a Keithly model 417 picoammeter (figure 3).

Figure 4 shows a typical calibration curve for vinyl chloride. Additional calibration data taken with a 25-cc sample loop indicate a full-scale response of 0 to 1 ppm with a noise equivalent concentration of 30 ppb and a minimum detectable limit of 60 ppb.

Figure 5 gives the chromatographic separation of vinyl chloride from similar unsaturated hydrocarbons using the chemiluminescent-GC system. Baseline separation of vinyl chloride is possible and sufficient resolution is present to permit the quantification of a number of other compounds. The chromatographic conditions could be optimized for each compound of interest.

CONCLUSIONS

An analysis technique has been developed which for the first time combines the chemiluminescent detector with chromatographic separation for measurement of trace compounds. Detection of vinyl chloride in the ppm and sub-ppm range with a linear signal from 0 to 10 ppm and a noise equivalent concentration of 30 ppb is possible. Trace concentrations of propylene, ethylene, and 1,2-dichloroethylene can also be measured with this system. No compounds have been found to interfere with the detection of vinyl chloride. A field monitor fabricated with use of the above technique would have an advantage of simpler operation, portability and specificity over existing procedures.

A more detailed account of this technique has been submitted to Environmental Science and Technology for publication.

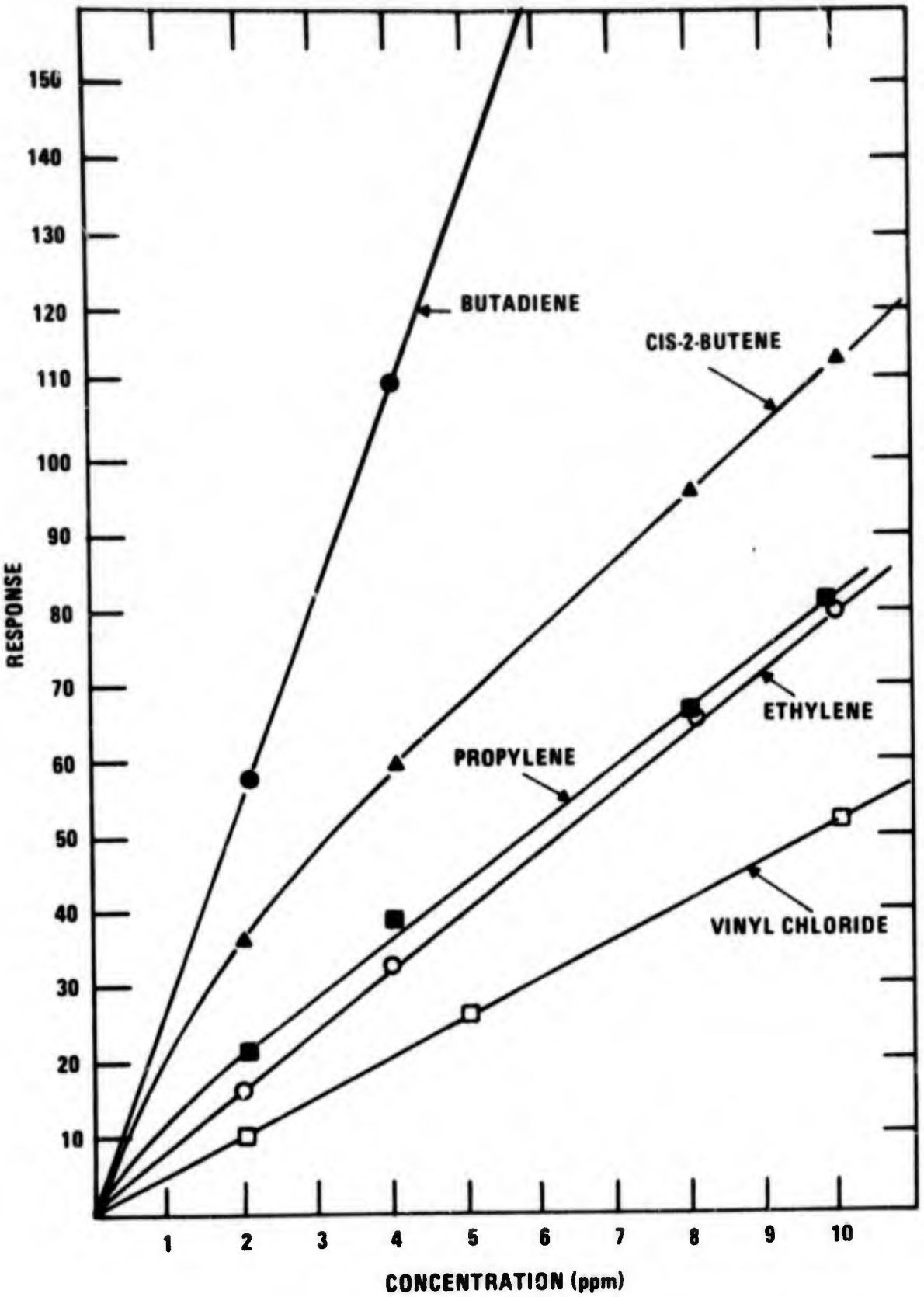

Figure 2. Response of Unsaturated Hydrocarbons Versus Concentration in ppm

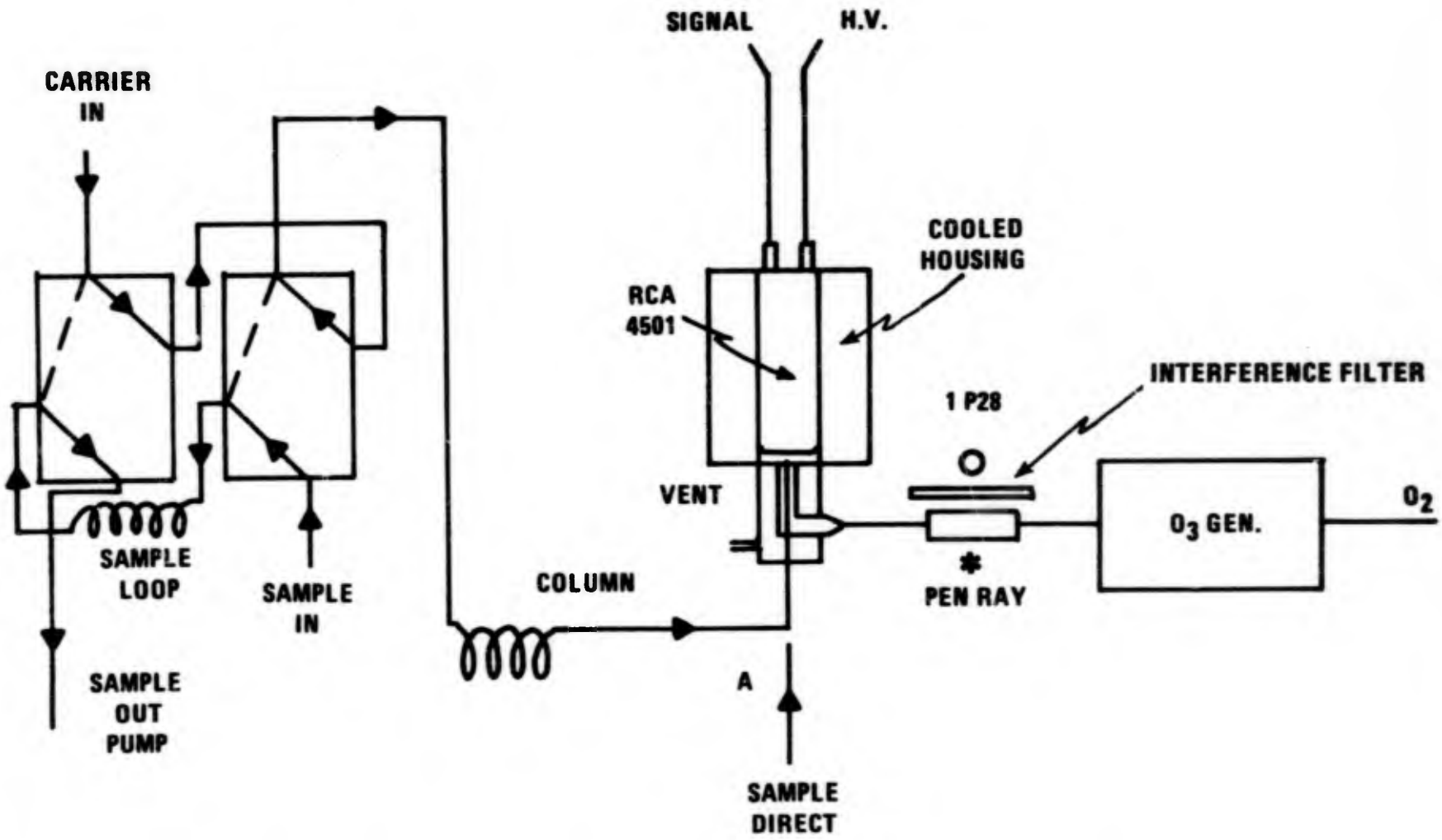

Figure 3. Diagram of Gas Chromatographic – Chemiluminescence Detector System

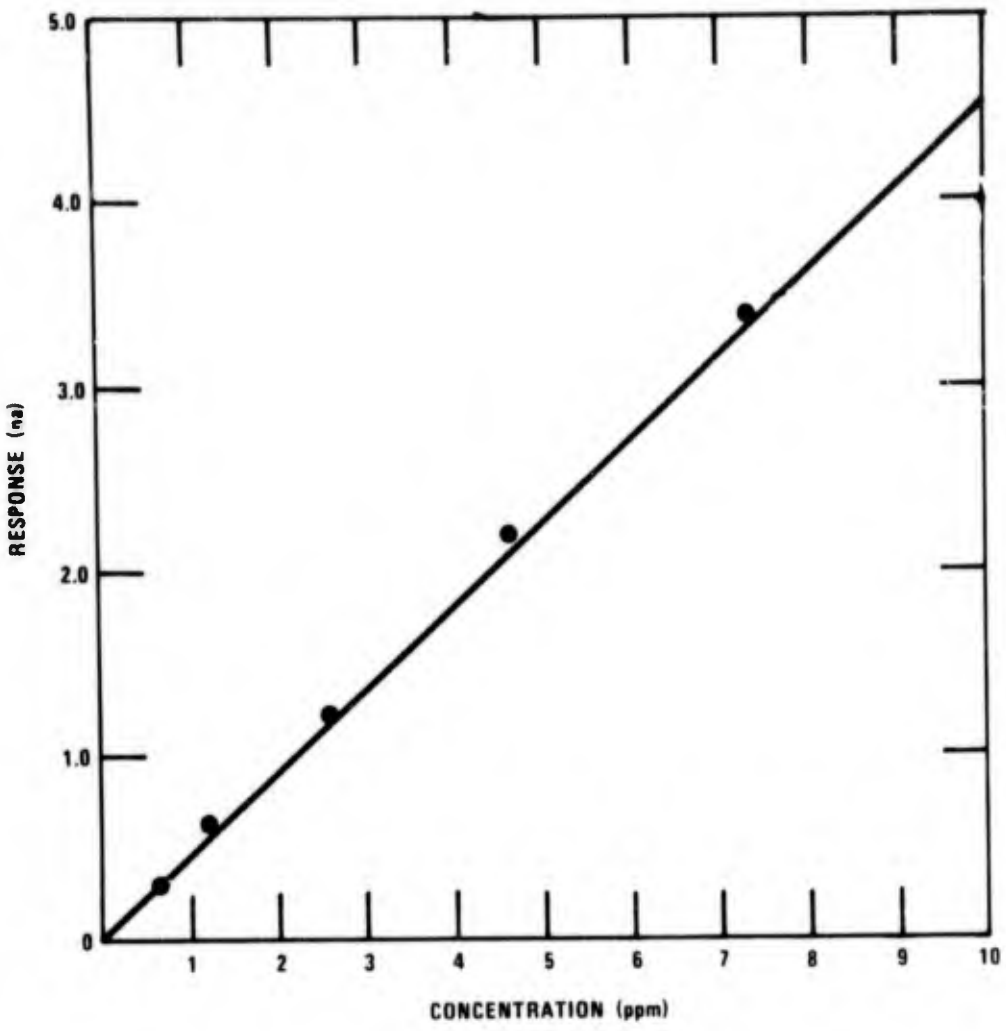

Figure 4. Calibration Curve for Vinyl Chloride

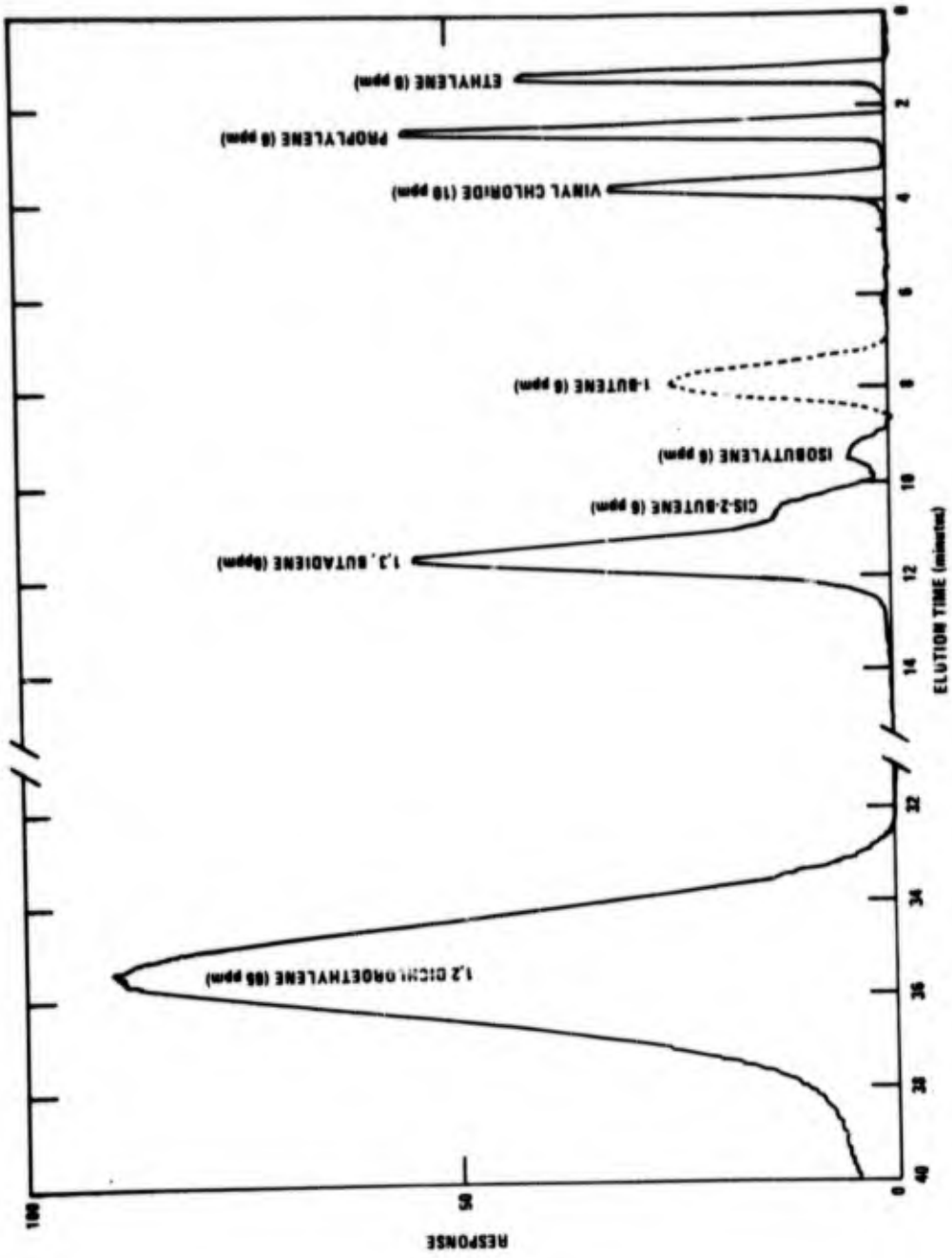

Figure 5. Chromatogram from GC-chemiluminescence System Showing Vinyl Chloride Separation
Conditions are column 10 ft. X 3/16 in. packed with 0.4% carbowax 1500
on carbopack A, temperature 23°C. ozone flow 30 cc/min. carrier flow
30 cc/min N_2, sample size 10 cc.

NEEDLE IN THE HAYSTACK ANALYSIS

by

Walter C. McCrone
McCrone Associates, Chicago, IL 60616

Trace analysis involves the detection of very low percentages of a substance in a relatively large sample. The trace, perhaps a part per billion in concentration, may be homogeneously distributed throughout the matrix or it may be present as discrete particles heterogeneously distributed. Examples might be asbestos fibers in Lake Superior water (heterogeneous) or mercury compounds dissolved in Mississippi river water (homogeneous).

Ultramicroanalysis describes the identification of very small samples single subnanogram particles, of relatively pure substances. The two types of analysis overlap when the trace component is heterogeneously distributed throughout a matrix. Each particle of the trace component is an ultramicroanalysis problem.

The polarizing microscope is an ideal tool for most ultramicroanalytical problems. If the partle can be magnified microscopically to the size of recognizable macroscopic objects, e.g., a car key, anchovy olive or a dime, we should expect to be able to identify it if we have seen it before and remember what it is or if we can refer to a reference set of pictures that includes the unidentified object (figures 1-4). Identification is based on observation of a group of obvious "identifying characteristics" such as size, shape, surface texture, transparency, color, refractive index (relative to the mount) and birefringence. These characteristics register almost instantaneously on the retina and in the brain and trigger the memory bank to identify the substance.

If the memory bank fails, additional identifying characteristics must be measured until the particle is identified. These additional characteristics include refractive indices, dispersion staining and other optical properties measurable by polarized–light microscopy. Also included, however, are x-ray or electron diffraction patterns; shape, size and surface texture by scanning or transmission electron microscopy; and elemental analysis by energy- or wavelength-dispersive x-ray analysis or by mass spectrometry using the ion microprobe. Very few particles characterized by one or more of these techniques fail to yield their identity.

Since all of these techniques, from polarized-light microscopy to the ion microprobe, are designed to determine significant identifying characteristics of microscopic objects we term the application of all of these tools and techniques microscopy. We begin each analysis with the simplest and quickest of these microscopical techniques, polarized-light microscopy. When necessary we continue through micro x-ray diffraction to electron microscopy and the microprobes until the particle is identified. Most often, the particle is identified at the first stage because we have a group of optical microscopists (with good memory banks) who can identify many thousands of particles at sight. The identification is so rapid that the results of an analysis of a sample containing many different substances will be tape-recorded. A small portion of a typical recording of a dust sample analysis might be transcribed as: coal (30 μm), quartz (2 15 μm particles), glass wool (15 × 300-μm), paper fiber (25 × 200-μm), brass machining chip (50-μm), power plant flyash (3 10-μm particles, 3 20-μm and 5 30-μm), limestone (50 particles <2-μm 20 5-μm, 2 30-μm and 1 50-μm particles), molding sand (100-μm), incinerator ash (10 particles 10- to 100-μm) etc. Identification and estimated dimensions take only as long as it takes to dictate the name and size.

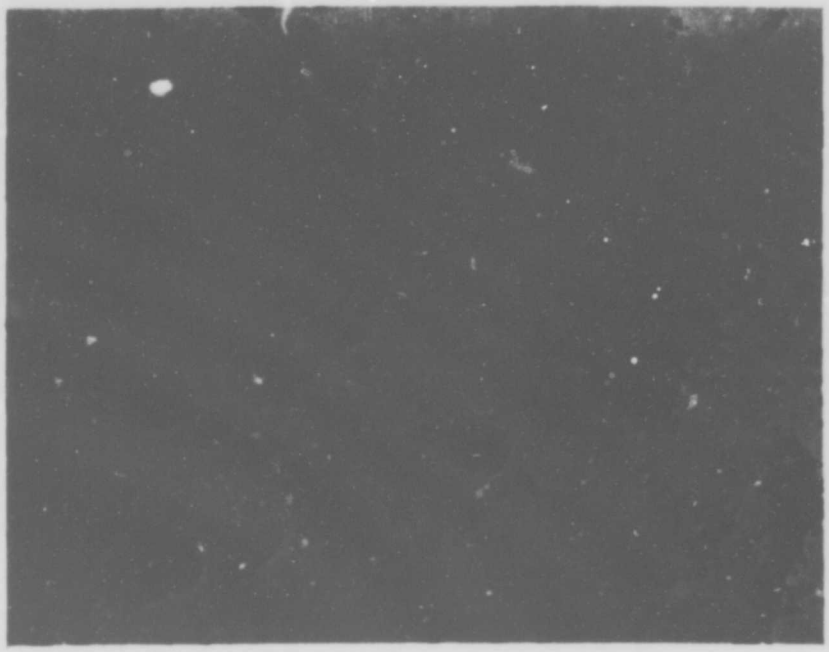

Figure 1. Pulverized Coal Boiler Flyash from a Power Plant Stack, Slightly Uncrossed Polars, Top Light, 200X

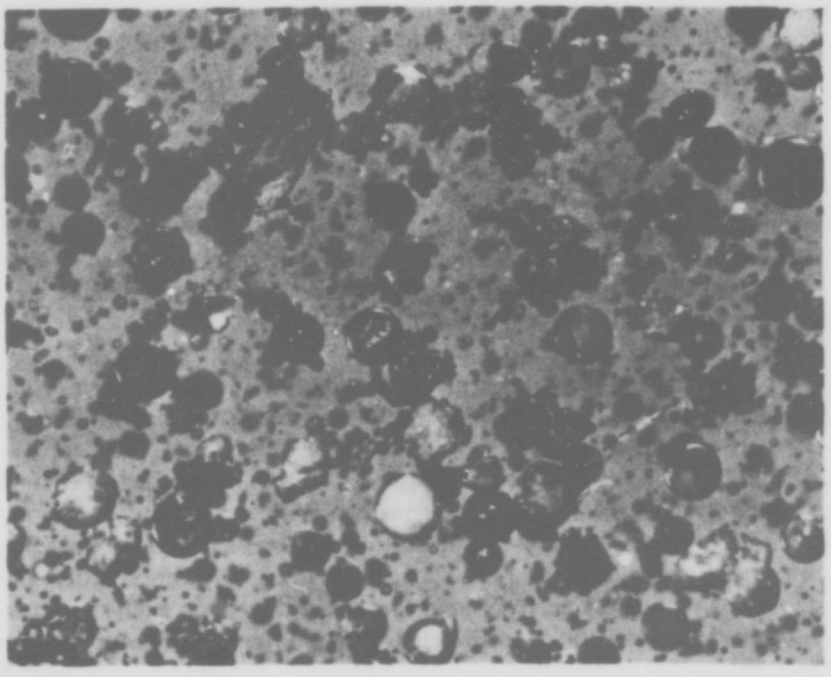

Figure 2. Oil Soot, Slightly Uncrossed Polars, Top Light, 200X

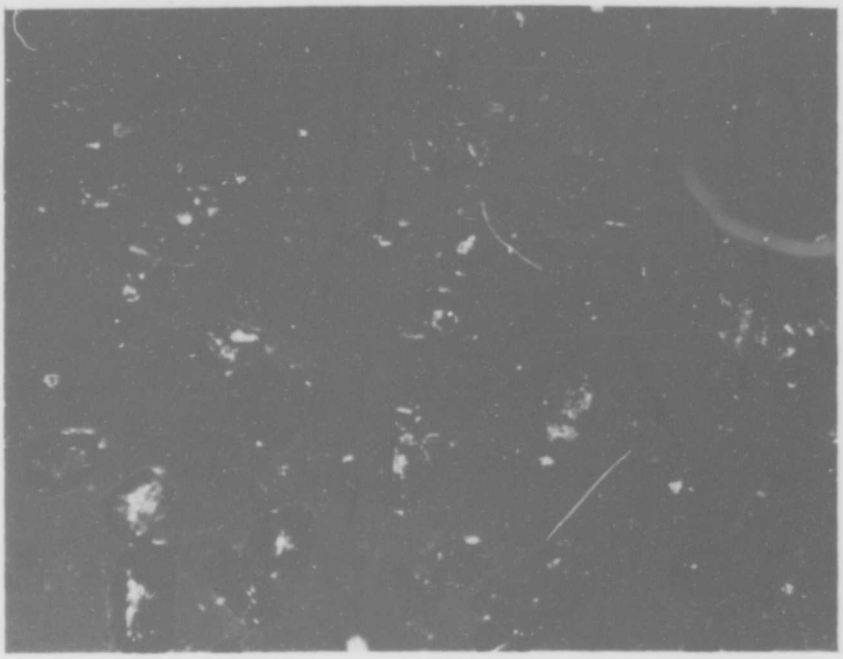

Figure 3. Foundry Sand, Slightly Uncrossed Polars, Top Light, 200X

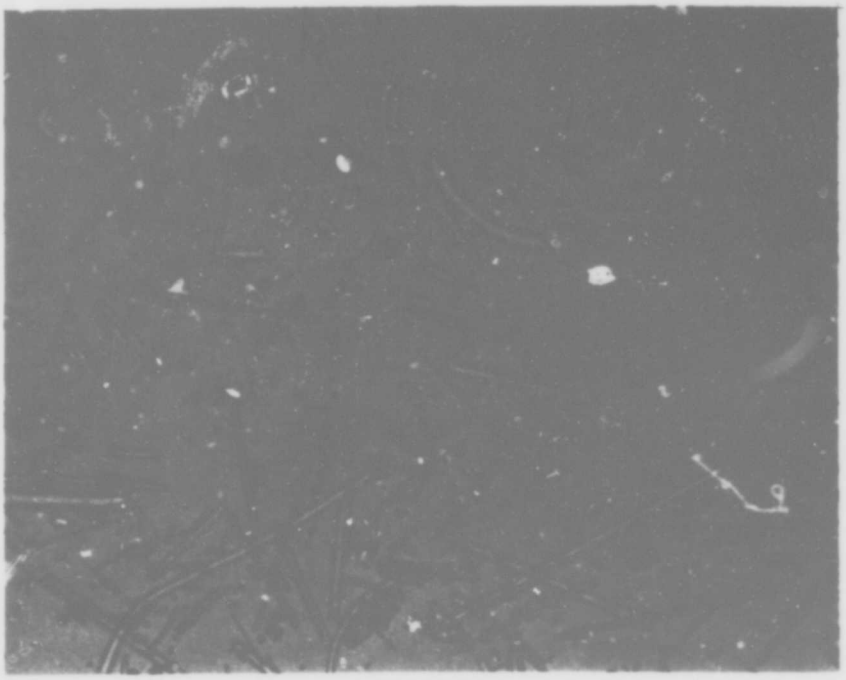

Figure 4. Mineral Wool, Slightly Uncrossed Polars, Top Light, 200X

Any particles not identified, if important enough, are isolated, washed clean and remounted for electron microscopy, microprobe or diffraction (figures 5 and 6). Fewer than 10 percent of unknown particles submitted for analysis require more than optical microscopy. This 10 percent, however, presents problems not the least of which is mounting on the proper substrate in such a way that the microanalyst can find each particle quickly and unequivocally. Although finder grids can be used for transmission electron microscopy, mounting a 1- to 5-μm particle at a specific spot on a highly polished beryllium surface requires great skill. We have a group of highly trained microscopists led by Anna Teetsov who manipulate and mount single tiny particles for all of the electron optical instruments. To make certain that the operators of these instruments quickly and dependably find the proper particle these girls draw tiny pictures a few tenths of a millimeter high on the bery'lium plate (figure 7). The microprobe operator is told to look for a meter high on the berryllium plate. The microprobe operator is told to look for a sailboat, bird, airplane, horse etc., and to analyze the particle on the mainsail, in the bird's eye, on the horse's tail etc. This apparent bit of whimsy has greatly aided the analyst in finding the proper particle quickly and confidently.

The methods used are the same whether the sample is river silt, atmospheric particles, moon dust, soil, or particles from parenteral solutions, hydraulic fluids, mine dust, clogged filters or industrial stacks. All particles in the sample can be identified or we can look for specific substances, e.g., in the sample there can be identified or we can look for specific compositions, e.g., asbestos in talc, free silica in mine dust, or explosive residues from a bombing or safe insulation in dust vacuumed from a burglar's clothing. Sometimes one or a few single particles must be identified, e.g., exotic crystals in human tissue, contaminants in drugs, foods, metals, polymers, paper etc. Finally, two samples often must be compared for identity of composition and source. This includes glass from the crime scene and glass on the shoes of a suspect or a hair from the crime scene with the hair from a suspect. The methods outlined above can solve all of these problems and, equally important, no other analytical methods would do the job except in special cases, e.g., DTA to detect chrysotile asbestos in talc. Even here microscopy does a superior job since it also sizes the fibers and often designates the particular source for that sample.

It is difficult to see why methods as powerful as these are not more often used.

Figure 5. Electron Microprobe Analyzer as Used for Small Particle Analysis

Figure 6. Ion Microprobe Analyzer

Figure 7. Two Pictures Drawn on Highly Polished Beryllium Plate as Keys to Location of Particles for Probe Analysis, Brightfield Top Light, 200X

SESSION III

Chairman: Mr. Joseph Hirata
US Drug Enforcement Administration

A DAY IN THE LIFE OF "CHOPPER"

by

Guy T. Barry, Ph.D., Deputy Director
Technical Services Division, US Customs Service, Washington, DC 20229

This is a film that illustrates the use of a biosensor by the US Customs Service to interdict contraband drugs in vehicles, packages and cargo at more than 300 ports of entry into the United States of America.

Despite the effectiveness of the biosensor dog in the examination of vehicles and mail packages, the use of this technique has several limitations. These include, among others, the nonpermissible use of dogs to examine people. As more than 200 million persons entered the United States during the 1975 fiscal year, it is apparent that no more than a fraction of these could be closely examined. Other mechanical sensor techniques are needed for examination to supplement the dog in the interdiction of drug contraband.

This future mechanical dog must be inexpensive, rugged, portable and have a high degree of reliability that will permit rapid examination in a large variety of operational conditions and environments that include people, ships, containers, mail cargo and all types of vehicles. The purpose of showing the film was to demonstrate some of the workday tasks that US Customs Service personnel have to do at the border and at ports of entry in the performance of the agency's mission. The development of a mechanical sensor to supplement the biosensor dog for drug interdiction is a major goal of the service. The successful design of a suitable mechanical sensor is posed as a challenge to those chemists and engineers present who are engaged in trace analysis detection and who are interested in assisting the Government to control the drug menace.

DETECTION OF VAPOR PHASE COMPOUNDS OF ILLICIT NARCOTICS

by

D. Hagel,* V. Laverty,* J. Santo,* and A. Fein**

SUMMARY

A number of adsorbents were tested for their collection efficiencies towards vapors associated with illicit narcotics. The purpose of the study was to characterize these vapors and evaluate the feasibility of developing a field instrument for detection of illicit drugs. Various metals, metal oxides, organic polymers and active carbon were screened as adsorbents, using GC, or GC-MS for analysis. A number of characteristic compounds were found to be associated with most of the drugs and were appreciably preconcentrated by various adsorbents. Based on the study, it appears feasible to develop a field detector for these materials.

INTRODUCTION

HYDRONAUTICS, Incorporated recently completed the first phase of a research program sponsored by the Drug Enforcement Administration.†

The purpose of the program was twofold; to identify and characterize compounds present in the vapor phase of *street samples* of seven types of narcotics (hashish, marijuana, marijuana resin, opium, morphine and heroin) and to evaluate the potential of the development of a field instrument for detection of illicit narcotics based on preconcentration of characteristic vapors associated with them. Complete chromatographic separation of hashish and marijuana resin vapors would require a capillary column, but as the study was a practical, qualitative, feasibility study, standard packed columns were used. Because the active compounds of these drugs have extremely low vapor pressures, there would be little chance to detect their vapors in field situations; however, other compounds that are inherent with the drugs such as the terpenes (in the cannabis and opium drugs' decomposition products), or manufacturing byproducts and impurities may serve as good indicators for the presence of illicit narcotics.

INSTRUMENTATION

The study was performed using an existing vapor preconcentrator, the Vapor Trace Sampler (VTS) which was originally developed in HYDRONAUTICS (Israel) for selective preconcentration of vapors of explosives. VTS Teflon plugs (figure 1) containing various adsorbents were used for testing the collection characteristics. A few modifications of the VTS allowed control of sampling rate and desorption temperature (between 200-250°C depending on the adsorbent used).

* HYDRONAUTICS, Incorporated, Laurel, Maryland.

** US Drug Enforcement Administration, Washington, DC

† Under contract No. J-LEAA-032-73.

The adsorbent materials tested were of four types:

- Metals: Pt, Pt-black, Nickel, Tungsten, and Palladium
- Metal oxides: SiO_2 and Al_2O_3 (coated on Pt or Ni wires)
- Polymers: SE-30, OV-17 and Texsil 400 (coated on Pt wire) and
- Active carbon (particles trapped in coiled Pt wire)

The preconcentrating unit of the VTS, the Teflon plug (figure 1) is installed in a stainless steel housing and during its operating cycle, it assumes three functional positions (figure 2):

- Sampling
- Purging of nonadsorbed vapors, and
- Injecting the sample, which is desorbed of adsorbent by heat supplied via electrical leads, into the GC column.

RESULTS

A summary of the results can be illustrated by a few representative figures and chromatograms, as follows:

Preconcentration-efficiencies and Characteristics

Figure 3 – presents a chromatogram of hashish headspace vapors, introduced to the GC by syringe injection (with no preconcentration). It can be seen that the concentration of high-molecular-weight compounds (far end of the spectrum) is considerably lower than the low-molecular-weight ones, an obvious result of their lower volatility.

Figure 4 – shows the difference in adsorption characteristics between Pd, NiO, SiO_2, and W, (the upper chromatogram represents a typical pattern obtained for this group of adsorbents) and Al_2O_3 (compare to figure 3). Whereas the Pd, NiO, SiO_2, and W, with decreasing efficiency, preferentially preconcentrate the high MW end of the spectrum and do not preconcentrate the low MW fraction, the Al_2O_3 preconcentrates low MW volatiles with high efficiency (note sensitivities and sampling time) while the high MW compounds are less efficiently collected.

Figure 5 – illustrates a comparison of the collection characteristics of active carbon and Al_2O_3 for headspace vapors of marijuana resin. It seems that the carbon preconcentrates very efficiently the whole range of volatiles of the marijuana resin (the same is true for other cannabis drugs) whereas Al_2O_3 has little affinity for high MW compounds, but very similar efficiency to carbon for low MW compounds.

Figure 6 – illustrates the configuration of the adsorbent in the VTS preconcentrator valve. The wire coil which entraps the charcoal particles is tight, and the loops are actually touching each other, thus blocking the contact between the sampled air and adsorbent; the estimated collection efficiency is less than 7.3% based on volume ratios.

Figure 7 – Despite the low collection efficiency, the preconcentration effect is still very high. The figure compares the result of syringe injection of a volume of hashish vapors equivalent to the volume of the adsorption channel, with sampling and preconcentrating for 3 minutes using an active carbon adsorbent in the configuration shown in figure 5.

Figure 8 – presents chromatograms obtained by preconcentrating opium vapors, using two different adsorbents. A very similar pattern can be observed for both.

Figure 9 – presents chromatograms obtained by preconcentrating morphine and cocaine headspace vapors. Surprisingly similar patterns are obtained for the two unrelated drugs, hinting perhaps to similar impurities present due to manufacturing processes.

Figure 10 – Using Al_2O_3 and Ni as adsorbents, for preconcentrating cocaine it was possible to detect (although in low concentration) a relatively high MW compound, at 175° oven temperature. The humps present in the high-temp range of the chromatograms in figure 9 indicate the existence of these compounds. The Ni adsorbent did not preconcentrate this compound until it got oxidized in repeated use.

Figure 11 – Although the heroin sample used was about two years old, a very small peak was persistently obtained after preconcentrating its headspace vapors on a Pd wire.

Figure 12 – summarizes qualitatively the collection efficiencies of the adsorbent materials tested for the various drugs.

Identification GC-MS Analysis

In order to characterize the vapors associated with the narcotics samples, the preconcentrator was interfaced with the GC-MS unit equipped with a data system

A quadrupole MS with a single-stage separator was found to be the most suitable for analyzing these trace-vapor mixtures, compared to the ones using double-stage and Biemon-Watson separators. A few representative results are shown in the following figures:

Figure 13 – A typical fingerprint was found for the cannabis family consisting of four terpenes, limonene, myrcene, Δ3-carene and caryophyllene (see figures 14 and 15 for mass spectra); the figure shows regenerated chromatograms of marijuana and hashish (partial) showing the compounds identified definitively. Additional terpenes ($C_{10}H_{16}$) were identified but due to insufficient separation were not yet definitively characterized (having such similar structure varying only in the location of one or two bonds, these compounds have to be almost ideally separated to achieve positive identification).

Figure 16 – shows the regenerated chromatograms obtained for cocaine and morphine using a charcoal adsorbent. Surprisingly the two narcotic samples had methyl and ethyl benzoates present in their vapors. From figure 17 it can be seen that one could expect these compounds to be present in cocaine head-space vapors; however, their presence in the morphine vapors is not expected, and might be due to cutting materials, manufacturing contaminants, or cross contamination.

Figure 18 – summarizes all compounds identified so far in the various drugs head-space vapors.

CONCLUSIONS

It has been proven in this study that there are, indeed, characteristic vapors associated with the various narcotics. Despite the relative inefficiency of the preconcentrator in its present form the vapors were collected and preconcentrated appreciably. It is anticipated that with an improved design of preconcentrator with the right combination of adsorbents, a collection efficiency greater by 2-3 orders of magnitude can be achieved, which would make it feasible to build a selective field detection instrument for illicit narcotics.

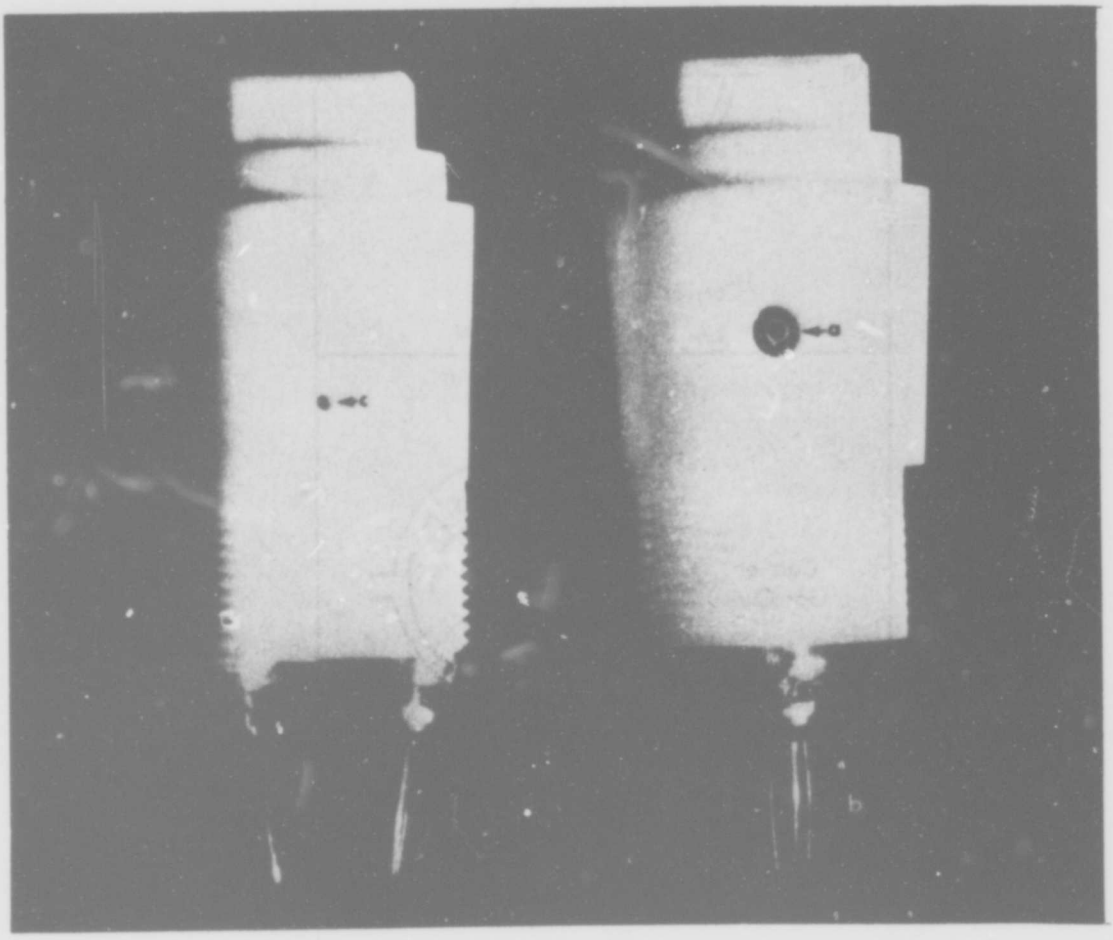

Figure 1. VTS Teflon Plug

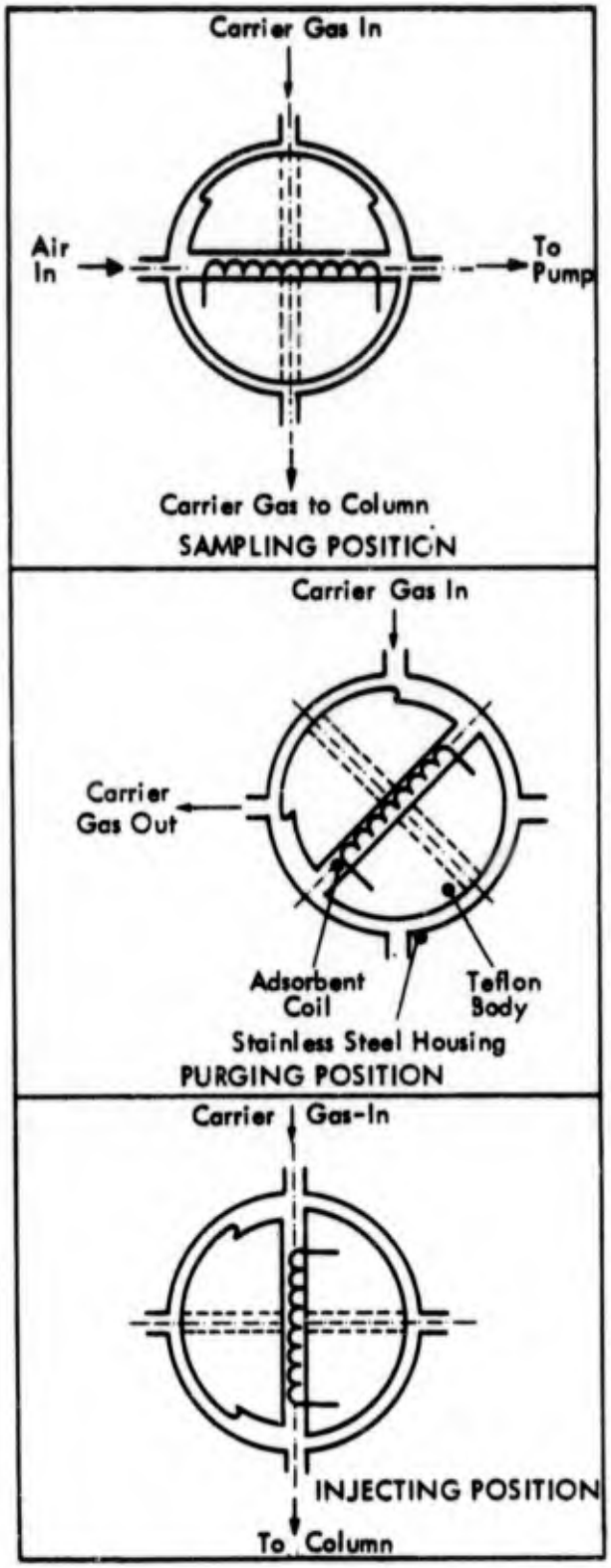

Figure 2. Functional Positions of Teflon Plug in VTS

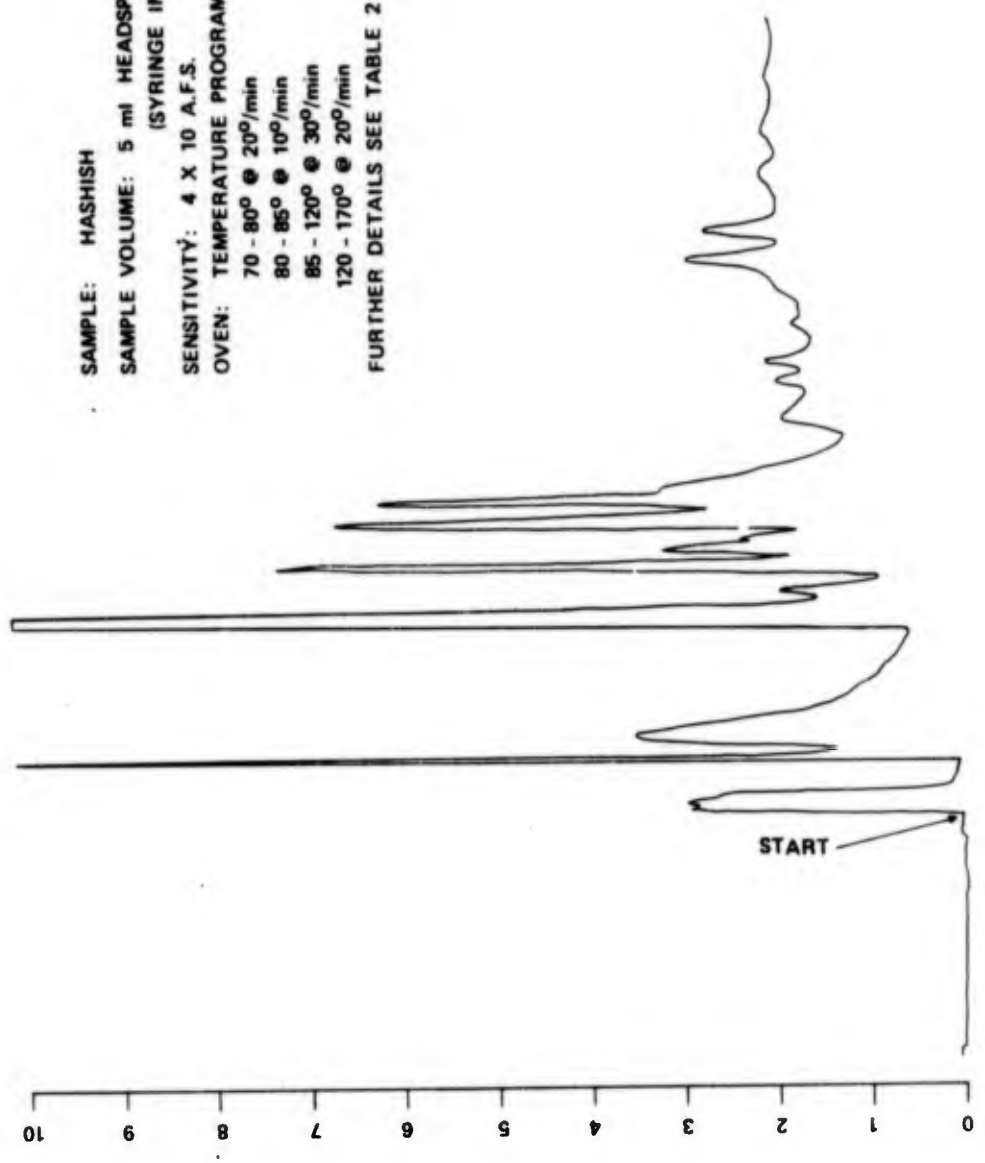

Figure 3. Chromatogram of Hashish Head-Space Vapors

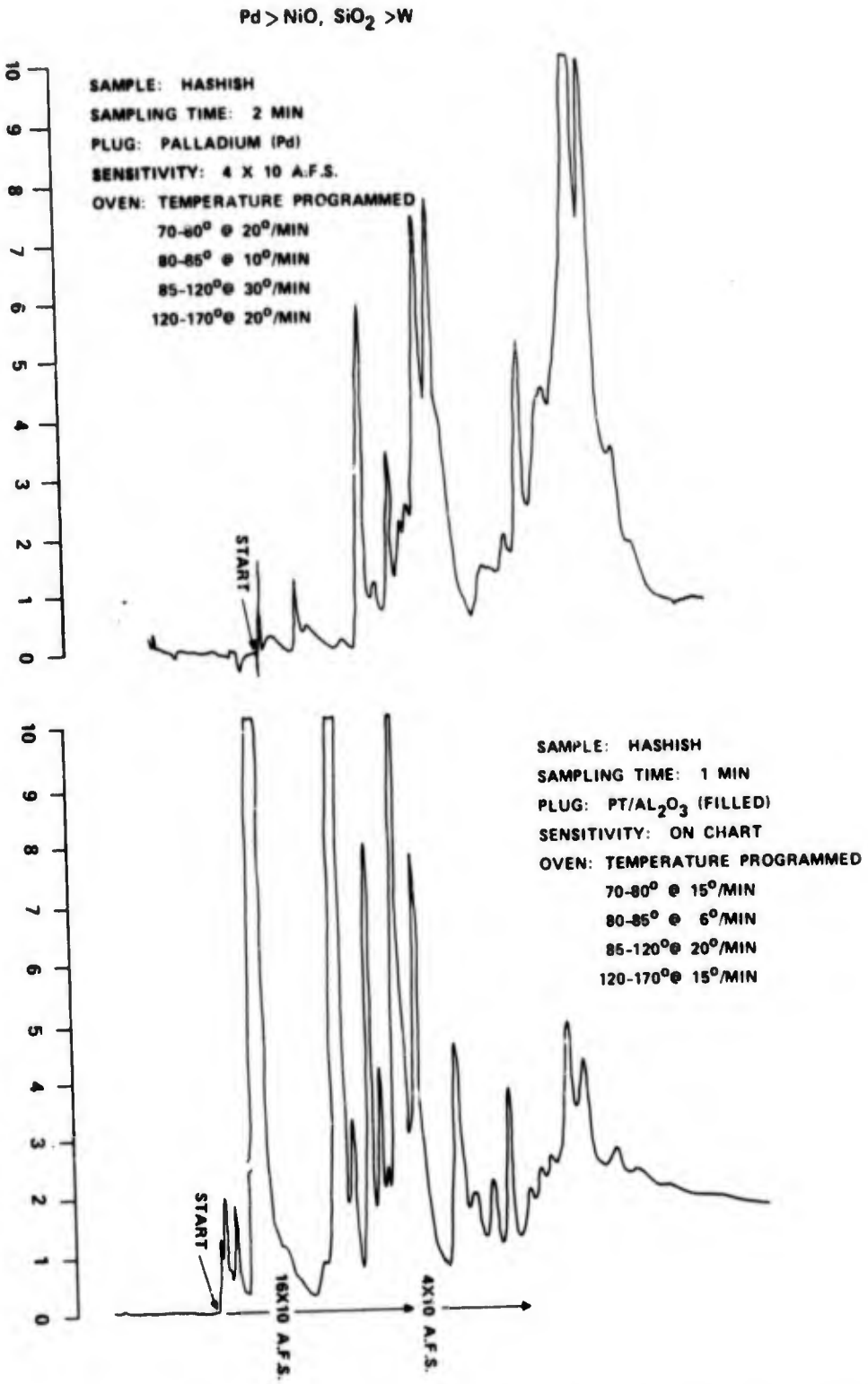

Figure 4. Difference in Absorption Characteristics Between Pd, NiO, S, O_2 and Al_2O_3

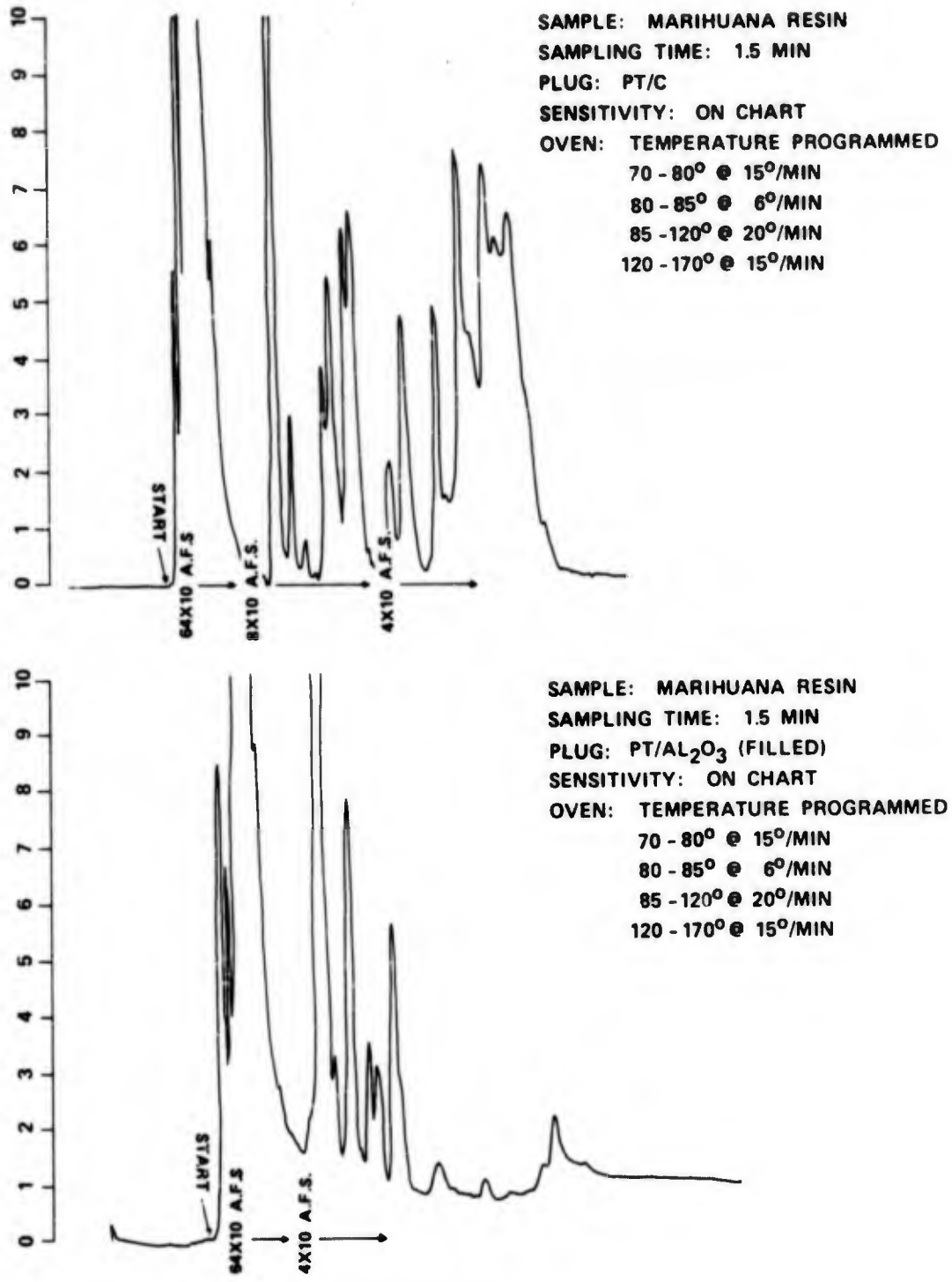

Figure 5. Comparison of Collection Characteristics of Active Carbon and Al_2O_3 for Head-Space Vapors of Marijuana Resin

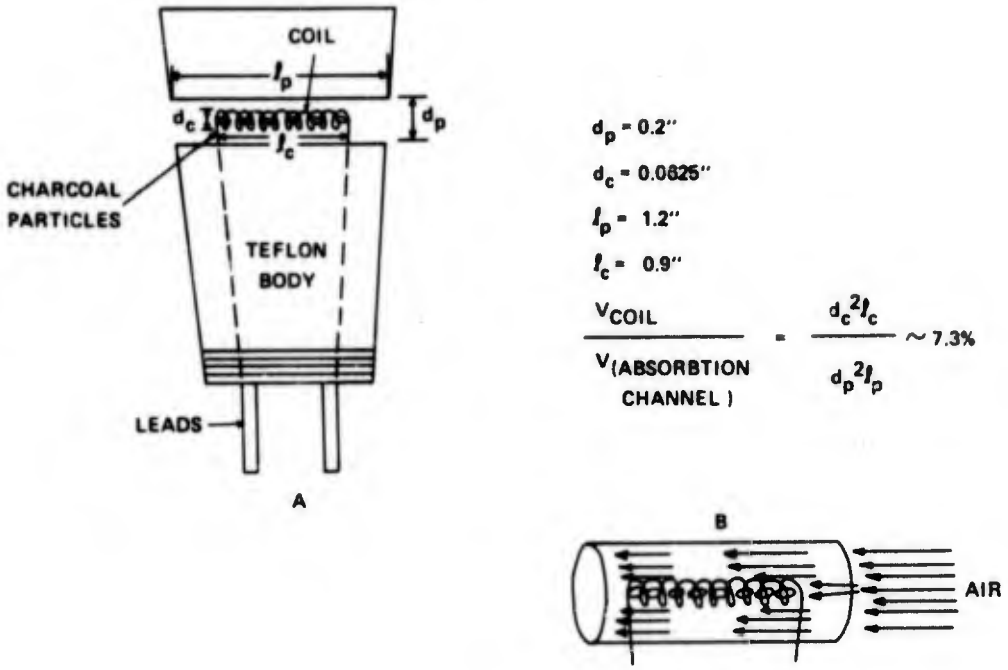

Figure 6. VTS Preconcentrator Valve

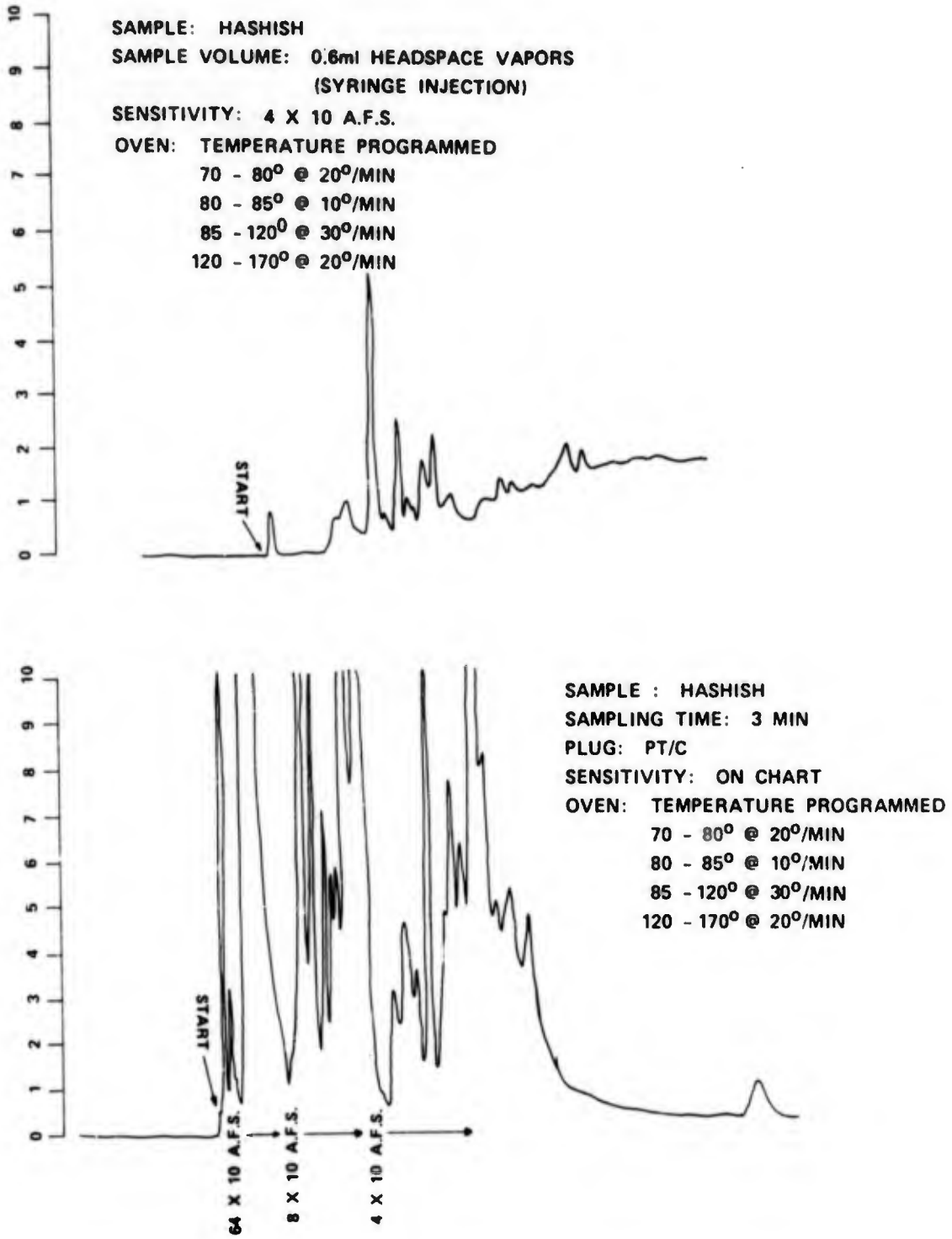

Figure 7. Syringe Injection of Hashish Vapors Compared to Preconcentration with Use of Active Carbon Adsorbent

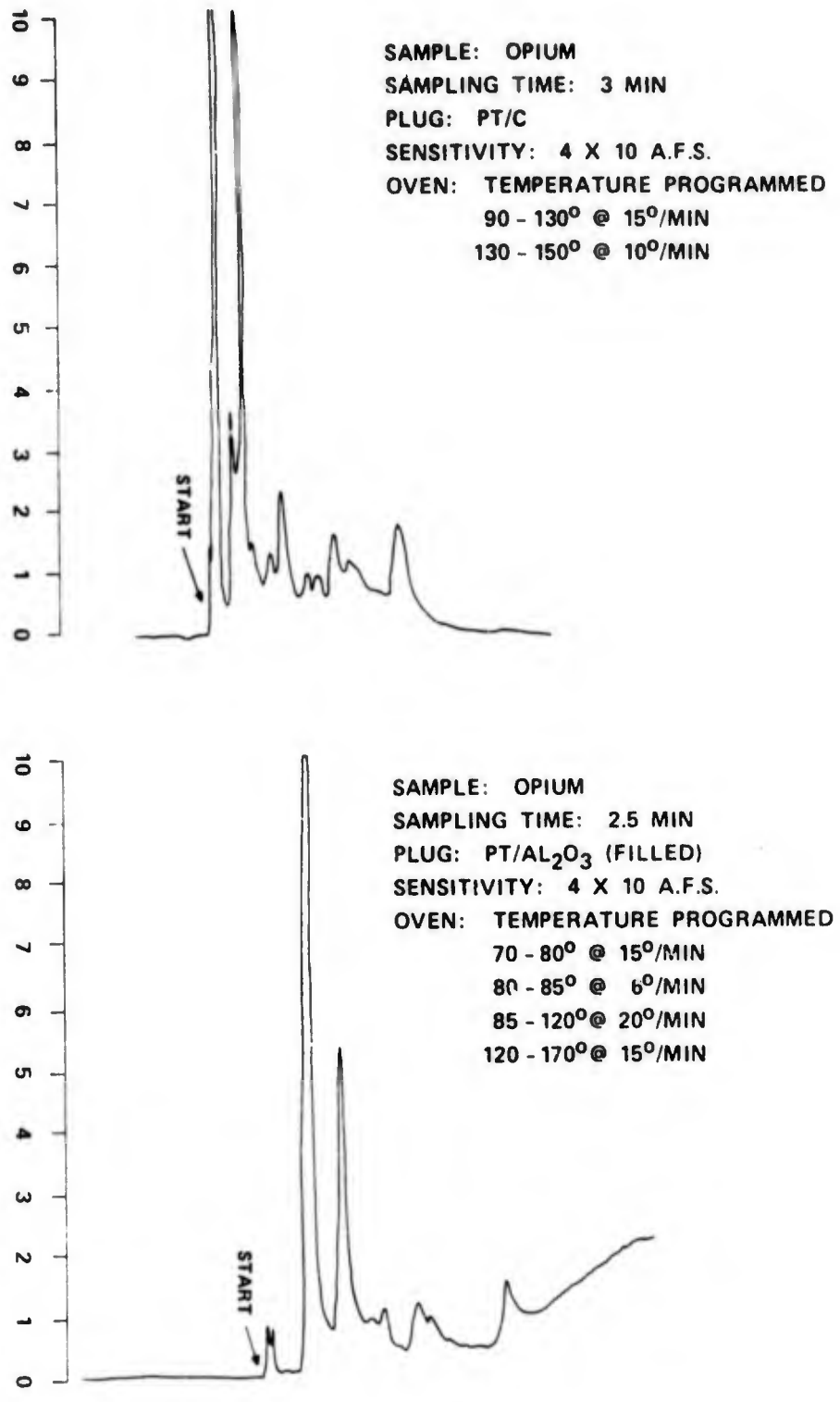

Figure 8. Chromatograms from Opium Vapors by Preconcentration and Use of Two Different Absorbents

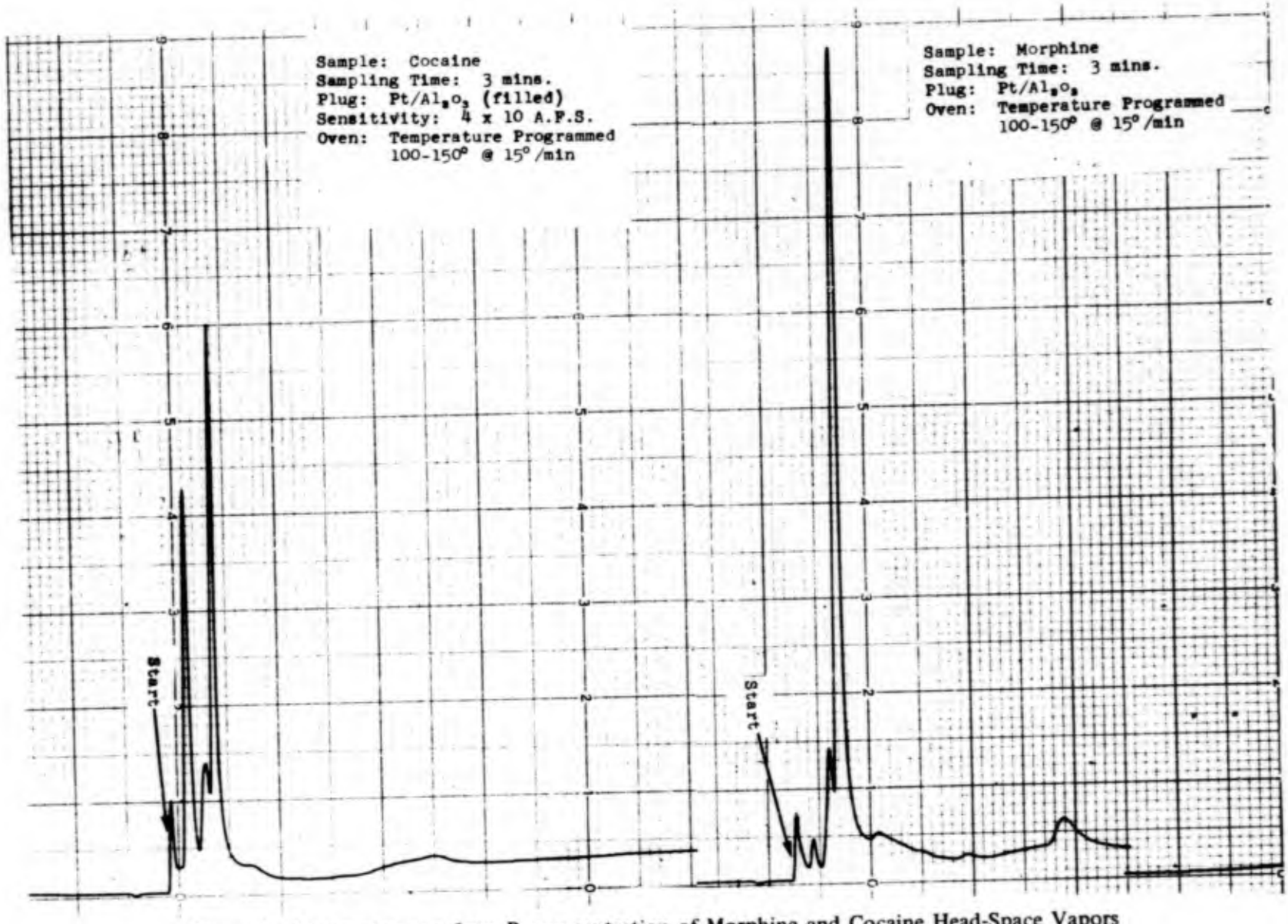

Figure 9. Chromatograms from Preconcentration of Morphine and Cocaine Head-Space Vapors

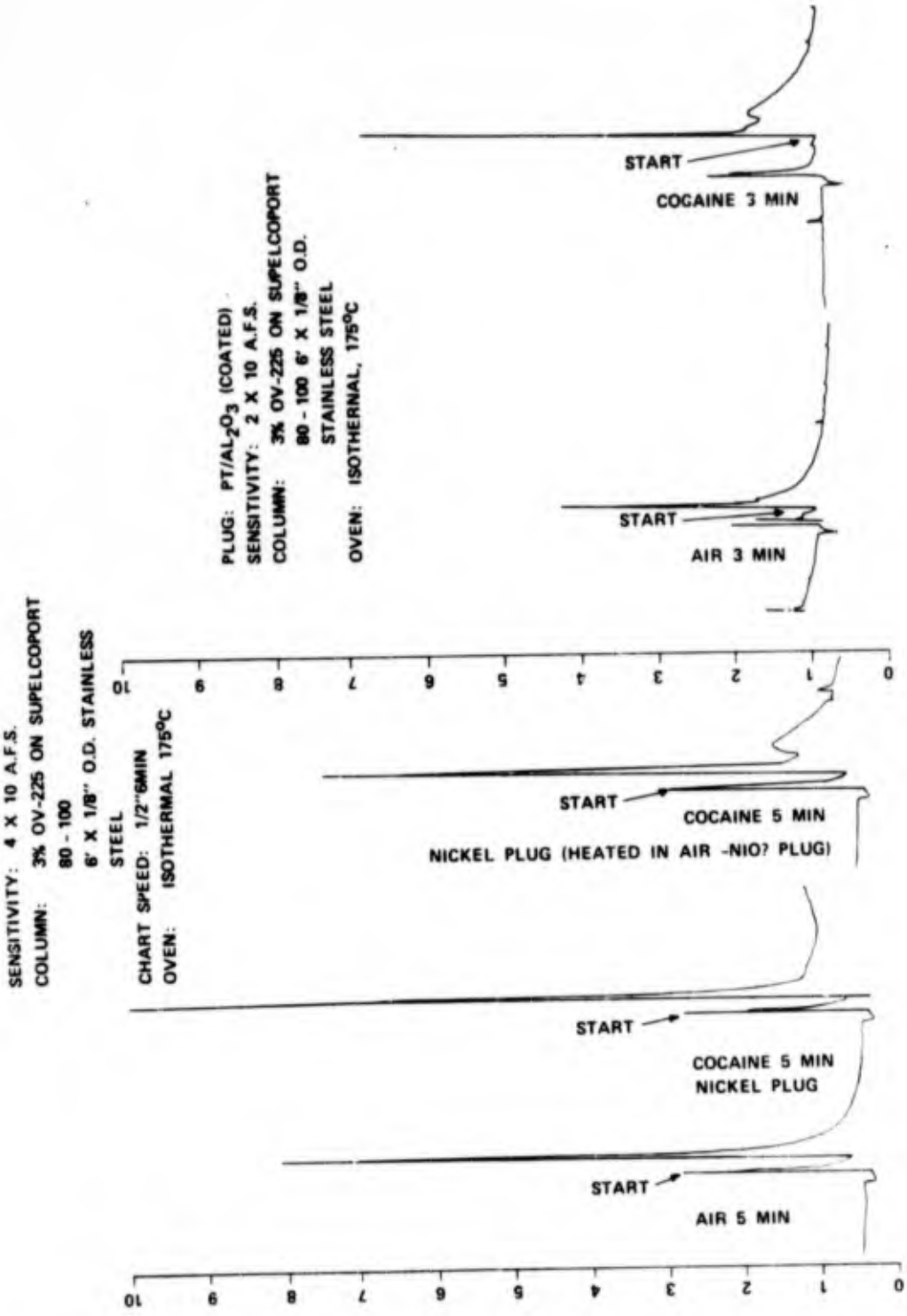

Figure 10. Detection of Relatively High-Molecular-Weight Compound

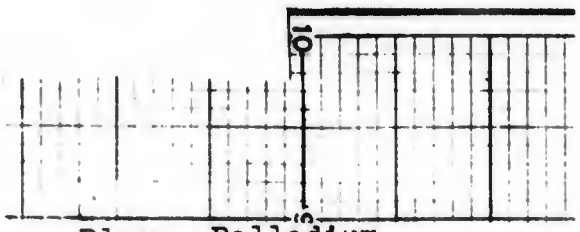

Plug: Palladium
Sensitivity: 2 x 10 A.F.S.
Chart Speed: 1/2"/min.
Oven: Temperature Programmed
95-170° @ 20°/min

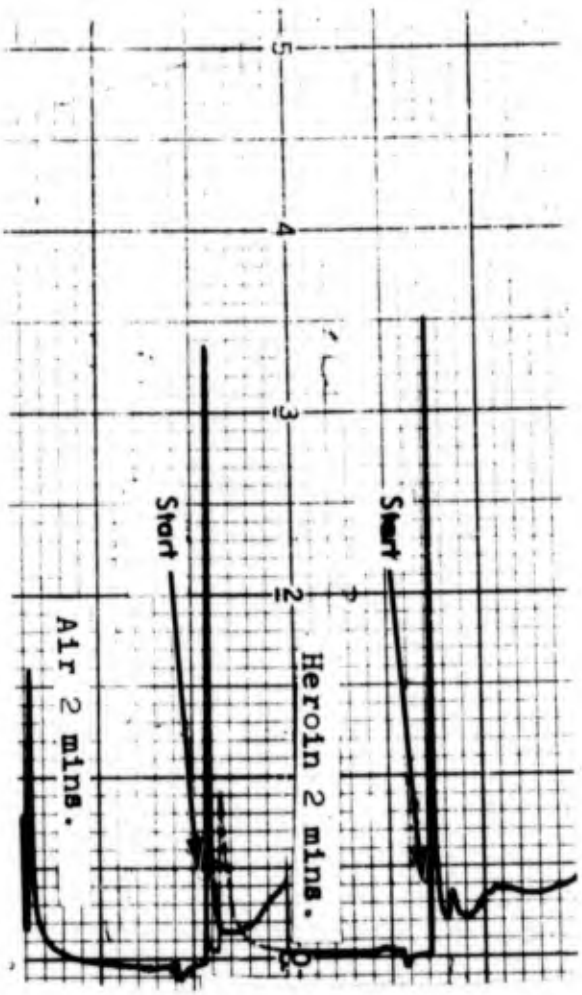

Figure 11. Small Peak from Heroin, Two-Years old, After Preconcentration of Vapors

Plug \ Drug	Hashish	Marihuana Resin	Marihuana	Opium	Morphine	Cocaine	Heroin
Platinum (Pt)	—[a]	—	—	—	—	—	—
Platinum black (Ni/Pt black, coated)	D[b]	C	D	—	—	—	—
Nickel (Ni)	C	B	D	—	—	?![d]	—
Tungsten (W)	C	B	—	—	—	—	—
Palladium (Pd)	C	B	C	D	D	D	D
Silicone dioxide (Pt/SiO_2, coated)	BC[c]	C	—	—	—	—	—
Aluminum Oxide (Pt/Al_2O_3, coated)	C	C	—	BC	BC	?!	—
Alumina (Pt/Al_2O_3, filled)	AB	AB	A	A	A	A	—
OV-17 (Pt/OV-17, coated)	BC	BC	C	C	C	C	—
SE-30 (Pt/SE-30, coated)	AB	B	A	C	D	D	—
Dexsil-400 (Pt/Dexsil, coated)	AB	AB	B	B	D	B	—
Activated Carbon (Pt/C, filled)	A	A	A	A	A	B	—

(a) No vapors detected
(b) Decreasing adsorption efficiency marked from A to D
(c) AB, BC etc., intermediate efficiency
(d) ?! - a small peak obtained, different from peaks obtained for cocaine by all other adsorbent, (See Pgs. 11, 15

Figure 12. Summary of Results for Adsorbents Tested

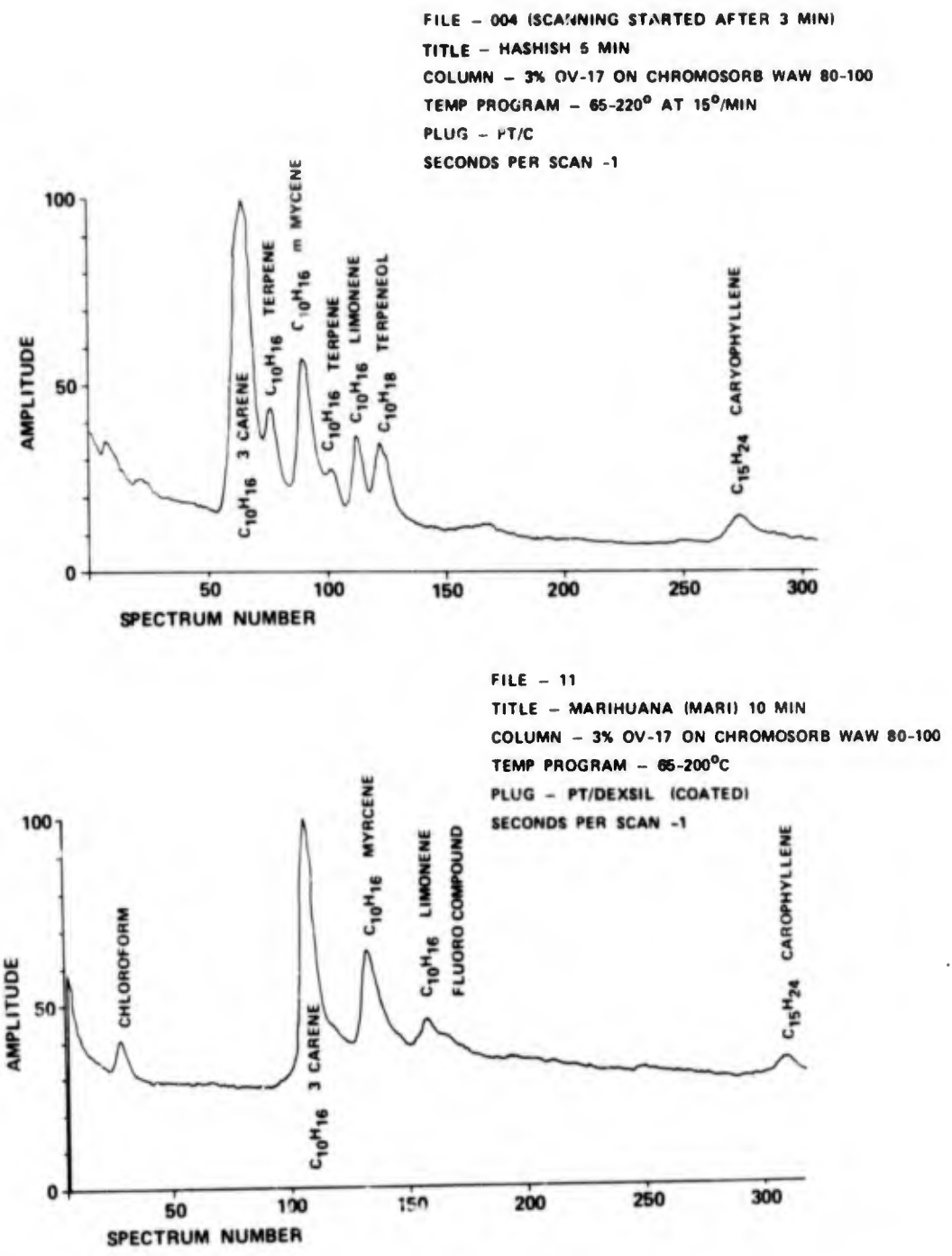

Figure 13. Regenerated Chromatograms of Marijuana and Hashish

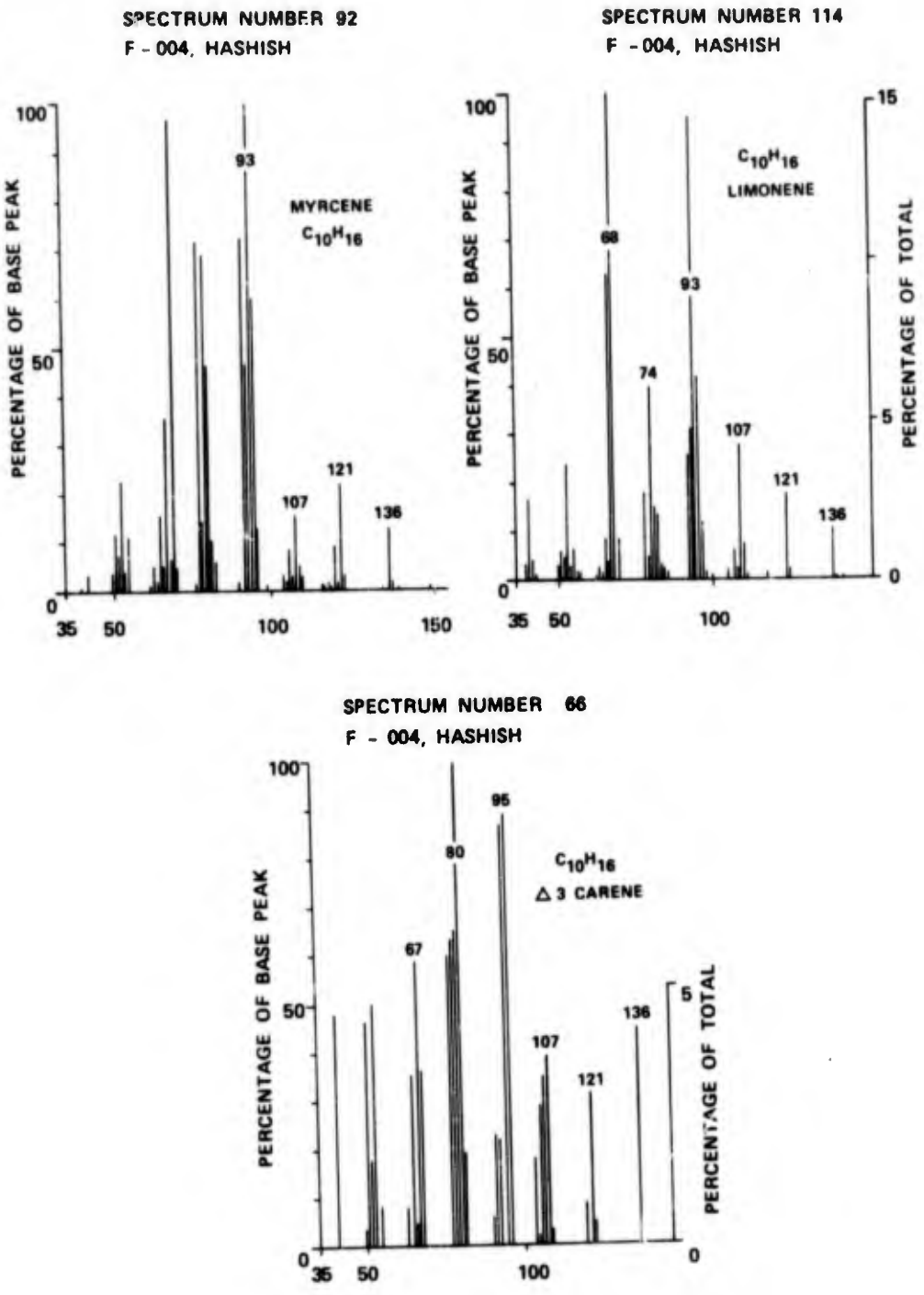

Figure 14. Mass Spectra for Figure 13: Spectra 66, 92, and 114

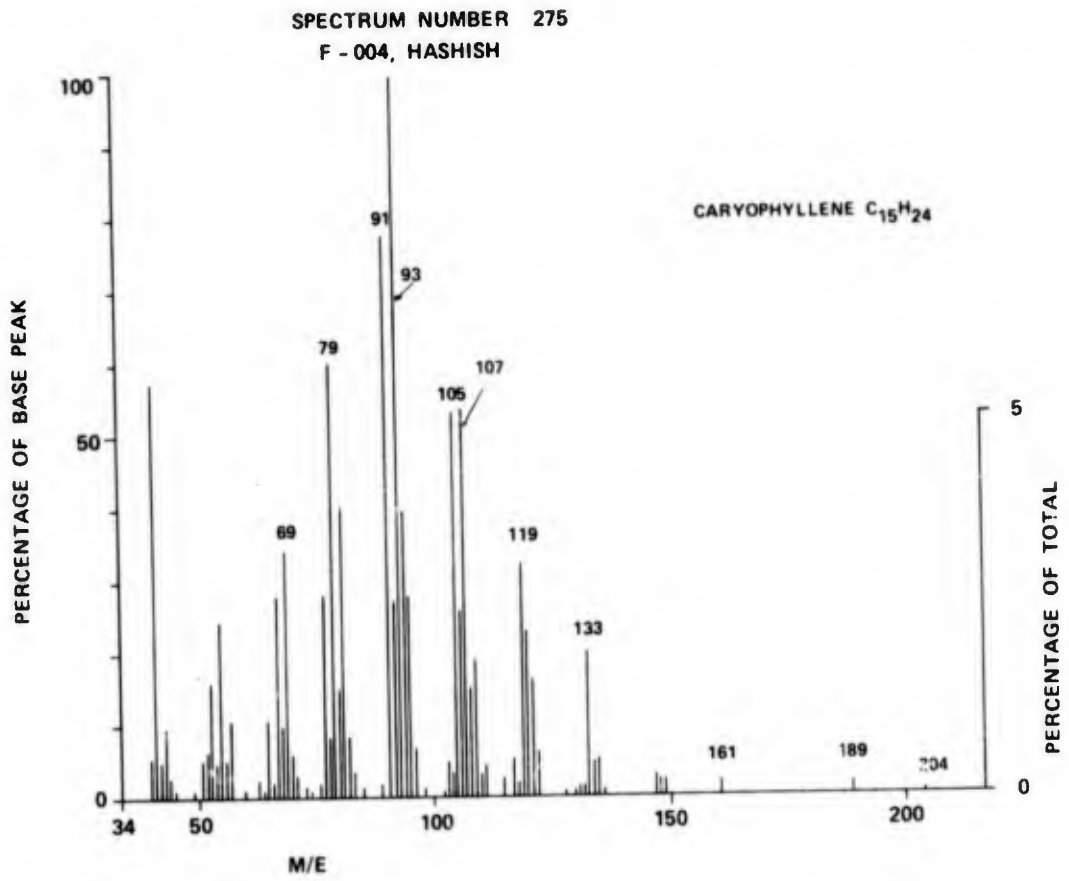

Figure 15. Mass Spectra for Figure 13: Spectrum 275

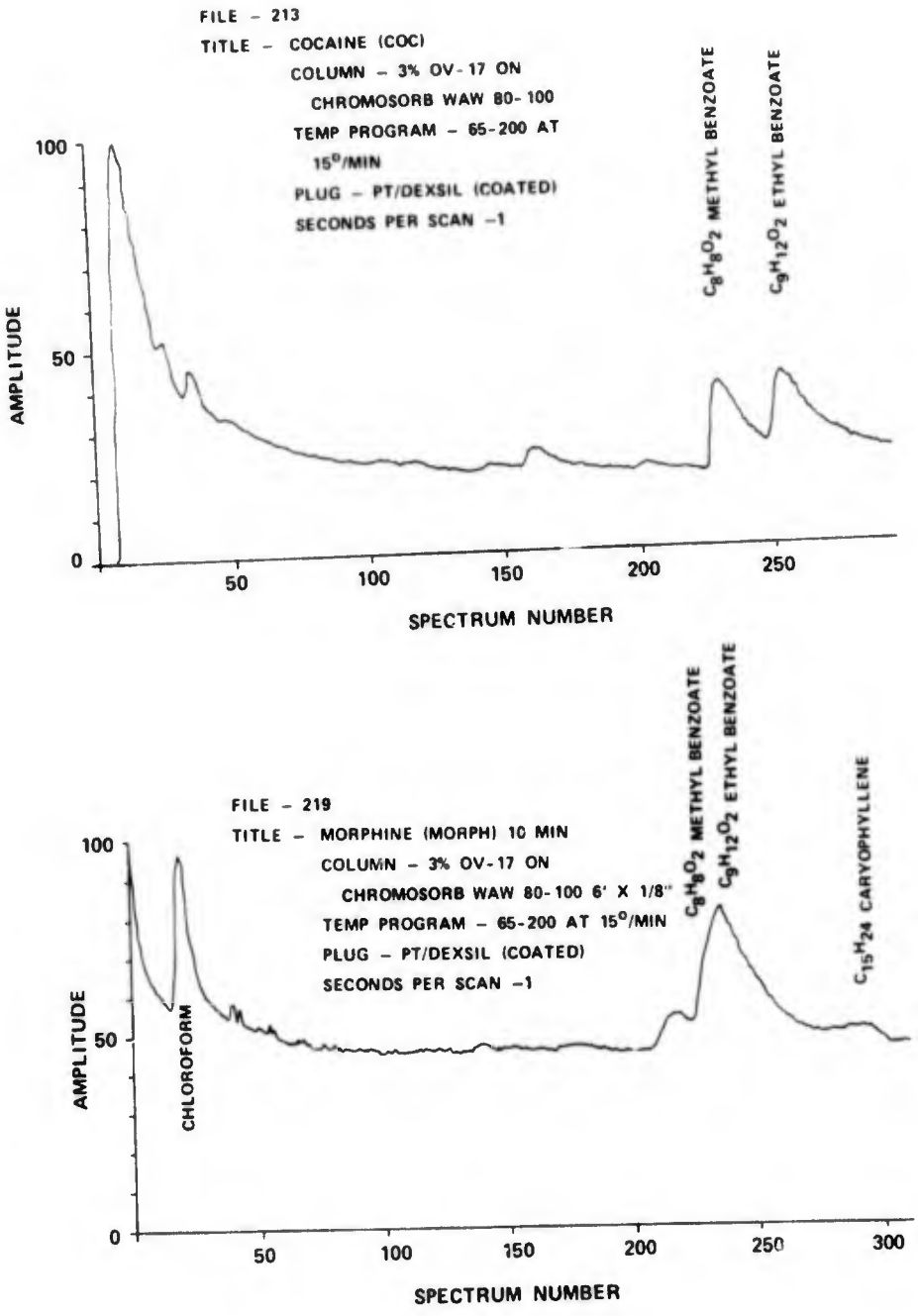

Figure 16. Regenerated Chromatograms Obtained for Cocaine and Morphine Using a Charcoal Adsorbent

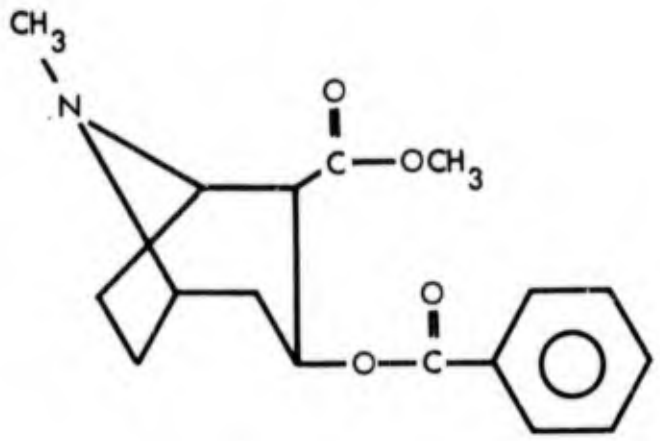

COCAINE

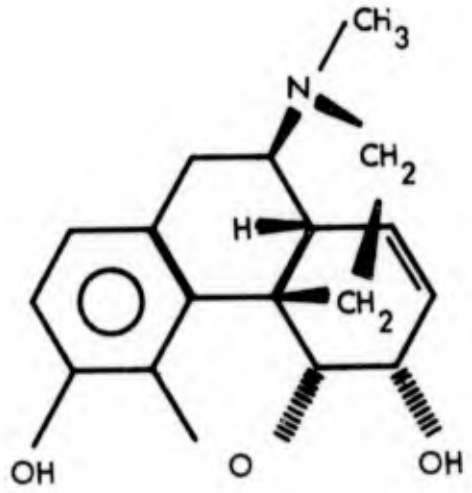

MORPHINE

Figure 17. Molecular Structures

HASHISH	MARIJUANA	MARIJUANA RESIN	OPIUM	MORPHINE	COCAINE
Δ_3-Carene	Δ_3-Carene	p-Cymene	Fenchene	Methyl benzoate	Methyl benzoate
Myrcene	Myrcene	Dimethyl-styrene	Caryo-phyllene	Ethyl benzoate	Ethyl benzoate
Limonene	Limonene		$C_{10}H_{16}$	B-Caryo-phyllene	
Caryo-phyllene	Caryo-phyllene	Caryo-phyllene	$3C_{10}H_{16}$ (terpenes)	Chloroform	
p-Cymene		$3C_{10}H_{16}$ (terpenes probably Limonene, Δ_3-Carene and Myrcene)			
Terpeneol					
O-Allyl-toluene					
$C_{10}H_{16}$ (terpenes)					

Figure 18. Vapor-Phase Compounds Identified from Street Samples of Illicit Narcotics

DETECTION OF NITROAROMATICS WITH PLASMA CHROMATOGRAPHY/PRECONCENTRATION

by

Glenn E. Spangler
US Army Mobility Equipment Research and Development Center
Fort Belvoir, VA 22060

Plasma chromatography has been developed in recent years to detect and identify trace constituents of organic vapors in gaseous mixtures with increased sensitivity and short analysis times. The Beta VII instrument as owned by USAMERDC consists of a drift tube along with supporting electronics for data analysis. The internal construction of the drift tube is illustrated in figure 1. Detection is achieved by subjecting the trace vapor molecules to ion-molecule reactions in a reagent carrier gas and analyzing the product ions with coupled-ion mobility-drift-tube spectrometry in a drift region. The molecules are drawn and/or carried into the reaction region of the instrument by either room air or a carrier gas and are ionized in the presence of a 11.5-millicurie ^{63}Ni radioactive source. The drift times of the product ions are measured with the aid of a pulsed grid, a constant electrostatic drift field, and fast or slow electronics depending on whether multiple-ion or single-ion monitoring is performed. For multiple-ion monitoring, signal-to-noise enhancement is achieved by using signal-averaging techniques and readout is an arrival time spectrum of ion current peaks separated by mobility differences.

Due to the extremely electornegative character of nitroaromatic compounds and the large cross sections offered by these compounds to charge transfer and ion-molecule reactions, negative-ion plasma chromatography has been found particularly suited for their detection and analysis. The purpose of the studies described here was to determine the nature of the ion-molecule reactions involved in the ionization of these compounds, to establish the feasibility of extending the detection capabilities of the instrumentation by using preconcentration techniques, and to demonstrate capability for the detection of land mines. It is impossible to discuss the results of all these experiments in just 20 minutes, but some of the more interesting ideas will be presented with the understanding that the details will become available in forthcoming publications.

The experimental work was performed on a Beta VII instrument utilizing various reagent carrier gases and ultrahigh purity nitrogen for the drift gas. Gases chosen for the reagent carrier gases included zero air containing less than ppm levels of water and hydrocarbons, ultrahigh purity nitrogen, laboratory air, and these gases in the presence of Cl^- anions generated from the dissociative capture of electrons by o-dichlorobenzene. All gases except laboratory air were passed through Linde 13X molecular sieve traps before introduction into the reaction or drift regions. The instrument temperatures were 202°C for the inlet, 166°C for the drift tube housing, and 180°C for the carrier gas. Resolution was optimized by using an 0.1-msec gate width and an electrostatic drift field of 214 volt/cm applied across an 8-inch drift length. The sample vapors were obtained from zone refined or recrystallized supplies of 2, 4, 6-TNT, reagent grade supplies of 2, 4-DNT, and reagent grade supplies of o-, m-, and p-nitrotoluene. Sample introduction was achieved through either a direct sniff of the vapor or by adsorption on a six-inch length of 0.021-inch diameter gold wire followed by desorption via indirect heating in the inlet of the instrument.

Summarized in figure 2 are the responses obtained for TNT. Three ion mobility peaks were observed having drift times of 14.6, 15.0, and 15.5 msec corresponding to reduced mobilities of 1.59, 1.54, and 1.49 $cm^2volt^{-1}sec^{-1}$ respectively. The top spectrum was obtained with a pure nitrogen carrier gas while the other spectra were obtained with increasing levels of laboratory air in the nitrogen carrier. It is observed that the ions at 15.5 msec are the dominant ions species in nitrogen while the ions at 15.0 msec become important in laboratory air. Since spectra similar to that obtained in laboratory air were obtained in the presence of zero air and the Cl^- anion, the ions at 15.5 msec appear to arise from reactions with free electrons. The ions at 15.0 msec appear to arise from ion-molecule reactions with reactant ions. The same phenomenon was also observed for the 13.9 and 14.5 msec ions of DNT as illustrated in figure 3 in the presence of increasing levels of the chloride anion. These ion peaks correspond to reduced mobilities of 1.67 and 1.61 $cm^2volt^{-1}sec^{-1}$ respectively. For mononitrotoluene, the fourth figure illustrates that, except for the hydrated OH^- or Cl^- ions which may or may not arise from the room air, a dominant ion response is observed in the presence of nitrogen while extensive fragmentation is observed in the presence of zero air. The ion peaks at 13.3 and 12.8 msec with reduced mobilities of 1.74 and 1.81 $cm^2volt^{-1}sec^{-1}$ are thought to correspond to the ion peaks described for DNT and TNT but instead of the 13.3 msec ion peak disappearing in favor of the 12.8-msec ion peak in the presence of Cl^-, the chloride attached ion peak at 15.0 msec was observed. The NO_2^- ion has a drift time of 8.7 msec and contributes to the mononitrotoluene spectrum in zero air.

When considering the possible ionization processes which might occur in negative-ion plasma chromatography, considerations must be given to electron capture. The probability of electron capture depends much on the energy of the electrons involved in the capture process. This energy in a nitrogen carrier gas can be estimated through the Townsend energy relatationship $3/2\eta KT$ where η is the Townsend energy factor. For the operating conditions of the plasma chromatograph, this energy is 0.49 ev. Since the energy lies below the appearance potentials of Christophorou, et al. for the dissociative capture of nitrotoluene, the ion formed in nitrogen is most likely the parent anion. However, if air or Cl^- is present, the electrons are thermalized to 0.057-ev ions which in turn cause fragmentation through ion-molecule reactions.

In order to substantiate this interpretation, arrangements were made to run several samples of TNT on a negative-ion chemionization source of a MS-9 mass spectrometer and an atmospheric pressure ionization source of a quadrupole mass spectrometer. The data on chemi-ionization were obtained with the facilities of Hunt at the University of Virginia and are displayed in the fifth figure. Ionization is achieved with a corona discharge in the presence of air, oxygen, or hydrogen/water reagent gas mixtures. Except for the reactant ions, the ions generated for TNT depended little on the type of reagent gas used in the instrument. The dominant ion was the TNT molecular anion with only slight evidence for the dissociation of NO_2 to form the $(M\text{-}NO_2)^-$ anion. This contradicts the interpretations of Karasek and Denney but supports the fact that NO_2^- is not observed in the negative ion spectrum for TNT in plasma chromatography. The ion peaks at masses 210 and 197 correspond to a loss of OH and NO respectively but in different ratios as observed by Yinon, Boettger, and Weber with 2-ev electron bombardment in negative-ion mass spectrometry. The data on atmospheric pressure ionization were obtained with the facilities of Horning, et al. at the Baylor School of Medicine. Ionization was achieved in the presence of a radioactive source and Cl^- with the resulting mass spectrum being dominated by a proton-abstracted anion with little evidence for additional fragmentation. The differences in response between chemionization and atmospheric pressure ionization are thought to be due to the slightly more energetic ions and electrons involved in the low pressure regime of chemionization and the acidity character of the chlorine anion in atmospheric pressure

ionization. In fact, when the discharge of the chemionization source was pushed into the glow discharge regime, dissociation of NO_2^- from TNT was observed as expected from the data of Boettger, et al. Consequently, the ions observed in plasma chromatography for the nitrotoluenes appear to be the molecular anion in the presence of nitrogen while the proton-abstracted anion becomes important in the presence of air, Cl^-, etc. This does not correlate well with mass assignments obtained from the empirical relationship provided by Cram and Chesler but empirical relationships must give way to mass-identified ions. Chloride attachment was not observed for DNT or TNT but was observed for o-mononitrotoluene. Tannenbaum et al. have reported chloride attachment for mononitrotoluene in chemionization mass spectroscopy.

The sensitivity of plasma chromatography to TNT vapor has been reported. Based on dilution flask measurements on a Beta VIIIS instrument detection limits were found to be near one part in 10^{11}. However, the electronic noise was 2×10^{-13} amp and grid transmissions were 40% for this instrument. The Beta VII instrument as owned by USAMERDC has a peak noise less than 8.5×10^{-14} amps and grid transmissions of about 90%. This would suggest that sensitivities of 2 parts in 10^{12} are achievable. Furthermore, the ionization processes in the presence of reactant ions are more efficient than the ionization processes in the presence of free electrons and sensitivity can be increased through the use of preconcentration. The simplest of all preconcentration devices is a gold wire with which the following series of experiments can be performed.

If a gold wire is allowed to collect vapor from a reservoir of TNT vapor for increasing lengths of time at room temperature and the collected vapor desorbed into the heated inlet of the instrument for analysis, the response of the instrument follows a relationship similar to that displayed in the sixth figure. Here σ is the surface coverage which is proportional to the instrumental response, α is the accomodation coefficient for adsorption, J is the impingent flux rate of material on the surface, and τ is the mean residence time spent by the molecule on the surface before desorption. Hence, the response builds up to a maximum value dependent on J which in turn depends on the partial pressure. Experimental data of this type fitted to the equation are displayed in figure 7. From the fit, the mean residence time for a TNT molecule on a gold surface is observed to be about 8.95 minutes. Such a large value for the residence time corresponds to a heat of adsorption of 21 kcal/mole which lies close to the heat of vaporization. Since it is thought that the maximum volume of vapor collected on a six-inch length of 0.021-inch diameter wire is near 20-30 cc, the sensitivity of the plasma chromatograph should be improved by about an order of magnitude with the technique. The volume of the reaction region is 4.7 cc, a factor of 5 below the collected volume. Such an increase in sensitivity has been preliminarily established experimentally by the sampling of saturated vapors for one second. Additional gains in sensitivity can be achieved by using larger surface areas for adsorption.

Using the gold wire sampling technique with its enhanced sensitivity an experiment was performed to measure the availability of TNT vapor from an encased mine. The mine chosen for analysis was an inert Italian antitank mine because the main charge well is easily exposed by unscrewing retainer rings and breaking gasket seals. Three tanks were prepared to collect vapor given off by the mine. One served as a blank containing no mine, a second served as a blank to establish background for an unloaded inert mine, and a third served as a sample containing a mine with a laboratory amount of recrystallized TNT deposited in the main explosive charge well. The tanks were sampled periodically through holes provided in one of the walls of each tank for about 3 months to watch the buildup of vapor. When the vapor concentrations reached a steady state, the response obtained on the plasma chromatograph were as displayed in figure 8.

The reactant ions were the only ions observed in the spectrum obtained on the air-filled tank. For the blank mine, an ion peak appeared at 18.7 msec originating from materials contained and being released from the hard-rubber pressure plate of the mine. For the TNT laden mine, a TNT related anion was observed at an estimated level of 4 part in 10^{12}. This is nearly three orders of magnitude below the saturated vapor pressure for TNT. Experiments of this type indicate a detection capability for antitank mines albeit only under very specialized sampling conditions of enclosed containers. Detection limits needed to establish a more practical detection capability appear very stringent.

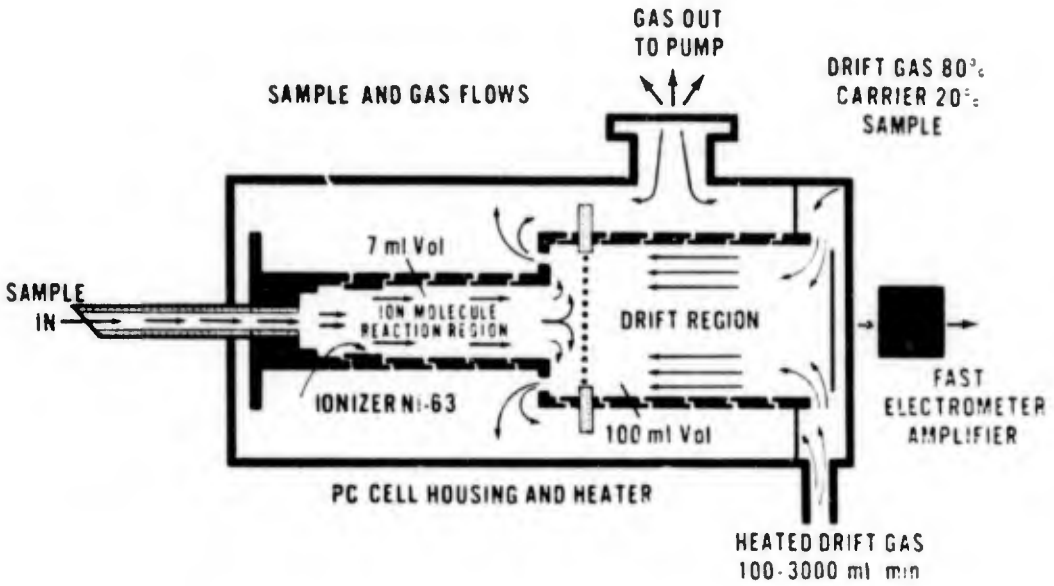

Figure 1. Internal Structure of Plasma Chromatograph

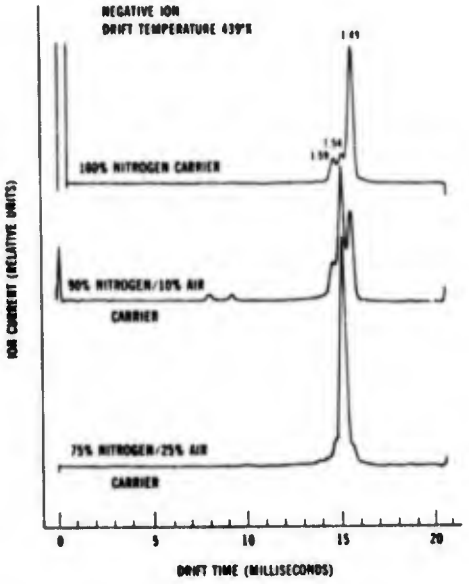

Figure 2. Ion Mobility Spectra of TNT Vapor

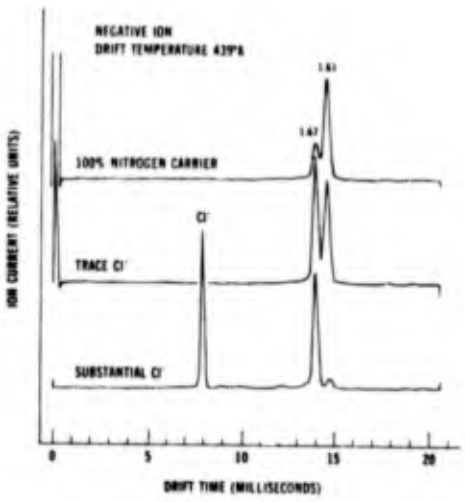

Figure 3. Ion Mobility Spectra for DNT

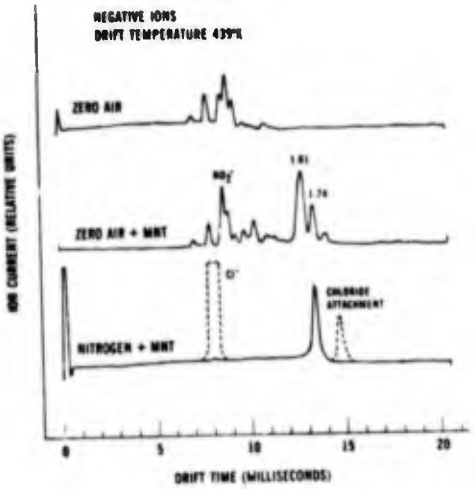

Figure 4. Ion Mobility Spectra for MNT

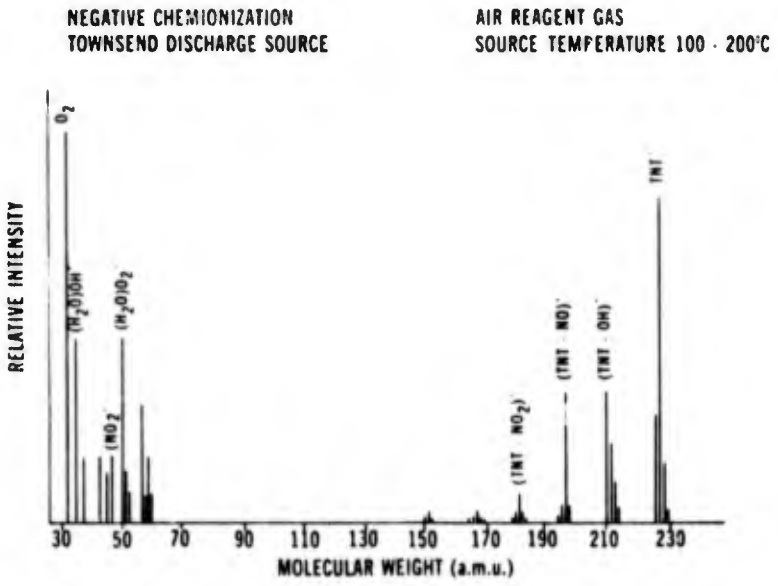

Figure 5. Mass Spectrum of TNT

$$\frac{d\sigma}{dt} = \alpha J - \frac{\sigma}{T} \qquad (1)$$

SOLUTION $\alpha, T \neq f(\sigma)$

$$\sigma = \alpha J T \left[1 - EXP\left(\frac{-t}{T}\right)\right] \qquad (2)$$

Figure 6. Differential Equation Describing Adsorption/Desorption

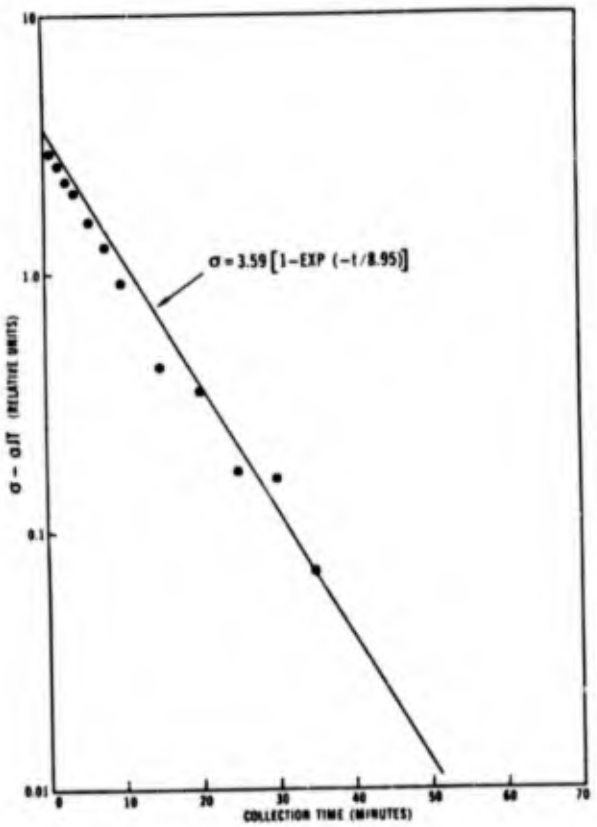

Figure 7. Integrated Response Versus Collection Time

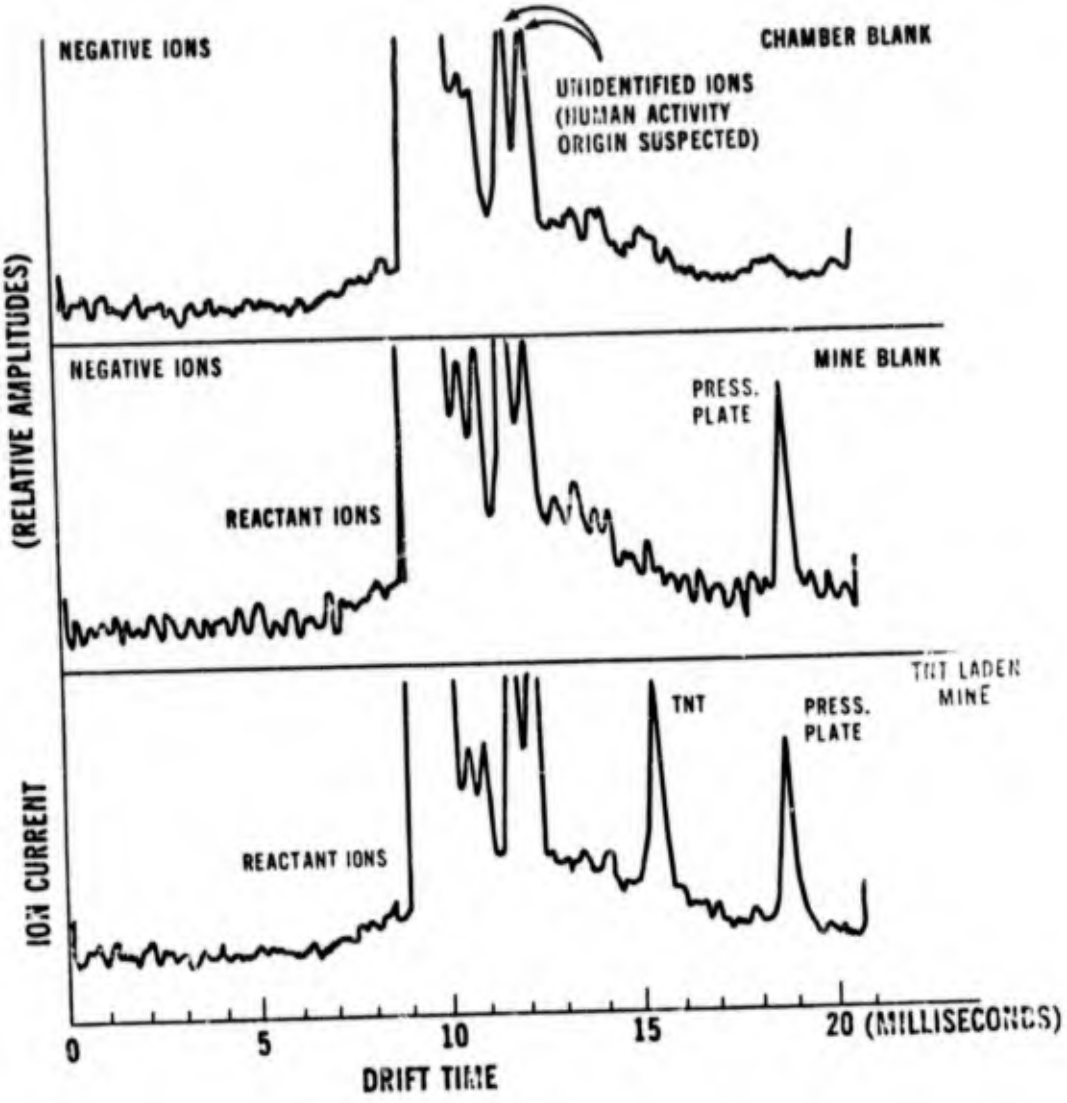

Figure 8. Detection of TNT from Mines

AN ULTRASENSITIVE FLAME PHOTOMETRIC DETECTOR FOR SULFUR DIOXIDE AND HYDROGEN SULFIDE

by

R. K. Stevens and Ralph Baumgardener
Environmental Protection Agency

H. E. Stubbs and A. W. Berger
Better Environmental Development Corporation
Newton, Massachusetts 02160

Conventional analytical techniques for measuring gaseous sulfur compounds such as SO_2 and H_2S at low part-per-billion concentrations are, at best, marginally sensitive at these levels. In order to determine the background sources and fate of these gases, improved analytical methods are required. This report describes the development and application of a new type of flame photometric detector capable of measuring sub-part-per-billion concentrations of sulfur dioxide and hydrogen sulfide. The instrument employs rare earth absorption filters to define a spectral band including the sulfur emission at 374 nm and an adjacent background comparison band. The first of these filters has a band pass of 10 nm and the second of 5 nm. An optical chopper alternatingly presents light from the two filters to a detector. Special signal-processing techniques are employed, permitting detection of sulfur compounds at levels below 1 ppb. Data taken in nonurban areas measuring ppb concentrations of H_2S and SO_2 will be presented.

The seven figures show how the instrument behaves along with some results from its use.

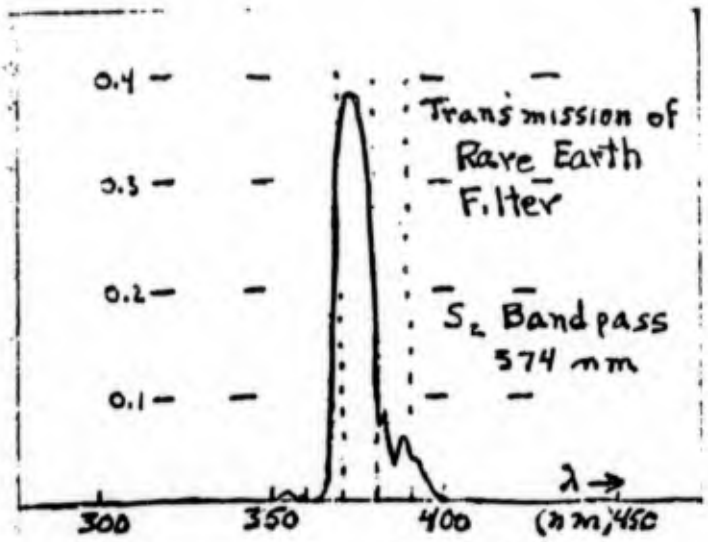

Figure 1. Response at 350-400nm

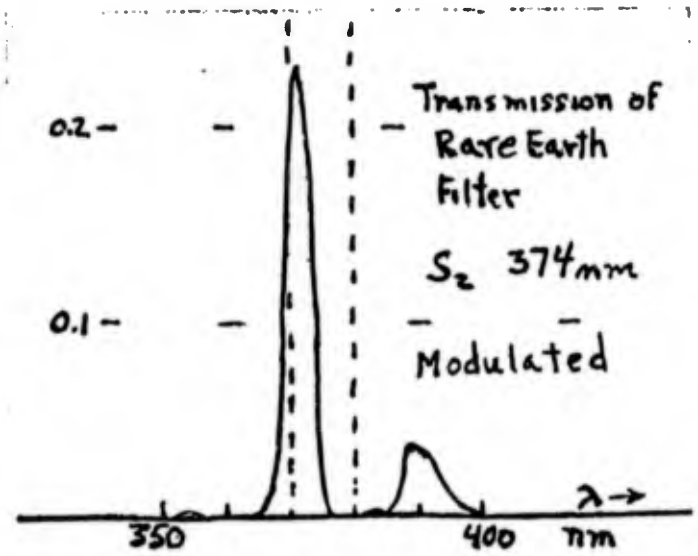

Figure 2. Another Response Curve at 350-400 nm

(Note change of scale)

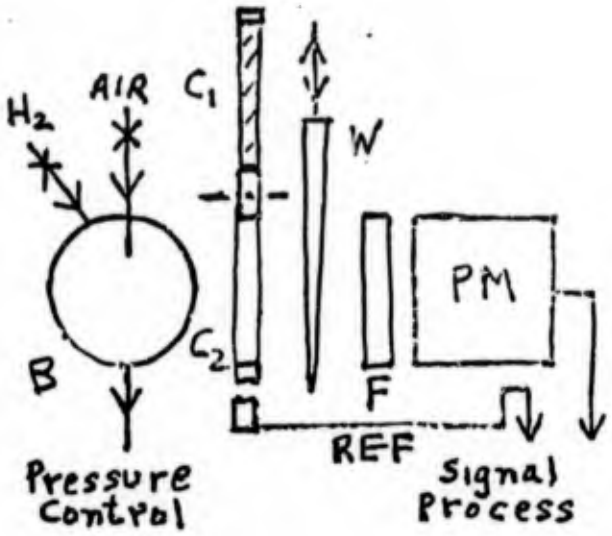

Figure 3. Photometer Optics

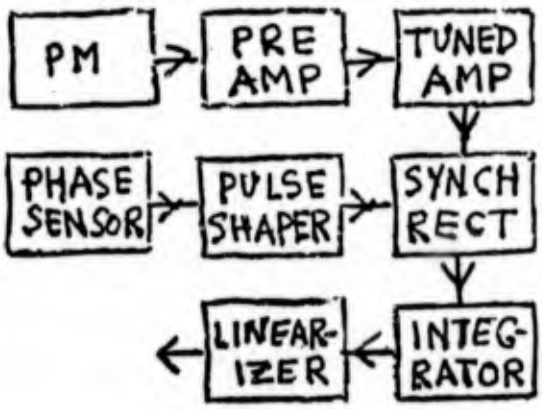

Figure 4. Photometer Electronics

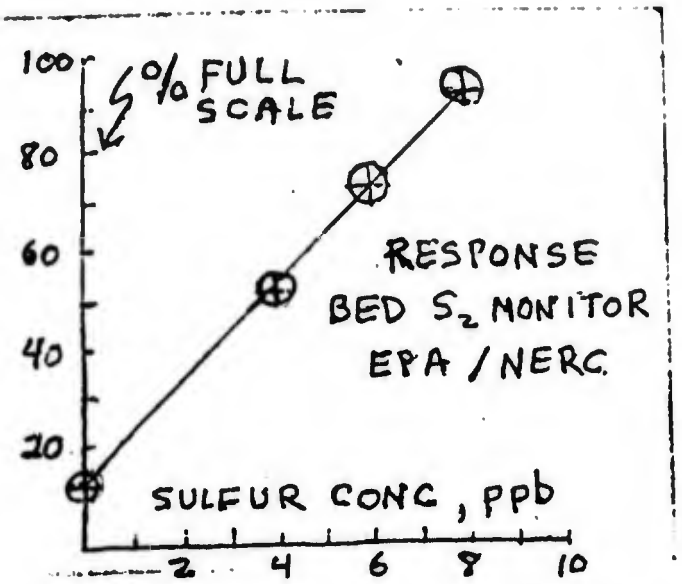

Figure 5. Response Versus Sulfur Concentration

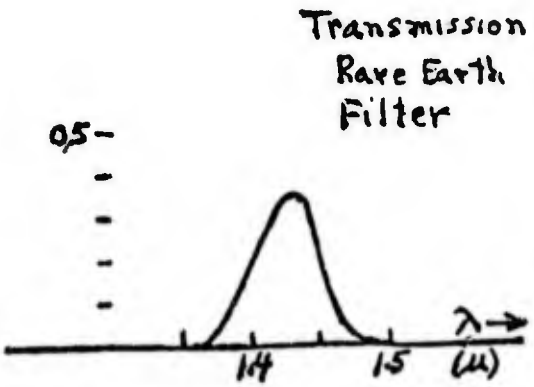

Figure 6. Water Monitor

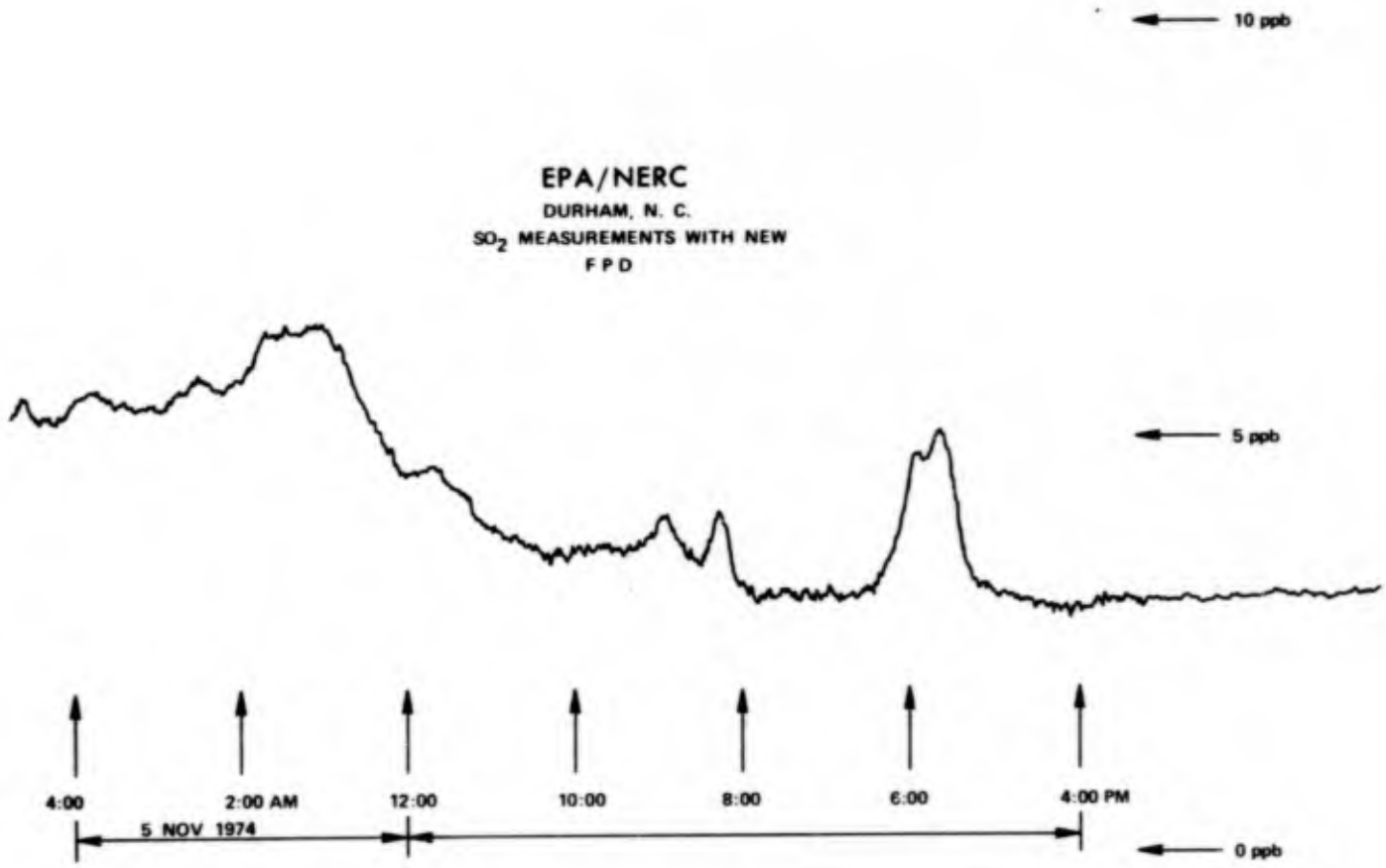

Figure 7. Ambient Sulfur Concentration, Research Triangle Park; 12 Hours

ANALYSIS OF TRACE CONSTITUENT DATA -- A PATTERN RECOGNITION APPROACH

by

H.T. McAdams and C.F. Holmes
CALSPAN CORPORATION
Buffalo, New York 14221

ABSTRACT

A survey is presented of data analysis techniques applicable to collected data of trace constituents. In particular, techniques are presented whereby the identification of sources can be accomplished based on chemical analysis of particulate effluents from several sources in a given area. Many of the methods presented fall under the general term of pattern recognition. In particular, the techniques of maximum likelihood theory are used to classify particulate effluents according to source. An example problem is solved and the applicability of other pattern recognition techniques to the problem of source identification is discussed.

1. INTRODUCTION

Particulate effluents which escape the suppressive mechanisms designed to eliminate them can be collected at distances downwind from the source. Often several sources may be present in one general area so that the sampling sites may well be collecting effluent particles from several different industrial operations. In order to pinpoint the sources of such pollutants so that environmental impact may be assessed and any necessary corrective measures may be taken, it would be desirable to have data analysis techniques available which could help identify sources of effluents on the basis of chemical or physical analysis of the effluent particles.

Clearly, there are cases where this is impossible. If two or more industrial sites are engaged in nearly identical operations, using similar raw materials, it is unlikely that chemical analysis of effluents will reveal differences enabling discrimination. However, there are other situations in which even minor differences in industrial processes will result in effluent particles sufficiently different to enable their separation and identification as to source. It can also be expected that these differences may be subtle enough to escape detection by visual examination of analytical data. It is this class of problems we would like to address in greater detail. Namely, given that subtle differences exist among particulate effluents from different sources within a general geographic area and similarities among particulates emanating from a single source, how can such factors be combined in a data analysis scheme which will allow the identification of the sources of particulates comprising a collected sample?

A method which is showing considerable promise in solving a class of problems typified by the above situation is a subset of artificial intelligence known as pattern recognition. Briefly stated, the general problem addressed is the classification of objects united by some (perhaps obscure) property into appropriate groups on the basis of indirect measurements made on these objects. The exact relationship by which the measurements are related to the classifying property may be unknown and theoretically inaccessible. But if the measurements (say elemental analysis of the effluent particulates) are related to the classifying property (source) in a manner not readily apparent, the techniques of pattern recognition can often provide the method by which the two are related and can provide an algorithm by which sources are identified on the basis of analytical information obtained from the particulate effluents.

This relatively new field of applied mathematics was originally developed to solve such problems as recognition of handwritten characters, analysis of speech patterns, image analysis, and signal discrimination.

More recently, chemists, physicists, and engineers have become aware of the potential of this tool and are applying pattern recognition to problems in their fields. Pattern recognition has been applied to the interpretation of analytical spectra,[1,2] the screening of drugs according to pharmacological efficacy,[3] surface characterization,[4] blood cell analysis,[5] and fingerprint identification.[6]

It is the purpose of this paper to propose pattern recognition as a useful tool in identification of effluent particulate sources. In the following sections some basic concepts of this tool are presented, a sample problem is introduced and solved, and some general remarks regarding the usefulness and limitations of this method are presented.

2. PATTERN RECOGNITION -- A PROLEGOMENON

Often the physical scientist/engineer is faced with the detection of a seemingly obscure property of a collection of objects based on indirect measurements made on the objects. Occasionally, the connection can be made through theoretical application of basic principles to the problem. More often, however, the connection between a common property and a given set of measurements is more subtle and requires a more empirical approach to its development. A somewhat ill-defined but nonetheless effective method of "guessing" the connection between measurements and a common property of objects is often used by scientists to deduce logical empirical relationships.

Pattern recognition, a subset of a much broader field known as "artificial intelligence," attempts to classify objects into appropriate groups according to measurements (called "features") made on these objects. Pattern recognition can be divided into <u>probabilistic</u> (parametric) approaches and <u>geometric</u> (nonparametric) approaches. In the probabilistic approach an estimate is made of probability density functions describing the underlying statistical distribution of the pattern features. Classification is then made using "maximum likelihood" (Bayesian) strategies. In the geometric (nonparametric) approach, relations between sets of objects are made on the basis of their "closeness" in some geometrical representation.

The field can be further divided into supervised learning and unsupervised learning. In supervised learning the classification algorithm is built upon objects for which both the features and the proper classification is known. The information thus assimilated is used to classify unknown objects based on their similarity (in some well-defined mathematical sense) to the known patterns. Unsupervised learning seeks to discover hitherto unknown relations between groups of objects by finding meaningful clusters of points reflecting the possible existence of relationships.

The particular scheme we have applied in this paper is a probabilistic one based on the occurrence of certain features capable of differentiating among classes of airborne particulate materials. An estimate is made of underlying probabilities of mutual occurrences of groups of pattern features from patterns whose proper classification is known. These probabilities are then incorporated into a maximum likelihood classification algorithm which can be used to classify unknown pattern sets. Details of the algorithm are presented in the Appendix and are developed heuristically below.

2.1 MAXIMUM LIKELIHOOD PRINCIPLE

The principle of maximum likelihood, as it applies to the problem under consideration, can be illustrated by a simple urn model. Consider two urns containing different mixtures of black and white balls (Figure 1). Let a ball be drawn randomly from one of the urns and let its color be communicated to a decision maker whose task is to "guess" which urn yielded the ball. It is assumed that the decision maker does not know the source of the ball but does know the relative proportions of black and white balls in the two urns. Suppose that, at the outset, one urn is as likely to be sampled as the other. It is evident, then, that if the ball drawn is black, it "most likely" came from urn I, but if it is white, it "most likely" came from urn II. If the decision maker calls I on black and II on white, therefore, his "batting average" will be 75% correct decisions.

Figure 1. URN MODEL DEMONSTRATING MAXIMUM LIKELIHOOD DECISION MAKING

The simple process described above becomes less straightforward if the two urns are not sampled with equal likelihood. Suppose, for example, that urn II is sampled much more often than urn I. It should now be apparent that a black ball does not necessarily imply a high probability that the ball came from urn I. Quite clearly, the decision making process needs to be adjusted to allow for the preference of the sampling process for urn II. This preference can be taken into account by proper attention to the "prior probability" that urn II will be sampled more frequently than urn I. As shown in the Appendix, Bayes' theorem provides the basis for such adjustment. In the event that urn II is sampled three times as often as urn I, drawing a black ball affords no basis for decision: the chances are 50/50 that either urn I or urn II was the source.

2.2 JOINT AND CONDITIONAL PROBABILITY FUNCTIONS

In many practical situations, the distinction between sources of items to be classified is not nearly as definitive as in the urn model discussed above. Items from the various sources may be very much "like" each other in the sense that no one attribute or feature stands out as a specific indicator of source. For example, suppose that urn II contains 51% black balls and that urn I contains 49% black balls. The slight "edge" of urn II over urn I is not a sufficient basis for decision making if one wants to be right "most of the time." Suppose, however, that there are several attributes, each exhibiting a slight edge with regard to probability of occurrence in one of the categories. If a sufficient number of these bits of information can be composited, it may well turn out that decisions can be made with relatively high probability of being correct even though decision based on any one item of information would be highly problematical.

Suppose, for example, that the balls differ not only in color but in shape: some are perfect spheres while others are recognizably distorted. Though the two shapes, like the two colors, may occur with about equal frequency in the two urns, the joint occurrence of color and shape may be considerably more indicative of source of origin than either color or shape considered alone.

A popular approach to consideration of joint probabilities is to regard the occurrence of the several attributes as statistically independent. In the above example, this assumption is equivalent to saying that the probability that a ball is black is the same whether the ball is perfect or malformed or, conversely, that the probability that the ball is perfect is the same whether the ball is black or white. Under such an assumption, the probability of occurrence of a perfect black ball is just the probability that the ball is black times the probability that the ball is perfect.

In many cases, of course, the assumption of independence is violated. The conditions "black" and "perfect" may tend to go together, and so may "white" and "imperfect." In such instances, decision making can be improved by incorporating conditional probabilities into the decision making process. Given that a ball is black, the probabilities associated with perfect and imperfect spheres take on one set of values; given that a ball is white, the shape probabilities take on a different set of values. Under these conditions, joint probabilities can no longer be computed by the product rule but must be determined directly for the four classes: white-perfect, white-imperfect, black-perfect, black-imperfect.

As the number of attributes is increased, the prospect for more complex forms of dependences presents itself. Thus one can speak of first-order dependence, second-order dependence, and so on according to the number of conditions which must be specified before probabilities for the occurrence of a particular feature can be specified.

It should be clear that as the number of features is increased, the number of combinatorial possibilities for dependences goes up very rapidly. For example, in a set of 10 features, there are 45 possible first-order dependencies alone; consequently, it is advantageous to incorporate into the decision making process only those dependencies which are in some sense "most important." The means whereby these primary dependences are singled out for inclusion in the decision-making algorithm is discussed in the Appendix.[7] The key concept is a measure called "mutual information." By means of this measure, the various first-order dependences can be ranked in order of their importance so that the most critical dependences can be incorporated into the decision algorithm.

3. EXAMPLE PROBLEM

3.1 SCENARIO

With the above preamble it is possible to demonstrate the technique of Bayesian classification by its application to a specific "scenario" which could conceivably arise in connection with particulate effluents as they affect air quality. Consider a situation wherein three industrial coal-burning operations are located in the same general geographic area. Each of these sites is producing fly ash particulates, some of which escape and are carried downwind where they adversely affect air quality. It is possible to sample the particulates at the sources (i.e., in the stacks), and it is also possible to sample the (combined) effluents downwind (Figure 2).

Figure 2. SCENARIO OF EXAMPLE PROBLEM

By means of scanning electron microscopy coupled with energy dispersive X-ray spectroscopy or electron microprobe analysis, it is possible to analyze these particulates for percent concentrations of the various chemical elements making up fly ash. Ten of the more important constituents of fly ash are: Carbon, Sodium, Magnesium, Aluminum, Silicon, Phosphorus, Sulfur, Potassium, Titanium, and Iron. Of these elements Al, Si, and Fe are major constituents; the rest are present in trace amounts (say 5% or less). These data can be normalized, digitized, and placed into a ten-component "pattern vector" characterizing each fly ash particle.

The problem we proposed to solve is the following: Given that samples of particulate effluents can be collected at each of the sources S_1, S_2, S_3, and at a downwind site C, estimate the percentages of the total sample collected at C which originated at each of the sources. The data to be used in this problem will be the concentrations of the ten chemical elements listed above.

It should be pointed out that this problem is not without its analogies in the "real world." In a project conducted for the Erie County Air Pollution Control Board, Calspan Corporation attempted an identification as to source of particulate effluents collected downwind from four sources within a local steel plant on the basis of data obtained from particles collected within the stacks.[8] Although the mathematical techniques presented here were not employed in that study, the problem itself is comparable.

3.2 DATA GENERATION

Fly ash from coal-burning power generation plants varies in chemical composition as a result of a number of factors, notably differences in the coal used as fuel and differences in efficiency of the combustion process. Conceivably, then, the particulate effluents from two or more generating plants might be expected to carry "fingerprints" by which their source

identity might be inferred. It is on this assumption that a collection of data was simulated. It is emphasized that the data, though believed to be "reasonable," were generated by purely random means for the express purpose of demonstrating how principles of pattern recognition might be applied in a particle-identification context.

Table 1 shows the bulk chemical composition of three fly ashes used in an experiment to evaluate the ability of fly ash to reclaim acidic surface-mined coal lands.[9]

Table 1

CHEMICAL ANALYSES OF FLY ASHES

	Ash #1	Ash #2	Ash #3
Chemical Analysis, wt pct			
Aluminum (Al_2O_3)	23.9	23.9	23.6
Silicon (SiO_2)	46.3	42.2	47.7
Iron (Fe_2O_3)	22.9	24.0	15.6
Phosphorus (P_2O_5)	.3	.2	.6
Titanium (TiO_2)	.9	.8	2.7
Calcium (CaO)	1.9	4.0	3.5
Magnesium (MgO)	.8	1.2	1.5
Potassium (K_2O)	2.2	2.2	2.2
Sodium (Na_2O)	.6	.6	1.9
Cobalt	.02	.02	ND*
Boron	.008	.02	ND
Manganese	.03	.05	ND
Copper	.02	.02	ND
Molybdenum	.007	ND*	ND
Carbon	5-7	12.4	1.54
Sulfur (total)	.24	.51	.34

Note that on a bulk basis the differences among the three ashes are slight for certain elements such as aluminum and silicon but are appreciable for other elements such as iron, titanium, and carbon.

*not determined

To generate data for a sample problem, the analyses of Table 1 were considered typical. Then, by means of a random number generator which used postulated variances, a collection of 1000 "particles" were "produced" for each of the three ashes and, finally, for 1000 particles constituting an arbitrary mix of the three sources. It was assumed that discrimination among sites would be based on individual-particle examination rather than on bulk sample analysis for two reasons: first, the collection of a bulk sample might be difficult and, second, the fly ash undoubtedly would be mixed with extraneous debris and would have to be identified as fly ash on the basis of its particle morphology. Consequently, identification of the fly-ash source would have to be based on chemical analysis of individual fly-ash particles by means of some technique such as electron microprobe or energy dispersive X-ray analysis as previously mentioned.

Figure 3 is a scanning electron micrograph of a sample of fly ash particles. Though these particles all look similar, they are revealed by energy dispersive X-ray (Figure 4) to vary considerably in composition. In particular, some appear to be relatively high in iron and low in silicon and aluminum, whereas for others the reverse appears to be true. In short, considerable variation in composition from particle to particle can, and most likely does, exist even within a given source of fly ash. The simulated data were constructed to reflect this postulated variation.

Consider, for example, the iron analyses in Table 1. It is postulated that individual particles from a composite sample of the three fly ashes might have a statistical distribution as shown in Figure 5. On an interval basis, one can hypothesize four ranges of iron content -- say trace, low, medium and high -- and can compute probabilities that particles from each of the three sources fall into the trace, low, medium, and high categories (states 1, 2, 3, or 4).

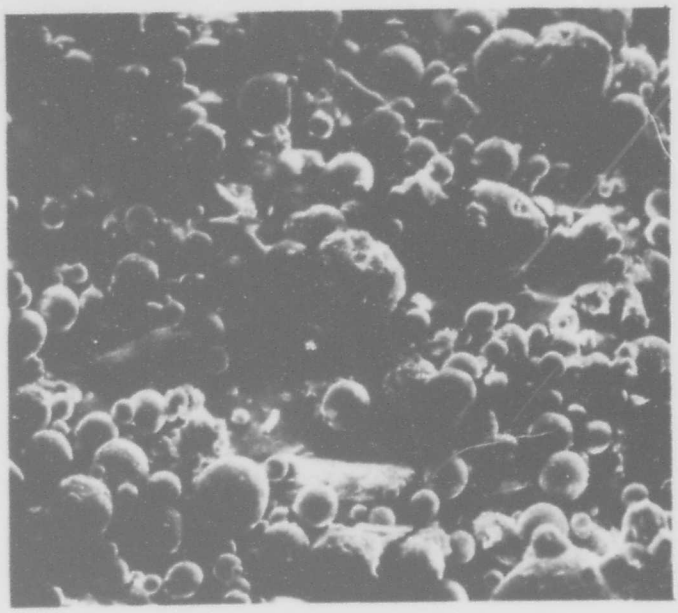

(A)

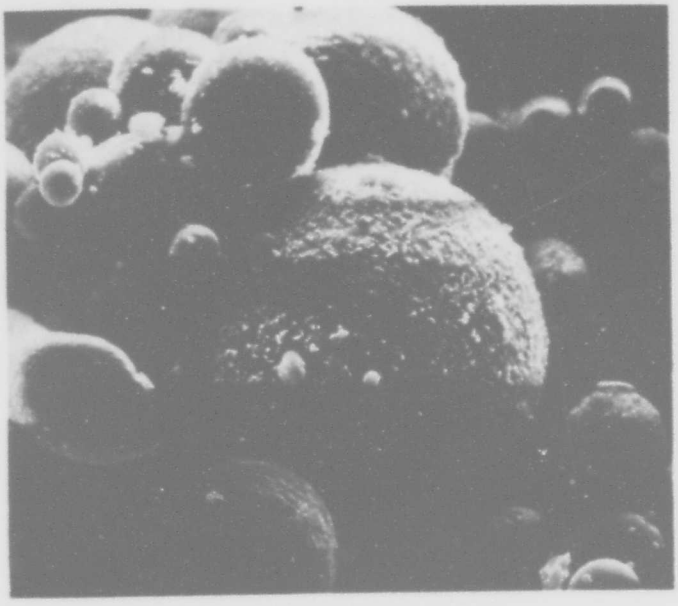

(B)

Figure 3 (A) SEM MICROGRAPH AT 400 X OF EASTLAKE PLANT MAGNETITE
(B) SEM MICROGRAPH AT 1600 X OF EASTLAKE PLANT MAGNETITE

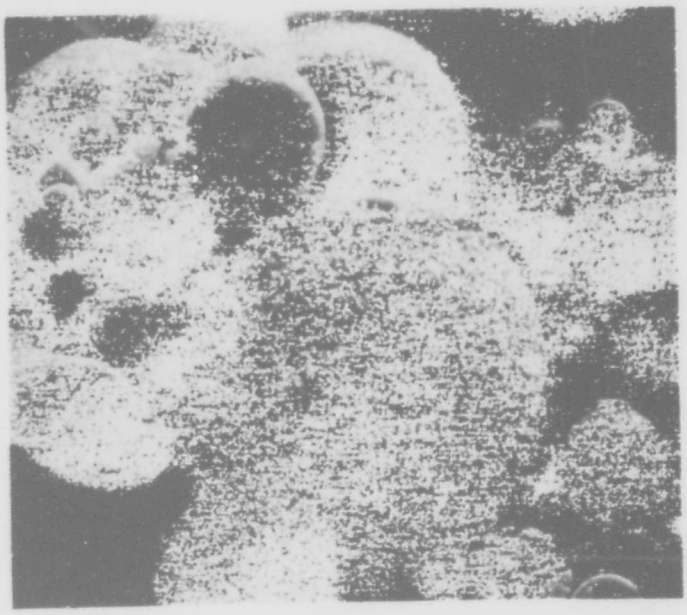

(A)

(B)

Figure 4 (A) IRON MAP OVERLAP ON SEM MICROGRAPH OF FIGURE 3 (B)
(B) SILICON AND ALUMINUM MAP OVERLAY ON SEM MICROGRAPH OF FIGURE 3 (B)

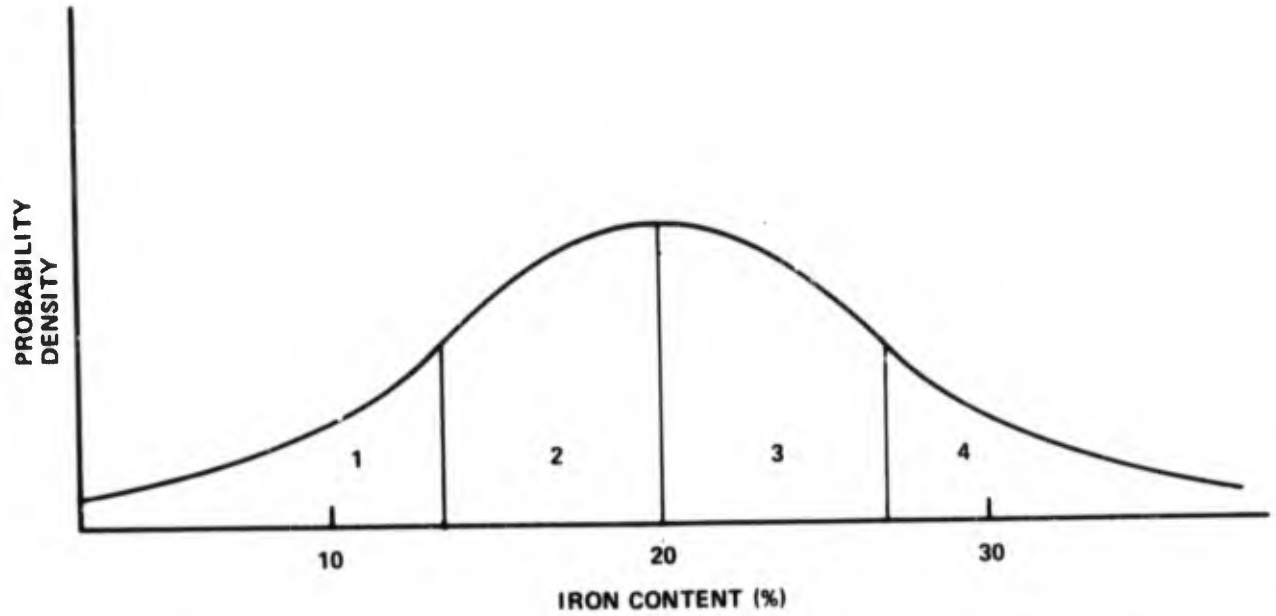

Figure 5 POSTULATED DISTRIBUTION OF IRON IN FLY-ASH PARTICLES

It is a reasonable assumption, therefore, that particles from fly ashes #1 and #2 would exhibit a distribution skewed toward the high-concentration range, whereas particles from fly ash #3 would exhibit a distribution skewed toward the low-concentration range. For purposes of the example experiment, these differences were realized by assigning the following probabilities to the iron ranges for the three fly ash samples.

	Trace	Low	Medium	High
Ash #1	5	15	50	30
Ash #2	5	15	50	30
Ash #3	30	50	15	5

Note the considerable amount of overlap of the three distributions; in particular, there is no distinction between ash #1 and ash #2 on the basis of iron alone.

The method of allocation of probabilities discussed above was applied to the ten elements: Al, Si, Fe, P, Ti, Na, Ca, Mg, K, and C with the results shown in Table 2.

Table 2

STATE PROBABILITIES FOR SELECTED CHEMICAL ELEMENTS IN FLY ASH

	ASH #1				ASH #2				ASH #3			
State	1	2	3	4	1	2	3	4	1	2	3	4
	Percent of Occurrences											
Al	15	35	35	15	15	35	35	15	15	35	35	15
Si	15	35	35	15	15	35	35	15	15	35	35	15
Fe	5	15	50	30	5	15	50	30	30	50	15	5
P	15	35	35	15	25	50	20	5	5	25	60	10
Ti	15	35	35	15	25	50	20	5	5	10	75	10
Na	15	35	35	15	15	35	35	15	5	5	80	10
Ca	25	50	15	10	5	20	50	25	15	35	35	15
Mg	30	50	15	5	15	35	35	15	5	15	50	30
K	15	35	35	15	15	35	35	15	15	35	35	15
C	15	35	35	15	5	5	75	15	15	75	5	5

In view of the apparent association between certain elements such as Fe and Si, however, it is not realistic to assume that the distributions of Table 2 are all statistically independent. To allow for the possibility of statistical dependence, it was assumed that Al, Si, Fe, and Ti were correlated to varying degrees and that this correlation was not the same for all three sources. Correlation implies that probabilities associated with these elements must be given as conditional, rather than as unconditional, probabilities.

Tables 3, 4 and 5 give the conditional probabilities which were used as inputs to the random generation process. In Table 1, which characterizes Ash #1, it is assumed that Al and Si always occur together and in the same state -- that is, if Al is in state 3, then Si is also in state 3. The four states have the probabilities 0.15, 0.35, 0.35, and 0.15. Note, however, that if Al and Si are in state 1, Fe is always in state 4, whereas if Al/Si is in state 4, then Fe will occur in state 1 with probability 0.3 and in state 2 with probability 0.7 but never in states 3 or 4. Finally, the state probabilities for Ti depend on knowing what state Fe is in. For example, when Fe is in the highest state, Ti has 0.5 probability of being in state 1 or state 2. When Fe is in its lowest state, however, Ti always occupies its highest state.

Table 3

CONDITIONAL PROBABILITIES FOR ASH #1

Al/Si (Read Down)	Fe (Read Down)	Ti (Read Across)			
.15	0	0	0	0	1.0
	0	0	0	.3	.7
	0	0	.4	.6	0
	1.0	.5	.5	0	0
.35	0	0	0	0	1.0
	0	0	0	.3	.7
	.6	0	.4	.6	0
	.4	.5	.5	0	0
.35	0	0	0	0	1.0
	.15	0	0	.3	.7
	.85	0	.4	.6	0
	0	.5	.5	0	0
.15	.3	0	0	0	1.0
	.7	0	0	.3	.7
	0	0	.4	.6	0
	0	.5	.5	0	0

Table 4

CONDITIONAL PROBABILITIES FOR ASH #2

Al/Si (Read Down)	Fe (Read Down)	Ti (Read Across)			
.15	0	.25	.50	.20	.05
	0	.25	.50	.20	.05
	0	.25	.50	.20	.05
	1.0	.25	.50	.20	.05
.35	0	.25	.50	.20	.05
	0	.25	.50	.20	.05
	.6	.25	.50	.20	.05
	.4	.25	.50	.20	.05
.35	0	.25	.50	.20	.05
	.15	.25	.50	.20	.05
	.85	.25	.50	.20	.05
	0	.25	.50	.20	.05
.15	.3	.25	.50	.20	.05
	.7	.25	.50	.20	.05
	0	.25	.50	.20	.05
	0	.25	.50	.20	.05

Table 5

CONDITIONAL PROBABILITIES FOR ASH # 3

Al/Si (Read Down)	Fe (Read Down)	Ti (Read Across)			
.15	.30	.3	0	.7	0
	.50	.3	0	.7	0
	.15	.3	0	.7	0
	.05	.3	0	.7	0
.35	.30	0	.3	.7	0
	.50	0	.3	.7	0
	.15	0	.3	.7	0
	.05	0	.3	.7	0
.35	.30	0	0	1.0	0
	.50	0	0	1.0	0
	.15	0	0	1.0	0
	.05	0	0	1.0	0
.15	.30	0	0	.3	.7
	.50	0	0	.3	.7
	.15	0	0	.3	.7
	.05	0	0	.3	.7

With the underlying probability distributions defined above, random "particles" were generated as strings of 10 digits, each digit of which was either 1, 2, 3, or 4. Position in the string denoted the element and the digit in that position denoted the concentration state for the element. For the purposes of the experiment, random numbers in the interval 0.0-1.0 were generated and states assigned according to whether the number fell within certain subranges defined so as to occur with the desired probabilities. The necessary conditional probabilities were generated in a similar way.

3.3 PARTICLE MIXTURE ANALYSIS

Consider three sources S_1, S_2, S_3 and a collection site C. Let it be assumed that a classification algorithm has been developed and that the performance of this algorithm is given by the "classification matrix" below.

		Item is classified as		
		S_1	S_2	S_3
Item belongs to	S_1	.7	.2	.1
	S_2	.2	.6	.2
	S_3	.1	.1	.8

The classification matrix simply tabulates, for each of the sources S_1, S_2, S_3, the probabilities that a particle from a given source will be assigned to S_1, S_2, or S_3. Perfect classification would be represented by a matrix having 1.0 in each principal diagonal position and zero elsewhere. In practice, however, perfect classification is seldom achieved and the off-diagonal elements of the matrix indicate the extent of misclassification indigeneous to the algorithm under consideration. How do errors of misclassification propagate when a composite mix of particles is involved, and how can these errors be accommodated under circumstances in which the prior probabilities are unknown?

To answer these questions, it is appropriate to proceed from the known to the unknown. Suppose that of all the particles collected at C, 20% originated in source S_1, 30% in source S_2, and 50% in source S_3. How would this collection of particles be assigned by the classification algorithm?

Of the 20% from S_1, 70% would be assigned to S_1, 20% to S_2, 10% to S_3. The corresponding fractions of the total collection so assigned would be

$$(0.2)\ (0.7) = 0.14 \text{ to } S_1$$

$$(0.2)\ (0.2) = 0.04 \text{ to } S_2$$

$$(0.2)\ (0.1) = 0.02 \text{ to } S_3$$

Of the 30% from S_2, 20% would be assigned to S_1, 60% to S_2, 20% to S_3. The corresponding fractions of the total collection so assigned would be

$$(0.3)\ (0.2) = 0.06 \text{ to } S_1$$
$$(0.3)\ (0.6) = 0.18 \text{ to } S_2$$
$$(0.3)\ (0.2) = 0.06 \text{ to } S_3$$

Of the 50% from S_3, 10% would be assigned to S_1, 10% to S_2, and 80% to S_3. The corresponding fractions of the total collection so assigned would be

$$(0.5)\ (0.1) = 0.05 \text{ to } S_1$$
$$(0.5)\ (0.1) = 0.05 \text{ to } S_1$$
$$(0.5)\ (0.8) = 0.40 \text{ to } S_2$$

Then, of <u>all</u> the particles collected,

$$0.14 + 0.06 + 0.05 = 0.25 \text{ would be assigned to } S_1$$
$$0.04 + 0.18 + 0.05 = 0.27 \text{ would be assigned to } S_2$$
$$0.02 + 0.06 + 0.40 = 0.48 \text{ would be assigned to } S_3$$

Note that the fractions 0.25, 0.27, 0.48 differ from the actual fractions 0.20, 0.30, and 0.50.

In practice, we will determine the assigned fractions, and the actual fractions will be unknown. Let x_1, x_2, x_3 denote the unknown fractions. Then, in the above problem,

$$0.7\,x_1 + 0.2\,x_2 + 0.1\,x_3 = 0.25$$
$$0.2\,x_1 + 0.6\,x_2 + 0.2\,x_3 = 0.27$$
$$0.1\,x_1 + 0.1\,x_2 + 0.8\,x_3 = 0.48$$

or, in matrix notation,

$$D\,\underline{x} = \underline{y}$$

where D is the classification matrix

$\underline{x}$ is the vector of prior probabilities

and $\underline{y}$ is the vector of posterior probabilities

Solution of the simultaneous equations will be seen to yield the prior probabilities assumed at the outset. The following section presents the results of applying this technique to the simulated data.

3.4 RESULTS

The results of applying the Bayesian approach to simulated data on fly ash particulates illustrate and reinforce the principles discussed above. Implementation of this algorithm is a two-stage proce s. In the first stage simulated elemental occurrences for fly ash particles from each of the three sources are used to construct estimates for the underlying probabilities of occurrence. In the second stage the probability that an "unknown" fly ash particle exists in each source is calculated, and the particle is classified as having come from that source for which its probability of occurrence is highest. The result of this exercise is a classification matrix D in which the element d_{ij} is the percent of particles known to have come from source i which was classified as having come from source j. Ideally, the diagonal elements would be 100% and the off-diagonal elements would be zero. In practice, some misclassification will occur, and the success of classification can be judged by the size of the diagonal elements.

Two Bayesian schemes were applied to these data. The first scheme invoked the assumption that the elements observed in the particles were statistically independent. This is clearly not a good assumption, since statistical dependence was built into the data. Accordingly, the second scheme invoked the assumption of first-order dependence among elements.[7] In each case 1000 particles from each of the three sources were used as the training set to construct estimates of the underlying probabilities. Then 1000 <u>different</u> particles from each of the three sources were run

through the algorithm and classified as to source. Finally, a mixture of 1000 particles taken from all three sources (i.e., particles taken "downwind" from the sources) were classified and "unscrambled" as to sources of origin.

The results of the classification under the assumption of statistical independence are shown below.

Table 6

CLASSIFICATION RESULTS ASSUMING STATISTICAL INDEPENDENCE OF ELEMENTS

		Source as Classified		
ACTUAL SOURCE		S_1	S_2	S_3
	S_1	74.2	17.0	8.8
	S_2	16.2	78.4	5.4
	S_3	6.4	3.1	90.5

The mixture of 1000 particles was then classified. Results showed 29.7% assigned to S_1, 45.9% assigned to S_2, and 24.4% assigned to S_3. Solution of the simultaneous equations indicated the prior probabilities to be 25.4%, 51.7%, and 23.4%. The actual mix employed in the simulation was 30%, 50%, and 20%.

A second set of results was obtained by classification under the assumption of first-order dependence among elements. The results of that classification are shown in Table 7.

Table 7

CLASSIFICATION RESULTS ASSUMING FIRST-ORDER DEPENDENCE AMONG ELEMENTS

		Source as Classified		
ACTUAL SOURCE		S_1	S_2	S_3
	S_1	83.4	13.4	3.2
	S_2	13.9	83.4	2.7
	S_3	3.3	2.2	94.5

Considerable improvement was obtained by taking into account the statistical dependence among elements. The mixture of particles was again classified, and the results were 32.6% classified into S_1, 46.6% classified into S_2, and 20.9% classified into S_3. The prior probabilities calculated by solving the set of linear equations were 30.2%, 50.2%, and 19.8%. Again the correct results were 30%, 50%, and 20%.

The classification results obtained under the assumption of first-order dependence is encouraging. The correct percentage of effluent from each source was identified to within two significant figures. The three "unknown" sets of 1000 particles each achieved good classification results. The potential of this method for identifying effluents collected downstream on the basis of information obtained at the sources is clearly illustrated.

4. CONCLUSION

The purpose of this paper has been to demonstrate that the techniques of pattern recognition exhibit potential value for the analysis of trace constituent data. Thus an example problem has been constructed and worked out in some detail using one of a vast array of pattern recognition techniques. The problem was constructed so as to include as much "realism" as possible and to preclude a trivial or facile solution.

The technique employed in this exercise was a maximum likelihood (Bayesian) classifier. There are available many other pattern recognition techniques. In particular, geometric (nonparametric) algorithms such as linear discriminant function analysis, Euclidean distance classification, and other supervised learning approaches may be applicable to this problem as well. The problem of identification of sources from data taken downwind may also be amenable to techniques available in unsupervised learning or cluster analysis. Techniques such as "non-linear mapping" may provide a graphic display method for sorting out and identifying data from several sources.

The results obtained by application of the maximum likelihood algorithm to the problem proposed here are encouraging. The data used in this exercise were simulated data designed to reflect real differences that were reflected in bulk analysis of real data from three fly ash producing sites. The data thus reflected differences in probabilities of elemental occurrence that accounted for the ability to discriminate among sources. This is not without physical merit, however, in that it is to be expected that such differences will arise in actual situations. The use of random number generators to create the data set further contributes to the "realism" of the example problem and illustrates the promise of these methods in attacking the problem of source identification. It is hoped that this demonstration problem will stimulate interest in the use of pattern recognition as a data analysis tool for trace constituent characterization.

APPENDIX

The maximum likelihood classification algorithms employed in this paper are based on a theorem of Bayes concerning the probability of occurrence of an event. Let $S_1, S_2, \ldots S_n$ denote one of n possible sources from which particulate effluents can emanate and let A be a "feature" or characteristic of a particle (e.g., an elemental concentration). Then the probability that a particle exhibiting the property A emanated from source Si, $P(S_i|A)$, is given by

$$P(S_i|A) = \frac{P(S_i)\ P(A|S_i)}{\sum_{j=1}^{n} P(S_j)P(A|S_j)} \qquad (A\text{-}1)$$

where $P(A|S_j)$ is the conditional probability that the property A will be observed given that S_j is the source sampled and $P(S_j)$ is the prior probability that S_j was the source from which the sample was drawn.

The probability $P(S_i|A)$ is referred to as an inverse probability and, given good estimates of the probabilities on the right side of Eq. (A-1), can be calculated for each source S_i. The source S_i for which the inverse probability is the greatest is, in fact, that source from which the particle is most likely to have emanated.

The application of the maximum likelihood strategy under the assumption of statistical independence of elemental occurrence requires the computation of the joint probability of occurrence of (in our problem) ten elemental concentration states as the product of the marginal distributions of the several states considered individually. Thus

$$P_j\ (x_1,\ x_2,\ \ldots\ x_{10}) = \prod_{i=1}^{10} P_{ji}\ (x_i) \qquad \text{(A-2)}$$

$P_j\ (x_1,\ x_2,\ \ldots\ x_{10})$ is the probability that the fly ash particle with concentration states $(x_1,\ x_2,\ \ldots\ x_{10})$ emanated from source S_j and $P_{ji}\ (x_i)$ is the marginal probability that concentration state x_i occurred in source S_i. These P_{ij}'s are estimated by the equation

$$P_{ij}\ (x_i) = n_{ij}\ (x_i)/N \qquad \text{(A-3)}$$

where n_{ij} is the number of times the concentration state x_i occurs in a sample from source S_i of size N. The $P_{ij}\ (x_i)$ functions are estimated from data contained in the training set, the function $P_j\ (x_1, x_2, \ldots x_{10})$ is calculated for each unknown particle, and the particle is assigned to that source for which P_j is largest.

As was pointed out in the text, the assumption of statistical independence of elements in fly ash particulates is a dubious one on chemical grounds. A method of accounting for some of the dependence among elements is based on "dependence trees."[7] Let $P_j\ (x_1,\ x_2,\ \ldots\ x_{10})$

denote the joint distribution of the 10 elements. This distribution can be approximated by

$$P_j\ (x_1, x_2, \ldots x_{10}) = \prod_{i=1}^{10} P\ (x_i | x_{j\ (i)}) \qquad \text{(A-4)}$$

implying a dependence relation $j(i)$ among the elements. This relation can be represented by a directed graph, or "dependence tree." For example, consider five variables (x_1, x_2, x_3, x_4, and x_5) for which the dependence tree is as follows:

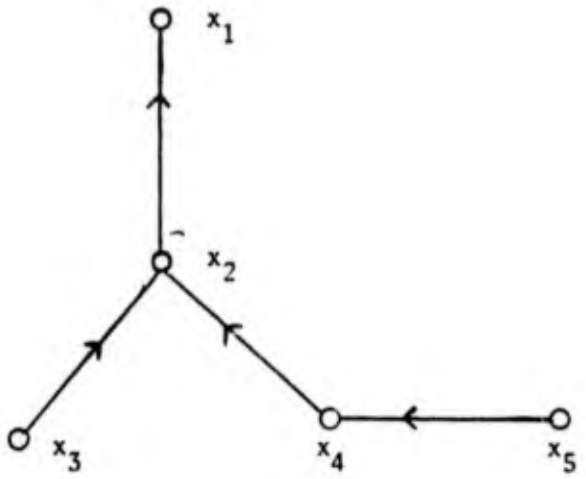

Then,

$$P(x_1, x_2, \ldots x_5) = P(x_1)\ P(x_2|x_1)\ P(x_3|x_2)\ P(x_4|x_2)\ P(x_5|x_4) \qquad \text{(A-5)}$$

where, for example, $P(x_5|x_4)$ means the probability that element 5 is in state x_5 given that element 4 is in state x_4. The dependence sequence is determined by extracting from the possible ordering sequence that one which best approximates the joint probability as a product of conditional probabilities. Unknowns are then classified as before.

REFERENCES

1. P.C. Jurs, B.R. Kowalski, and T.L. Isenhour, Anal. Chem., 41, 21, (1969).

2. B.R. Kowalski, and C.F. Bender, J. Amer. Chem. Soc., 94, 5632, and references therein.

3. K.C. Chu, Anal. Chem., 46, 1181, 1974.

4. T.R. Thomas, C.F. Holmes, H.T. McAdams, and J.C. Bernard, Proc. Int. Eng. Conf., 1975.

5. J.W. Becus and E.E. Gose, I.E.E.E. Trans. SMC, SMC-2, 513 (1972).

6. C.W. Swonger, "Applications of Fingerprint Identification Technology to Criminal Identification and Security Systems," presented at the First International Conference on Electronic Crime Countermeasures, Edinburgh, Scotland, 1973.

7. C.K. Chow and C.N. Liu, I.E.E.E. Trans. on Information Theory, IT-14, 462 (1968).

8. C. Easterbrook, "Analysis and Characterization of Airborne Particulates in Erie County, New York," Calspan Report to Erie County Department of Health, 1974.

9. J.P. Capp and L.M. Adams, "Reclamation of Acid Spoil with Power Plant Fly Ash," presented at Mined-Land Redevelopment Workshop, Pittsburgh, Kansas.

DETERMINATION OF CONCENTRATION OF EXPLOSIVES IN AIR BY ISOTOPE DILUTION

Gilbert A. St. John, James H. McReynolds, and Michael Anbar
Mass Spectrometry Research Center
Stanford Research Institute
Menlo Park, California 94025

The design of instrumentation for the detection of explosives or narcotics, and the application of such devices under field conditions must take into account many parameters including:

(1) Static vapor pressure of pure material

(2) Static vapor pressure of material over explosive

(3) Rate of evaporation from explosive

(4) Rate of equilibration with surfaces

(5) Extent of adsorption on particulate matter in air

(6) Rate of equilibration with particulate matter

(7) Rate of penetration through barriers.

The first requirement is to obtain reliable information regarding the concentration in air of the materials in question in pure state at room temperature under equilibrium conditions. The next important task is to ascertain the concentrations in air over impure technical products or composites under equilibrium conditions; these will, as a rule, be lower than those over the pure material. Information on the rates of adsorption on surfaces, desorption from surfaces, and diffusion through packaging materials requires measurement of concentrations in air of the materials in question, but now under dynamic conditions. Such practical measurements would involve determination of concentrations 1 to 3 orders of magnitude below those of the equilibrium values.

Many of the materials in question (e.g., TNT, RDX, PETN, heroin, cocaine) have very low vapor pressures (of the order of microtorrs) which produce equilibrium concentrations in air of the order of ppb (v/v). The determination

of the concentrations in air of such materials under dynamic conditions requires sampling of air with minimum disturbance and thus limits the sample size to small volumes of air (10 to 50 ml). Ten ml of air would contain such materials in amounts of the order of 0.1 ng, even under equilibrium conditions, and only picogram amounts under dynamic non-equilibrium conditions.

Because of excessive adsorption of such nonvolatile polar materials on the walls of the sampling vessels or the inlet system of the measuring device, the quantitative determination of such small amounts of material is extremely difficult, even if detection systems of sufficient sensitivity were available. Monolayer adsorption involves 10^{15} molecules per cm^2; thus, at 1% saturation, a sampling vessel with 10 cm^2 area would have about 10^{-8} g of TNT adsorbed on its walls, i.e., approximately 100 times more material than it would contain in the gas phase at room temperature under equilibrium conditions with bulk TNT.

Isotope dilution analysis (using stable isotopes as labels) overcomes this difficulty. In this technique we add a known amount (100 to 10,000 times larger) of isotopic carrier to the sample and determine the abundance ratio of unlabeled to labeled material by mass spectrometry. In order to attain sizable dilution factors (> 100) without interference from the natural abundance of the heavy isotopes, carrier molecules multilabeled with a number of isotopic heavy atoms are used. It is preferable to use carriers with molecular weights 5 to 8 amu higher than the material at its natural isotopic composition.

Field ionization mass spectrometry is the analytical method of choice for the assay of unlabeled and labeled materials because it produces almost exclusively unaltered molecular ions, as can be seen from the following figures. Figure 1 shows a field ionization spectrum of pure hydrocarbon compared with that of an electron impact spectrum of the same. Figure 2 is the field ionization spectrum of DNT. Figure 3 is a spectrum of hexalabeled DNT. Note the absence of any significant amount of the unlabeled material in the isotopic carrier. Figure 4 is an analogous spectrum of pentalabeled TNT. Figures 5 and 6 are the spectra of multilabeled RDX and PETN, respectively.

The determination of the concentrations in air under equilibrium conditions was carried out by rapid transfer of 50 ml of air equilibrated with the pure explosive in a 3-liter vessel to an evacuated sampling vessel containing 100 to 400 ng of multilabeled carriers. The air was removed from the sample vessel by freezing and pumping; the material was dissolved in an appropriate solvent (e.g., benzene) and transferred to the mass spectrometer using a solid sample probe.

The equilibrium vapor pressures of a number of pure explosives determined by this technique are presented in Table 1. In the case of nonvolatile explosives (e.g., nitrocellulose), volatile additives present in smokeless powders may be detected by air monitors. A number of volatile additives have been detected and identified by monitoring the effluents from powder samples by field ionization mass spectrometry at room temperature. Figure 7 shows a few examples of such spectra. The materials positively identified are diphenylamine, DNT, sym diphenyldiethyl urea (ethyl centralite), and its methyl analog, as well as dibutylphthalate. The compound at mass 198 is tentatively identified as dinitrocresol. Tables 2a and 2b summarize the findings on over 30 kinds of smokeless powders. Using the isotope dilution technique we are presently able to measure the equilibrium concentrations in air of these additives over a number of smokeless powders. These concentrations will evidently be lower than those of the neat materials.

The nonfragmenting nature of field ionization mass spectrometry also makes it a unique tool for characterization and identification of explosives by the content of their volatile constituents. This can be seen from the molecular weight profiles of the volatile constituents of smokeless powders (Figure 7) as well as from the characteristic fingerprint of the volatile constituents of dynamites (Figures 8 and 9). Higher resolution field ionization mass spectrometry can characterize even more complex mixtures and identify them through their molecular weight profiles as is exemplified for different crude oils in Figure 10.

This research has been sponsored by the U.S. Postal Service under Contract No. 74-00810.

Table 1

ROOM TEMPERATURE ($25^{o} \pm 2^{o}C$) VAPOR PRESSURES OF EXPLOSIVE COMPOUNDS OBTAINED BY THE ISOTOPE DILUTION METHOD

Compound	Concentration (g/cc)	P (torr)	Moles/Mole
EGDN	2.5×10^{-7}	2.8×10^{-2}	37 ppm
DNT	1.3×10^{-9}	1.4×10^{-4}	184 ppb
NG	3.2×10^{-10}	2.4×10^{-5}	31 ppb
PETN	1.0×10^{-10}	5.3×10^{-6}	7 ppb
TNT	4.0×10^{-11}	3.0×10^{-6}	4 ppb
RDX	8.0×10^{-12}	6.1×10^{-7}	0.8 ppb

Table 2a

SMOKELESS POWDER	Diphenyl-amine m/e 169	Dinitro-toluene m/e 182	Dinitro-cresol m/e 198	Methyl-centralite m/e 240	Ethyl-centralite m/e 268	Dibutyl-phthalate m/e 278
#1 Hercules 2400	++++				+++	++
#2 Hercules Unique					++++	
#3 Hercules Green Dot	++++					
#4 Hercules Herco	++++					
#5 Hercules Bullseye					++++	
#6 Hercules Red Dot	++++				+++	
#7 Hercules 21	+++				++++	
#8 Hercules 11	+++				++++	
#9 Hercules 7	+++				++++	
#10 Alcon A17	+++					++++
#11 Dupont IMR-4198	+++	++++				
#12 Winchester 760BR	++++	+	++			+++
#13 Winchester 630P	++++	++	+++			
#14 Winchester AA20S	++++	++	+++			
#15 Winchester 450LS	++++	++	+++			

Table 2b

SMOKELESS POWDER	Diphenyl-amine m/e 169	Dinitro-toluene m/e 182	Dinitro-cresol m/e 198	Methyl-centralite m/e 240	Ethyl-centralite m/e 268	Dibutyl-phthalate m/e 278
#16 Winchester 500	++++	++	+++			
#17 Winchester AA12S	++++	++	+++			
#18 Winchester 540MS	++++	++	+++			
#19 Winchester AA665S	++++	++	+++			
#20 Winchester 630BR	++++	++	+++			
#21 Winchester 780BR	++++	++	+++			
#22 Winchester 230P	+++	++	++++			
#23 Winchester 748BR	++++	+	+++			++
#24 Winchester 680 BR	++++	+	+++			++
#25 Hodgdon H335	++++	++	+++			+
#26 Hodgdon H110	++++	+	++			+++
#27 Hodgdon H380	++++	+	++			+++
#28 Hodgdon BL-C	++++	+	++			+++
#29 Hodgdon H870	++++		++			+++
#30 Russian 7.62 mm	++++					
#31 Dupont HSKOR	++++	+++				
#32 Dupont IMR	+++	++++			+	
#33 Hodgdon 4895	+++	+		++++	++	
#34 Alcon Al-5	++++					

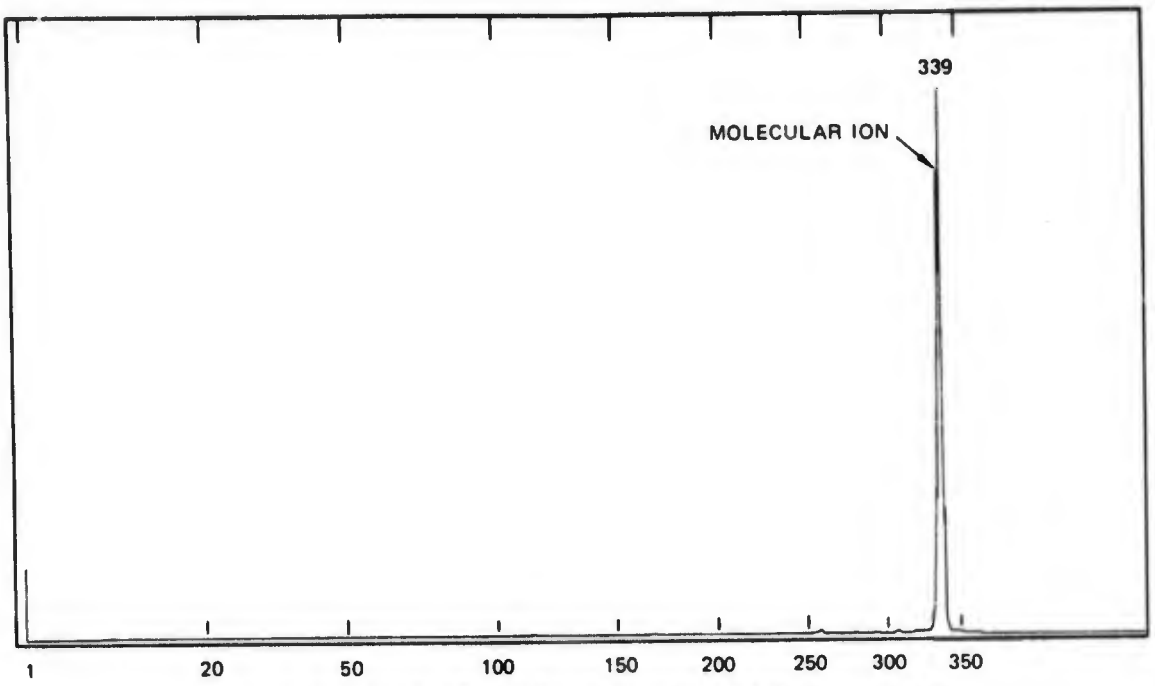

FIELD IONIZATION SPECTRUM OF n-TETRACOSANE, M.W. = 338.67

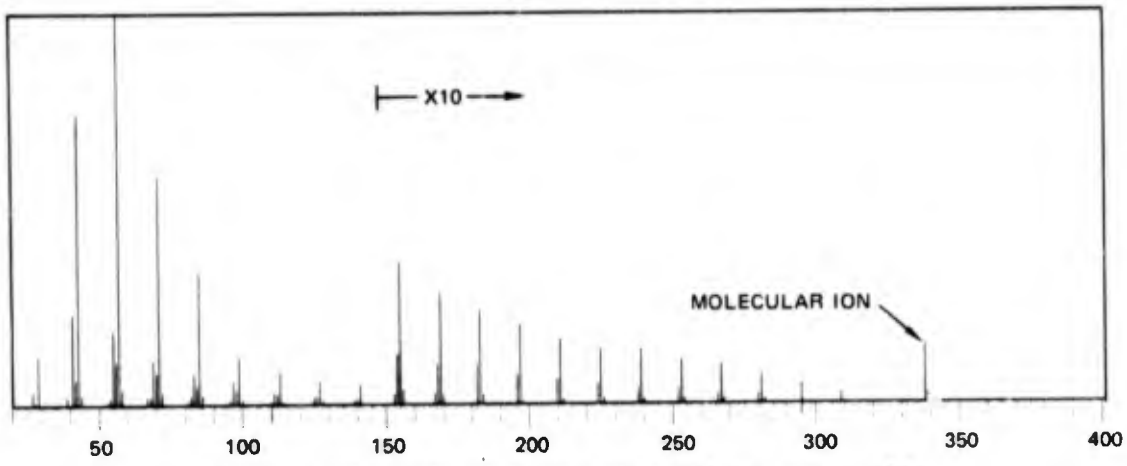

ELECTRON IMPACT SPECTRUM OF n-TETRACOSANE, M.W. = 338.67

SA-2028-12

FIGURE 1

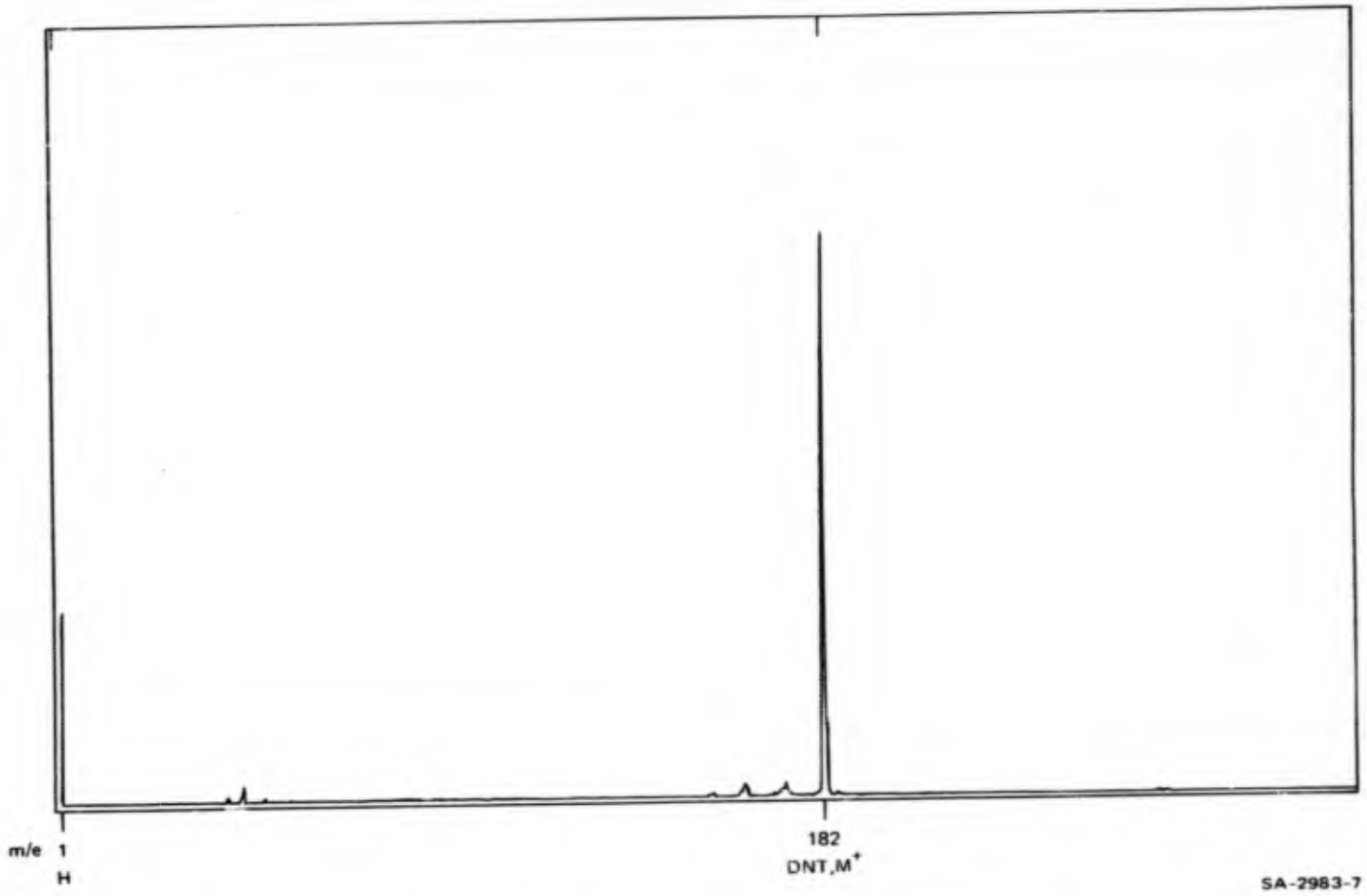

FIGURE 2 FIELD IONIZATION SPECTRUM OF UNLABELED DNT

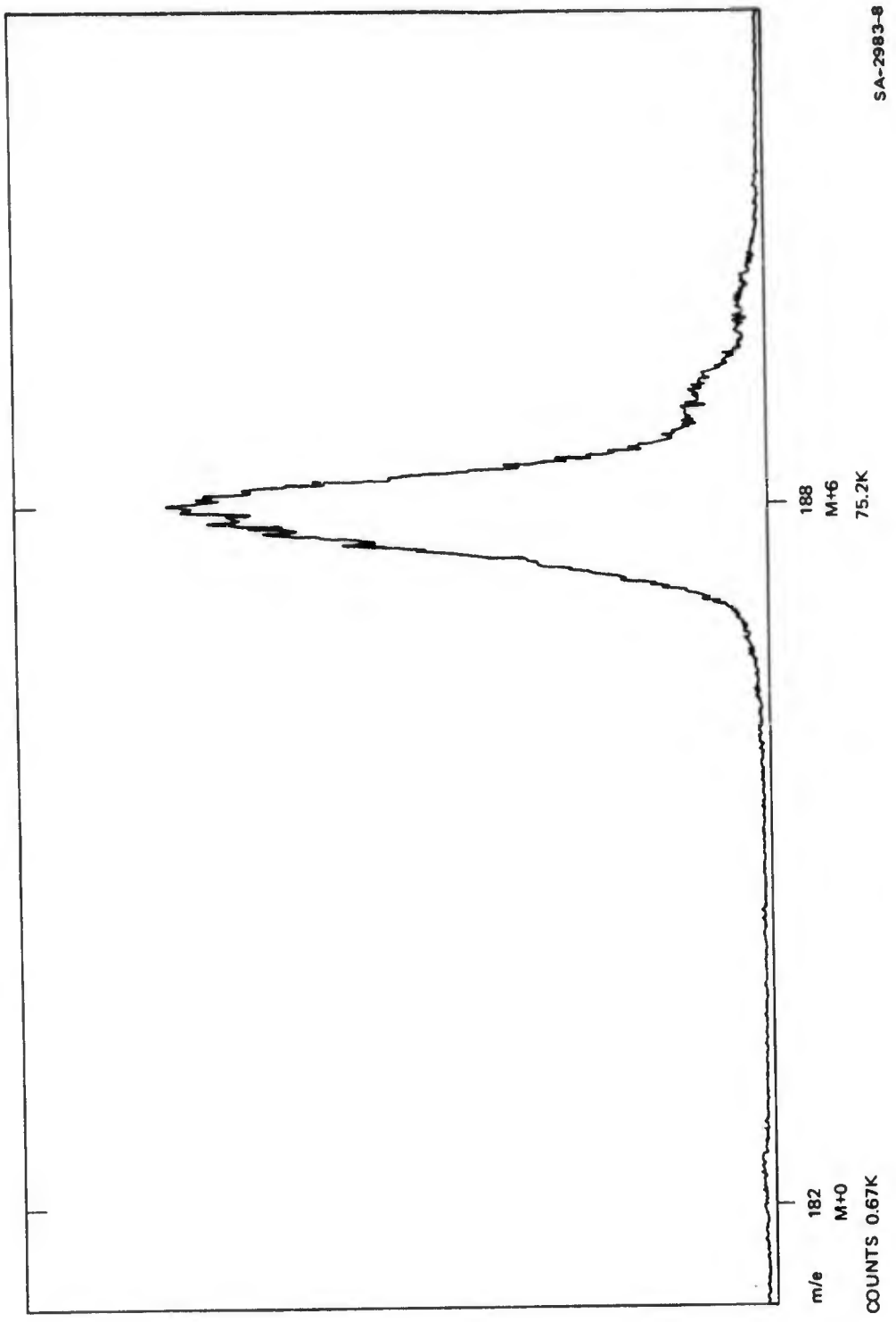

FIGURE 3 MOLECULAR ION REGION OF d_6-DNT

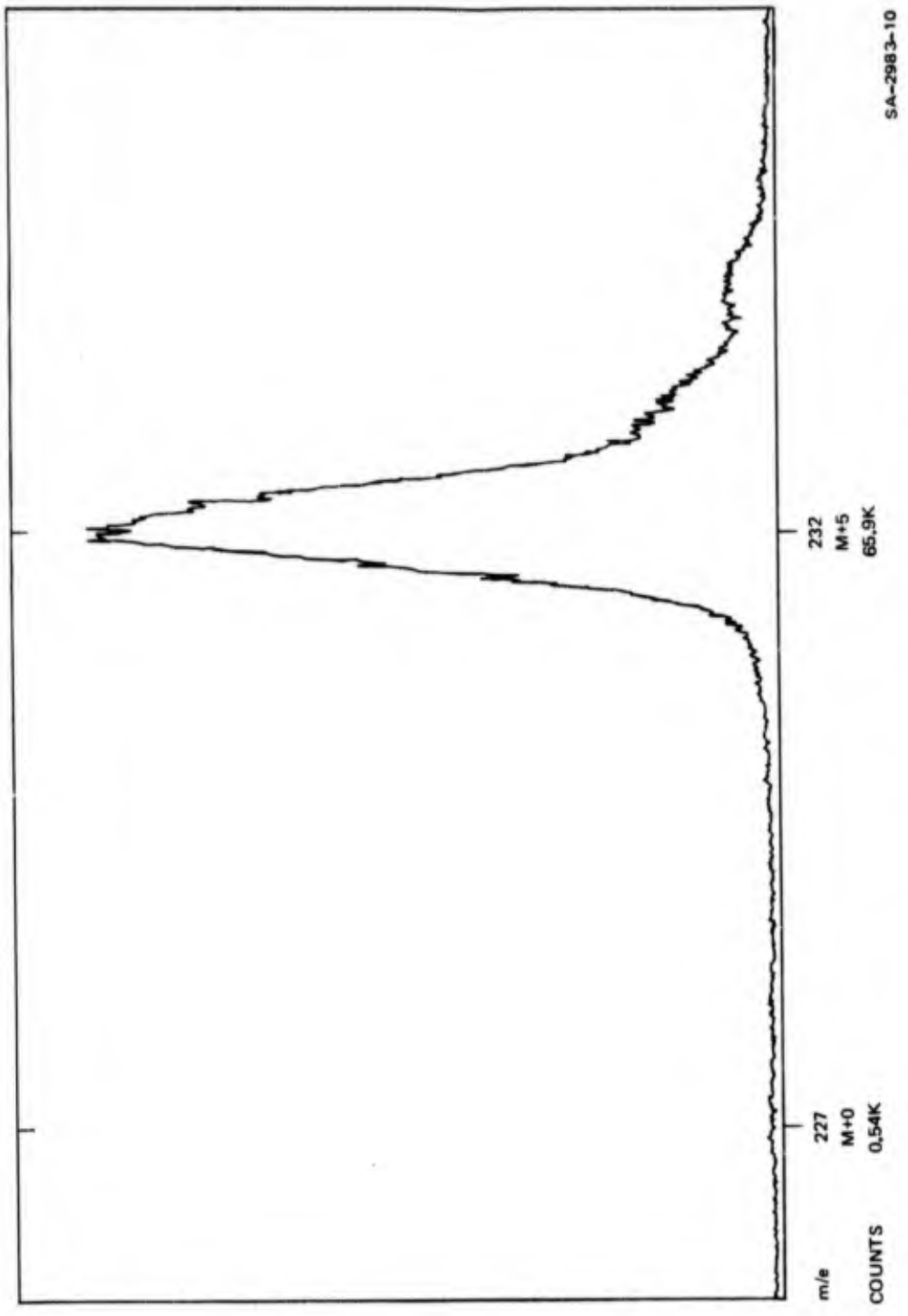

FIGURE 4 MOLECULAR REGION OF d_5-TNT

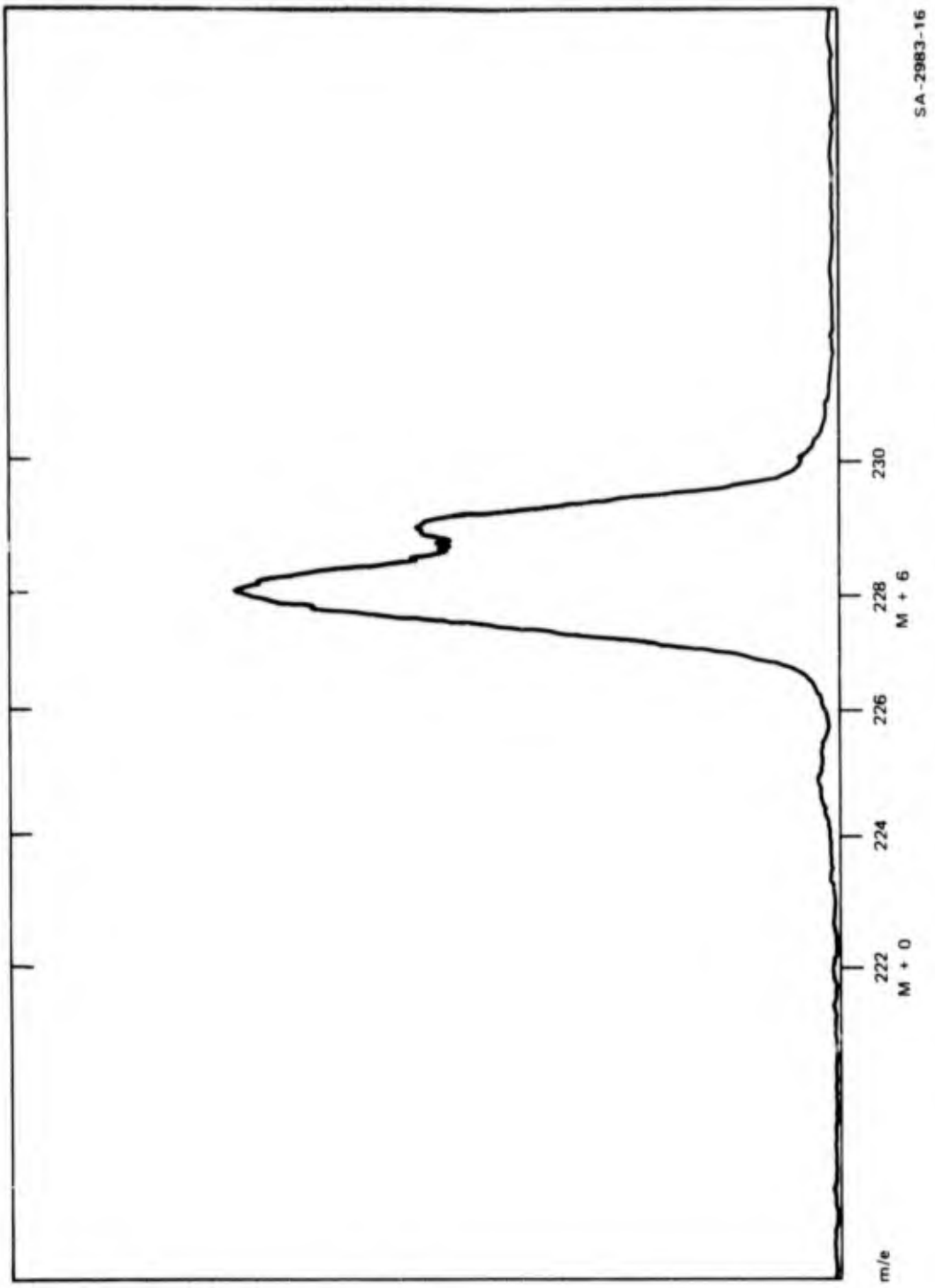

FIGURE 5 MOLECULAR ION REGION OF d_6-RDX

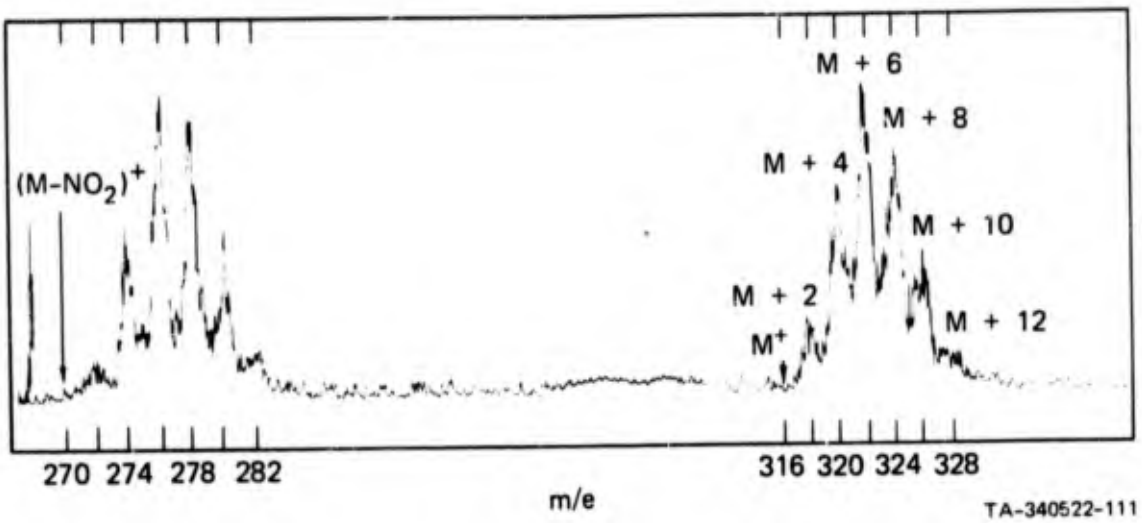

FIGURE 6 PETN MULTILABELED WITH O^{18}, M.W. 316

Source temperature: 100°C.

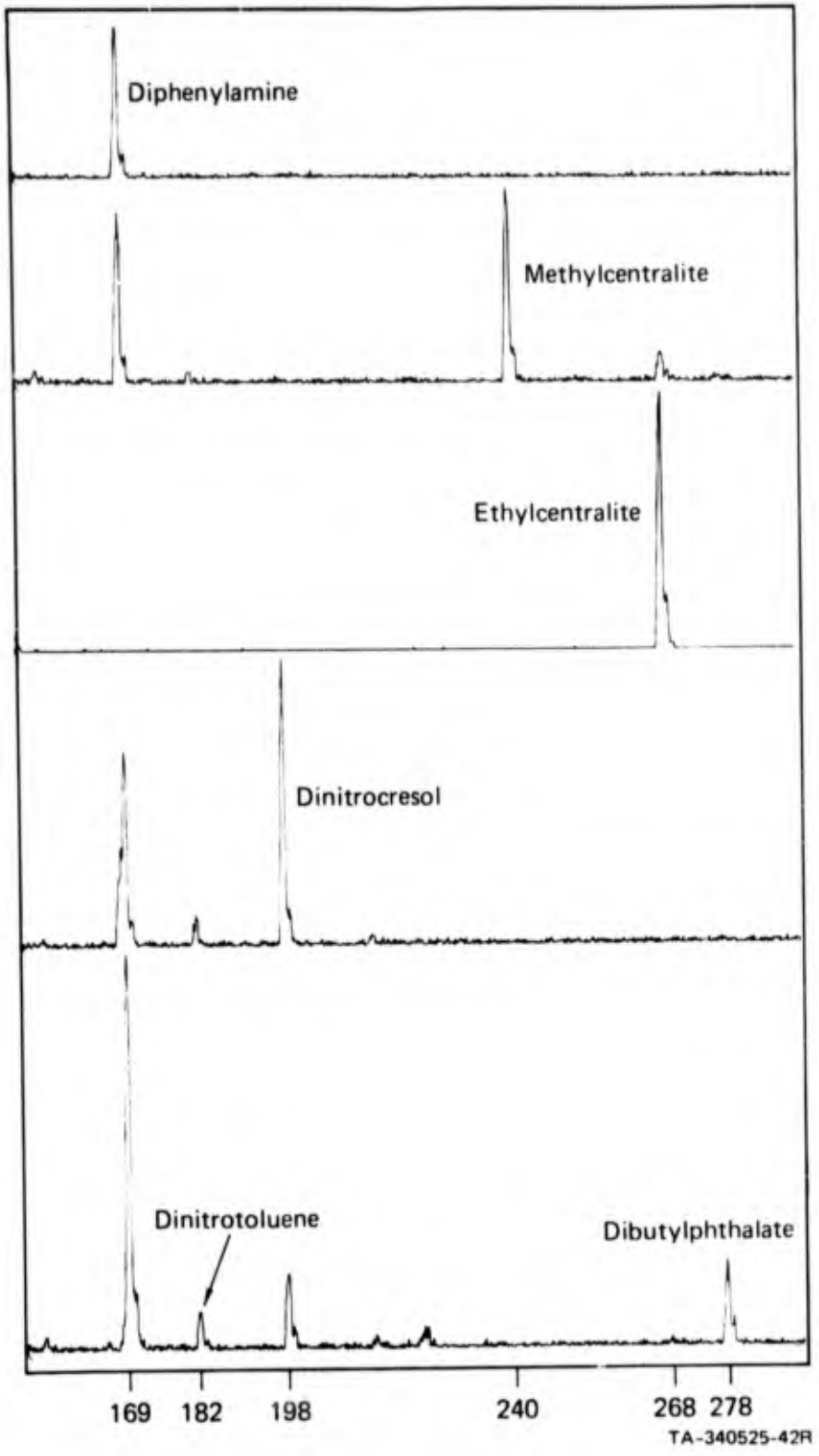

FIGURE 7 VOLATILE EFFLUENTS OF SMOKELESS POWDERS AT ROOM TEMPERATURE

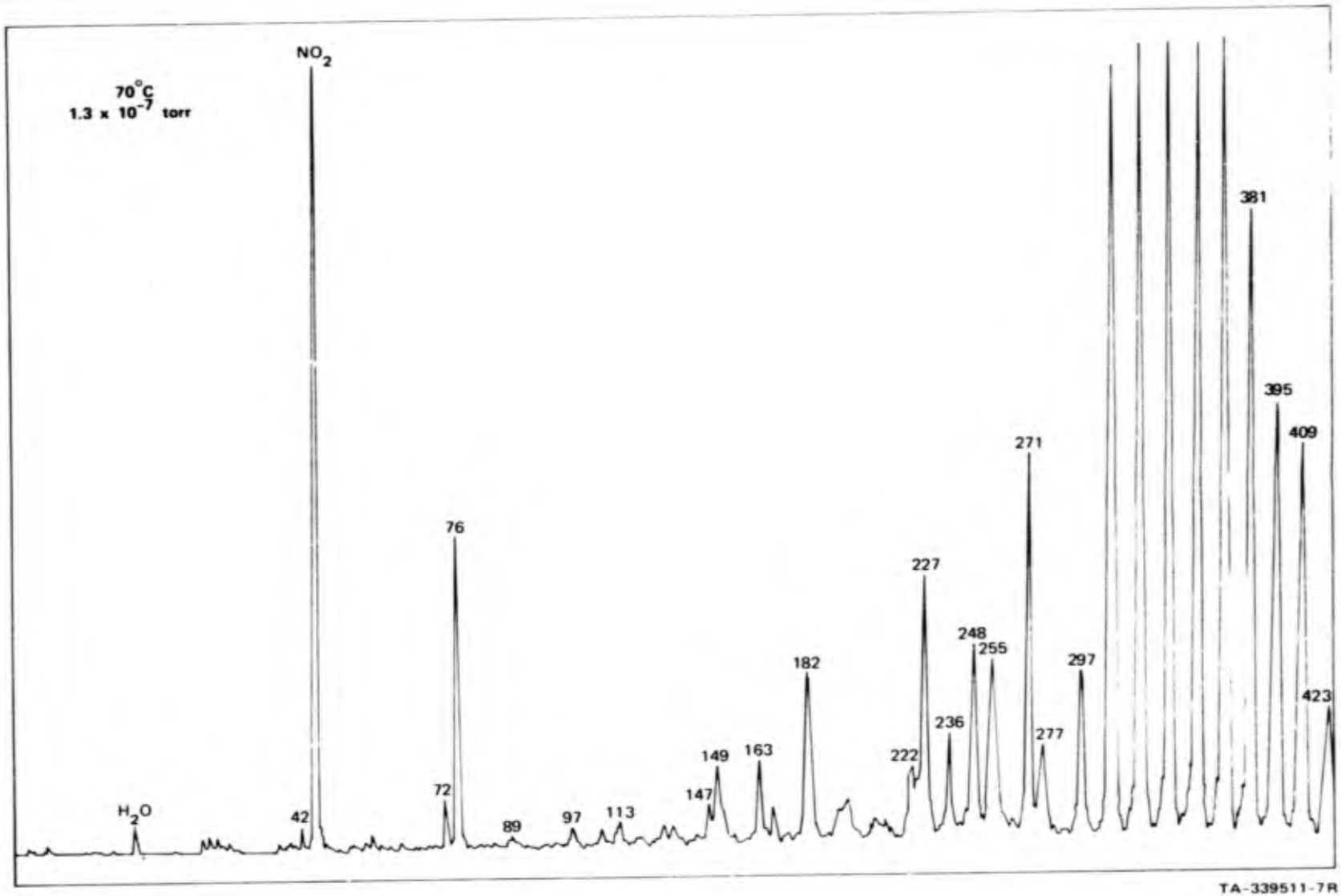

FIGURE 8 FINGERPRINT SPECTRUM OF DYNAMITE RED ARROW 70%

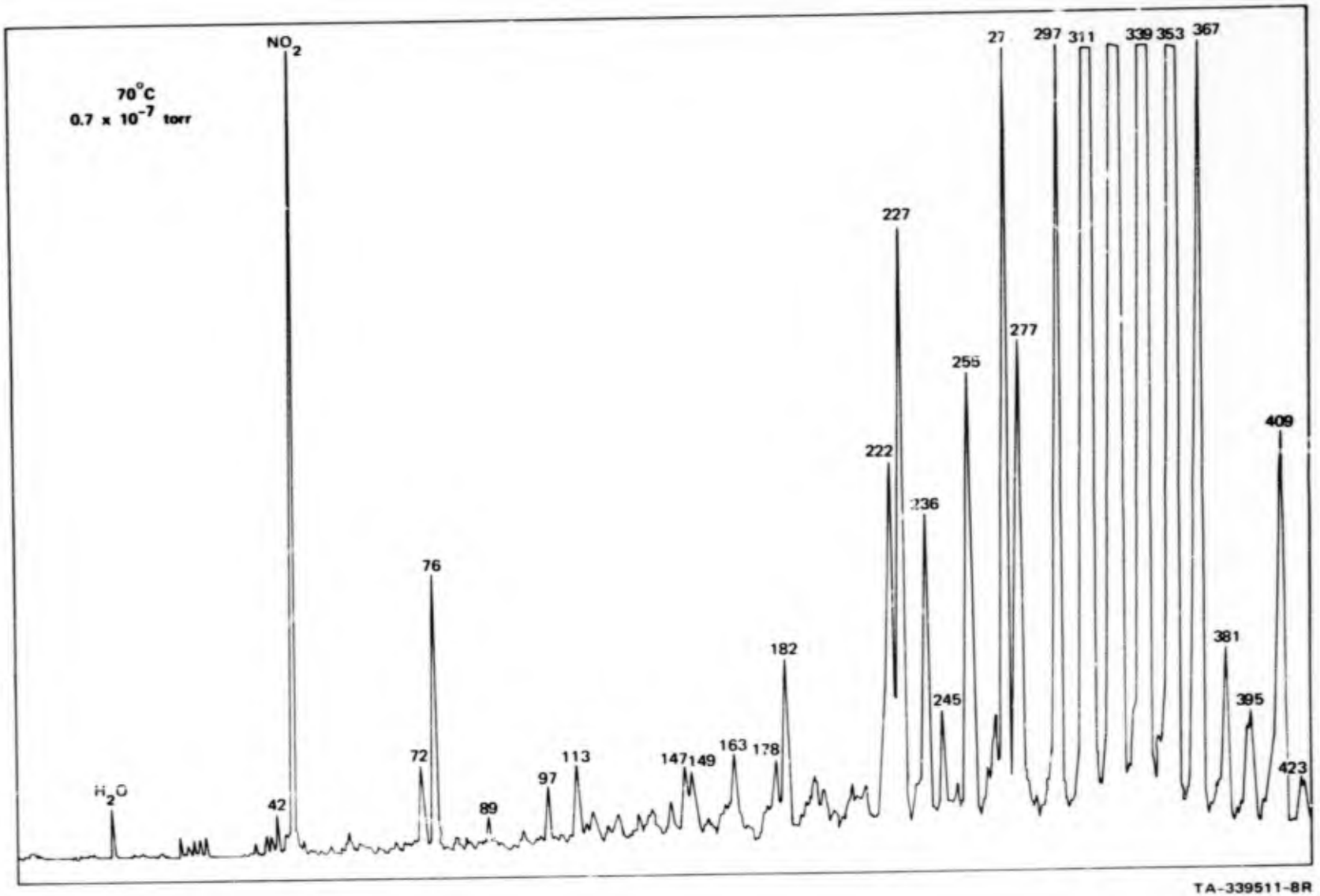

FIGURE 9 FINGERPRINT SPECTRUM OF DYNAMITE RED CROSS EXTRA 50%

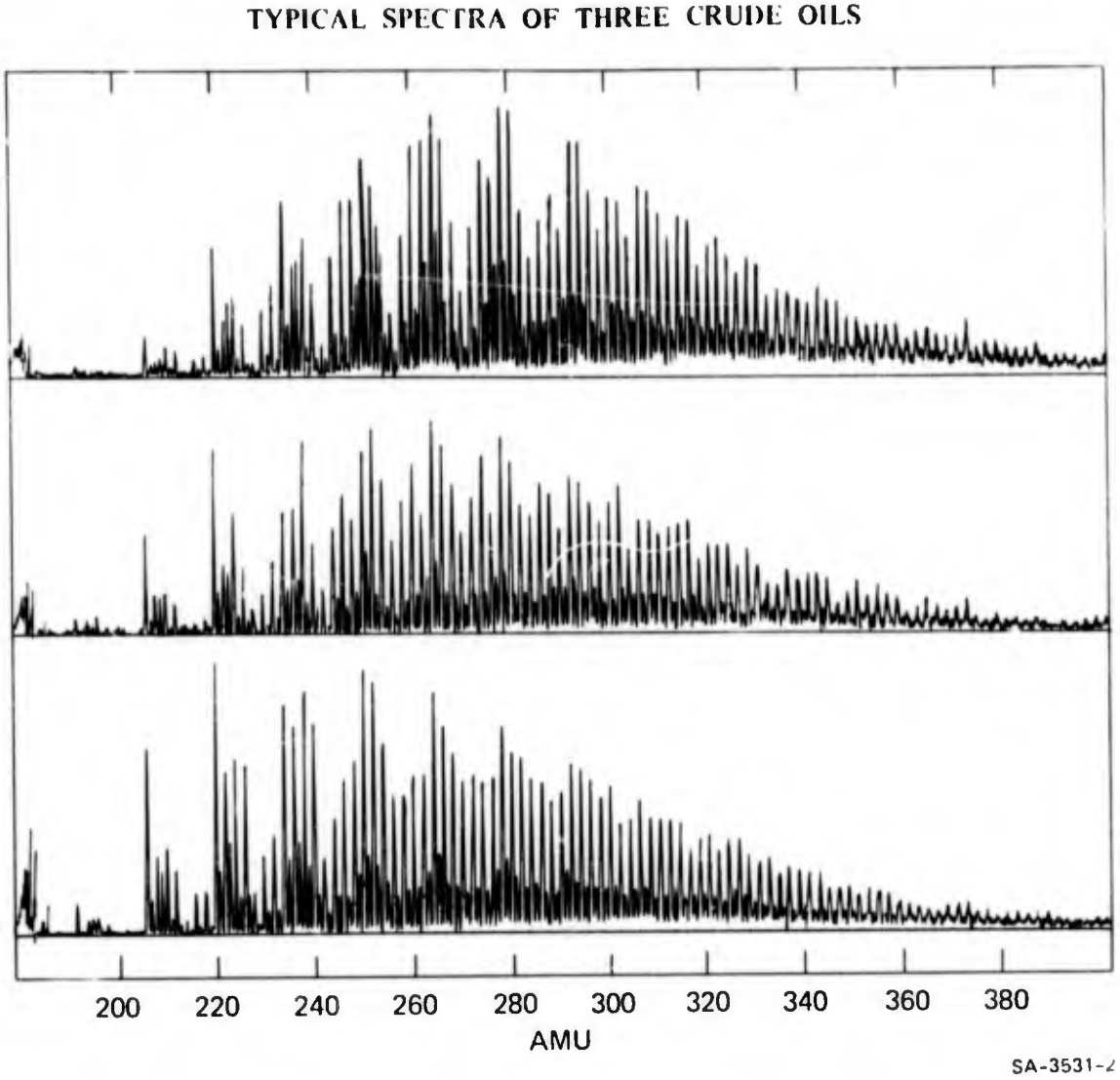

FIGURE 10 TYPICAL SPECTRA OF THREE CRUDE OILS

SESSION IV

Chairman: Mr. Robert Moll
Edgewood Arsenal

RECENTLY DEVELOPED ENZYMATIC SYSTEM FOR ENVIRONMENTAL MONITORING

by

Louis H. Goodson and William B. Jacobs
Midwest Research Institute
Kansas City, Missouri 64110

An instrument known as the Continuous Aqueous Monitor, CAM-1, which uses gel entrapped cholinesterase for the rapid detection of cholinesterase inhibitors in water, has been reported earlier[1,2,3] (Slide 1). This apparatus has been shown to be useful for the detection of toxic and subtoxic levels of organophosphates and carbamates in water supplies. In this instrument the enzyme pad with its gel entrapped cholinesterase acts like a dosimeter; by measuring the activity of the enzyme pad before and after exposure to inhibitors, it is possible to correlate loss of enzyme activity with quantity of inhibitor reacted with the immobilized enzyme.

In an effort to detect very low levels of organophosphate inhibitors in air, the CAM-1 instrument was converted into an air monitor by adding a concentrator to extract the organophosphates from large volumes of air into small volumes of water and making some adjustments in flow rates. A breadboard model of this system is shown in Slide 2. In this system, the inhibitor solution is pumped from the air-liquid separator of the concentrator assembly to the enzyme pad; as in the case of the CAM-1, the reduction in activity of the enzyme pad is determined automatically and is used as an indicator of the amount of inhibitor in the air sampled.

A flow diagram showing the concentrator and electrochemical enzyme cell is shown in Slide 3. Operation of this instrument with a 3-min detection cycle in which inhibitor solution from the concentrator is contacted with the enzyme pad for the first 2 min of the cycle and the residual activity of the enzyme pad was measured during the last minute of the cycle, permits detection of low levels of airborne inhibitors. Slide 4 shows typical data which can be obtained with this air monitoring system. By reading up from the bottom of the strip-chart recording, it will be noted that a stable baseline voltage was obtained for the first 3-1/2 hr of monitoring. At the end of this 3-1/2 hr-period, the pure air was replaced with a stream of air containing 0.0001 µg GB/liter for three 3-min cycles. The increase in voltage from 320 to 360 mV accompanying this exposure is typical of responses to these low levels of agents. Greater responses to this same concentration of GB are possible by increasing the air flow rates into the concentrator or by increasing the contact time of the inhibitor solution with the enzyme

pad. It should be noted that a new stable baseline voltage was established after the exposure to GB was terminated; also, there was adequate enzyme left on the pad so that other responses to GB could have been measured before it was necessary to insert a new enzyme pad into the cell. In the present example, eel cholinesterase was entrapped on the enzyme pad and a solution of 2.5×10^{-4} M acetylthiocholine iodide in 0.08 M Tris buffer, pH 6.75, was pumped through the enzyme pad; at the same time, a constant current of 2.0 μA was applied to the electrodes in contact with the enzyme pad. In this manner, a voltage change inversely proportional to the change in enzyme activity of the enzyme pad was measured once each cycle.

Experiments show that immobilized cholinesterase offers a practical method for monitoring both air and water for toxic or sub-toxic levels of cholinesterase inhibitors on a real time basis. Sensitivity, selectivity, and rapid display of the results are features which justify the use of systems of this kind in environmental monitoring.

1. L. H. Goodson and W. B. Jacobs, A rapid detection system for organo phosphates in water. Proceedings of the 1972 National Conference of Hazardous Material Spills, Sponsored by EPA and University of Houston, Houston, Texas, March 21-23, 1972, pp 129-136.

2. L. H. Goodson, W. B. Jacobs, and A. W. Davis, An immobilized cholinesterase product for the rapid detection of enzyme inhibitors in air or water, Anal. Biochem., 51(2):362-367 (1973).

3. L. H. Goodson and W. B. Jacobs, Use of immobilized enzyme product in water monitoring, Proceedings of the 1974 National Conference on Control of Hazardous Material Spills, Sponsored by American Institute of Chemical Engineers and EPA, San Francisco, California, August 25-28, 1974, pp 292-299.

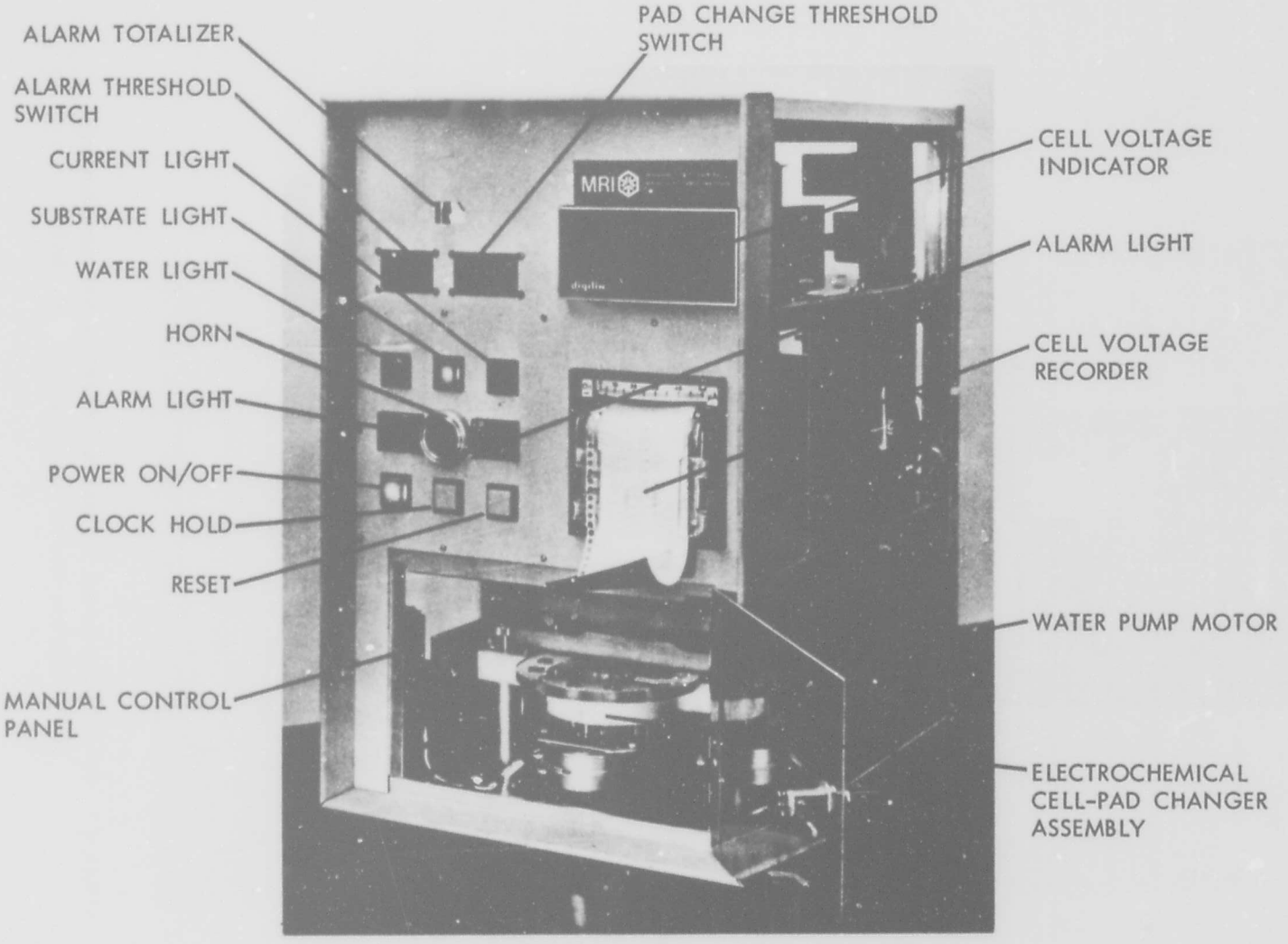

Slide 1. Continuous Aqueous Monitor, CAM-1

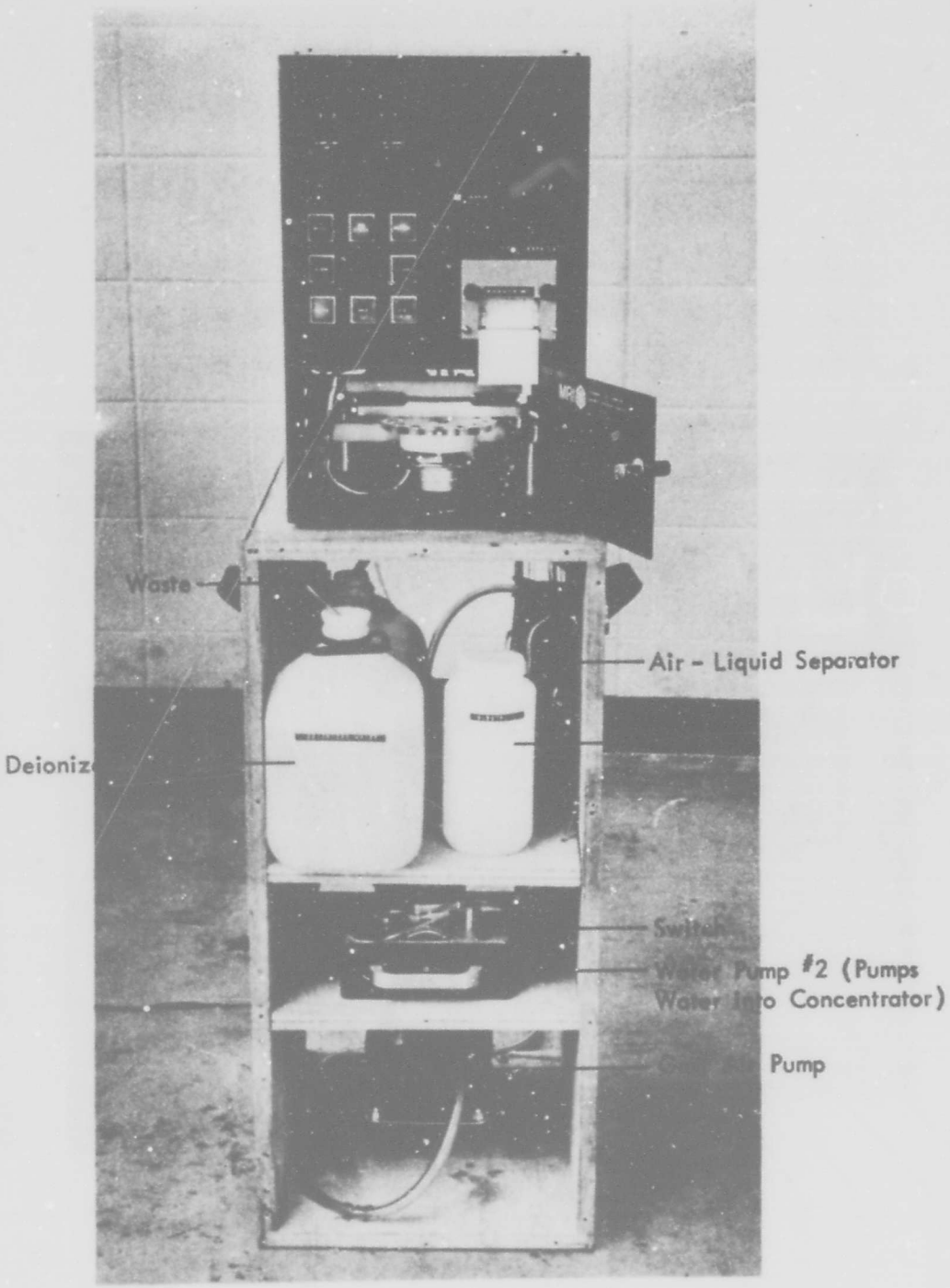

Slide 2. Breadboard Model of Air monitoring System Showing CAM-1 System Above and Concentrator Below

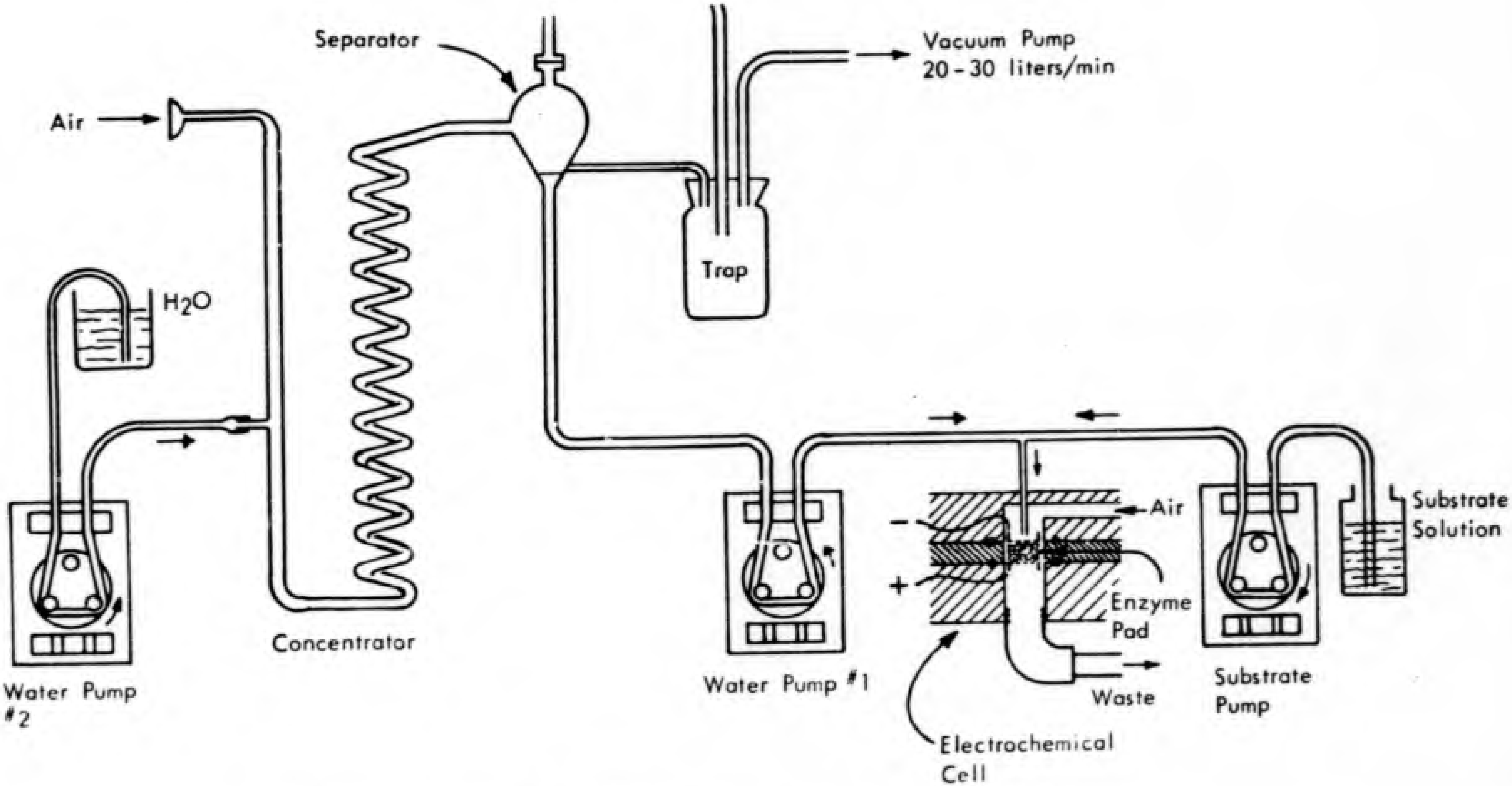

Slide 3. [illegible] Diagram of Air Monitoring System (i.e., CAM-1 system plus concentrator)

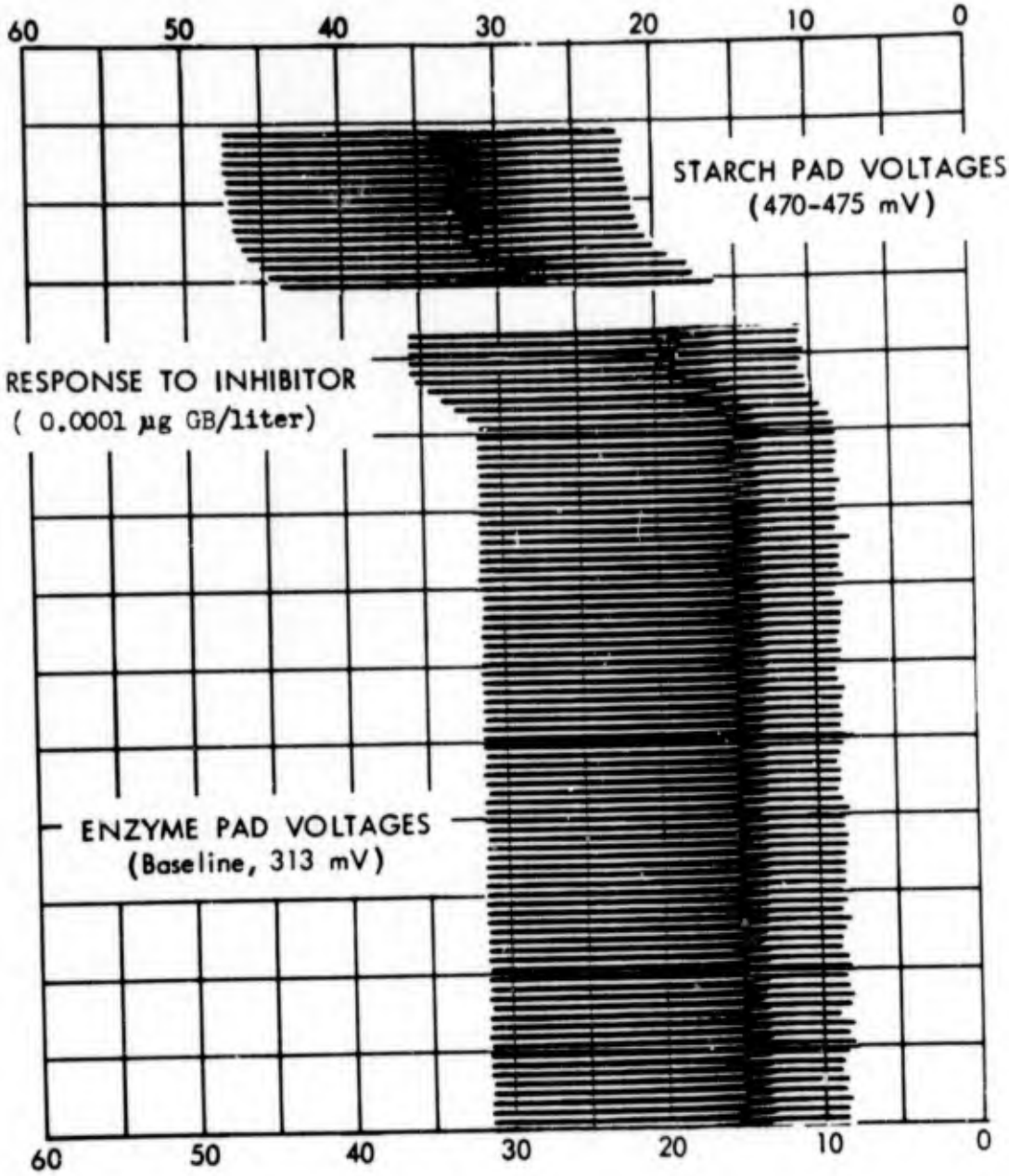

Slide 4. Strip Chart Recording from Air Monitor

DETECTION OF POLLUTANTS BY CHEMICAL AGENT DETECTION TECHNOLOGY

by

Harvey Tannenbaum

The Edgewood Arsenal military mission of developing detection devices for chemical agents, is, at the same time, consistent and inconsistent with the requirements for the detection of pollutants. It is consistent with it in that we are developing trace contaminant detectors of high reliability for field use, and inconsistent in that our detectors, for their military role, are designed specifically so as not to respond to the pollutants that might be encountered in the battlefield or other potential use situations. In the course of these developments, however, in encountering what we call "interference" problems from specific atmospheric pollutants, we go to considerable effort to eliminate such responses. In the absence of concern for chemical agents, of course, without these correction factors, we might have a very useful pollution detection device. In other cases, a modification of the system or technique, as I will describe, can make the approach applicable to certain pollutant-monitoring uses.

We are developing basically three types of detection devices. There are two types of automatic threshold alarm devices, these being "point sampling" and "remote sensing." We define the point samplers as those which must be in the sampled environment to function and remote sensors, as the name implies, which can detect remotely, without the detector necessarily being in or even near the contaminant being detected. The last type is the "kit", which we might call a miniature chemical-reagent kit packaged in a convenient field configuration and simplified for use by unskilled personnel. There are obvious specialized applications for each of these types of detectors. The most obvious application of our detection devices, developed primarily for nerve agents, is for the detection and monitoring of organophosphorus insectides, which find wide use today. Requirements have been established by Federal agencies for acceptable levels of contamination for a wide range of these compounds, and a review based upon our experimental measurements to date, indicates that a number of our devices of the kits and automatic alarms types can meet these requirements in sensitivity and, probably as well, in other specifications.

As typical of these devices, we have the standardized M8 Automatic Alarm which is a rugged, portable automatic detector. It will operate for more than 12 hours before requiring minimum servicing by replacing solutions, filter and battery. It is an electrochemical-type detector which detects either directly, or by conversion through an oxime reaction, the cyanide ion, measuring the resultant detector-cell current and triggering the alarm circuit. It will detect as little as 0.2 mg/m^3 (equivalent to .04 ppm) of organophosphorus compounds in less than 2 minutes, responding more quickly to higher concentrations. Atmospheric cyanide is removed by a prefilter, limiting the response to compounds of the type of interest.

By eliminating the prefilter we have a detector which will respond with comparable sensitivities to cyanide and hydrogen sulfide. Sensitivities have been measured to be approximately 0.1 mg/m^3 for both H_2S and HCN, equivalent to fractions of a part per million. It might be noted that OSHA Maximum Allowable Exposure (8-hour weighted average) is 10 ppm for HCN and 20 ppm for H_2S.

The enzyme alarm, a system now in exploratory development, employs a concept well established. Our development problems relate primarily to instrumentation suitable for military field applications, although the detection concept is well founded. It employs cholinesterase and a suitable substrate, relying for detection on the enzymatic reaction which duplicates the human physiological response. It thus provides assurance of detecting any anticholinesterase agent, has a very high degree of specificity and a sensitivity which exceeds any other point-sampling alarm It will detect organophosphorus compound concentrations of as low as 0.001 mg/m^3, equivalent to a fraction of a part per billion.

In its designed operational mode, and for applications where one is not concerned with a militarized piece of hardware, the current enzyme alarm system provides an ultrasensitive automatic monitor and warning device for organophosphorus insecticides. It does require servicing to replace enzyme pads and battery each 12 hours, but use of line power could simplify this requirement. Elimination of other of our rigorous military requirements also could permit unattended operation for longer periods by modification of the enzyme design features.

Another of our point-sampling detectors of interest is the ionization detector. This is based upon ion cluster spectrometry. Dr. Harden will be discussing the theoretical aspects of this detector in detail in the following paper, so it will suffice to state now that the detector is designed to respond to positively charged ion clusters above a certain mass. The organophosphorus insecticide compounds generally fall in this category; we have found none to date to which it does not respond with sensitivities of better than 0.1 mg/m^3, equivalent to less than a tenth of a part per billion with response times ranging from almost instantaneous to less than a minute. Similar responses have been measured for carbamates. Interference studies, conducted in a wide range of normal and industrially polluted atmospheres have not revealed any interference problems, although in the laboratory a large number of compounds can generate significant responses. The work being conducted by Dr. Harden and others is directed toward improving the specificity of this detector, along with other objectives. The significant advantage of the ionization detector is that is is a physical technique, thus eliminating the periodic-servicing requirement. As long as power is supplied, the system can run unattended for days, or even weeks, at a time. It is hoped that the basic studies now under way will enable us eventually to design sensor cells to respond to specified classes of compounds. The ability to specify responses to predetermined mass ranges and the nature of the charge on the ion cluster will, hopefully, permit us to attain the required degree of specificity for intended applications.

In addition to automatic point-sampling devices of the type just described, we are also developing new kits for the detection of chemical agents. These differ in function from the automatic alarms in their military application, since they require some form of manual operation. The automatic alarm provides warning, permitting troops to take proper protective action and the kits are then used, while troops are in protective gear, to monitor the atmosphere to determine when it is safe to remove the protective equipment. They are designed to provide greater sensitivity and to be more specific in identifying the nature of the threat. Several kits have been standardized over the years for both air and water monitoring, and a major program is now under way to develop a simplified kit to replace several of the current military items. The XM256 Kit is designed to monitor and identify low concentrations of a number of chemical agents, using packaging concepts which greatly simplify use of the kit. It has four test spots for

the detection of all major nerve, blood and blistering agents. These are in a 3-by-6-inch plastic sampler with premeasured reagents in finger-crushable glass ampules. By following simple, prescribed procedures, the user can identify the nature of the chemical agent in the atmosphere. All agents being tested for are simultaneously sampled. Including sampling time, in about fourteen minutes the complete range of chemical agents can be monitored. Compounds in the same classes as the chemical agents can be monitored with these kits, including the organophosphorus insecticides, cyanide and arsenicals. A related program EPA funded, is now under way at Edgewood Arsenal to develop a water-monitoring kit for monitoring a wide range of contaminants. EPA is concerned about 370 compounds, and a model list of 33 is being used in the development studies. It appears that 18 tests will provide a sufficiently broad detection scheme. These include pH, conductivity, colorimetric, enzyme, volatile and high-molecular-weight organics, heavy metals and a variety of inorganic ions. Prototypes of the selected design will be available and tested before the end of the calendar year.

Another application of our detection technology is Liquid Agent Detection (LAD) paper. It is a detector paper which has been made more storable and resistant to interferences and abrasion. It consists of a paper bonded to a plastic film coated with an adhesive, in turn protected by a silicone release paper. The detector paper incorporates a detector dye and a green camouflage dye. When a liquid chemical aerosol impacts on the surface it dissolves the detector dye and stains the paper red. The Department of Forestry has expressed interest in using this as marker to trace the application of inseciticides over forest areas. LAD has been shown to respond to a number of liquid insecticides and some of their solvent carriers.

In general, with respect to point-sampling alarms and kits, there are a number of direct potential applications for organophosphorus insecticides for agricultural applications. Modifications of current techniques, which may be as simple as removing a prefilter, or adaptation by change of enzyme or reagent, may permit application of our field hardware for other pollution-monitoring applications as well. A significant factor to bear in mind is that these are developed for rugged field use by relatively untrained personnel and high reliability.

Remote sensing for pollution monitoring has different types of applications. It may be used for monitoring of ambient atmospheres over large urban areas, where one is interested in an integrated concentration level, or with some techniques mapping pollutant clouds over large areas. It may also be applied to police areas that are not readily monitored by other techniques, such as remotely monitoring stack or other effluents from suspect manufacturing facilities. Because of the comparative complexity and higher costs of remote-sensing systems at present, their applications are of necessity limited to unique functions which can be justified on the basis of an otherwise unattainable capability or cost effectiveness standpoint as compared to multiple use of point-samplers. This discussion will be limited to the remote-sensing techniques with which we are directly involved, although there are additional approaches, most of them related to these, which are being studied elsewhere.

The most advanced of our techniques, insofar as our development cycle is concerned is Passive LOPAIR (Long-Path Infrared). The concept is based upon the detection of distinctive spectral absorption or emission of the compound to be monitored when viewed against a passive background of a temperature different than that of the ambient air. When

viewed against a cold sky background, one would see the spectral emission of atmospheric species such as water, carbon dioxide and contaminants present in sufficiently high concentration. When looking at terrain, buildings, etc., backgrounds warmer than ambient air, absorption would then be seen. Systems are programmed to monitor discrete spectral frequencies in such a way as to preclude interference responses. To do this, we have devised a simulation and spectral optimization program which derives a spectral program which we then implement in our versatile hardware. The efficacy of this technique has now been verified by field testing and we are now fabricating advanced systems with even greater capacity for adding to the spectral programming and enhancing the potential applications of the system. As mentioned earlier, our major efforts now are dedicated to problems associated primarily with military applications, rather than the basic concept of performing the monitoring function. In a fixed installation, where an active radiation source might be used or with a cooperative reflector and radiation source, the capabilities of the system could be greatly enhanced with respect to sensitivity and reliability. We have conducted successful tests with SO_2 from simulated smokestacks.

A related remote-sensing technique in exploratory development is similarly based upon long-path absorption, but uses an active laser radiation source. For detection of chemical agents the conventional CO_2 laser is not optimum since there is a significant gap in the spectral region of interest. However, the use of isotopic $C^{13}O_2$ shifts the lasing frequencies so that we may select the desired monitoring frequencies. With the use of a cooperative reflector there is abundant signal to operate over a range of several miles from a convenient low power laser and the EPA has, in fact, been developing this approach with the contractor who initiated our efforts. Our military concept, however, is to use topographic reflectors of convenience, thus permitting use in situations where a cooperative reflector cannot be emplaced. Systems have been designed and fabricated which permit spectral scanning or rapid sequential scanning of selected lasing lines for proper discrimination. We are planning to initiate efforts very shortly to apply our simulation and spectral optimization program to the laser technique for remote sensing. We are also initiating efforts to build a more fieldable system for more intensive exploratory studies. We will be investigating various instrumentation techniques, such as direct versus heterodyne signal detection and the potential use of capillary wave-guide lasers to reduce size and power requirements. The technique, like Passive LOPAIR, is adaptable to any contaminant possessing characteristic spectral signatures in the 8 to 13 μm spectral region.

Another laser approach we are investigating, this directly applied to pollution monitoring, is the application of laser elastic-backscatter differential-absorption measurements. This effort is jointly sponsored by Edgewood Arsenal, EPA-NERC and CUNY; the latter is doing the work. Present efforts are using a dye laser tuned to lines on and off an absorption peak of NO_2 at about 448 nanometers. Remote measurements have been made at ranges of up to one kilometer, with detection levels as low as 0.06 ppm. These values were checked by bubbler analysis to within .01 ppm. These studies are now being extended to the monitoring of SO_2. An important aspect of this technique is that, by virtue of using a time-gated system it is possible to determine the range to the pollutant and to map the pollutant cloud.

The last of the remote-sensing techniques we are studying is the remote Raman. Here we are using the back-scattered Raman shifted radiation generated by a pulsed laser irradiating the atmosphere. The shifted frequencies permit identification of the species, and by

time-gating the pulse we can determine the range to the contaminant and map the pollutant cloud. The present system operates at ranges of over two kilometers, and has monitored a number of atmospheric species as well as SO_2, kerosene and DIMP. All are referenced to atmospheric nitrogen, which permits quantitative measurements to be made. Calculations have been made as to projected sensitivities for various pollutants.

With respect to remote sensors, in general, they are less sensitive than point samplers, but do permit measurements to be made under conditions often otherwise impossible, and can perform large-area monitoring and surveillance. The rapidly developing technology associated with these techniques is likely to make them much more cost-effective in the near future, as well as improving their performance capabilities.

In summary, present chemical agent detector technology offers available solutions for monitoring of organophosphorus insecticides, which present a significant health hazard. The same technology, with minor modification, offers potential for pollutants such as H_2S and HCN in configuration and design which is probably superior to other techniques in use. The technology base developed in the course of these program efforts offers potential for application to other pollution-monitoring problems, as evidenced by ongoing efforts by Edgewood Arsenal, other Government agencies and a number of our present and previous contractors who are applying their gained expertise in pollution applications.

As Lead Laboratory for AMC for R&D for Pollution Abatement and Environmental Control Technology, and with our specific responsibility for the monitoring instrumentation for the R&D program, we are coordinating with other Government agencies and contractors and participating, as required both by in-house and contractual programs. We hope that the expertise we have accumulated over the many years of experience in trace gas detection will continue to play a key role in the important area of pollution monitoring

CONCENTRATIONS FOR DILUTE PLUMES RELEASED AT GROUND LEVEL AND DISPERSING UNDER DIFFERENT SURFACE AND ATMOSPHERIC CONDITIONS

by

P. B. S. Lissaman
E. R. Bate, Jr.
Aero Vironment, Inc., Pasadena, California

J. Hirata
US Department of Justice
Washington, DC

ABSTRACT

Concentration at a downwind surface receptor of contaminant released from a ground level point source is estimated. Because of meander of the plume, concentration is expressed as a probability. Effects of ground surface and ambient atmospheric conditions are considered in model, as well as building wake effects.

The long-term average centerline plume concentration is given as a function of downwind distance from a point source located on planar terrain. Effects of wind speed, ground roughness, heat flux, and the wake of a nearby structure are incorporated in the diffusion relations. The ratio of peak to mean plume concentrations, a function of the sampling time of the sensing instrument, and a result of the meander of the plume on either side of the wind axis, is discussed. This ratio (the gain) is expressed as a function of the exceedance probability, the probability that a given reading will be larger than an assigned level. The information presented in the paper is in a form suitable for immediate, operational use in actual field situations.

The results of the paper can be used for air quality estimation, for specifying detection instrument sensitivity, or for developing plume tracing strategies.

NOMENCLATURE

		Units
A_p	Area of plume	m^2
A_w	Area of wake region behind structure	m^2
a	Fluctuating velocity component	m/sec
B	Meander dispersion	m
C	Long-term average concentration	ppb
C'	Long-term average concentration modified by wake of structure	ppb
C^*	Instantaneous concentration on wind axis	ppb
C_o	Instantaneous concentration on instantaneous center of plume	ppb
H	Heat flux	$cal/cm^2/min$
L	Horizontal dimension of structure	m
n	Constant for determining concentration	$\frac{ppb\ m\ km^2}{gram}$
N	Number of sensors	
N_H	Heat flux number	
N_R	Roughness number	
P	Exceedance probability	
Q	Source release	grams/sec
t	Time	sec
u	Mean wind velocity at z = 10 m	m/sec
u_r	Roughness reduced wind speed	m/sec
x	Horizontal coordinate in direction of wind	m or km
y	Horizontal coordinate transverse to wind	m
Y	Meander displacement from wind axis	m

NOMENCLATURE (continued)

		Units
z	Vertical coordinate	m
β	Linear growth factor of meander	
ϵ	Atmospheric dissipation rate	cm^2/sec^3
ζ	Transformed coordinate	m
η	Transformed coordinate	m
λ	Ratio of horizontal to vertical dispersion	-
ν	Transformed time	sec
ξ	Transformed coordinate	m
σ	Dispersion	m
χ	Downwind concentration variation, $\frac{C}{Q}$	$\frac{sec}{m\ km^2}$
φ	Angle between mean wind direction and line joining receptor to source	

TABLE OF CONTENTS

	ABSTRACT	i
	NOMENCLATURE	ii
1.	INTRODUCTION	1-1
2.	PLUME CHARACTERISTICS	2-1
	2.1 Plume Concentrations	2-1
	2.2 Factors Effecting Dispersion	2-3
	2.3 Effects of the Wakes of Structures	2-5
	2.4 Typical Results for Concentration	2-7
3.	PLUME MEANDER	3-1
	3.1 General	3-1
	3.2 Gain Exceedance Probability	3-3
	3.3 Off Axis Exceedances	3-6
	3.4 Building Wake	3-6
	3.5 Multiple and Moving Sensors	3-7
4.	NUMERICAL INPUTS TO MODEL	4-1
	4.1 Determination of Heat Flux	4-1
	4.2 Ground Roughness	4-4
5.	CONCLUSIONS	5-1
6.	REFERENCES	6-1

1. INTRODUCTION

The manner in which material disperses in the atmosphere is of considerable importance in plume tracing studies and in predicting downwind concentrations from stationary sources. A properly validated mathematical diffusion model will thus allow the geometry of the plumes from such sources to be analyzed with respect to the geography of the area in which they are located. Decisions relating to the characteristics, the operation, or the location of a sensor in a particular situation may be quantitatively evaluated in terms of the measured or estimated downwind plume size and concentration.

This paper describes a rational general technique to estimate the peak and mean plume concentration taking into account the effects of wind, ground roughness, insolation, atmospheric stability, and building wakes. Such information is operationally useful not only to estimate concentration levels, but also to design or specify sensors to detect dilute plumes.

The material emanating from a source is convected by the mean ambient wind in the prevailing wind direction. The growth of the resulting plume of material as it is convected downwind is due to atmospheric dispersion. This dispersion results from the action of the turbulent transport of the atmosphere. The factors involved in the generation of this atmospheric turbulence are a combination of the effects of the velocity of the wind, the roughness of the ground over which the wind is blowing, and the heat flux through the atmosphere itself.

With point source releases, the meander of the plume is an important effect causing a significant difference between short-term and long-term concentration readings. An illustration of this effect is shown in Figure 1, from a recent AeroVironment field experiment. This shows an elevated point release from a smoke bomb attached to

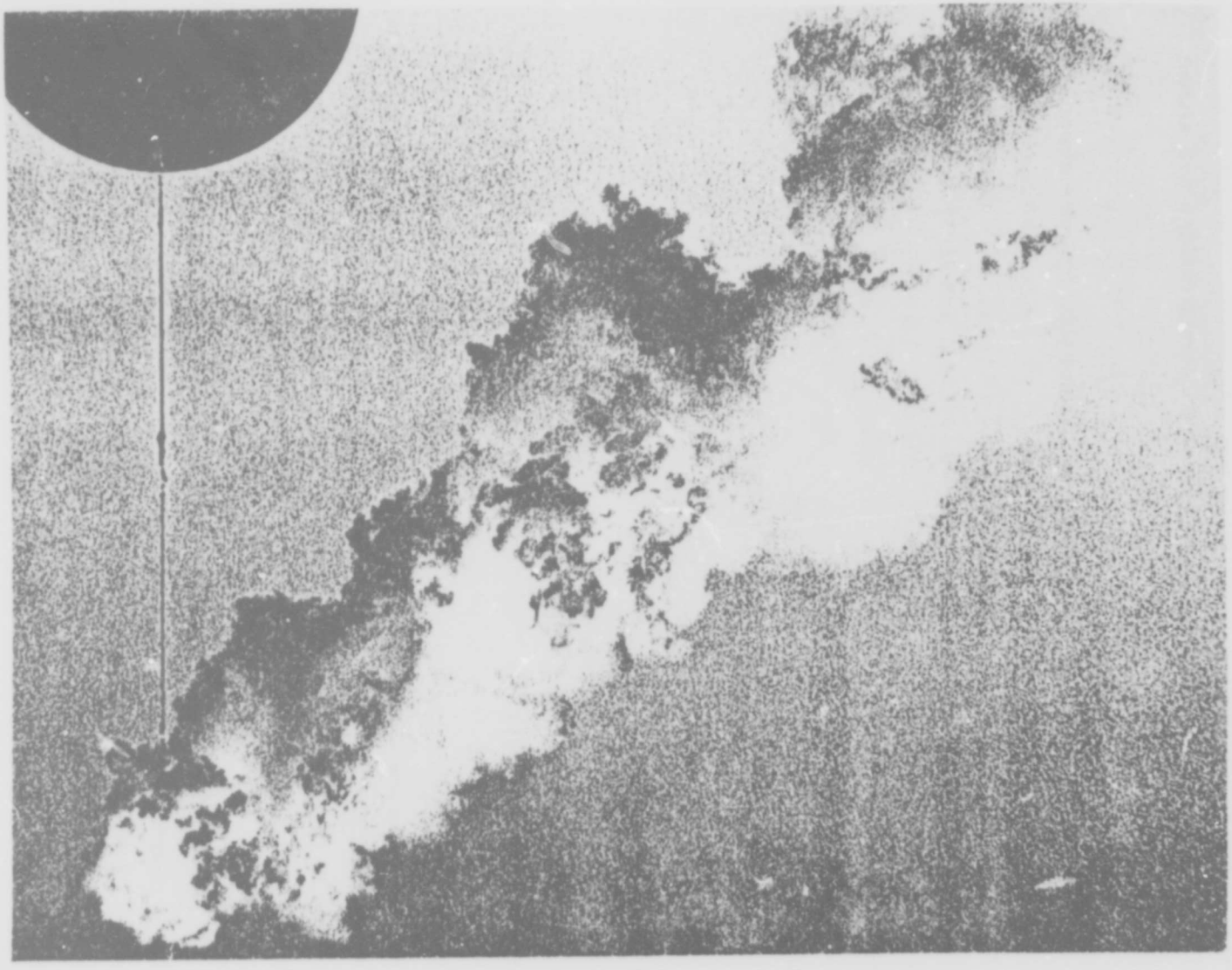

Figure 1. Structure of Point Release in Light Wind.

a tethered balloon at 30 m altitude, in conditions of a light breeze in an unstable atmosphere. The photo, taken at 1/250 sec exposure, clearly shows convection, meander, and dispersion. The general site and ambient conditions affecting plume concentrations are shown in Figure 2.

Lissaman (1973) has developed a mathematical plume concentration model in which the effects of ground roughness and heat flux are explicitly used to determine the turbulent transport velocities, and hence the plume dispersion. This has great practical significance from the standpoint of determining plume characteristics under actual field conditions. The steady-state solution of this model results in an expression for the long-term average concentration distribution for an inert plume. Numerous field observations conducted by AeroVironment (1974) have validated Lissaman's model.

The downwind concentration at a given receptor due to a plume from a point source will vary with time, so the short-term concentration will generally be different from the long time average centerline concentration predicted by the model. Both the instantaneous and averaged concentrations as read by a downwind detection instrument will be altered from the predicted plume centerline concentrations due to the statistical variation in actual plume location resulting from meander. Any meaningful use of the concentration model for point sources and short measuring times must properly correct predicted model centerline concentrations to account for instrument sampling time and plume meander.

This paper presents a method of determining expected downwind plume concentrations from isolated sources, taking into account the nature of the surrounding terrain, the atmospheric conditions, and the nature and sampling time of the measuring instrument. It presents this information in a practical and useful manner for application to field test conditions.

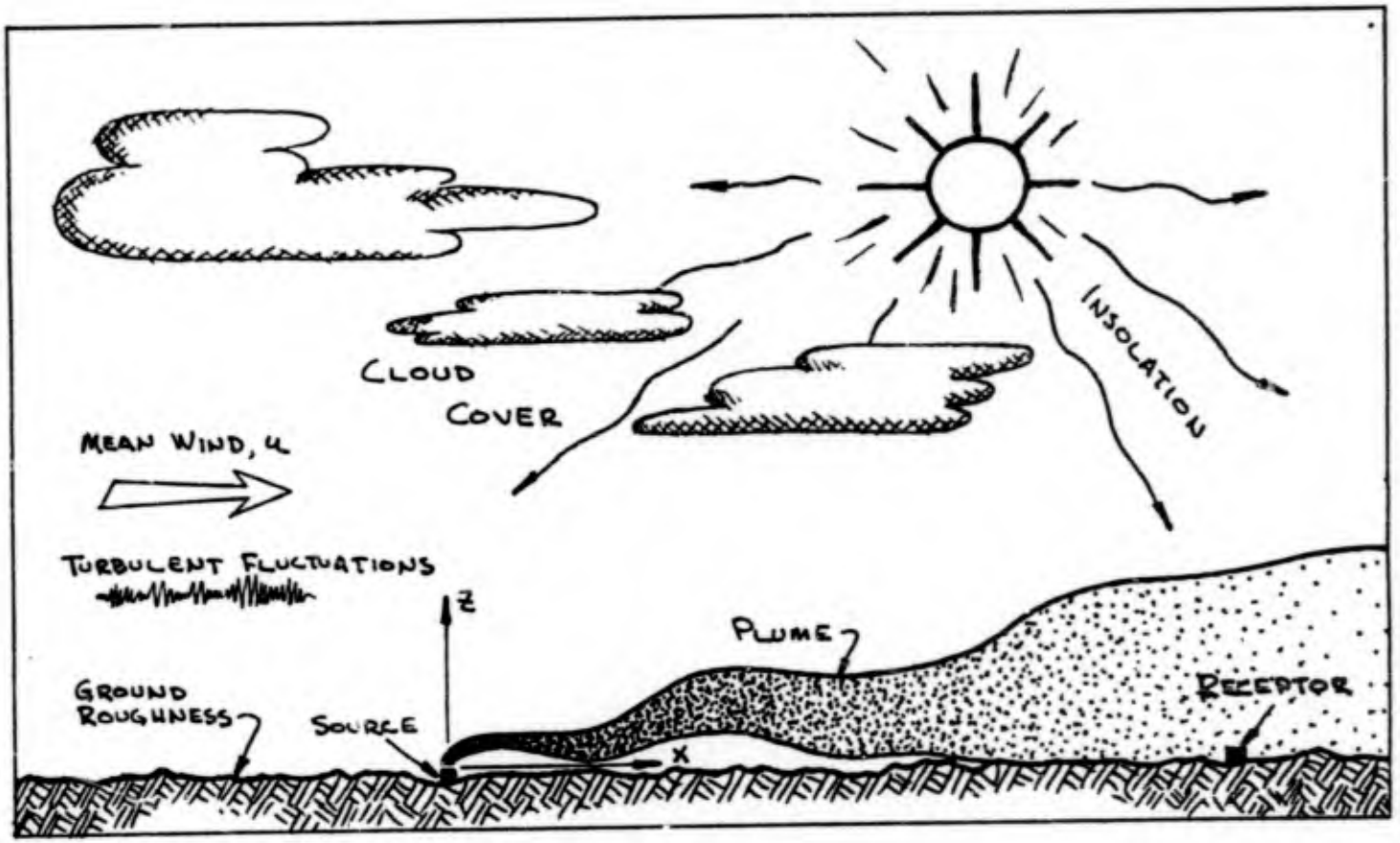

Figure 2. Factors Influencing Plume Dispersion.

2. PLUME CHARACTERISTICS

2.1 Plume Concentrations

The fundamental model is based on the short-term asymptotic result of Taylor's Theorem (1921), in which it is shown that the rms dispersion, σ , for short time, t , is $\sigma = at$, where a is the dispersion speed. Taylor shows that a may be taken as the rms turbulent fluctuations in the direction of σ . The condition of "short" time implies t is small compared with the Lagrangian time scale of the process. Justification for this is given by Lissaman (1973). Replacing the transfer coefficient, $k \sim a\sigma$, by terms containing the proper scales, the formal diffusion equation for the concentration χ can then be written as

$$\frac{\partial \chi}{\partial t} + u \frac{\partial \chi}{\partial x} = \frac{\partial}{\partial x} \left(a_x \sigma_x \frac{\partial \chi}{\partial x}\right) + \frac{\partial}{\partial y} \left(a_y \sigma_y \frac{\partial \chi}{\partial y}\right) + \frac{\partial}{\partial z} \left(a_z \sigma_z \frac{\partial \chi}{\partial z}\right) \quad . \qquad (1)$$

For a invariant with space and time, and from Taylor's result, $a\sigma = a^2 t$, Eqn. (1) becomes:

$$\frac{\partial \chi}{\partial t} + u \frac{\partial \chi}{\partial x} = t \left(a_x^2 \frac{\partial^2 \chi}{\partial x^2} + a_y^2 \frac{\partial^2 \chi}{\partial y^2} + a_z^2 \frac{\partial^2 \chi}{\partial z^2}\right) \quad . \qquad (2)$$

The transformations of $\nu = t^2/2$, $\xi = x - ut$, $\eta = y$, and $\zeta = z$ reduce Eqn. (2) to:

$$\chi_\nu = a_x^2 \chi_{\xi\xi} + a_y^2 \chi_{\eta\eta} + a_z^2 \chi_{\zeta\zeta} \quad , \qquad (3)$$

which is simply the diffusion equation in a coordinate system moving with the wind. An exact unsteady solution for Eqn. (3) with an instantaneous point release can be written down. The specific steady case for which $t \to \infty$, representing a fully developed plume from a continuous release, is given by:

$$\frac{a_y a_z}{a_x} x^2 (2\pi)^{3/2} \chi = \exp\left[-\left(\frac{u}{a_x}\right)^2\right] + \frac{u}{a_x}\sqrt{\frac{\pi}{2}}\left(1 + \operatorname{erf}\frac{u}{a_x\sqrt{2}}\right) \quad . \quad (4)$$

Over a short downwind distance, the ratios of the horizontal and vertical dispersion speeds may be assumed to vary in a coupled manner, so that

$$\frac{a_x}{a_z} = \frac{a_y}{a_z} = \lambda \quad .$$

With this assumption, the variation in downwind plume concentration may be expressed as:

$$\chi = \frac{\exp\left[-\left(\frac{u}{\lambda a_z}\right)^2\right] + \frac{u}{\lambda a_z}\sqrt{(\pi/2)}\left(1 + \operatorname{erf}\frac{u}{\lambda a_z\sqrt{2}}\right)}{a_z x^2 (2\pi)^{3/2}} \quad . \quad (5)$$

In general, λ is a function of downwind distance, x, and atmospheric stability. The determination of λ will be discussed in a later section.

In proper dimensional units, the plume concentration, $C = \chi n Q$, where Q is the source release rate, and n is a constant selected for the desired units of concentration. For Q in grams/sec, x in km, and a_z in m/sec, $n = 1.67$ for C expressed in ppb by mass in air. It must be noted that this is a proper dimensionless quantity of parts per billion by mass. That is, we use the ratio of contaminant mass to air mass in a given volume. For some air quality regulations a different unit is used, being parts by mass per unit volume (e.g., micrograms per cubic meter). For comparison, proper conversion factors must be used. Throughout, a conservative contaminant is assumed, that is, it is inert, with no deposition.

2.2 Factors Effecting Dispersion

Vertical Turbulent Velocity

For a given situation in which the release rate, the wind velocity, and the desired downwind receptor distance are all specified, the other factors which effect plume concentration are the vertical and horizontal dispersion speeds. It is shown by Lissaman (1973) that these dispersion speeds are functions of the wind speed, u, the ground roughness, z_o, and the heat flux, H. A particularly useful feature is the relationship between a_z and the heat flux, the wind speed, and the ground roughness. The turbulent dissipation rate, ϵ, is expressed in terms of the turbulent mechanical production due to wind shear and that due to buoyancy -- the only production mechanisms. The wind shear results from the Lumley and Panofsky (1964) self-similar diabatic wind profile. These relationships are coupled to give an expression for the vertical fluctuating velocity component. The results are presented below as an algorithm which is suitable for programming. The wind speed is expressed as a roughness reduced wind speed also described in the cited paper.

Vertical Turbulence

1. For $H < 0$ and $u_r < 13.2\ (-H)^{1/3}$; $a_z = 0$

2. For $H > 0$ and $u_r < 6.96\ (H)^{1/3}$; $a_z = .87\ H^{1/3}$

3. Otherwise, $a_z = .125\ u_r$

Roughness Reduced Wind Speed

$$u_r = \frac{4.6u}{\ell n\left(\frac{10}{z_o}\right)}$$

Here, u and a_z are the wind speed and the rms vertical turbulence, respectively in m/sec at z = 10 m , z_o is the ground roughness in m , and H is the heat flux in cal/cm^2/min.

Ratio of Horizontal to Vertical Turbulent Velocities

It is becoming increasingly clear that Pasquill's diffusion curves ("Meteorology and Atomic Energy", 1968) are not sufficiently general to give reasonable accuracy for different values of heat flux and ground roughness. Furthermore, Pasquill's curves give the dispersion, σ , as a function of downstream distance and not the turbulent velocities themselves.

However, the ratio of horizontal to vertical dispersion would be the same for similar ratios of the turbulent velocities at the same downwind distance. Hence, λ can be easily determined from the ratios of the Pasquill dispersion estimates as a function of downwind distance. Also, it can be assumed that these ratios would only be weakly dependent upon heat flux and ground roughness, and hence the Pasquill stability classifications will adequately specify broad ranges of applicability of λ which match the actual conditions.

Thus, λ was determined as the ratio of horizontal to vertical dispersion as a function of downwind distance from Pasquill's diffusion estimate curves, and presented for each of his stability classes. This procedure was done for two different ranges in downwind distance, $1 \leq x \leq 5$ km and $0.2 \leq x \leq 2$ km. The best straight line fit between the end points in each range was determined for both σ_z and σ_y . The ratio of these resulting functional relationships then formed the relationship for λ . Table 2-1, below, presents the results of these operations.

Table 2-1. The Ratios of Horizontal to Vertical Fluctuation Velocities as Functions of Downwind Distance and Pasquill Stability Class.

Pasquill Stability Class	λ (x)	
	$0.2 \leq x \leq 2$ km	$1 \leq x \leq 5$ km
A	$.25\, x^{-1.1}$	$.404\, x^{-2.94}$
B	$.90\, x^{-.4}$	$1.33\, x^{-.89}$
C	1.58	$1.64\, x^{0.5}$
D	$2.24\, x^{.2}$	$2.25\, x^{.25}$
E	$2.57\, x^{.2}$	$2.39\, x^{.26}$
F	$2.57\, x^{.2}$	$2.71\, x^{.32}$

2.3 Effects of the Wakes of Structures

For a source release in or near the lee side of a building, the plume material immediately mixes with and fills the wake area of the separated flow behind the building. Thus the concentration is reduced from the value that would exist in the absence of the building. For the plume area, A_p, and the wake area, A_w, at the same downwind location, the modified concentration, C', becomes:

$$C' = \frac{C}{1 + \frac{A_w}{A_p}} \quad .$$

The area of the plume is given by:

$$A_p = \frac{\pi}{2} \sigma_y \sigma_z = \frac{\pi}{2} \lambda (\sigma_z)^2 \quad .$$

The vertical dispersion and the fluctuating vertical velocity are related by:

$$\sigma_z = \frac{a_z x}{u} \quad ,$$

so that:

$$A_p = \frac{\pi}{2} \lambda \left(\frac{a_z x}{u}\right)^2 \times 10^6 \quad , \text{ for } x \text{ in km} .$$

The wake area is taken from "Meteorology and Atomic Energy" (1968) as:

$$A_w = \frac{\pi r^2}{2} \quad ,$$

where:

$$r = 1.57 L \left(\frac{x}{L}\right)^{1/3} \quad . \tag{6}$$

Here, L is the width of the building, and the height of the building is L/2. For L in m and x in km,

$$A_w = 386 L^{4/3} x^{2/3} \quad .$$

Thus:

$$C' = \frac{C}{1 + \frac{.00246}{\lambda} \left(\frac{u}{a_z}\right)^2 \left(\frac{L}{x}\right)^{4/3}} \quad . \tag{7}$$

The plume concentrations obtained from Eqn. (5) may be modified according to Eqn. (7) to obtain the concentrations downwind from a sharp edged building approximately twice as wide as it is high. Buildings of other shapes and proportions would result in modifications to Eqn. (6), which are beyond the scope of this paper. The reader is referred to Section 5.5 of "Meteorology and Atomic Energy" for a more comprehensive discussion of this subject.

2.4 Typical Results for Concentration

The preceding analysis assumes a plume ensemble average. Thus it may be considered to be the sensor reading taken over an infinitely long averaging time. The concentration equation contains terms which explicitly express the effects of different input parameters. For example, Figure 3 shows concentration under unstable conditions with small roughness. We observe the interesting effect that concentration at a given receptor does not vary in a simple inverse fashion with wind speed, as implied by some formulations. In fact, for conditions fixed, there exists a wind speed for which concentration is a maximum. To understand this consider a situation of positive heat flux, initially in calm conditions. The contaminant will disperse in a hemispherical manner, dispersed by convective turbulence. If a light wind develops, the contaminant is all blown downwind, while the dispersing turbulence is not greatly changed. This will double the concentration at a downwind receptor. As the wind speed increases dispersion increases due to mechanical turbulence generation, increasing plume growth rate with time, but the time of flight to a receptor is reduced, so that concentration there may still increase. As the wind becomes stronger the increase in turbulence will offset the reduced flight time so that eventually the concentration starts to drop.

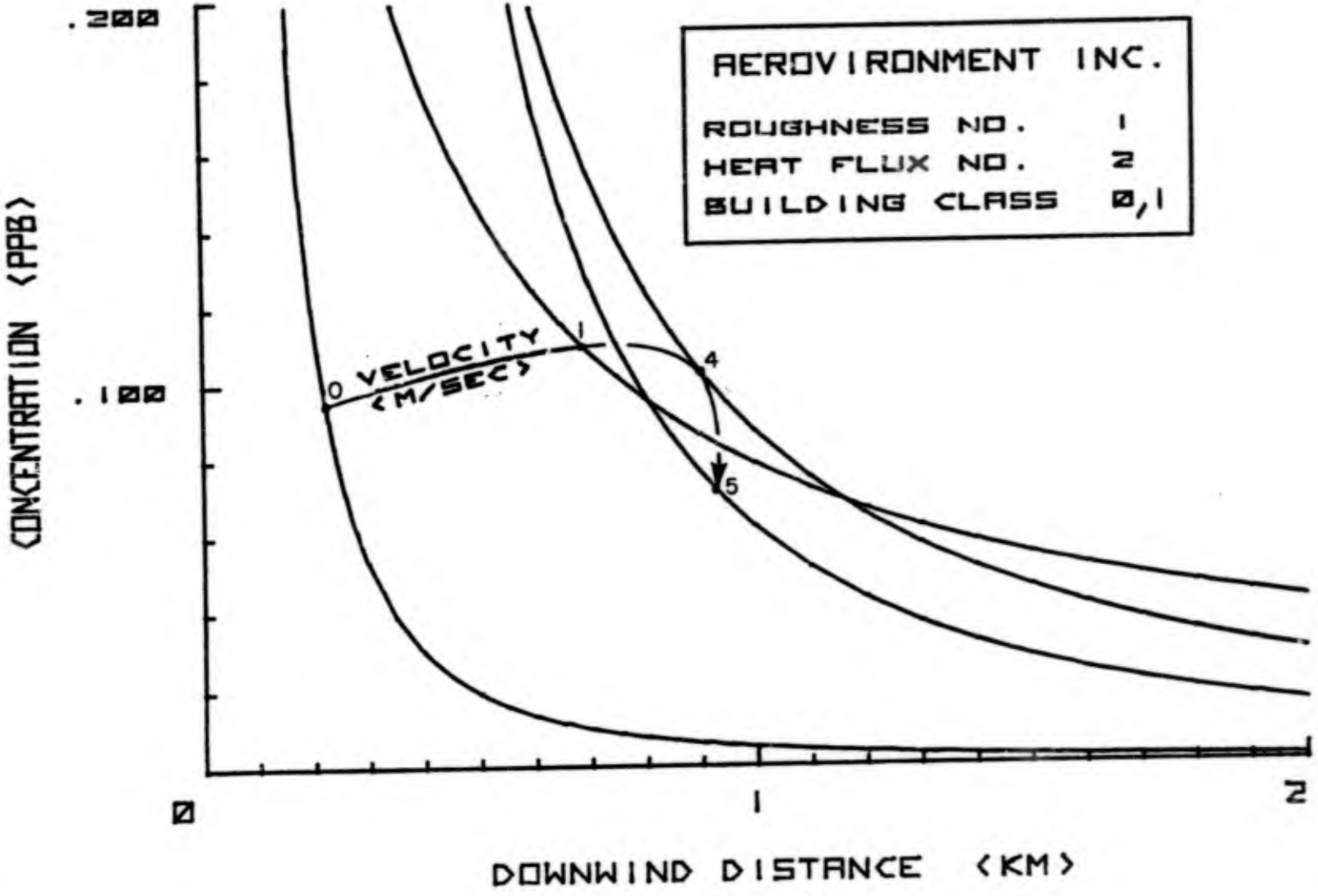

Figure 3. Downwind Concentration Under Unstable Conditions With Small Roughness.

Under extremely stable conditions, with small roughness a different situation occurs. Here, as shown in Figure 4, we have increasingly higher concentrations with wind speed, since because of the high stability the wind is not very effective in generating turbulence.

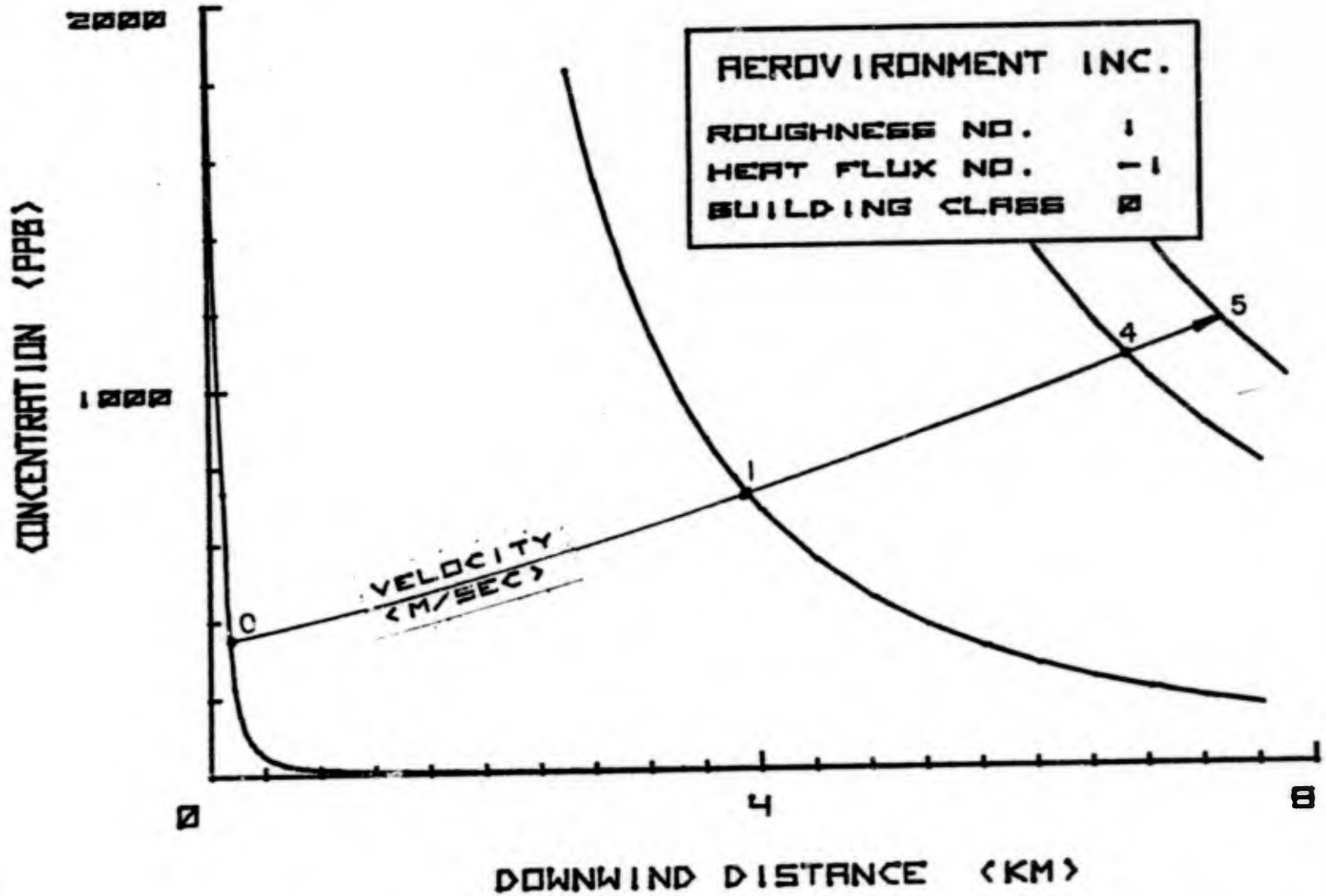

Figure 4. Diwnwind Concentration Under Stable Conditions With Small Roughness.

3. PLUME MEANDER

3.1 General

The sinuous path of a plume is a well known phenomenon. The plume centerline does not follow the mean wind but makes excursions, the vertical deviations being called looping, the horizontal, meander (Figure 5). If no distinction is required both vertical and horizontal motions will be referred to here as meander.

It is presumed that meander is caused by large eddies of relatively long time scale superimposed on the small scale turbulence. Theoretically all meander properties could be computed from knowledge of the turbulent power spectrum. However, certain conceptual difficulties occur here, since any continuous power spectrum will not give rise to the meander observed with real plumes. For a continuous type spectrum the meander would be a continuous function of the sampling time, increasing with this time. This does not appear to be the case with a plume where the meander properties appear to be disconnected from the small scale dispersion. For example, if a photograph is taken of a plume, its appearance will depend upon the exposure time. It appears that for exposures of less than five seconds the discrete sinuous appearance of the plume is maintained, while for exposures of 15 minutes, the fully diffuse meandered plume is recorded.

In the analysis of the previous section, it is implied that the ensemble average is taken as the mean concentration. This implies that the concentration is averaged over all possible positions, or conversely that the sampling time is long compared with the plume meander time. Thus the value given here is the long time average, which is the lowest value of the concentration. This is illustrated in Figure 6.

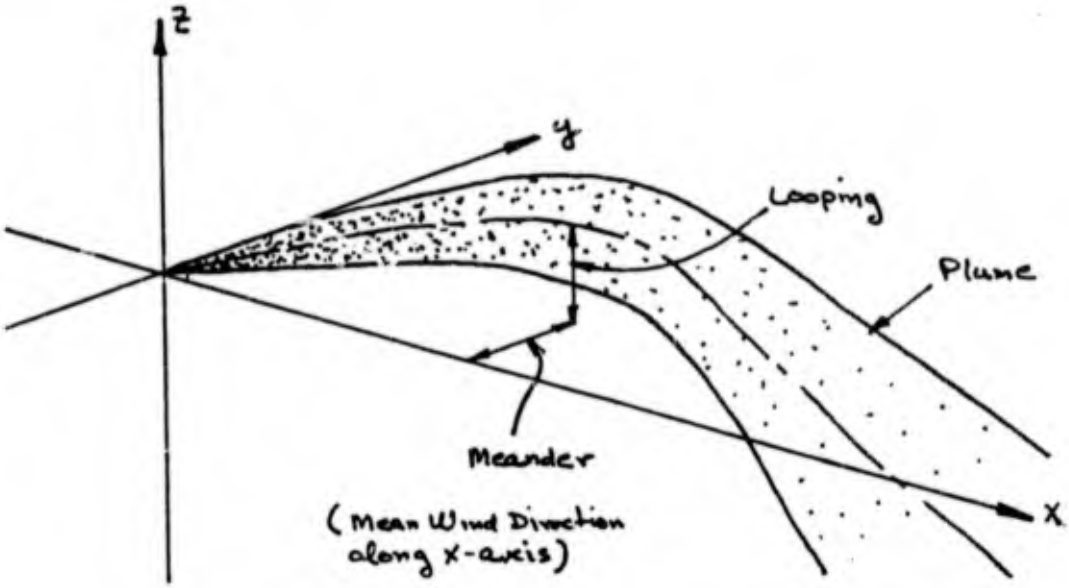

Figure 5. Meander and Looping of a Plume.

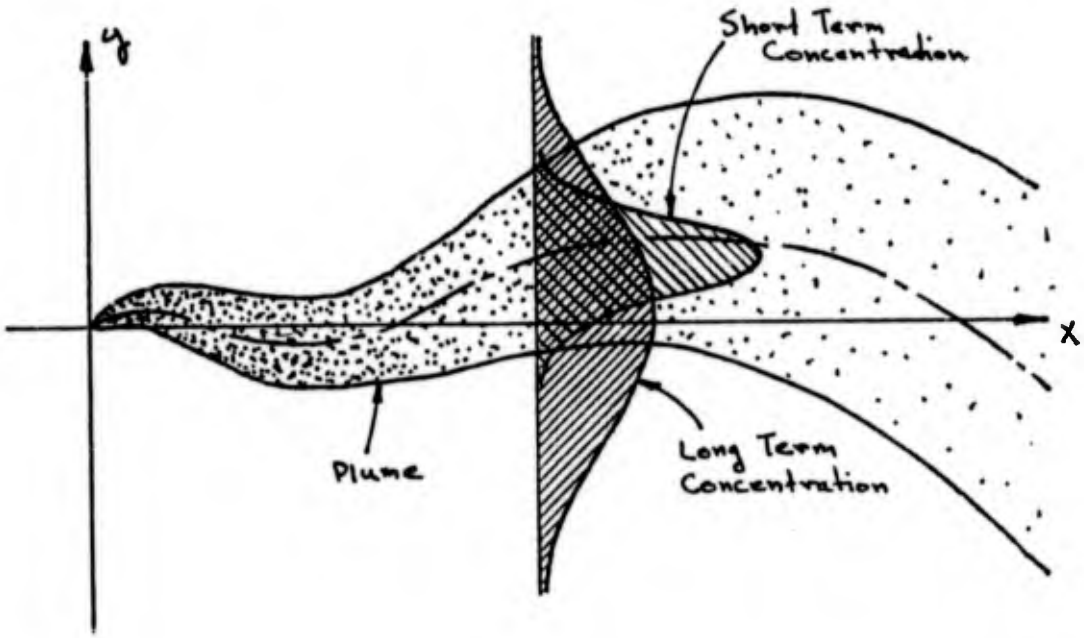

Figure 6. Short Time and Long Time Concentration Distributions.

For the purposes of this paper it was appropriate to assume that meander and dispersion are two discrete uncoupled parameters, both Gaussian and both functions of downwind distance and atmospheric turbulence. On this basis it is possible to compute maximum plume concentrations for short sampling times, and to express these in the forms of exceedance probabilities.

This approach is the asymptotic limit of the sampling times, in that the short-term concentration applies to zero sampling time, the long-term to infinite sampling time. The effect of finite sampling time is not treated, since it is assumed that the sensor instruments, having response time less than a few seconds, correspond to zero sampling time.

Thus, we have computed the long-term average in the preceding section. However, our instruments will detect short-term averages, which will always be higher than this value. The gain is defined as the ratio of the short-term concentration to the long-term centerline average.

3.2 Gain Exceedance Probability

At a given downwind position, assume the local dispersion is given by b and the meander by Y (Figure 7); then the short-term concentration on the wind axis, C* , is given by

$$C^* = C_o \exp(-Y^2/2b^2) \quad ,$$

where C_o is the short-term concentration on instantaneous plume centerline and b is instantaneous dispersion. Now, if the meander is Gaussian, of magnitude B , then the probability P that the concentration will exceed C is the probability that the meander will be less than Y

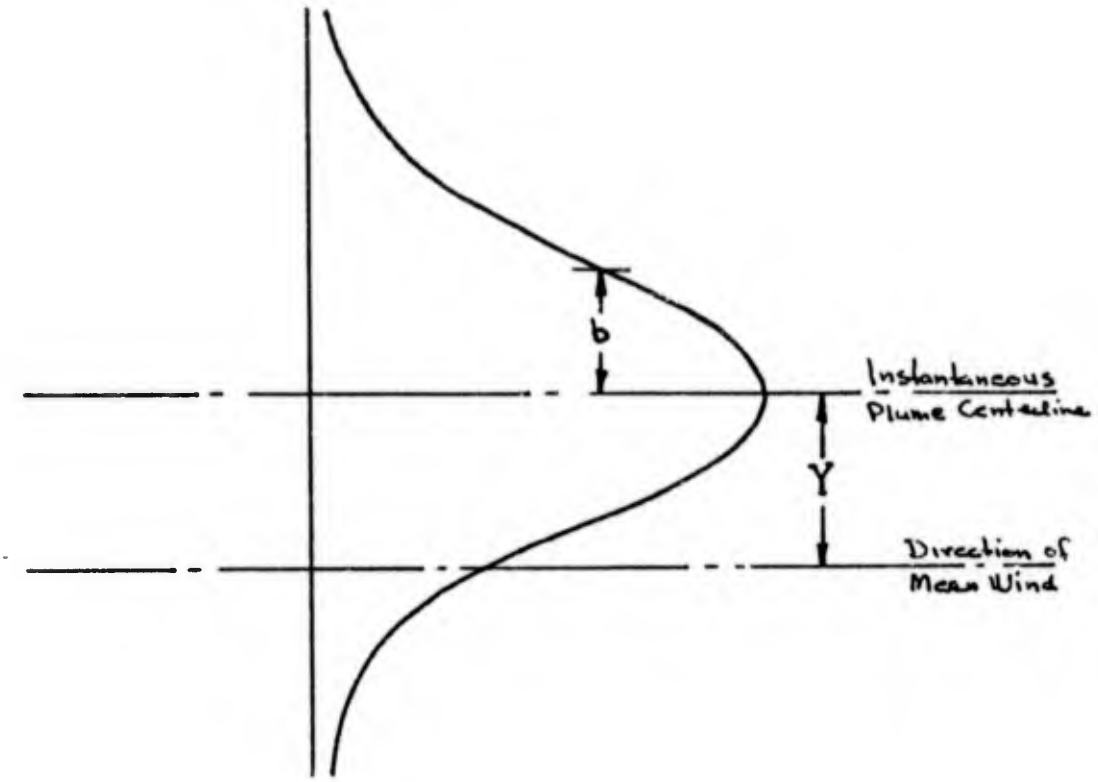

Figure 7. Centerline Concentration for Plume with Meander of Y .

$$P = \frac{1}{\sqrt{2\pi}} \int_{-Y}^{+Y} \exp(-Y^2/2B^2)\, dY$$

$$= \text{erf}(Y/\sqrt{2}B) \quad .$$

On the other hand, the long-term wind axis average is given by

$$C = \frac{C_o}{\sqrt{2\pi}B} \int_{-\infty}^{\infty} \exp(-Y^2/2b^2 - Y^2/2B^2)\, dY$$

$$= C_o/\sqrt{1 + B^2/b^2}$$

where $\sqrt{b^2+B^2}$ is the long-term dispersion, σ . Now the gain G is defined as $C/\overline{C}$ and the exceedance probability of a specified gain given by

$$P(G) \equiv \text{erf}(Y/\sqrt{2}\, B)$$

with Y/σ defined by the ratio C/C_o .

We note that the previous section defines the long-term dispersion, σ , in giving the long-term average. If B is specified one can determine b , hence Y for a given G and then P .

It is assumed that both b , B are linear functions of x so that exceedance probabilities are not functions of downwind distance. There is very limited information on B , the meander scale. For our purposes we assume that it is a function of atmospheric stability only.

The values of B can be inferred from reported peak to average concentration ratios. Although experimental data here is sparse and not extensively correlated we can obtain some estimates. From Gifford

(1960) we assume that peak to average concentration ratios are 5, 3, 2 for unstable, ueutral, and stable cases. Then, taking a linear approximation of the Pasquill results for long-term average it is possible to infer the magnitude of B . Assume B to vary linearly up to about 1 km we write B as $B - \beta x$ and use the values listed below:

Atmospheric Stability	β
Unstable	0.21
Neutral	.071
Stable	.033

Gifford predicts gains to vary with receptor distance, but for simplicity we have ignored this effect.

3.3 Off Axis Exceedances

With the above assumptions the off axis exceedance can be computed in a similar fashion. Since all scales are linearly dependent on x , the downwind axis, it is found that the exceedance probabilities are constant along lines at fixed angles to the mean wind. Along a line inclined at φ to the mean wind it can be shown that the exceedance probability is given by

$$P = \frac{1}{2}\left[\operatorname{erf}\{x \tan\varphi + Y)/\sqrt{2}\,B\} - \operatorname{erf}\{(x \tan\varphi - Y)/\sqrt{2}\,B\}\right]$$

where other quantities are defined in a similar way taking receptor offset into account.

3.4 Building Wake

In the case of dispersion in a building wake it is clear that initially the concentration at right angles to the wind will not have a Gaussian distribution. Presumably it will have more of a uniform ("top hat") type distribution. However, it is known that a few scale lengths

behind bluff bodies the wake properties are generally Gaussian in nature. Consistent with the other approximations involved in this analysis, we will assume the concentration behind a building is Gaussian, at the receptor distances of interest. Thus the exceedance probability estimation follows the same lines as before.

3.5 Typical Exceedance Curves

Two extreme cases of exceedance probability curves are shown. In Figure 8 we have the case of a very unstable atmosphere (positive heat flux) with minimal effects of building wake because the atmospheric dispersion is much larger than the wake dispersion. Here we see that gain is quite large, and that for up to 10° off axis receptors there is not much change in gain probability.

On the other hand, for a stable atmosphere with a building wake we get the curves shown in Figure 9. The features here are that the plume width is much larger than the meander. Thus, the gain is always rather small. Also, because of the very small meander it is seen that the exceedance probability is very sensitive to receptor angle φ, so that receptors must be close to wind direction for significant gains.

3.6 Multiple and Moving Sensors

The effect of multiple and moving sensors is inserted in a simple fashion, assuming that the meander correlation time is about 15 minutes. for N sensors taking short-term averages and operating for less than 15 minutes it is assumed that the probability that at least one sensor will detect a signal is $1 - \prod_{i=1}^{N}(1-P_i)$ where P_i is the detection probability of each sensor. For a single sensor on the wind axis sampling for more than 15 minutes it is assumed that maximum gain will always be detected. For a sensor moving at right angles to the wind it is assumed that maximum gain will always be detected.

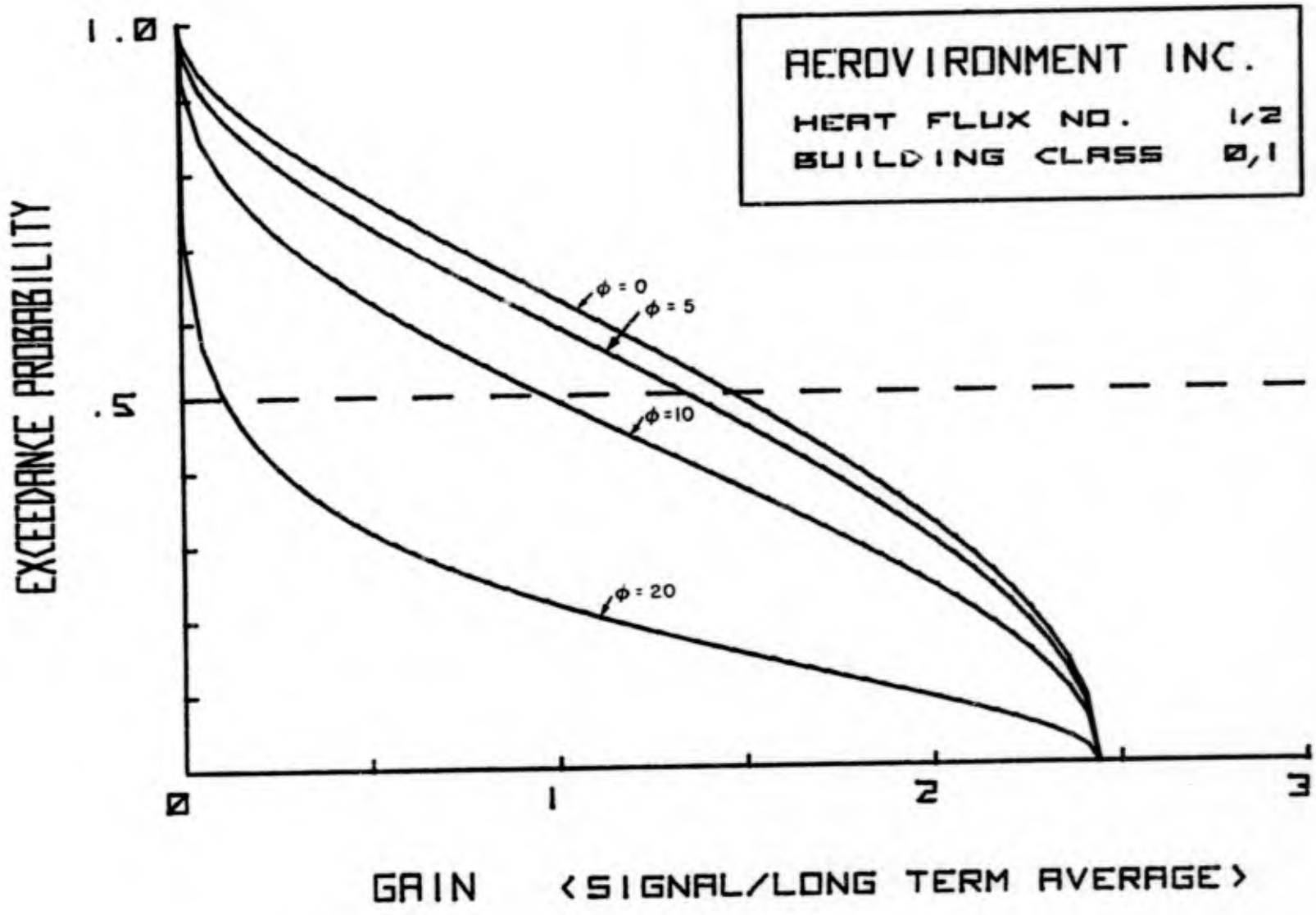

Figure 8. Exceedance Probability for Unstable Case.

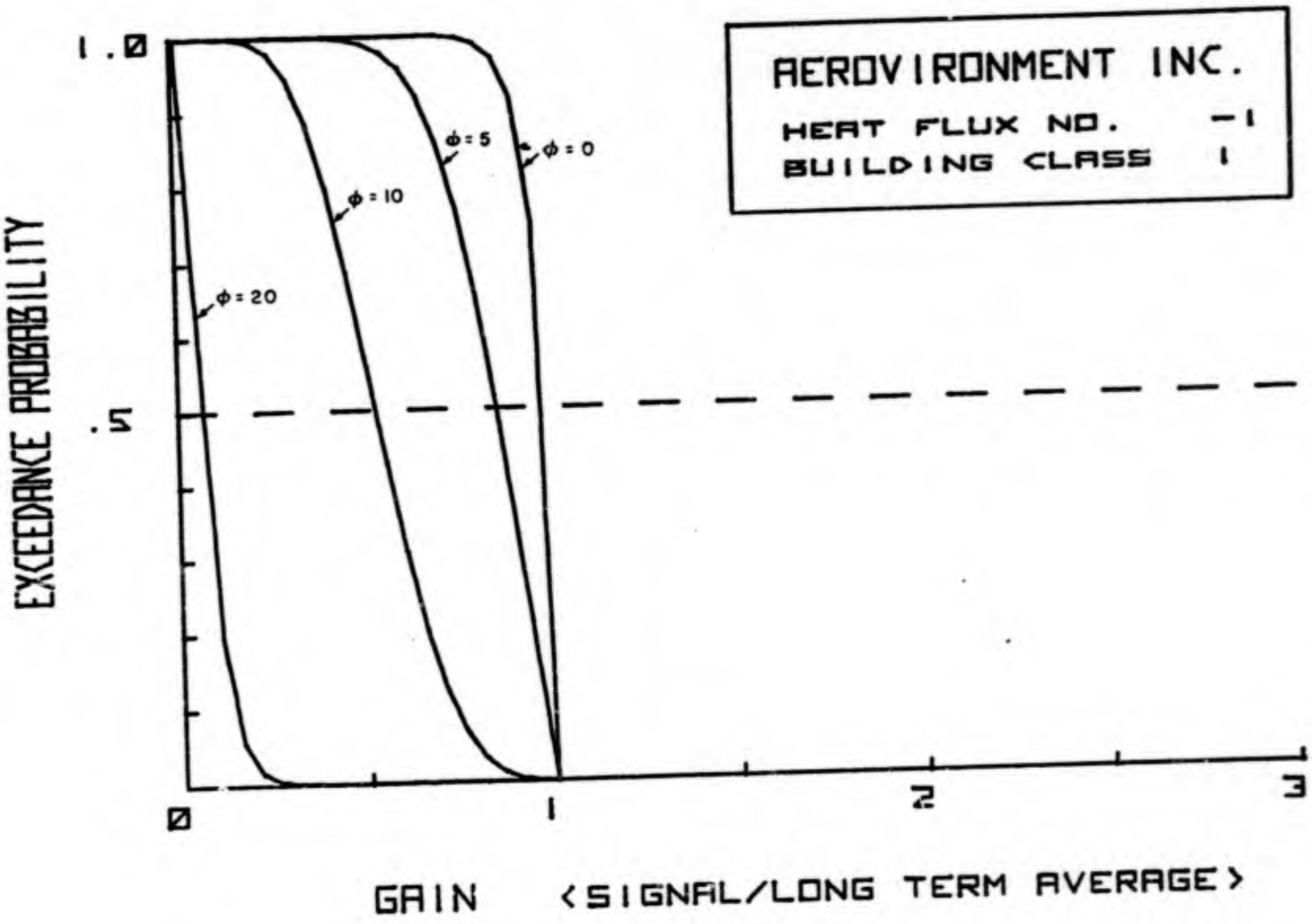

Figure 9. Exceedance Probability for Stable Case With Building.

4. NUMERICAL INPUTS TO MODEL

The downwind concentrations predicted by the model are a function of both the specified parameters and the variable parameters. Specified parameters include the source release, Q, the downwind distance, x, and the wind speed, u. The variable parameters include the heat flux, H, and the ground roughness, z_o, and depend totally upon the conditions at and near the location of the release. Here, we determine the numerical values of these variable parameters and the conditions which affect them.

4.1 Determination of Heat Flux

The heat flux is a function of the insolation in the region of interest. Since actual values of insolation are usually not available, it is convenient to define certain broad categories of insolation and to assign them a heat flux number, N_H. These heat flux numbers are then related to observable quantities in the field. Some precision is sacrificed by doing this, but the convenience in applying the model to actual field conditions more than compensates. The heat flux numbers are directly related to the Pasquill insolation. Table 4-1 lists the heat flux numbers, the associated values of the heat flux, and the conditions for which they apply.

Table 4-1. Heat Flux

Heat Flux No., N_H	Heat Flux, H ($cal/cm^2/min$)	Pasquill Insolation
-1	-.060	Nighttime, ≤ 3/8 cloudiness
0	0	Nighttime, ≥ 1/2 cloudiness Daytime - slight
1	.175	Daytime - moderate
2	.350	Daytime - strong

For daytime insolation, the condition of slight pertains to early morning or early evening; moderate to mid-morning and afternoon; and strong to direct, overhead sun with no sky cover.

The insolation is modified by position on the earth (latitude), season of the year, and sky cover.

If α is the angle of the sun from the vertical (in degrees) at latitude θ, then:

$$\alpha = |\theta - \zeta\gamma| ,$$

where

$\gamma = -1$	for winter
$\gamma = 0$	for spring and fall
$\gamma = +1$	for summer
$\zeta = 23.5^\circ$	(the tilt angle of the earth)

The value, $\cos \alpha$, represents the variation of insolation, with $\cos \alpha = 1$ ($\alpha = 0$), representing the maximum (sun directly overhead).

Variations in insolation due to latitude were examined over a range $\theta = 0^\circ$ to 50° in 10° steps for the three seasonal categories. The only significant variation within the range of heat flux numbers prescribed occurred between latitudes 20°-50° for winter. Thus, latitude variation of insolation is presented in two broad categories, $\theta = 0^\circ$-20° and $\theta = 20^\circ$-50°. Seasonal variation is also presented in two broad categories; winter, and the combination of summer, spring, and fall. Table 4-2 shows the clear sky, mid-day heat flux numbers for these combinations as functions of the prescribed latitude ranges, and seasonal categories. Table 4-3 then shows the heat flux numbers that are operationally significant in the field for the same variation in latitude and season for different sky conditions.

Table 4-2. Clear Sky Midday Heat Flux Numbers.

Latitude	Season	
	Summer, Spring, Fall	Winter
0°-20°	2	2
20°-50°	2	1

Table 4-3. Operational Heal Flux Numbers, N_H

Latitude	Sky Conditions				
	Day			Night	
	Clear*	1/2 Overcast	Overcast	1/2 Overcast	Clear
	Summer, Spring, Fall				
0°-20°	2	1	0	0	-1
20°-50°	2	1	0	0	-1
	Winter				
0°-20°	2	1	0	0	-1
20°-50°	1	0	0	0	-1

*Note: For one hour after sunrise and one hour before sunset, use $N_H = 0$; for early morning and late afternoon use $N_H = 1$.

For operational use, the appropriate heat flux number is selected from Table 4-3, and then the actual heat flux is determined from Table 4-1. This value is then used to determine the vertical turbulent velocity in Section 2. 2. If the actual value of heat flux is

available from direct measurement in the field, it will provide a more accurate determination of the turbulent velocity.

4.2 Ground Roughness

In a similar manner to the heat flux numbers, the ground roughness can be specified as a roughness number for field use. However, ground roughness is a fairly easy quantity to obtain and hence the roughness number is not as operationally useful as the heat flux number.

Table 4-4 presents the roughness, z_o, in m and a roughness number, N_R, for each of several categories of terrain. The value of z_o is directly used to calculate the roughness reduced wind speed in Section 2.2. The roughness for terrain not included in the table can be interpolated from the cases that are listed.

Table 4-4. Roughness for Various Types of Terrain.

Roughness No. N_R	Roughness, z_o (m)	Terrain Types
1	.022	Ice, smooth water, snow, lawn or smooth, long grass, smooth sand desert
2	.220	Fully grown crops, bushes, and small trees, rocky desert
3	.800	Residential buildings, park-like trees
4	2.20	Forest areas, city and commercial buildings

5. CONCLUSIONS

The procedures described give a rational method for determining concentration and exceedance probability for a wide range of ground roughness heat flux, and wind speed. The analysis is confined to roughly planar (not hilly) terrain and ground level releases. However, elevated releases, or the effect of an inversion layer can easily be inserted into the equations by standard image methods.

The basic equation and constants have been extensively validated for line sources during various AeroVironment freeway air quality programs. For point releases, however, the meander term becomes significant. Experiments on this have not been done by AeroVironment, but it is believed that the best available data has been used.

A valuable aspect of this particular approach is that because all effects are explicitly represented in the model, as more data becomes available, it can be inserted into the equations. Thus the accuracy of the model can be improved as more experimental data becomes available.

6. REFERENCES

AeroVironment Staff (1974): Air Quality Analysis and Impact Study Routes 85 and 87 in the San Jose Area. AV Final Report AV FR 232 to Division of Highways, District 04, State of California.

Gifford, F. A. (1959): Peak to Average Concentration Ratios According to a Fluctuating Plume Model. Int. J. Air and Water Poll., 3, pp. 253-260.

Lissaman, P. B. S. (1973): A Simple Unsteady Concentration Model Explicitly Incorporating Ground Roughness and Heat Flux. Paper presented at the 66th Annual Meeting of the Air Pollution Control Association, Chicago, Ill.

Lumley, L. V., and H. A. Panofsky (1964): The Structure of Atmospheric Turbulence. Interscience Publishers, John Wiley and Sons, New York.

Taylor, G. I. (1921): Diffusion by Continuous Movement. Proc. London Mathematical Soc., Vol. 20, pp. 196-212.

U. S. Department of Commerce (1968): Meteorology and Atomic Energy. Prepared for the U. S. Atomic Energy Commission, David H. Slade, Ed., pp. 221-255.

SESSION V

Chairman: Dr. Erskine Harton
US Department of Transportation

BUREAU OF MINES GAS DETECTION SENSOR RESEARCH

by

George H. Schnakenberg
Research Physicist
Industrial Hazards and Communications
Pittsburgh Mining and Safety Research Center
Bureau of Mines
US Department of the Interior
Pittsburgh, Pennsylvania 15213

ABSTRACT

The gas detector sensor research program directly supports the Fire and Explosion Prevention and Industrial Hygiene programs of the Bureau. The work is concentrated on development of new sensors and prototype instrumentation for the detection of combustible and toxic gases. Specifically, the primary gases of concern are methane, carbon monoxide, nitrogen dioxide, nitric oxide, oxygen, and carbon dioxide. The ultimate objective is to develop transducers of suitable size, specificity, power consumption, and longevity for use in small light-weight portable handheld direct-reading instruments and for use in personal dosimeters or alarms. The transducer state of the art for each gas is presented. In-house and contract research programs are discussed in terms of the objectives and methods of approach (NDIR, electrochemical, and solid state) and accomplishments and time frame for usable hardware.

I. INTRODUCTION.

A. Gases of Interest.

The mining industry is obligated to ensure by Federal law that "all active workings shall be ventilated by air containing not less than 19.5 volume percentum of oxygen, not more than 0.5 volume percentum of carbon dioxide, and no harmful quantities of other noxious or poisonous gases." As people become more conscious of the health hazards and as diesel equipment is introduced into the coal mines, it becomes imperative that suitable, reliable and accurate instruments be developed and made available to measure these toxic gases which in sufficient quantities can be harmful to man.

Currently the concern is with the following gases: Methane (CH_4) at 2%, carbon monoxide (CO) at 50 ppm (parts per million), oxides of nitrogen (NO_x), especially nitrogen dioxide (NO_2) at 5 ppm ceiling, NO at 25 ppm, oxygen (O_2) deficiency at 19.5%, carbon dioxide (CO_2) at 0.5%, and other diesel combustion products such as aldehydes and higher molecular-weight hydrocarbons. Generally speaking, the detection methods for gas identification and measurement are rather straightforward for all but the miscellaneous diesel exhaust products. Extensive research investigations, however, are currently going on which will pin down those combustion products for which detection methods may have to be developed. I consider methane, CO, and the oxides of nitrogen, especially NO_2, to be the gases of special priority for concern.

B. Air-Monitoring Systems.

There are many gas-monitoring and measuring devices which can be placed in the mine to monitor air quality. These devices range from large mine-monitoring stations to small low-power personal dosimeters. Each device places different requirements on the performance of the gas-sensing transducer. Specifically these are:

1. Mine-monitoring stations with data link to mine control center.

2. Stationary area monitors.

3. Portable work area monitors.

4. Onboard (diesel) vehicle monitors similar in function to present methane monitors.

5. Handheld inspection instruments for spot checks.

6. Personal devices such as dosimeters.

A summary of the important instrument characteristics for each category is given in table 1. The immediate long-term objective of Bureau gas-detection instrumentation research and development is to produce suitable transducer/readout systems for the handheld-inspection-type instruments since all the other gas-measuring and monitoring systems, except for the personal devices, have requirements which are less restrictive in size, weight, and power requirements than those for the handheld instruments.

C. Gas Detection Method.

The coal mine environment is one in which high relative humidity, dust, shock and vibration, and explosive atmospheres are commonplace and, although the temperature deep within a mine is fairly constant, it can differ greatly from the temperature at the surface where the instrument calibration generally occurs. What then are the most promising detection methods for these conditions?

Based on our knowledge of the state of the art today, the following approaches hold the most promise for use in coal mines:

1. Catalytic oxidation

2. Electrochemical gas transducers

3. Chemical absorbents

4. Nondispersive optical absorption

5. Electrical conductivity changes in semiconducting elements

When the *catalytic oxidation* process is used to detect methane and carbon monoxide, the heated catalyst, mounted in some way to a resistance element, increases in temperature owing to the burning of the contaminant gas. This temperature rise is sensed by a change in resistance of the heated element, providing an electrical signal. The catalytic combustion method is used extensively in most methane detectors and serves also as a basis for the Hopcolite CO detectors. However, Hopcolite is rendered insensitive by high humidities and some methane elements are fragile and show a change in calibration upon an exposure to a high concentration of methane. In addition, methane concentrations greater than about 10% give low readings since there is insufficient oxygen to completely oxidize the methane.

In *electrochemical gas transducers* the air sample is passed over a membrane through which the contaminant gas passes. It undergoes a chemical reaction upon contact with a special electrode in an electrolyte. This reaction generates an electric current which is related to the partial pressure of the contaminant gas. This type of sensor is most suitable for the detection of O_2, CO, NO, NO_2, and NO_x. These sensors can be ruggedly constructed and work well in the high humidity level of the mine air.

The type of detection method which I have called the *chemical absorbent* method includes such devices as stain tubes and chemically coated tape systems in which a controlled volume of gas meets with a chemical solid to produce a color change. The color changes appear as a length or intensity of stain. In the so-called paper tape systems a long paper tape has been coated with a chemical substance which changes color when exposed to a specific contaminant (NO_2, H_2S, or CO). The air sample is drawn over a small piece of the tape. The color change is measured optically to give a signal proportional to the product of the gas concentration and exposure time.

Nondispersive optical absorption methods use the fact that each contaminant gas of interest can absorb light at specific wavelengths (or colors). These absorption bands can be used to identify the gas and the amount of absorption can be used to measure the quantity of gas present. This method uses hot filaments as the light sources. These sources pose a problem in permissibility design. Clever implementation of this method can minimize the effects of dust and interfering gases.

The final method which may be applicable for gas detection in coal mines uses a *semiconducting element* which changes its resistance in a manner related to the concentration of contaminant gas near its surface. The present Figaro TGS sensor uses this principle but lacks selectivity and reproducibility. These devices are inexpensive and lightweight and consume little electrical power.

All of the foregoing methods, except the nondispersive method, use transducers which are inherently permissible, are low power consumers, and are small and lightweight. There are a number of other methods for gas detection. A description of these methods and a list of available instruments have been summarized in several articles. One of them is in Vol 7, No. 11, November 1973, of Environmental Science and Technology, pages 1011 through 1017. It is by Craig D. Hollowell and Ralph D. McLaughlin. Table 2 is my summary of most gas detection methods used today.

II. AVAILABLE GAS DETECTION DEVICES.

Generally speaking, there are very vew gas detection instruments available that have been designed for use in coal mines. Methanometers and methane monitors are the obvious exception. Again I will discuss the availability of these devices categorized by detection methods.

Methane and carbon monoxide have traditionally been measured by handheld portable battery-operated catalytic combustion-type detectors. The CO detectors using Hopcolite are sensitive to relative humidity so the sample must be dried. For measuring CO near the threshold limit value (TLV) (50 ppm) these devices are not really adequate. Some catalytic methane sensors can be poisoned and desensitized by exposure to a high level of methane or low-level silicone compounds. A full-scale evaluation program is planned to examine the effects of temperature and relative humidity on instrument calibration.

Stain tubes are being used in mines and many brands are available that can measure CO, NO, NO_2, and CO_2 among others. An extensive evaluation program is continuing at the Bureau to evaluate the performance of these devices under simulated mine environments. Results show (see Bureau of Mines I.C. 7811, Accuracy and Precision of Several Portable Gas Detectors, by H. B. Carroll, Jr. and F. E. Armstrong) that the observer is the major source of error with these devices. Variations in the reading for gas concentration near the threshold or ceiling limit value can vary from the true value by as much as 50 percent or more. But these tubes are the only readily available portable method that can measure all the toxic gases in mines.

There have been some recent advances in the electrochemical sensor technology. There are several approved battery-operated, handheld meters and alarms available for measuring oxygen levels in coal mines. An approved portable battery-operated unit is also available for measuring carbon monoxide at levels near the TLV (50 ppm) with good stability and accuracy although it has not been designed specifically for use in the severe mine environments.

Unfortunately, there are no comparable devices to measure the oxides of nitrogen. None of the commercially available instruments are battery operated or are packaged suitably for use in the mine, although they are generally small in size and relatively lightweight. They are reasonably accurate in the low part-per-million range, yet require frequent calibration and have response times ranging from seconds to tens of minutes. I think this area holds the most promise for handheld gas detection devices. The Bureau is planning an extensive research and development program in this area, starting with fundamental research on electrochemical gas measurement techniques.

Currently, available gas analysis instruments using nondispersive absorption are suitable only for surface monitoring of CO, methane, or CO_2. They are expensive and are not likely to go underground in great numbers.

III. BUREAU RESEARCH EFFORTS.

In general toxic gas detection devices have not been designed for underground use. To this end, then, the Bureau will be devising suitable performance specifications for instruments which will be used in the underground coal mine environment.

Long-term research programs are underway to improve the overall performance and availability of gas detection instruments for use underground. These programs will be outlined below. The general procedure which is used is (1) to define the contaminant to be measured; (2) to survey the available devices and keep abreast with new technological developments; (3) to choose those devices which use methods which seem compatible with restrictions imposed by the mine environment; (4) evaluate devices available to determine applicability; and (5) to perform the necessary research that will yield the suitable instruments.

The Bureau has a 5-year gas-detection-instrumentation-research program. The ultimate purpose of this program is to develop or refine gas detection methods and develop the necessary hardware, the gas-sensing elements, needed electronics, and packaging in a suitable form for use as a personal dosimeter or alarm for all the hazardous gases that could be found in coal mines. In doing this the Bureau will also, in a shorter time frame have developed small handheld gas-detectors for CO, NO, NO_2, etc., similar in size and function to the present methanometers. This research effort will be carried out through in-house investigations and specific contract research programs, based upon in-house findings.

Currently several areas of research into methods of gas detection are very active and are summarized here:

1. Contract H0230050 with ANDROS, Inc., is using nondispersive optical absorption methods in a unique and clever way described in the following presentation to detect part-per-million levels of NO_2, CO, and percent levels of CH_4 (or possibly CO_2, if necessary). The final instrument will be a battery-operated, handheld multigas device for spot checking toxic gases in the mine atmosphere. It could also be used as the sensor for stationary monitors and vehicle monitors. A prototype should be available in about 6 months.

2. The Bureau of Mines Bartlesville Energy Research Center (BERC) is developing a CO_2 monitor and alarm for mounting on diesel-powered equipment. By monitoring the CO_2 level of the diesel intake air, the instrument gives an indication of the extent of dilution of the diesel exhaust by the ventilation air. With this information available, the operator can minimize the diesel rebreathing its own exhaust and can shut down the diesel operation if air quality becomes unsafe for prolonged exposure. By keeping the CO_2 level in the safe region below one-half percent, the operator can be reasonably sure that the other diesel exhaust gases, CO, and the oxides of nitrogen are being diluted to a safe level as well. The first prototype has undergone field tests; the second-generation monitors are to be delivered and field tested in the near future. Nondispersive infrared absorption is the detection method used.

3. In addition to the multigas detector in item 1 above, Brown University (Grant G0101740) has successfully produced infrared-emitting diodes which emit in the methane absorption band, 3.3 micrometers. These devices are being used with a solid state Indium Arsenide detecting diode as the methane detector for a handheld methanometer. Instrumentation design utilizing these devices is being done at the Pittsburgh Mining and Safety Research Center (PMSRC).

4. A grant, G0133066, was given to New York University to develop CO, NO, and NO_2 dosimeters. Molecular diffusion along a path depends upon (1) ratio of path length to cross sectional area, (2) ambient temperature, and (3) difference in gas concentration along the path. The NO_2 concentration is kept at zero by a chemical absorbent at the closed end of the

tube. The amount of NO_2 absorbed, determined later by chemical analysis, depends only upon the exposure time and the ambient NO_2 level, all other factors being constant. The device is specific to NO_2, is insensitive to air flow and weighs only 7 grams. These devices are passive samplers in that a chemical absorbent of the gas being measured samples the atmosphere through a controlled orifice. The sampling rate is controlled by molecular diffusion of the gas in air. Small NO_2 samplers using this principle were developed and are currently in field tests. Dosimeters for CO and NO are currently under development.

5. The principle by which the semiconductor Figaro TGS sensor detects "almost everything" is being investigated by Research Triangle Institute under Bureau contract H0346015 to see if a semiconducting detector can be developed which is selective and sensitive only to carbon monoxide. When such a substance is found, a handheld CO meter with a low range of 0-100 ppm will be made. In addition, such a transducer could be used in a CO dosimeter/alarm.

6. The Bureau is also supporting the development of an optical stain tube reader which will remove the observer error from stain tube measurements. A bench-type setup has proved the feasibility of such a device. Along the same lines a prototype sub-part-per-million-range NO_2 dosimeter using the change in optical reflectance of a chemically impregnated silica-gel-coated tape as the detection method will soon be undergoing in-mine field tests. It is self-powered by rechargeable batteries and fits a 6-in by 6-in. by 6-in. box.

7. Two prototype multigas Mine Air Monitors (O_2, CO, and NO_2) using available electrochemical-type sensors were developed for the Bureau of Mines under contract H0122044 with Texas Instruments. These devices, already in field trial, are hand-carryable, train-case-sized battery-operated air monitors for use near the working face. These units can run unattended for 30 hours on a single battery recharging. Should the CO or NO_2 level rise above a set threshold or an O_2 level or fall below a set threshold, an alarm will sound. The actual gas concentration, state of battery charge, and threshold levels can be read on a digital meter. Complete design drawings, schematics, and specifications for this device are available from the Bureau of Mines.

8. Perhaps the most promising research area is in the electrochemical-type transducers for CO, NO, and NO_2. These devices are inherently low-power devices and in fact, generate their current in proportion to gas concentration. This type of device is ideal for use in dosimeter/alarm devices. In the next several years, the Bureau of Mines will be putting a great deal of effort and money into the development of both electrochemical transducers. Although several instruments using electrochemical transducers are on the market, only a few can be used in a coal mine and none of these were specifically designed for such use. The transducers themselves are in their infancy and it does not seem likely that they will be improved or specifically designed for use in mines without a Bureau of Mines program of coordinating and funding in-house research, university grants, and contracts. Carbon monoxide will be the target gas for our initial efforts.

SUMMARY

To ensure adequate coal mine air quality, especially with the introduction of diesel-powered equipment and to improve instruments used to detect methane, the Bureau of Mines is carrying on an extensive research effort into the development of better gas-sensing transducers. A discussion of candidate gas detection methods was presented emphasizing electrochemical methods, nondispersive optical absorption, chemical absorption, and gas-sensitive semiconductor methods. The target gases are CH_4, CO, NO, NO_2, CO_2, and O_2.

The availability of suitable detectors for mine use was pointed out. Most are not suitable, with methane detectors and possibly oxygen detectors being an exception, and only the methanometers have been designed specifically for use in coal mines. Contract research and development have produced a prototype portable Mine Air Monitor for CO, O_2, and NO_2 using state of the art electrochemical transducers; a passive NO_2 sampler using an absorbing chemical; and an infrared emitting diode for use in NDIR methane detection. Current contract research should produce a small handheld CO, CH_4, NO_2 gas detector using nondispersive absorption, passive samplers for CO and NO, optical stain tube reader for all gases for which there are tubes, an infrared diode methanometer, and a low-power semiconductor CO detector.

Table 1. In-Mine Gas Detection Applications and Requirements

I. Mine-monitoring stations	
Function:	Stationary monitors with or without data link to central location; local alarm or readout
Gases:	Probably CH_4, CO, NO_2, O_2
Power:	Either unlimited or intrinsically safe power available
Size:	Standard rack mounting
Environment:	Little or no shock, vibration, or temperature variation, continuously wet and dusty
Operating requirements:	Very little maintenance, infrequent or automatic calibration in situ, continuous operation, low operating cost, fail safe, accurate, and precise
Candidate methods:	Nondispersive absorption, sealed electrochemical cells, chemiluminescent
II. Portable work area monitors	
Function:	Local breathing-air-quality alarm at face, possible wireless link to communications station (alarm condition), local alarm or readout
Gases:	CH_4, CO, NO_2, O_2
Power:	At least 10 hours continuous operation from rechargeable batteries
Size:	Hand carryable, train case size
Environment:	Shock, large temperature variation, wet and dusty

Table 1. (Contd)

Operating requirements:	Weekly maintenance and calibration, continuous, reasonably accurate and precise
Candidate methods:	Sealed electrochemical cells, semiconductor
III. Vehicle monitors	
Function:	Breathing-air quality monitor onboard diesel- or electric-powered face equipment, local alarm and readout; possible wireless link to central control, possible vehicle shutdown at alarm
Gases:	CH_4, CO, CO_2, NO_2, O_2 others
Power:	Unlimited (100W) 12 or 24 volts, direct current
Size:	Small low profile, heavy/permissibly enclosed
Environment:	Shock, vibration, temperature variation, wet and dusty
Operating requirements:	Little maintenance, infrequent calibration, short warmup time, nonmicrophonic, ruggedly constructed, continuous operation, reasonably accurate and precise
Candidate methods:	Nondispersive absorption, catalytic combustion, sealed electrochemical cells, semiconductor
IV. Portable handheld devices	
Function:	To replace stain tubes, spot-checking gas concentrations by operators and inspectors
Gases:	CH_4, O_2, and all toxic gases
Power:	10-hour operation at a 10-to-20-percent duty cycle, rechargeable or replaceable batteries
Size:	Small, less than 10 pounds. Single gas – handheld multigas – shoulder-strap-carried box
Environment:	Shock, temperature variation, wet and dusty
Operating requirements:	Accurate and precise, short warmup and measuring time, weekly maintenance and calibration long shelf or storage life between uses
Candidate methods:	Nondispersive, absorption, sealed electrochemical cells, semiconductor catalytic combustion

Table 1. (Contd)

V.	Personal devices	
	Function:	To provide alarm or dosage measurement to wearer or mine industrial hygienist
	Gases:	O_2, CO, NO_2, NO
	Power:	Little, if any; self-contained battery or cap lamp reserve
	Size:	Small, pocket-sized; integral part of hat
	Environment:	Some shock, wet and dusty, temperature variations
	Operating requirements:	Low cost, infrequent or no calibration, reasonably accurate and precise
	Candidate methods:	Chemical absorption, sealed electrochemical cells

Table 2. Gas Detection Methods

I. Optical absorption spectroscopy

A. Nondispersive absorption spectrometer

1. Nondispersive infrared (NDIR) [CO, CO_2, HC]

2. Dual isotope fluorescence [CO only]

3. Ultraviolet (UV) and visible nondispersive absorption [SO_2 NO_x]

4. Mercury substitution UV absorption [CO]

5. Laser techniques [many gases]

6. Dual isotope correlation [many gases]

B. Dispersive spectrometers

1. General dispersive absorption spectrometers [SO_2, NO_x, CO, or HC]

2. Correlation spectrometers [SO_2 or NO_x]

II. Chemical reaction methods

A. Electrochemical

1. Conductimetric [SO_2]

2. Amperometric [SO_2, NO_x, CO]

3. Chemical-sensing electrode [SO_2, H_2S, NO_x, NO_2, CO]

B. Colorimetric

1. Solutions [SO_2, NO_x]

2. Dry chemical-impregnated tape [H_2S, NO_2, CO]

3. Stain tubes [many gases]

III. Other standard methods

A. Chemiluminescent [NO_x]

B. Mass spectrometers [many except CO]

C. Condensation nuclei formation [SO_2, submicron particulates, smoke]

IV. Other methods

A. Bioluminescence [many gases]

B. Microwave spectroscopy

C. Semiconductor detectors [CO, H_2, HC]

D. Quartz microbalance

RESEARCH IN THE USE OF LIQUID CRYSTALS IN CHEMICAL DETECTION*

by

Edward J. Poziomek, Thaddeus J. Novak, and Raymond A. Mackay

Chemical Laboratory, Edgewood Arsenal, Aberdeen Proving Ground MD 21010

This report reviews current technology on the use of liquid crystals for chemical detection of organic vapors. Emphasis is placed on the research performed at Edgewood Arsenal. An introduction to the nature of liquid crystals is supplied. The effect of bulk impurities on the transparency of liquid crystals is described. The Department of Defense programs in the subject area are reviewed. Considerations in the use of liquid crystals for chemical detection are discussed. Details are given on the use of microporous polypropylene films impregnated with liquid crystals. Current technology would allow the development of simple liquid-crystal detector devices for the detection of organic chemical vapors in the parts-per-million concentration range. The detection would not require instrumental monitoring; it would be nonspecific reversible and temperature insensitive. Suggestions for future research are supplied.

I. INTRODUCTION.

For those unfamiliar with liquid crystals, a convenient introduction is available in a book and several articles.[1-4]

The history on liquid crystals goes back to 1888 when the Austrian botanist, Friedrich Reinitzer,[5] found that cholesteryl benzoate appeared to have two melting points. At 145°C the solid turned into a cloudy liquid; at 179°C it melted. Lehmann[6] in 1889 showed that the cloudy liquid contained many regions that appeared to have a crystal-like molecular structure, i.e., ordered areas which were optically anisotropic. In other words, there was a defined temperature range where it behaved as a liquid (in its mechanical properties) and as a solid (in its optical properties). Lehmann suggested the name liquid crystal to describe this behavior.

About 5 percent of all organic compounds are transformed at their melting point into liquid crystals. These are termed thermotropic mesophases. There may be more than one discrete mesosophase exhibited by a particular compound. The fluidity of a liquid crystal may vary from a paste to that of a free flowing liquid. There are also lyotropic mesophases, i.e., those formed by mixing substances. A soap-water solution is an example. The liquid crystals described in the present paper belong to the thermotropic class.

Practical application of liquid crystals to chemical detection is minimal in comparison to the use of these substances in temperature measurements,[7-9] medical

* The use of trade names in this report does not constitute an official endorsement or approval of the use of such commercial hardware or software. This report may not be cited for purposes of advertisement.

thermography,[10] quality control[11,12] and low-powered electro-optic and digital displays.[13-15] Liquid crystals have also been related to living systems and are important in biological research.[16-18] Many important cell components such as lipids and phospholipids form mesophases in solution. Also, it has been shown that the change in the partitioning of cholesterol between lipoprotein mesophases with age is a strong biophysical factor in arteriosclerosis and coronary thrombosis. Publications covering the chemistry of liquid crystals,[19] and applications in chemistry[20] and physics,[21] are available.

The molecules of liquid crystals are long, relatively straight, and rigid, in other words, rodlike. Mutual lateral interactions constrain the molecules to be parallel to each other. Conventionally, there are three types of liquid crystals, namely, smectic, nematic and cholesteric.

Smectic is derived from the Greek word for *soap*. The molecules of a smectic liquid crystal are arranged side by side in a series of layers. Within each layer the molecules can be arranged in rows or at random Since hardly any interaction occurs between the ends of the molecules, the layers are free to slide over each other giving the properties of a two-dimensional fluid. Smectic liquid crystals are optically positive, i.e., the velocity of light transmitted perpendicular to the layers is less than that transmitted parallel. The *high viscosity* and *surface tension* of smectic phases are a consequence of the high degree of order. A number of smectic states have been identified depending mostly on molecular arrangements. Techniques such as thermal analysis, microscopy, miscibility relationships in binary systems and x-ray analysis have been used to identify and assign smectic phases. Smectic liquid crystals have been used as solvents in electron spin resonance, Mossbauer spectroscopy and electrooptical memory devices.

A second major class of liquid crystals is the nematic one. *Nematic* is taken from the Greek work for *thread* because thread-like structures are observed when viewing a sample under a microscope. The nematic liquid crystals are not as highly ordered as are the smectic ones. The long axes are parallel, however, the molecules are not separated into layers. The time and spacially averaged parallel orientation of the long molecular axes occurs within relatively small domains. As one result, nematics are much less viscous than smectics. The degree of order is about 0.3-0.8 and decreases further with increases in temperature. Parallel orientation of the molecules over large regions can be achieved only by expenditure of additional energy. Nematics respond to electric and magnetic fields in much the same way as iron filings do. Changes in order are observable as changes in optical properties such as transparency, birefringence, or color. Impurities will induce such changes. Indeed as will be discussed later in this report, attempts are being made to use the effect as a signal in the detection of chemicals which have been absorbed by liquid crystals.

The cholesteric mesophase represents a special case of the nematic structure in that the long axes of the molecules are parallel to the plane of the layers. As mentioned earlier, cholesteric liquid crystals were first described with cholesteryl esters. The preferred direction of the long molecular axes in each layer is rotated through a constant angle (averaging 15 minutes of arc) relative to that in the next layer giving the appearance of a "twisted" nematic structure. A helical path is described. High optical rotation and circular dichroism result from the twisted structure. The property of circular dichroism is responsible for the characteristic iridescent color

formed when cholesteric liquid crystal films are illuminated by white light. The light is broken into two components, one with an electric vector rotating clockwise, the other counter-clockwise. One component is reflected, the other is absorbed or transmitted. The wavelength of the reflected light is sensitive to temperature as well as any effect which causes a disturbance of the molecular arrangement. Thus, sheer stresses or the addition of chemicals result in changes of the reflected wavelength.

II. EFFECT OF IMPURITIES ON OPTICAL CHARACTERISTICS OF LIQUID CRYSTALS.

The liquid crystal research at Edgewood Arsenal which relates to the effect of impurities on the optical characteristics of liquid crystals can be divided into three major categories:

Effect of bulk impurities on transparency

Effect of bulk impurities on transition temperatures

Fluorescence emission of impurities

A simple technique was developed to measure the transparency of liquid crystal films at any specific wavelength (ultraviolet to near infrared) versus temperature.[22] The procedure involves heating a sample held in a lead spacer between calcium fluoride plates in a brass holder placed in a Cary 14 spectrophotometer. Thus, the technique provides a spectrophotometric method of following transitions which occur from the solid to the isotropic liquid phases. The technique was found to be reliable with regard to the detection of the transition and the accuracy and reproducibility of the temperature range over which the transition occurs. The cell was designed so that the events corresponding to transparency curve features can be checked by using a microscope.

Using the above-mentioned procedure, transparency characteristics were determined for cholesteryl myristate, decanoate and nonanoate from the solid to the isotropic phases at fixed wavelengths of 300, 400, 500, 700, and 2,500 nm.[23] The transparency characteristics of cholesteryl nonanoate while being cooled from the liquid phase were also determined. All transitions previously reported utilizing techniques such as microscopy, differential thermal analysis, and differential scanning colorimetry were observed. The method compares very favorably with other techniques in regard to the detection of transitions and dichroic scattering. The degree of light scattering varies as a function of the incident wavelength, but the temperature ranges over which the transitions occur are reproducible. The shapes of the transparency curves do vary markedly between compounds as would be expected.

The effect of bulk impurities on the transparency of cholesteryl nonanoate has been determined.[24] In one variation, the transparency was measured at a fixed wavelength (500 nm) as the sample was allowed to cool at a fixed rate (0.8°C/min) from the isotropic liquid to the smectic phase. The effects on transition temperature and temperature of maximum dichroic scattering by each of nine solutes at a concentration of 0.5% were determined. Of the solutes examined, anthracene and methyl benzilate exhibited the greatest changes (1.8-3.4°C difference in the various transitions compared to those found for cholesteryl nonanoate alone).

Since the solute is soluble in all three phases (cholesteric, smectic, and isotropic liquid), the depression of the transition temperature depends on both the transition enthalpy of cholesteryl nonanoate (h°) and the distribution coefficient (D) of the solute between the phases. An "effective" enthalpy (h) can be calculated from the slope of the line, which on the basis of thermodynamics is related to h° and D by equation 1.[24]

$$h = \frac{h^\circ}{(1 - D)} \qquad (1)$$

where

$$D = X^{\beta}/X^{\alpha}$$

and

X = mole fraction of solute,

and

h° = enthalpy of transition from phase α to phase β.

The results for methyl benzilate were reported[16] as follows:

Transition (α - β)	h°, cal/g[25]	h, cal/g	D
Isotropic-cholesteric	0.22	2.24	0.902
Smectic-cholesteric	0.11	1.62	0.932

The wavelength of maximum dichroic scattering (λ_{max}) is related to the pitch of the helix (Z) and the average refractive index (n). Added solute will in general change both Z and n, and thus λ_{max}. Apparently, the decrease in temperature necessary to compensate for the effect of the added solute is proportional to the solute concentration. A similar relationship has been noted for the dependence of the nematic temperature of a compensated cholesteric liquid-crystal solvent on the concentration of added steroidal solute.[26] a typical dependence of λ_{max} on concentration (C) at constant temperature and λ_{max} on temperature at constant C have been shown for anthracene as a solute in cholesteryl nonanoate. Both methods are about equally sensitive. The relationships were found to be nonlinear.

The effects of recrystallization technique, recrystallization solvent and added impurities (diisopropyl methylphosphonate and pyrene) on the transparency of cholesteryl nonanoate in the solid state have been studied.* The studies indicate that the purer the sample the more transparent it is in the solid state. Addition of impurities leads to a transparency

* Poziomek, E. J., and Novak, T. J. Unpublished results.

decrease with a minimum (corresponding to a transparency maximum) appearing in solid state transparency versus temperature curves. The purer the sample the more impurity is needed before a minimum appears in the solid state transparency curve. A sample of cholesteryl nonanoate recrystallized from hexane scattered much more light than did those obtained from either ethanol or acetone. Cholesteryl nonanoate recrystallized from acetone was found to be the most transparent in the solid state.

Investigators working with cholesteryl esters in chemical detection applications require knowledge of how the ester was purified. The recrystallization solvent affects not only the solid state transparency but also the transition temperatures and the wavelength position of maximum dichroic scattering.

The fluorescence emission of impurities (using pyrene and phenanthrene as examples) dissolved in cholesteryl nonanoate has been examined as a function of temperature at various excitation wavelengths.[27] As the samples were cooled the curves exhibited prominent emission intensity increases. The temperatures at which the line slope increases and/or later "peaks" correspond within several degrees to isotropic-cholesteric and cholesteric-smectic transition temperatures were reported previously. The increase in fluorescence is most likely due to an increase in effective path length due to scattering of the exciting light by the mesophases. This is consistent with the general similarity between major features of the fluorescence and transparency curves.

III. DEPARTMENT OF DEFENSE PROGRAMS ON THE USE OF LIQUID CRYSTALS FOR CHEMICAL DETECTION.

The Department of Defense has considerable interest in various applications which utilize liquid crystals. The use of liquid crystals in chemical detection stems back a decade to the Air Force-sponsored research of Fergason.[28] The Air Force has continued to sponsor this type of research with emphasis on the use of instrumental readout.[29,30] Cholesteryl esters were utilized primarily.

For about five years the Army Research Office has sponsored basic research related to eventual use of liquid crystals in detection. Examples of the work can be found in the publications of Martire,[31-36] and also Bulkin.[37] Though the Air Force work was not duplicated in any way, the emphasis of the research was placed on cholesteryl esters. The Army Research Office has continued to sponsor the work of both Martire and Bulkin.

Currently, Martire is studying solute-induced nematic to isotropic transitions. Bulkin has been studying the interaction of organic solutes with liquid crystal solvents by utilziing infrared, far infrared and Raman techniques. He has also applied a cholesteric liquid crystal detector to a detection-identification scheme involving gas chromatography and infrared spectroscopy. The Army Research Office began recently to sponsor liquid crystal research by M. Labes. This investigator is well known for his research in electric field effects on various properties of liquid crystals.[38,39]

Edgewood Arsenal has been interested in the development of chemical vapor detectors which are very sensitive, simple to use and do not require instrumental monitoring. Gas-solid chemical reactions would be ideally suited for such applications but the fundamental technology does not exist. The problems encountered in the design of gas-solid reactions for detection purposes have been outlined.[40] Edgewood Arsenal interest in liquid crystal films as simple detectors goes back to 1972 when a preliminary communication was published on the visual detection between crossed polarizers, of the absorption of organic vapors in the liquid crystal film.[41]

IV. CONSIDERATIONS IN THE USE OF LIQUID CRYSTALS FOR CHEMICAL DETECTION.

The major factors to be considered in the detection of vapors using liquid crystals include film preparation film thickness, specificity, sensitivity and temperature effects. One also has to take into account the rate of diffusion of the materials to be detected in the liquid crystal film.

In the preparation of cholesteric liquid crystal films Fergason and coworkers[28-30] reported using a solution of 10-15 percent by weight of the liquid crystal usually in petroleum ether. A liquid crystal combination (e.g., cholesteryl chloride, cholesteryl oleyl carbonate and cholesteryl nonanoate) was chosen so that the dichroic scattering was detectable at room temperature. Two drops of the solution were placed on a Mylar film stretched by a hoop. The evaporation of the solvent resulted in a thin layer (approximately 25 μ) with a surface area of about 1 inch. The Mylar^R hoop was then positioned in the glass vacuum bell jar over an aluminum or copper block whose temperature could be measured and carefully controlled. The vessel was evacuated and the sample injected as a liquid with a microliter syringe. The reflection of light (monochromator source) by the liquid crystal film was detected by a photomultiplier. Parts per million of various organic vapors could be detected easily. Parts per billion have been claimed but this would have to involve the most ideal conditions and approach the limit of the instrumental monitoring capability.

The magnitude of the shift in wavelength of maximum dichroic scattering was found to depend on the nature and vapor phase concentration of the solute (i.e., the material to be detected). The wavelength shift was linear in the vapor-phase concentration range studied. Martire has reported that per mole fraction increment dissolved small dipolar and/or hydrogen-bonding solutes (e.g., chloroform and methanol) are most effective in producing red shifts, while large nonpolar solutes (e.g., nonane) are most effective in producing blue shifts.

In essence, nonselective detection of organic vapors at the ppm level appears practical with cholesteric liquid crystals but only if the temperature is controlled carefully. Warning devices, in the form of badges containing a *cholesteric* liquid crystalline film to be worn by personnel do not appear practical at this time.

V. USE OF MICROPOROUS POLYPROPYLENE IMPREGNATED WITH LIQUID CRYSTALS.

Since the use of cholesteric liquid crystals did not appear to offer promise as a system for simple detectors, Edgewood Arsenal research turned towards the smectics and nematics. Visual detection between crossed polarizers of organic vapors on various liquid crystal films was described in a preliminary communication in 1972.[41] A detailed paper appeared recently in Molecular Crystals and Liquid Crystals.*

For the preliminary screening tests the candidate liquid crystal was smeared thinly on a microscope slide or on the inside surface of a test tube. A modification involved mixing the liquid crystal (three parts) with fumed alumina (Alon^R), (one part) in order to prevent film creeping.

The normal procedure involved impregnating microporous polypropylene film (Celgard 2400) with the liquid crystal. Best results were achieved by first stretching the film using double wooden hoops. A piece (approximately 9 sq cm) of the stretched film was then mounted on a cardboard making a window A simple method of mounting involved placing the film onto the window opening previously lined with cellophane tape which was sticky on both sides. Excess film was then trimmed off.

A drop of the liquid crystal was then placed on the film and the excess wiped off by using absorbent tissue. Actually both sides of the film were rubbed repeatedly with the tissue until a uniform color field was evident when the film was viewed between crossed polars of a hand polariscope. In some instances it was found useful to expose the impregnated polymer to CH_2Cl_2 vapors (using a hypodermic syringe) then repeat the rubbing.

Several experiments were also performed using a polarizing microscope. In these cases the film was mounted over a 0.63-cm hole in a cardboard support.

A qualitative screening of several different liquid crystals was conducted in order to select materials for more detailed study. The nematic, cholesteric and smectic mesophases were represented. Tests were performed at room temperature or higher to maintain a particular mesophase of the material being examined. All of the liquid crystals tested gave a positive test but the nematics responded faster than the others. Since only a limited number of liquid crystals were examined, the possibility of obtaining a very sensitive nonnematic system cannot be overruled. The nematics, N (p-methoxybenzylidene)-p-n-butylaniline (MBBA), and N-(p-ethoxybenzylidene)-p-n-butylaniline (EBBA), were studied The results were compared to those obtained with a smectic, 3-N (p-ethoxybenzylidene)-6-n-butylpyridine (EBBP). The preparation and properties of MBBA and EBBA are well reported.[42,43] Champa[44] has described the preparation of EBBP.

It was found convenient to utilize microporous polypropylene as the matrix for the liquid crystals. The polymer film properties were as follows: thickness, 24 μm weight,

* Poziomek, E.J., Novak, T. J., and Mackay, R. A. Mol. Cryst. and Liq. Cryst. 27, 175 (1974).

1.2 mg/sq cm; pore size, <0.1 μm surface area 50 sq m/gm. The amount of liquid crystal loading was approximately 0.7 mg per sq cm of film.

Cardboard containing a window of liquid crystal impregnated polypropylene film was mounted with cellophane tape on the inside of a 1-liter flask. The flask was positioned between crossed polars of a band polariscope oriented to give the film a visual green color. Use of a fluorescent lamp in combination with polars from a commercial microscope gave brighter colors than did the polariscope.

Test atmosphere was prepared by allowing microliter quantities of the substance to be detected to evaporate in the stoppered flask. The exact quantity introduced was determined by weighing the microliter syringe filled and after emptying. The flask was equipped with a miniature fan which allowed equilibration to occur rapidly. The fan was operated for 1 minute after the test substance was introduced. The motor was turned off and the color of the film was checked. A change in color from green to orange was interpreted as positive detection of the vapor. The concentrations of various organic vapors required to give the color change with several different liquid crystals are shown in table 1.

Microporous polypropylene impregnated with a liquid crystal (mesomorphic state) and placed between crossed polars gives any one of several colors depending on the orientation of the polars. Rotation of the film or the polars lead to the appearance of several different colors. As mentioned, if the film is fixed so that the observed color is green, sufficient absorption of organic vapor will change the color to orange. The same color can be caused by heating the film above the isotropic transition point of the liquid crystal impregnant. Actually, different colors are observed within a 6° range of the transition point (table 2). The initial green is much lighter than the green noted in the sequence of colors near the transition point.

The liquid crystal-impregnated films are essentially acting as birefringent retarders when viewed through a polariscope. A smear on glass appears as a bright yellow white field. Impregnated polypropylene films give different colors depending on whether the liquid crystal is in a mesophase or an isotropic phase. It should be emphasized that the polypropylene itself is birefringent. The same color effects noted in raising the temperature of the impregnated films were also noted in the chemical detection aspects irrespective of the organic vapor tested. Undoubtedly the effect of the organic vapor absorption is to lower the isotropic transition to the test temperature (in most cases, the ambient one). Colors are observed when the unimpregnated film is rotated between crossed polars. Furthermore, droplets of any of the twenty-five organic liquid tests (including liquid crystals in the isotropic state) give the same color against a particular background color of the unimpregnated film, e.g., orange against green. Liquid crystals in a mesomorphic state show a different color than the isotropic liquids. The observed difference was utilized in the design of the organic vapor detector.

Of the nematics examined, the most sensitive detector was MBBA. This was also the one with the lowest isotropic transition temperature. Nematics with high isotropic transition temperatures were much less sensitive. In other words, more organic vapor needs to be absorbed in order to effect a transition from mesophase to isotropic liquid.

Table 1 Concentrations of Organic Vapors Effecting a Visually Observable Change of Liquid Crystal Films[a]

Organic vapor	Concentration
	ppm[b]
MBBA[c]	
Trimethylphosphate	1
α-Picoline	3
Pyridine	5
Dioxane	10
Tetrahydrofuran	15
Nitromethane	20
Acetonitrile	25
Ethyl acetate	40
Isopropanol	45
Methanol	50
Diethylamine	50
Chloroform	50
Acetone	60
Petroleum ether (b.p. 30-60°C)	270
50% MBBA + 50% EBBA[c]	
Trimethylphosphate	<3
Acetic acid	7
α-Picoline	10
Pyridine	19
Tetrahydrofuran	24
Dioxane	37
Nitromethane	70
Acetonitrile	110
Chloroform	190
Methanol	230
Carbon tetrachloride	250
Methylene chloride	400
EBBA[d]	
Tetrahydrofuran	6
α-Picoline	7
Pyridine	15
Dioxane	35
Nitromethane	40
Acetonitrile	52
Diethylamine	77
Acetone	110
Methylene chloride	240
Carbon tetrachloride	290
Petroleum ether (b.p. 30-60°C)	1200

a Tests performed at room temperature (approximately 27°C) The films were viewed using a hand polariscope.

b Weight volume.

c Nematic liquid crystal. Impregnated on Celgard 2400 microporous polypropylene film Color change from green to orange with several colors in between.

d Smectic mesophase. Impregnated on Celgard 2400 microporous polypropylene film. Color change from red to orange with several colors in between.

Table 2. Effect of Temperature on Observed Colors of Liquid Crystal Films[a]

Liquid crystal	Temperature	Colors
	°C	
MEBA	20-34	Green
	34-37	Red
	37-39	Green
	39-40	Purple
	>40	Orange
EBBA	20-72	Green
	72-74	Red
	74-76	Green
	76-78	Purple
	>78	Orange

a Celgard 2400 impregnated with the liquid crystal, supercooling effect noted with EBBA; colors viewed through a polariscope during the heating of the films. The same colors are observed when the films are cooled.

b This figure corresponds to the isotropic transition temperature.

In comparison to the other detectors listed in table 1, the MBBP was found least attractive. The detection sensitivity is low and the observed colors are not bright. The poor response does not appear totally related to the isotropic transition temperature. The pyridine derivative is smectic at room temperature and goes through other phase changes (including a nematic one) before reaching the isotropic state.

It is apparent on examining table 1 that the detection is nonspecific. There is no particular correlation evident between detectable concentration and properties of the organics other than that the more polar materials are more easily detected. Neither water vapor nor water droplets affect the liquid crystal-impregnated detector films.

The detection effects shown in table 1 are relatively insensitive to fluctuations in room temperature since the isotropic transition of the liquid crystals examined lie well above room temperature. Also, the effects are reversible, i.e., removal of the films from the organic vapor atmosphere restores the original color.

The polypropylene detector films are visually clear and do not feel wet or "greasy" to the touch. It is recommended that the films be used within a day of being prepared because of the possibility of their absorbing nonvolatile compounds or chemically reactive ones over a period of time. The benzylidene aniline derivatives are not especially stable since the C=N- group is a particularly labile one.

The major advantage of the detection technique reported in this publication over the one utilizing optical reflection from cholesteric liquid crystals is simplicity. Uniformly thin films are easily prepared and handled. Temperature control is relatively unimportant. Instrumental monitoring is not required but could be adapted easily if an application deems it. A hand polariscope with an electric light source was used but natural light could serve as well. In contrast optimum utilization of techniques based on optical reflection from cholesteric liquid crystals requires instruments such as a temperature regulator, incident light source and photocell as well as electronic output. Achievement of detection by visual observation is complicated since the observed color depends on the angle of viewing. This is not as critical with the nematogen-polypropylene film.

VI. CONSIDERATIONS FOR FUTURE WORK.

Current technology would allow the development of simple liquid crystal devices for the detection of organic chemical vapors in the parts-per-million concentration range. The detection would not require instrumental monitoring; it would be nonspecific, reversible and temperature insensitive.

Higher sensitivity (while retaining nonspecificity and reversibility) can be obtained with the microporous polypropylene films impregnated with liquid crystals by:

(a) Operating at temperatures closer to the isotropic transition temperatures.

(b) Operating at room temperature but choosing a liquid crystal system with a lower isotropic transition temperature, or

(c) Using the detection signal a color change which occurs prior to the formation of an isotropic phase.

Each of the above possibilities requires closer control on temperature and more careful monitoring. The sensitivity can be bettered by at least one order of magnitude (depending on the material detected and the choice of liquid crystal detector) if the first color change is used as the detection signal. This is illustrated with several examples in table 3.

A combination of increased sensitivity, selectivity and nonreversibility can be achieved if:

(a) The liquid crystal reacts with the material to be detected, or

(b) The liquid crystal system is combined with a chemical which reacts with the material to be detected.

Examples of this effect have been reported.[28,41]

Table 3. Color Changes of Liquid Crystal Films Exposed to Various Concentrations of Organic Vapors[a]

Concentration[b]	Color
ppm	
Liquid crystal: 70% MBBA	
Organic vapor: tetrahydrofuran	
<1.0	Green
1.5	Red
3.0	Orange
4.5	Green
6.0	Blue
7.5	Violet
>15	Orange
Liquid crystal: 70% MBBA + 30% EBBA	
Organic vapor: acetonitrile	
<35	Green
55	Blue
70	Red
80	Orange
90	Green
95	Blue
100	Violet
>110	Orange

a Celgard 2400 microporous polypropylene films impregnated with the liquid crystal, exposed to organic vapor and examined between crossed polars of a polariscope.

c Weight/volume.

Liquid crystals such as MBBA and EBBA are not very stable. Future work should utilize room temperature nematics such as reported by Gray.[45]

LITERATURE CITED

1. Porter, R. S., and Johnson, J. F. Liquid Crystals and Ordered Fluids. Plenum Press, New York, NY 10011 (1970).

2. Brown, G. H., and Shaw W. G. Chem. Rev. *57*, 1049 (1957).

3. Fergason, J. L. Sci. Am., *211* (2), 76 (August 1964).

4. Heilmeier, G. H. ibid, *222* (4), 100 (April 1970).

5. Reinitzer, F. Wiener Monatschr. Chem., *9*,421 (1888).

6. Lehmann, O. Z. Phys. Chem. *4*, 462 (1889).

7. Woodmonsee, W. E. Mater. Eval. 564 (October 1966).

8. Fergason, J. L. Appl. Opt. *9*, 1729 (1968).

9. Klein, E. J. Astronaut. & Aeronaut., 70 (July 1968).

10. Selawry, O., Holland, J., and Selawry, H. Mol. Cryst., *1*, 445 (1966).

11. Brown, S. P. Mat. Eval. 163 (August 1968).

12. Fergason, J. L., and Lauriente, M. Electron. Des., *15*, 71 (1967).

13. Heilmeier, G. H., Zanoni, L. A., and Barton, L. A. Proc. IEEE, *56*, 1162 (1968).

14. Soref, R. A. Applied Optics, *9*, 1323 (1970).

15. Heilmeier, G. H., and Goldmacher, J. E. Proc. IEEE *57*, 34 (1969).

16. Fergason, J. L., and Brown, G. H. J. Am. Oil Chem Soc. *45*, (3) 120 (1969).

17. Robinson, C., Mol. Cryst. *1*, 666 (1966).

18. Steward, G. T. Adv. in Chem. *63*, 141 (1967).

19. Van Meter, J. P. Eastman Org. Chem. Bull., *45* No. 1, 1973.

20. Brown, G. H. Anal. Chem. *41* (13), 27A (November 1973).

21. Petrie, S. E. B., Biicher, H. K., Klingbiel, R. T., and Rose, P. I. Eastman Org. Chem. Bull., *45*, No. 2 (1973).

22. Novak, T. J., Poziomek, E. J., and Mackay, R. A. Rev Sci. Instrum., *42*, 124 (1971).

23. Poziomek, E. J., Novak, T. J., and Mackay, R. A. Mol. Cryst. Liq. Cryst. *15*, 283 (1972).

24. Novak, T. J., Poziomek, E. J., and Mackay, R. A. Ibid, *20*, 203 (1973).

25. Barrall, E., Porter, R., and Johnson, J. J. Phys. Chem. *71*, 1224 (1967).

26. Baessler, H., and Labes, M. M. J. Chem. Phys. *52*, 631 (1970).

27. Novak, T. J., Mackay, R. A., and Poziomek, E. J. Mol. Cryst. Liq. Cryst. *20*, 213 (1973).

28. Fergason, J. L., Goldberg, N. N., and Jones, C. H. Detection of Gases by Use of Liquid Crystals. Technical Report No. RADC-TR 64-569, US Department of Commerce, August 1965.

29. Toliver, W. H., Roach, C. G., Roundy, R. W., and Hoffman P. E. Aerosp. Med. *40*, 35 (1969).

30. Toliver, W. H., Fergason, J. L., Sharpless, E., and Hoffman, P. E. ibid, *41*, 18 (1970).

31. Martire, D. E., Blasco, P. A., Carone, P. F., Chow, L. C., and Vicini, H. J. Phys. Chem., *72* 3489 (1968).

32. Chow, L. C., and Martire, D. E. J. Phys. Chem., *73*, 1127 (1969).

33. Schnur, J. M., and Martire, D. E. Anal. Chem. *43*, 1201 (1971).

34. Chow L. C., and Martire, D. E. J. Phys. Chem., *75*, 2005 (1971).

35. Chow L. C., and Martire, D. E. Mol. Cryst. Liq. Cryst. *14*, 293 (1971).

36. Peterson, H. T., and Martire, D. E. Mol. Cryst. Liq. Cryst. *25*, 89 (1974).

37. Lephardt, J. O., and Bulkin, B. J. Anal. Chem. *45*, 706 (1973).

38. Baessler, H., and Labes, M. M. J. Chem. Phys. *51*, 1846 (1969).

39. Baessler, H., Laronge, M. T., and Labes, M. M. ibid, 3213 (1969).

40. Hillenbrand, L. J., Jr., Lugash, M. N., Poziomek, E. J., and Kramer, D. N. Microchem. J. *7*, 78 (1963).

41. Novak, T. J., Poziomek, E. J., and Mackay, R. A. Anal. Lett. *5*, 187 (1972).

42. Kelker, H., and Scheurle, B. Angew. Chem. Internat. Ed. Engl. *8*, 884 (1969).

43. Flannery, J. B., Jr., and Hass, E. J. Phys. Chem., *74*, 3611 (1969).

44. Champa, R. A., Mol. Cryst. Liq. Cryst., *16*, 175 (1972).

45. Gray, G. W., Harrison, K. J., and Nash, J. A. 166th National Meeting, American Chemical Society, Chicago 1973. Abstract COLL 142.

MICROWAVE-INDUCED EMISSION SPECTROSCOPY: A NEW ANALYTICAL TOOL FOR ULTRATRACE ELEMENT DETERMINATION OF INDUSTRIAL, CLINICAL AND ENVIRONMENTAL INTEREST

by

G. W. Wooten

ABSTRACT

A laboratory model microwave-induced emission spectrometer system has been developed and fabricated which will extend ultratrace element analysis technology. This instrument, which employs low wattage microwave-induced gas discharges to excite atomic and diatomic emission, exhibits a high degree of specificity and sensitivity for metallic and nonmetallic elements in organic or inorganic substances, in any physical state, and in a variety of matrices of industrial, clinical, and/or environmental concern. Trace metals have been analyzed in matrices ranging from river waters to blood and other biologicals, and food products. No pretreatment or concentration steps are required for most analyses. A sensitivity approaching 10^{-14} gram has been achieved for elemental mercury while working limits in the order of 10^{-12} - 10^{-13} gram are obtained routinely for many metals with good reproducibility. Pesticide and similar analyses can be performed by employing this instrument as a selective and highly sensitive gas chromatographic detector. Performance studies conducted thus far indicate that the sensitivity obtained with the microwave-induced emission instrument meets or exceeds the absolute detection limits afforded by the most sensitive atomic spectrometric procedures available today.

Figures 1-23, which follow, reveal considerable information about the structure and possible uses of this spectrometer system.

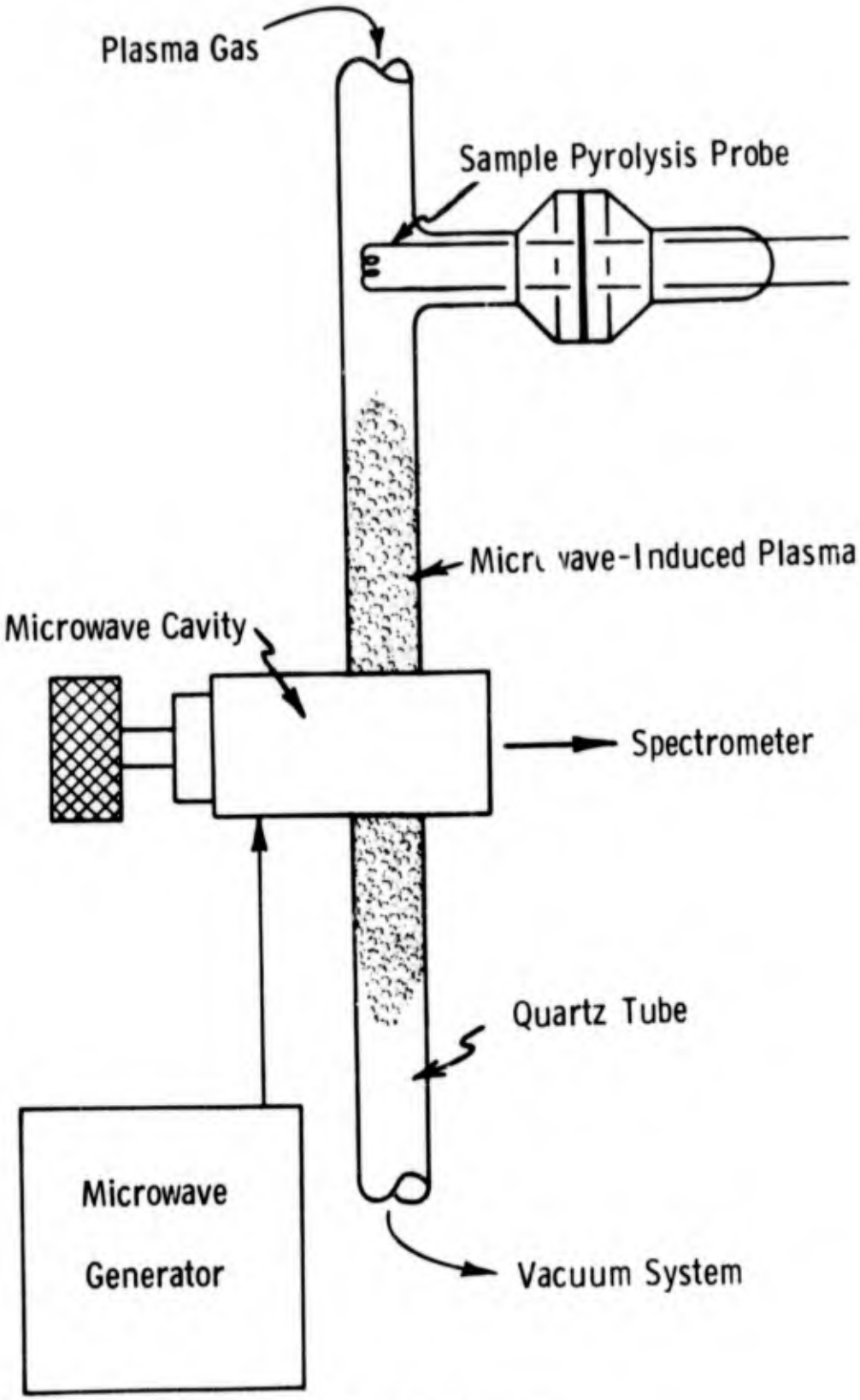

Figure 1. Schematics

- High Electron-To-Gas Temperatures Ratios Are Attained
- Microwave Discharge Can Be Generated At Pressures Ranging From Below One Torr To Above Atmospheric
- Compound Formation, Chemiluminescence and Other Processes Associated With Flame Excitation Are Not Observed
- Low Pressure Operation Results In A Substantial Decrease In Collisional Deactivation Of Excited States
- Emitted Radiation Is Comparatively Free From Self-Reversal Effects
- Discharge Fluid Can Range From Inert To Highly Reactive Gases

Figure 2. Summary of Properties

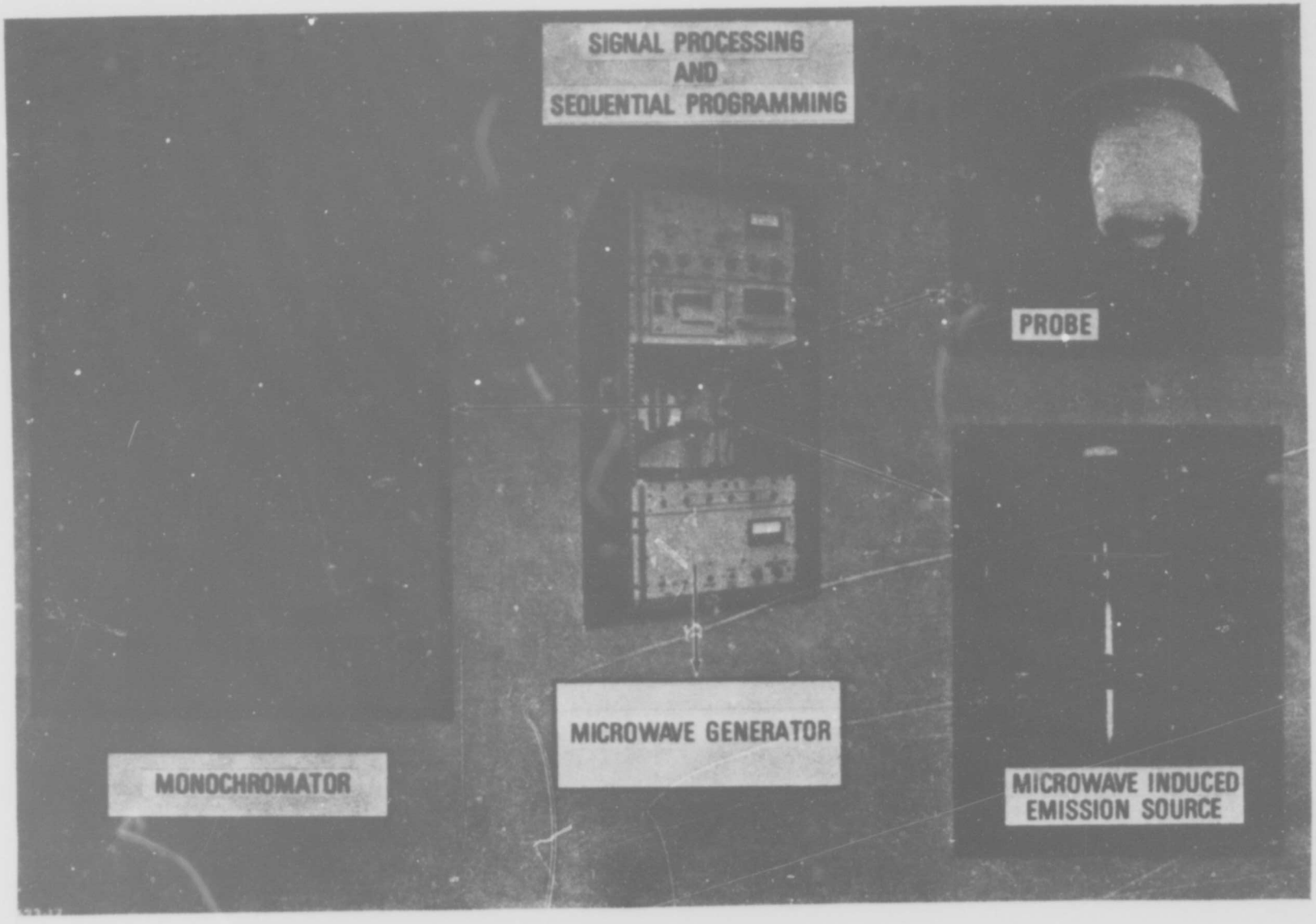

Figure 3. Explanatory Photos

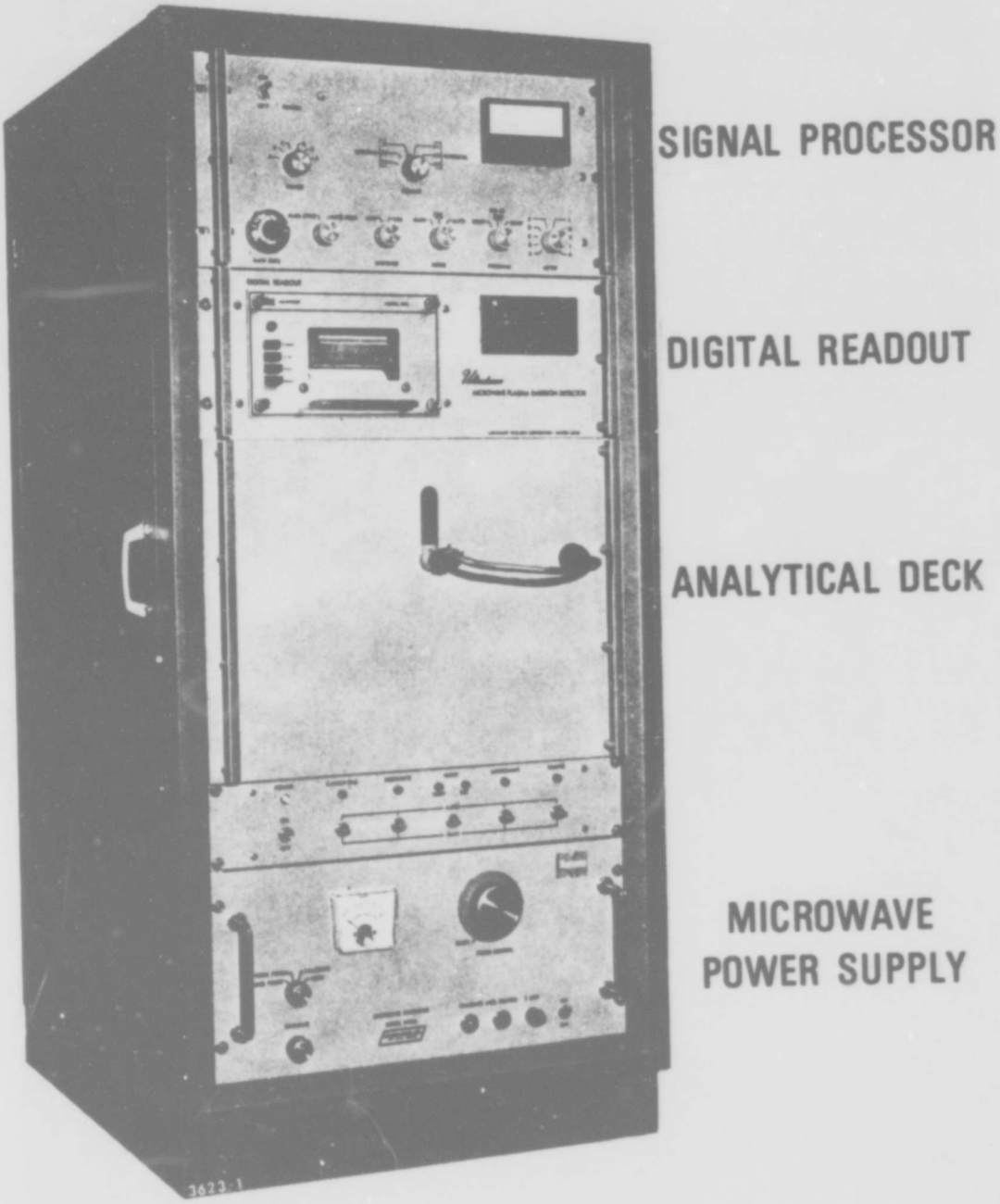

Figure 4. "Ultratrace" Microwave-Induced Emission Spectrometer

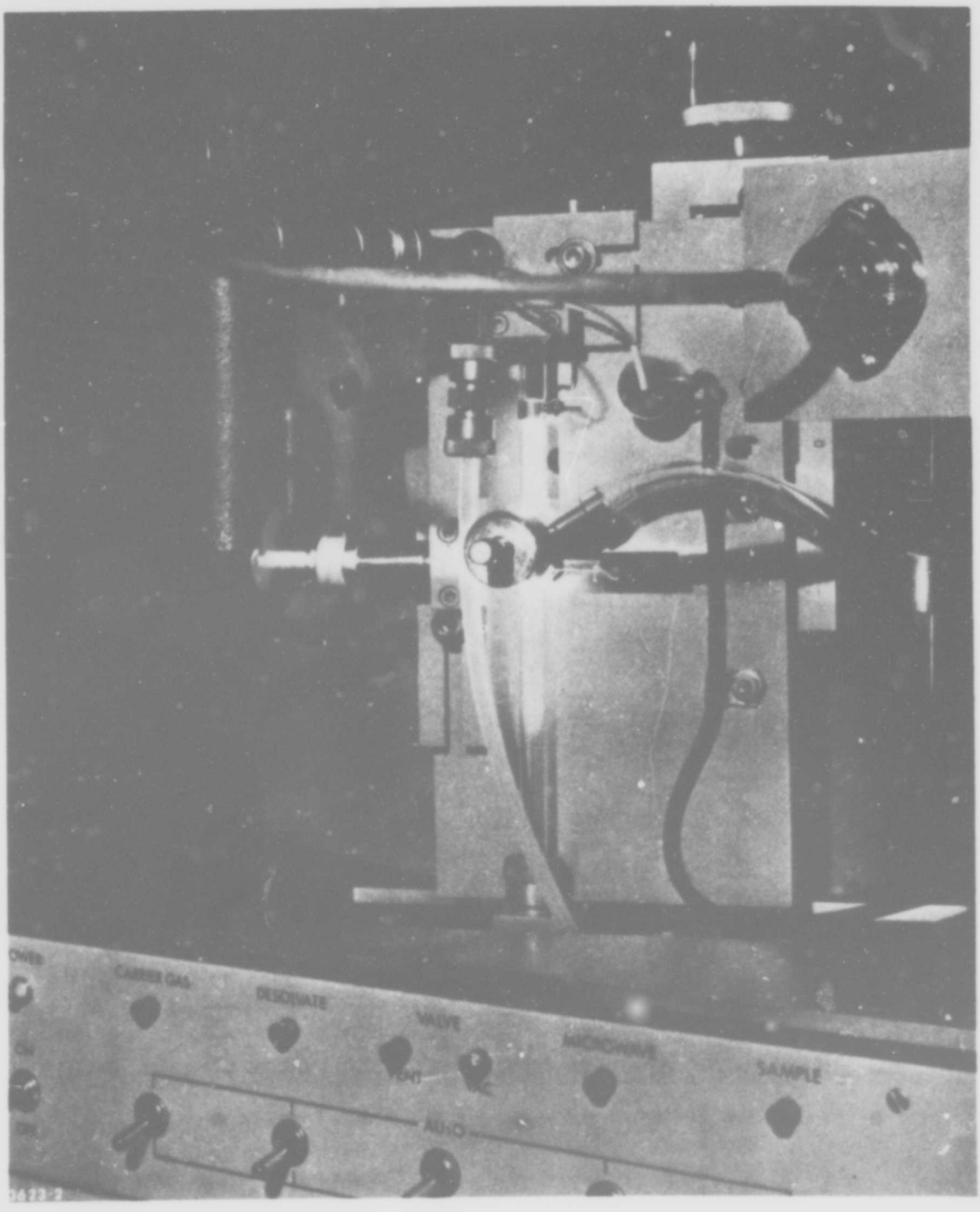

Figure 5. Microwave Plasma Excitation Assembly

- Probe Desolvation Heating Interval
- Carrier Gas Flow
- Sample System Vent and Vacuum Control
- Microwave Generator Output
- Sample Injection from the Probe
- Automatic Baseline Corrector
- Amplifier Integrator Operations
- Digital Panel Meter Readout
- Digital Printer (including the chart meter control)
- Total Cycle Time

Figure 6. Functions Controlled by Program

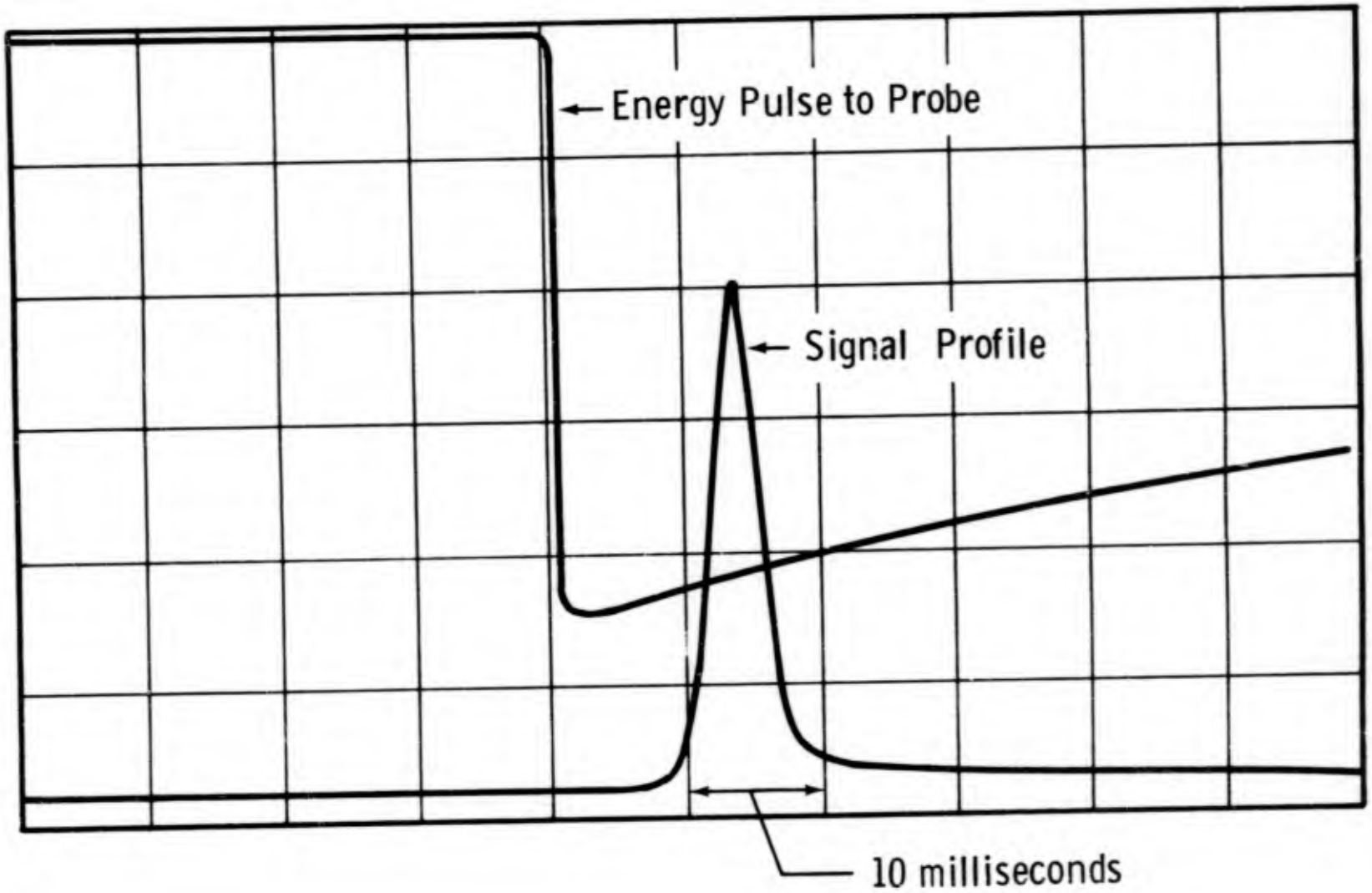

Figure 7. Pulsed Probe Format

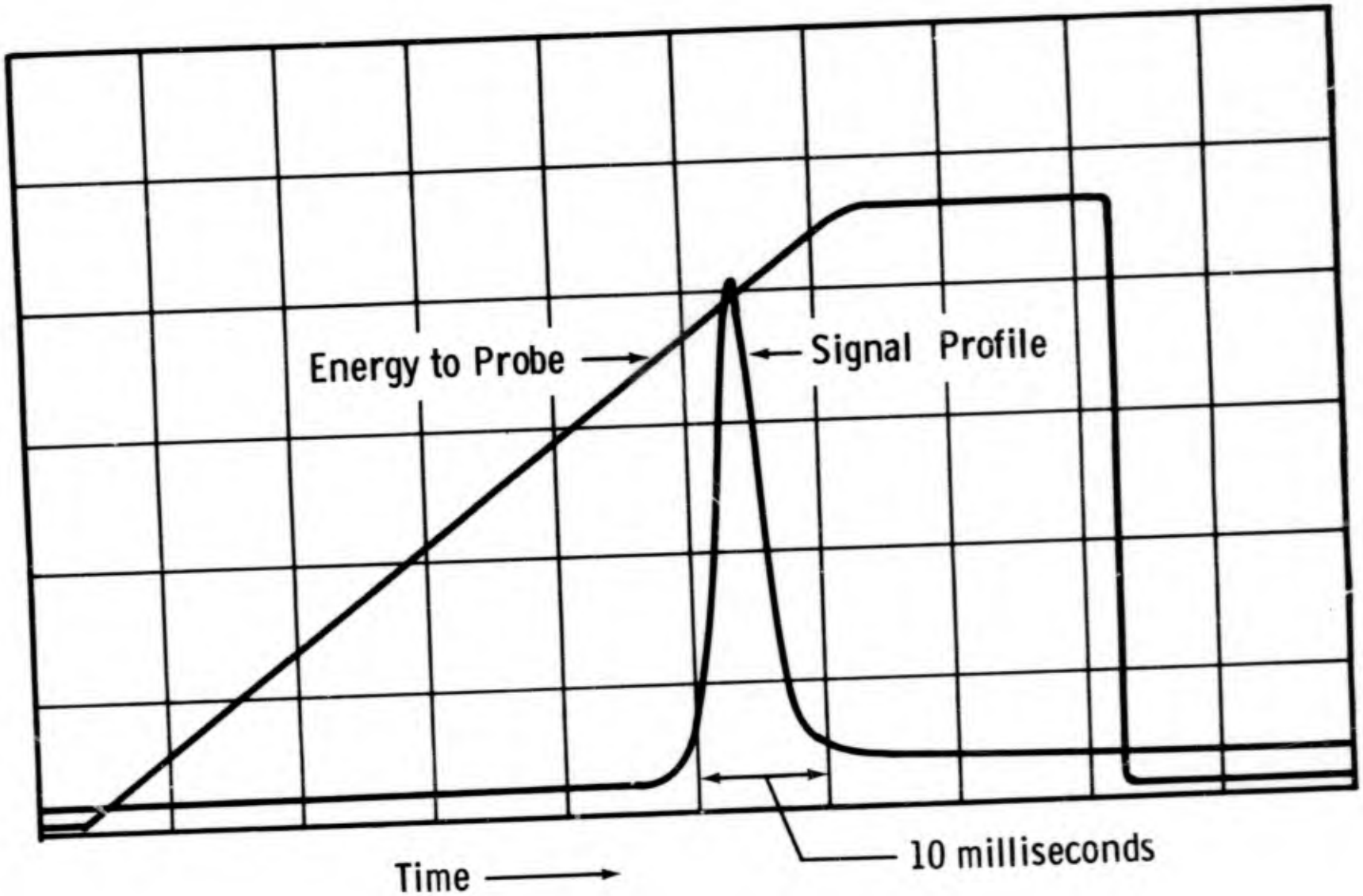

Figure 8. Temperature Programmed Probe Format

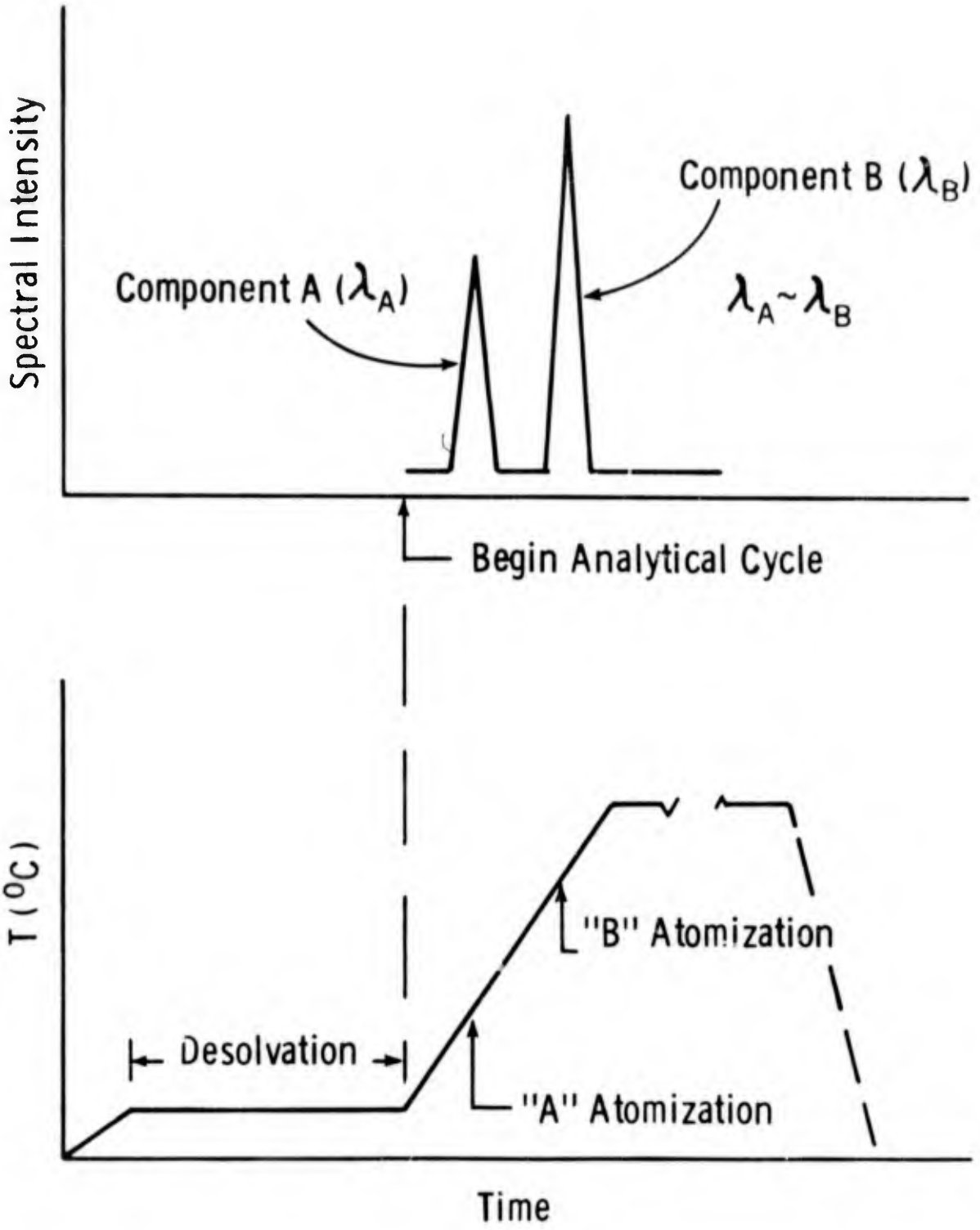

Figure 9. Probe Temperature Program

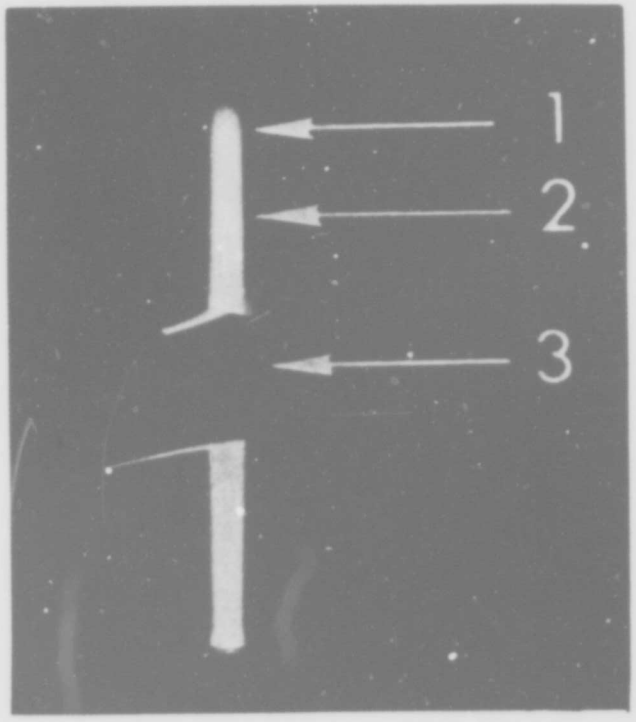

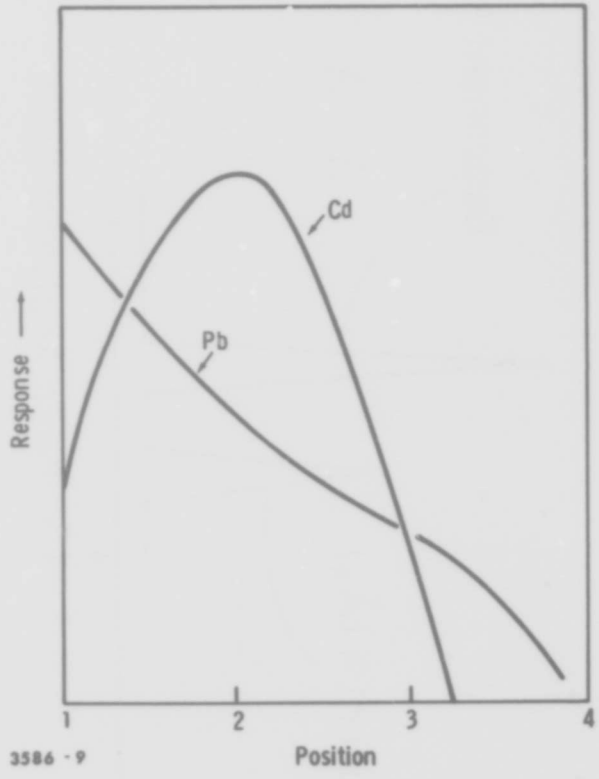

Figure 10. Instrument Response – Plasma Position Relationship

- Discharge Tube - 6mm O.D. X 5mm I.D. Spectrosil Quartz
- Discharge Gas - Helium
- Microwave Power - 50 watts forward
  0 watts reverse
- Gas Flow Rate - 250cc/minute
- System Pressure - 4-5 torr
- Pyrolysis Probe - 10 mil Tantalum Filament
  Capacitive Discharge Firing Mode –
  Sustained Probe Format
  Charging Rate - 7 volts at 5.6 amps
- Sample Size - 5 ul
- Discharge Zone Observed - Leading Edge of Discharge
- Data Acquisition - Spectral Mode

Figure 11. Instrument Operating Parameter

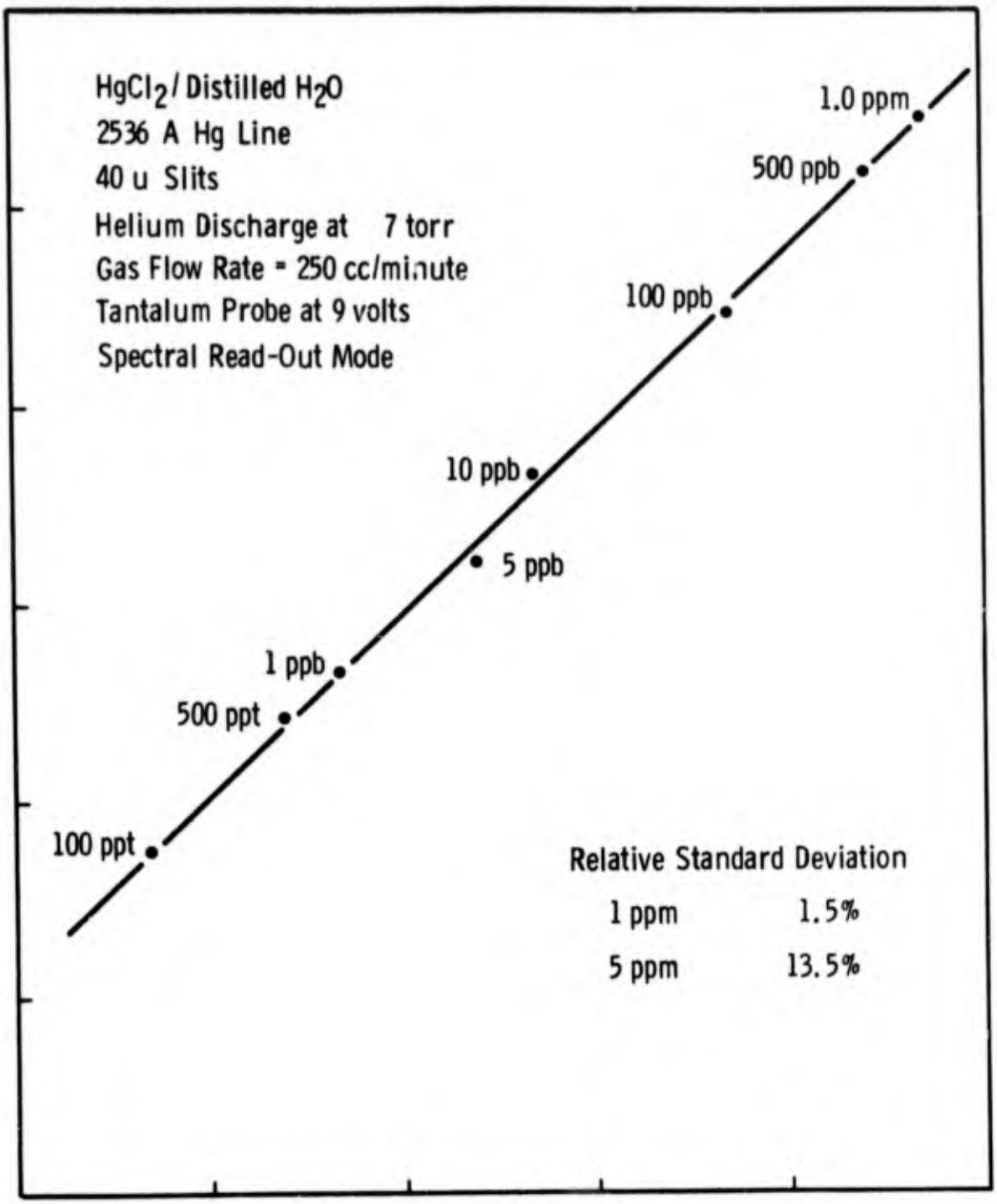

Figure 12. Instrument Performance

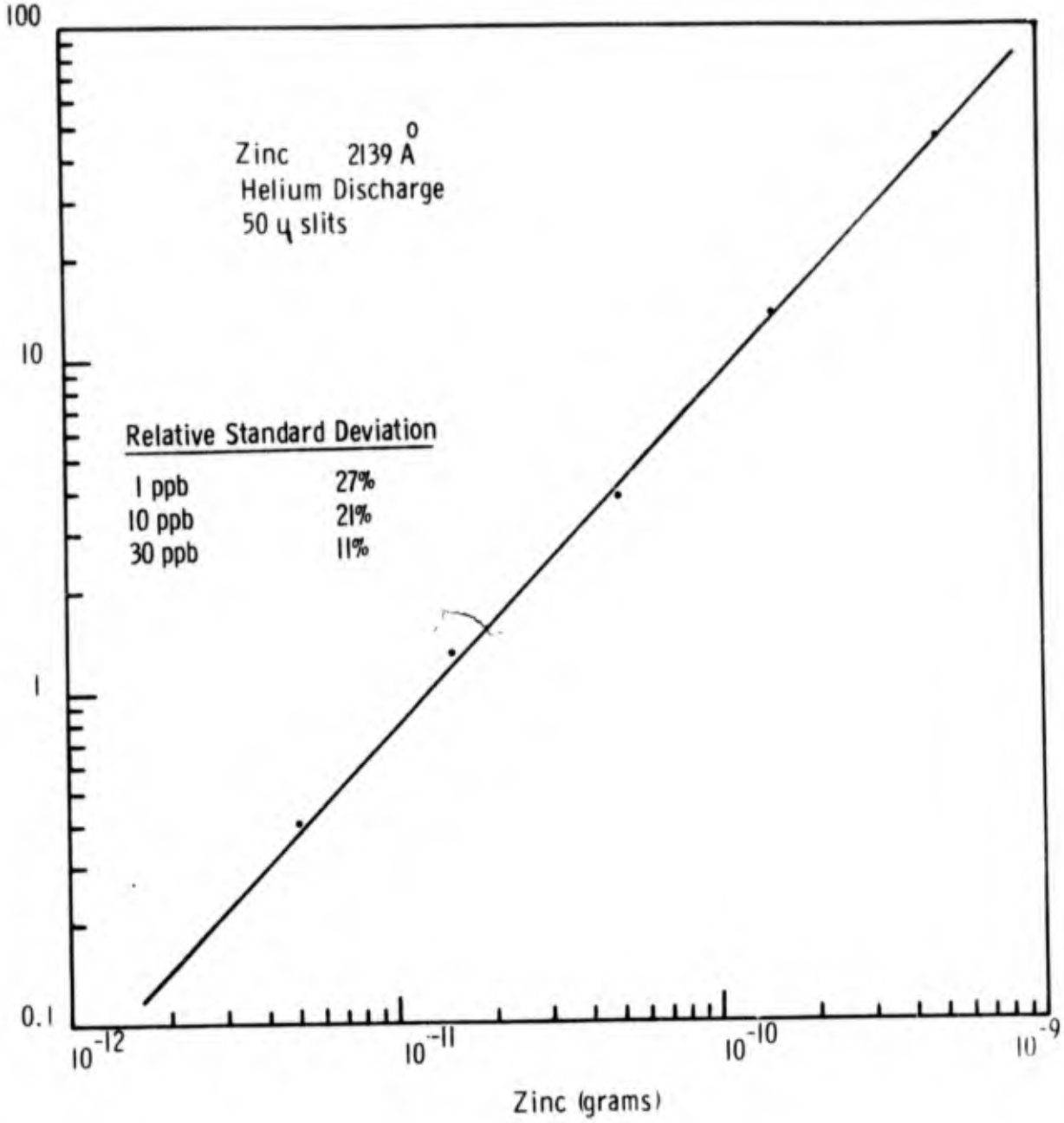

Figure 13. Instrument Response to Zinc

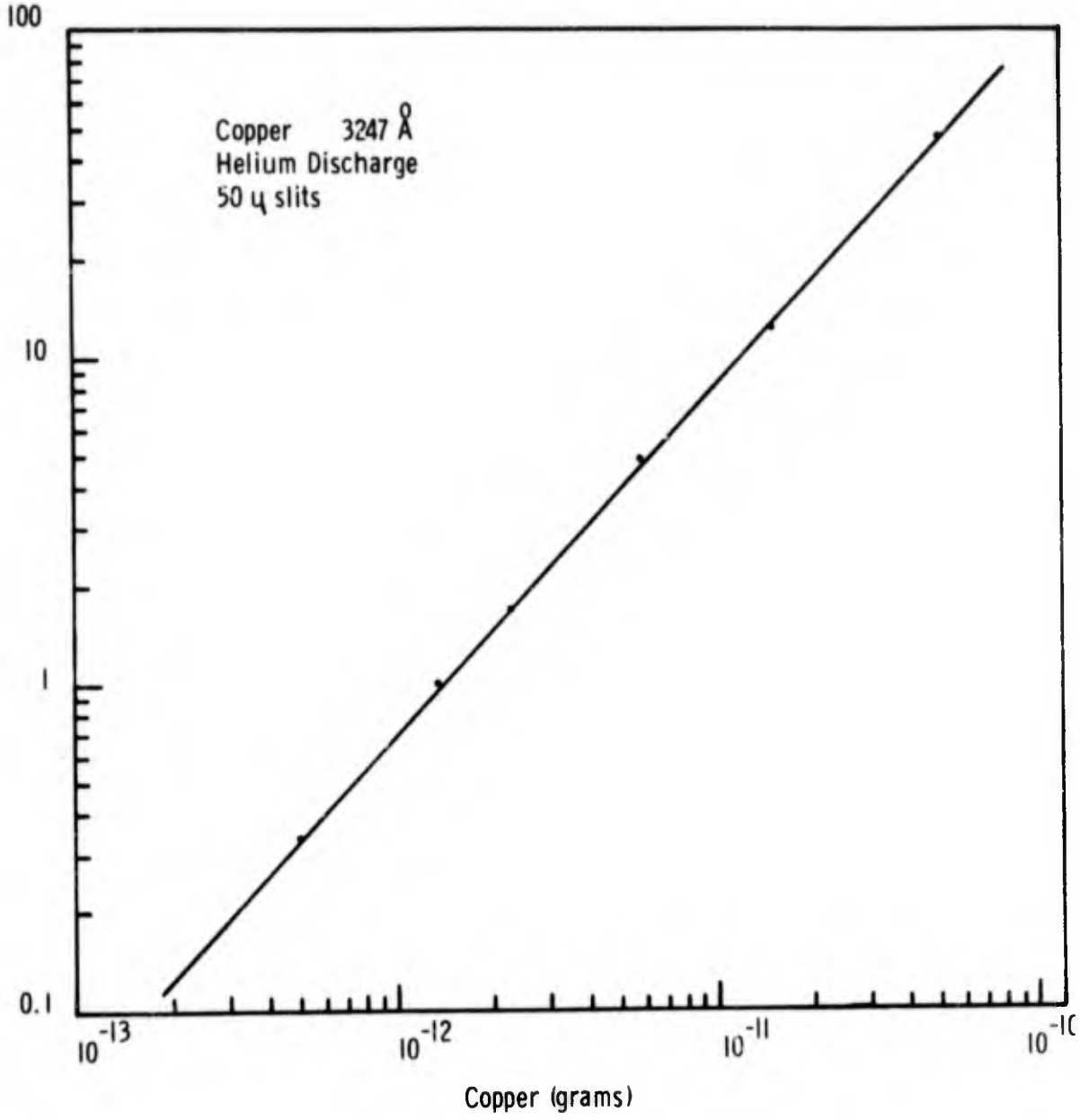

Figure 14. Instrument Response to Copper

Element	Ultratrace (1) (grams)	Microwave-Induced Plasma (2) (grams)	Inductively-Coupled Plasma (3) (grams)	Flameless Atomic Absorption (4) (grams)
As	1×10^{-11}	------	8×10^{-8}	6×10^{-10}
Cd	1×10^{-13}	3×10^{-12}	4×10^{-10}	7×10^{-12}
Zn	2×10^{-12}	9×10^{-12}	4×10^{-9}	4×10^{-12}
Pb	2×10^{-11}	4×10^{-12}	2×10^{-9}	3×10^{-11}
Fe	1×10^{-11}	------	1×10^{-9}	2×10^{-10}
Co	4×10^{-11}	------	6×10^{-10}	7×10^{-11}
Mg	3×10^{-12}	5×10^{-13}	2×10^{-10}	------
Mn	2×10^{-12}	------	2×10^{-10}	2×10^{-11}
Cu	1×10^{-13}	2×10^{-12}	2×10^{-10}	2×10^{-11}
Hg	5×10^{-13}	6×10^{-12}	4×10^{-8}	2×10^{-9}

(1) Monsanto Research Corporation – Microwave-Induced Emission Spectrometer
(2) L.R. Layman & G.M. Hieftje, Anal. Chem. Vol. 47, 194 (1975)
(3) V.A. Fassel & R.N. Kniseley, Anal. Chem. Vol. 46, 1110 (1974)
(4) Averaged values from a number of sources

Figure 15. Sensitivity Comparisons of Atomic Spectrometric Techniques

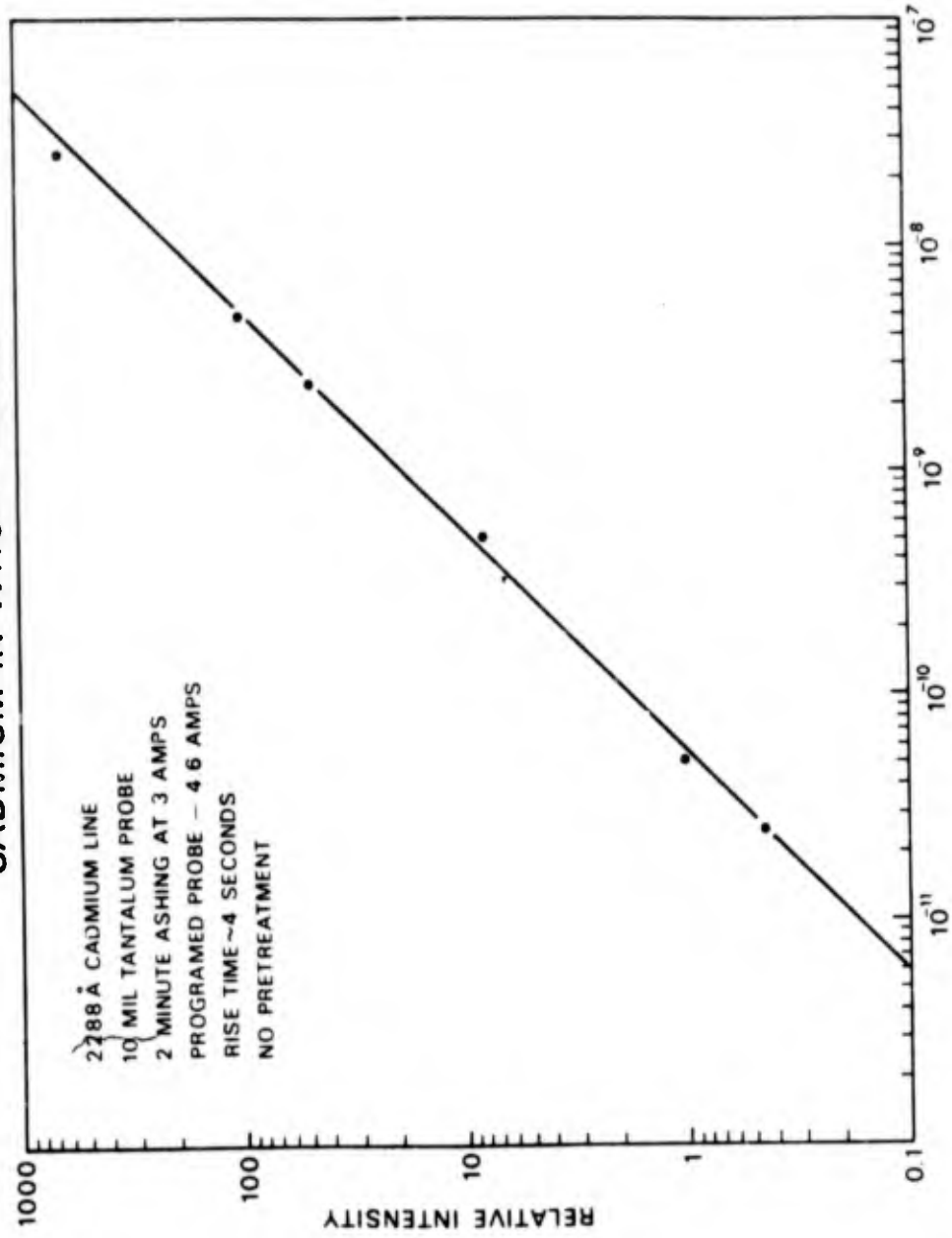

Figure 16. Cadmium in Whole Blood

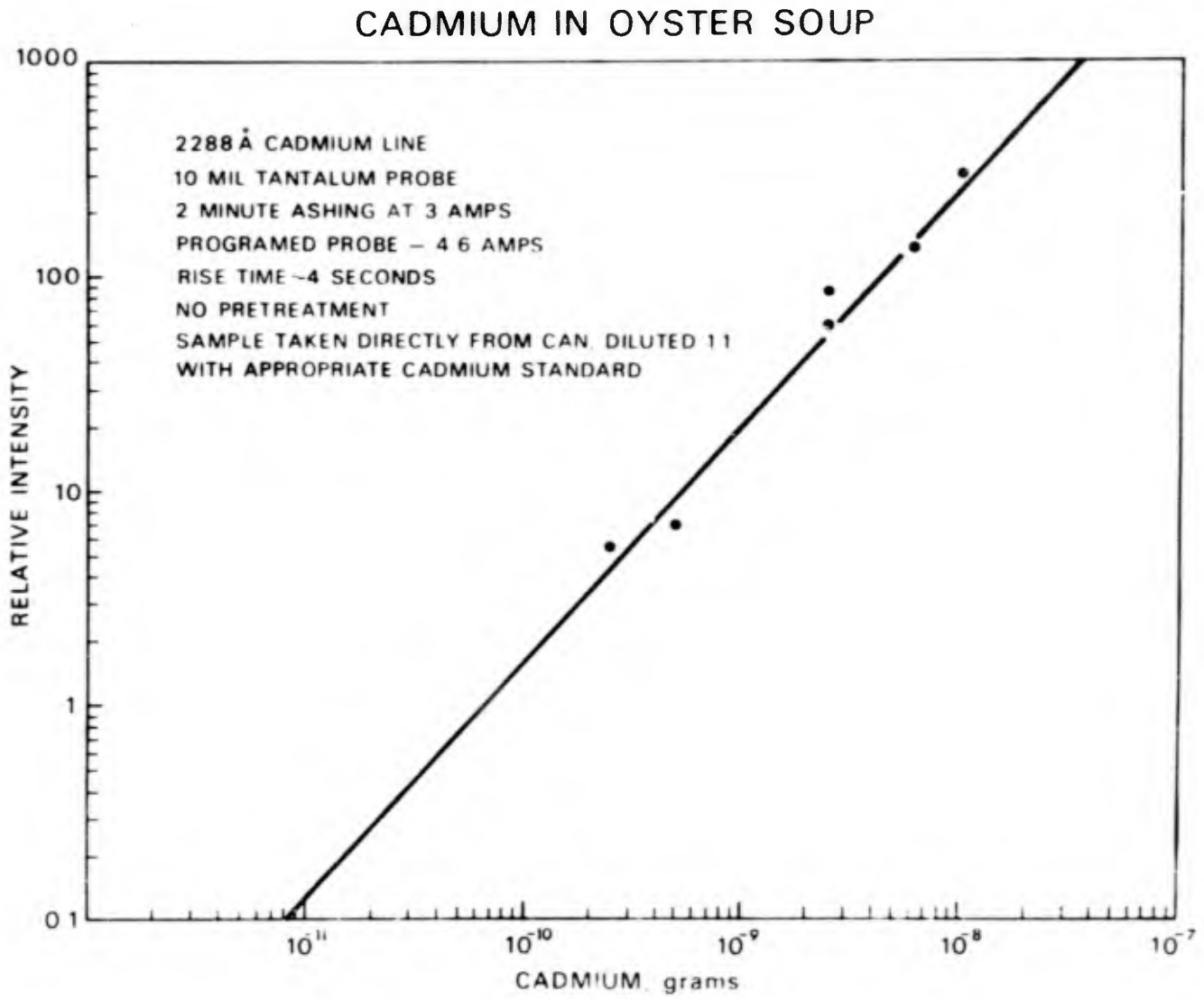

Figure 17. Cadmium in Oyster Soup

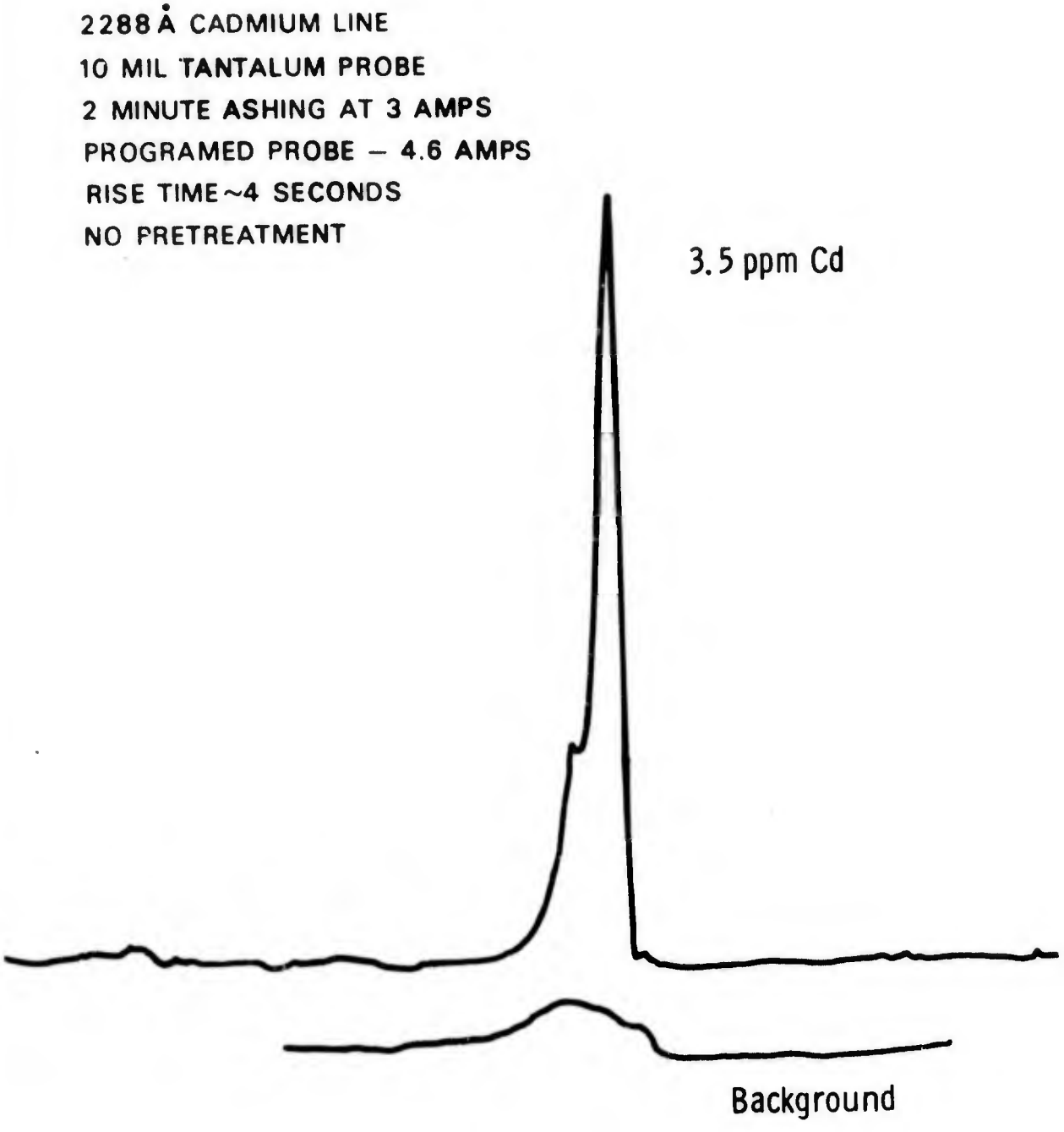

Figure 18. Cadmium in Oyster Tissue

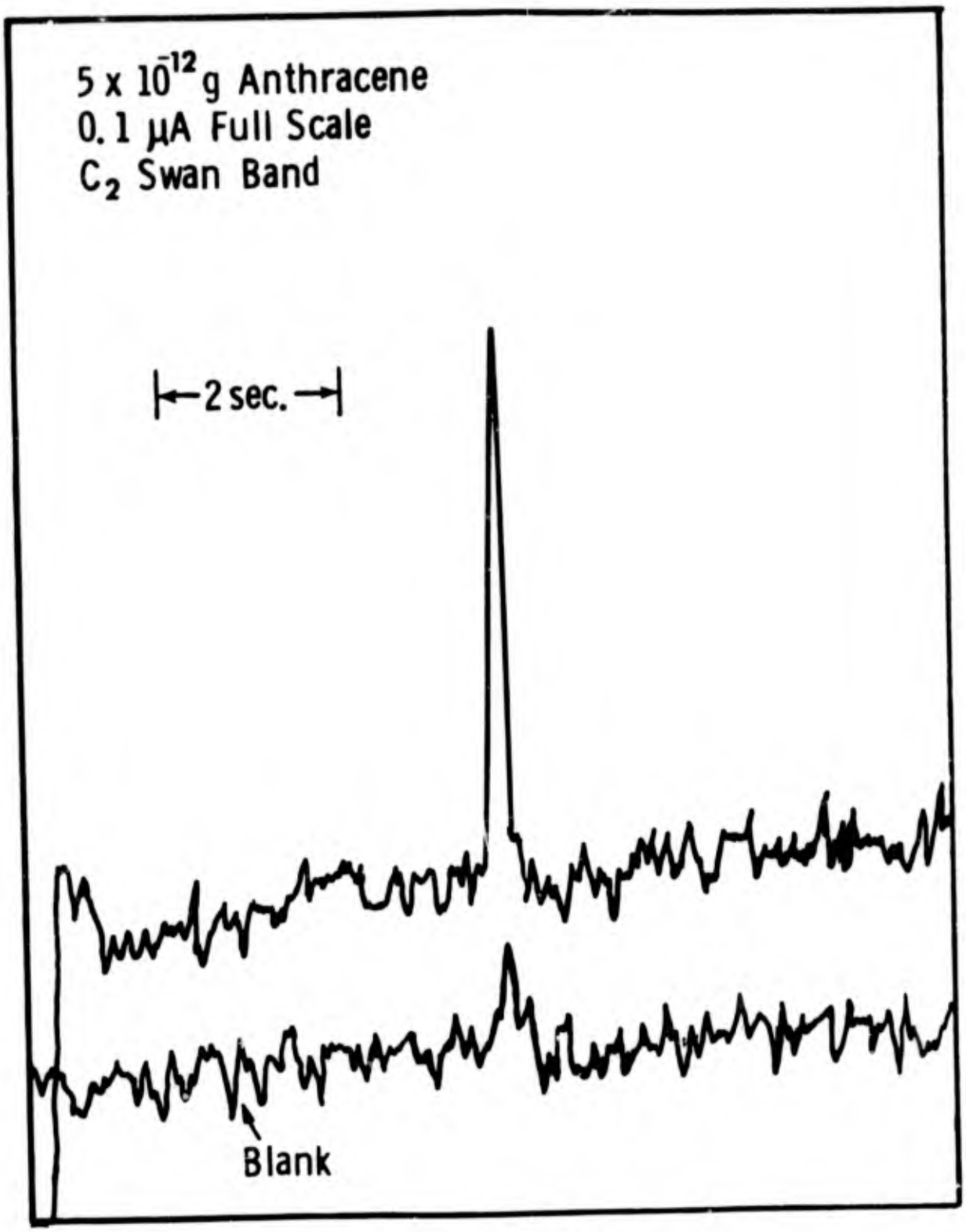

Figure 19. Detection of Anthracene

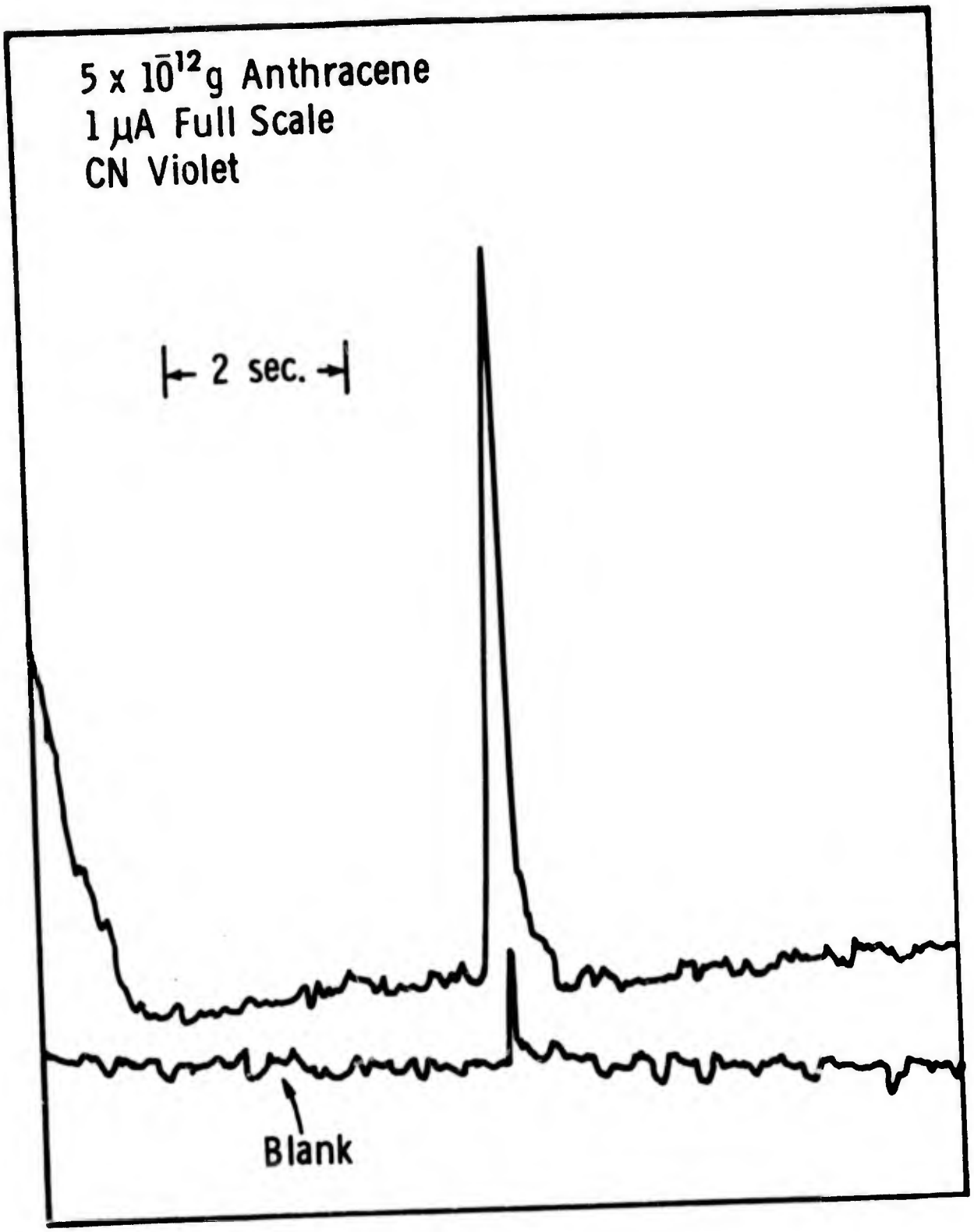

Figure 20. Anthracene, but Use of More Current

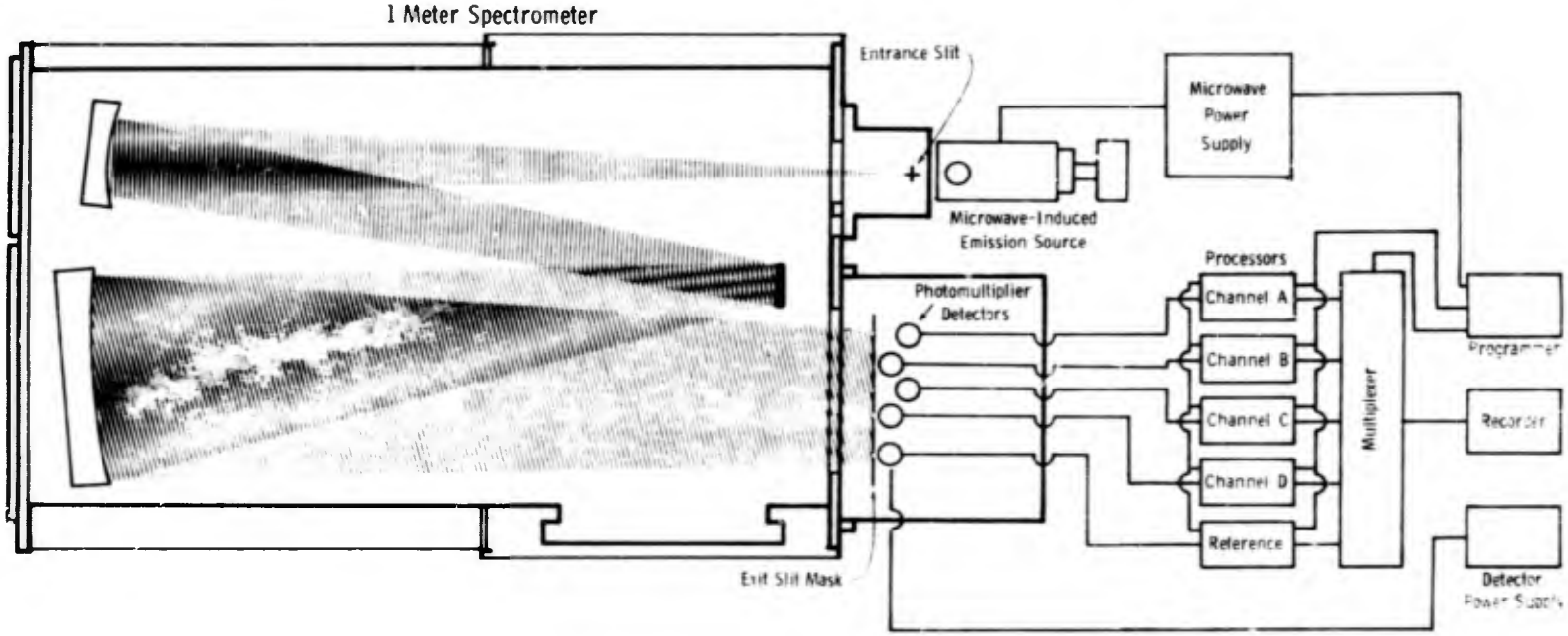

Figure 21. Multi-Channel Microwave-Induced Emission Spectrometer

REVERSE TRANSCRIPTASE FROM AVIAN MYELOBLASTOSIS VIRUS: A ZINC METALLOENZYME

D. S. Auld,* H. Kawaguchi,* D. M. Livingston† and B. L. Vallee*††

*The Biophysics Research Laboratory, Department of Biological Chemistry, Harvard Medical School, Division of Medical Biology, Peter Bent Brigham Hospital, Boston, Massachusetts and the Viral Lymphoma and Leukemia Branch, National Cancer Institute, National Institute of Health, Bethesda, Maryland, 20014

Received March 4,1974

Previous postulates of a relationship between a zinc enzyme and the leukemic process (1,2) have led to the identification of the RNA dependent DNA polymerase -- reverse transcriptase -- of avian myeloblastosis virus as a zinc metalloenzyme. Microwave induced emission spectrometry provides a microanalytical system capable of measuring precisely 10^{-11} to 10^{-14} g atoms of metal in microgram amounts of enzyme, orders of magnitude more sensitive than other, conventional methods. The chromatographic fraction with highest enzymatic activity contains 1.5×10^{-11} g atoms of zinc per 1.4 µg of protein, corresponding to 1.7 to 1.9 g atoms of zinc per mole of enzyme for a molecular weight previously determined either as 1.6 or 1.8×10^5. The Zn/activity ratio is constant in the active fractions. Copper, iron and manganese are absent, i.e., at or below their limits of detection, 10^{-13} to 10^{-14} g atoms. Agents known to chelate zinc inhibit the enzyme while their nonchelating isomers do not. The data underline the participation of zinc in nucleic acid metabolism and bear importantly upon the lesions which accompany leukemia and zinc deficiency.

Figure 22. Reprint of a Paper

- High sensitivity
- Little sample preparation
- No sample memory effects
- Utilizes small samples
- Multi-element capability
- Non-metal capability

Figure 23 Summary of Ultratrace

SIMULTANEOUS DETERMINATION OF ZINC, LEAD AND CADMIUM ION CONCENTRATION IN CONTAMINATED SEA WATER USING DIRECT CURRENT POLAROGRAPHY

by

Joseph H. Klein and Steven Diamond, Midn 1/C
US Naval Academy, Annapolis Maryland 21402

SUMMARY

A need for a faster, more accurate method of identifying, and quantifying metal ions in contaminated sea water can be seen by the recent published literature. Polarography appears to be a natural method for this work since the high concentrations of sodium, calcium and magnesium salts which hinder other methods of analysis aid polarography. This paper presents a fast, accurate means of identifying and analyzing sea water for zinc, lead, and cadmium in sea water without prior concentration or treatment. The three ions, zinc, lead, and cadmium can be determined simultaneously and can be estimated at any level greater than one part per million

I. INTRODUCTION.

Examination of the Environmental Protection Data Base Publication MPS 2.4 and 3.2 shows a striking lack of reference to polarographic methods for water analysis. Only a very brief treatment of polarographic methods appears in Standard Methods for the Examination of Water and Waste Water, 13th ed., and no reference at all to the examination of sea water is included.

A thorough search of the literature since 1922, revealed only a few articles involving the examination of sea water or other highly saline waters by polarography. Whitnack* reported that seawater acted as an excellent supporting electrolyte and recommended that polarography be given more consideration as an analytical tool in oceanography.

Most of the work reported involved the trace analysis of metal ions in sea water after some means of concentration, and in general, worked in the area of 1 to 10 parts per billion concentration. No reference was found which used standard direct current polarography to examine sea water for gross metal ion concentration.

This report describes a method of analyzing contaminated seawater for Zn^{++}, Pb^{++}, and Cd^{++} ions at levels greater than 1 part per million without prior sample concentration.

* Whitnack, Gerald C. Applications of Cathode Ray Polarography in the Field of Polarography. Journal of the Electroanalytical Society, 2, 110 (1961).

II. EXPERIMENTAL.

A. Apparatus and Material.

Two standard direct current polarographs were used in this work: (1) Beckman Electroscan 30 and (2) Heath Kit EUA 19.-2. The dropping mercury electrode was Heath Built Model EUA 10-6. pH measurements were made with a Beckman Expandomatic pH meter. Supplies of clean fresh seawater were obtained from Wrightsville Beach, N.C., approximately 1 mile off shore and from Key West, Florida approximately 5 miles off the Eastern reef.

All reagents used were of analytical reagent grade or better.

B. Polarographic Traces of Clean Seawater.

In order to corroborate Whitnack's report that seawater served as a good supporting electrolyte and to observe the characteristics of the instruments and cells, several polarograms were produced of clean seawater. The polarogram of Key West seawater and of Wrightsville Beach seawater showed almost identical traces. The increase in diffusion current waves due to metal ion concentrations could be detected between 0.00 volts and -1.5 volts versus S.C.E.

These polarograms corroborate Whitnack's work. Seawater serves as a good supporting electrolyte for polarographic studies in seawater.

C. Determination of Cd+2 Ions in Seawater.

A standard Cd^{++} ion solution was prepared by dissolving 11.2 g (0.1 mole) of Cd metal 99.99% pure obtained from Electronic Space Products Inc. in 1 molar HCl and was diluted to one liter. This stock solution was then used to prepare solutions of known Cd^{++} concentration in fresh seawater. In general, no maxima suppressor was needed but for uniformity 3 drops of 2.0% triton X 100 were added to each 100 ml of sample. The samples of cadmium ion in seawater whose concentrations varied from 10^{-2} molar to 10^{-4} molar were then scanned polarographically from 0.00 to -1.0 volts versus S.C.E. A well-defined wave appeared at an E 1/2 voltage versus S.C.E. of -0.60 and the diffusion current was proportional to concentration (see table 1). All solutions were scanned at the pH of the seawater used. A plot of the data appears in figure 1.*

A second series of solutions was then prepared varying in Cd^{++} ion concentration from 10^{-4} molar to 10^{-5} molar. Again, well-defined polarographic waves were obtained and the diffusion current was proportional to the cadmium ion concentration. (See table 2 and figure 2).

The data shows that Cd^{++} ion concentrations in seawater can be accurately estimated at levels of 1 ppm or greater in seawater without prior sample treatment by direct current polarography.

D. Determination of Zn^{++} Ions in Seawater.

A standard Zn^{++} ion solution was prepared by dissolving 6.5 g (0.1 mole) of Zn metal 99.99% pure, obtained from Electronic Space Products, Inc. in 1 molar HCl and diluting to one liter. This stock solution was then used to prepare solutions of known Zn^{++} concentration in fresh

* The tables at the top of the figures are referred to by the same number as the figure on which they appear throughout this paper.

seawater. To each 100 ml of solution 3 drops of 2% triton X 100 were added. The samples of zinc ion in seawater whose concentrations varied from 10^{-2} to 10^{-5} molar were then scanned polarographically from 0.00 to -1.5 volts versus S.C.E. A well-defined wave appeared at an E 1/2 voltage of -0.96 volts versus S.C.E. The diffusion current for these waves was proportional to the zinc ion concentration. All solutions were scanned at the pH of the seawater used, 8.2. A plot of this data appears in figure 3.

A second series of solutions of zinc ion in seawater were prepared varying the zinc ion concentration from 10^{-4} to 10^{-5} molar. A plot of this data also appears in figure 4.

These data indicate that zinc ion concentrations in seawater can be accurately estimated at levels of 1 ppm or greater in seawater without prior sample treatment by direct current polarography.

E. Determination of Pb^{++} Ions in Seawater.

A standard Pb^{++} ion solution was prepared by dissolving 1.0000 g of 99.99% pure lead in 1M nitric acid and diluting to one liter with distilled water. This stock solution containing 1000 ppm Pb^{++} ion was then used to prepare solutions of known Pb^{++} ion concentration in seawater.

Due to the low solubility of lead hydroxide and lead chloride, precipitation occurred at pH of 8.2, even at lead ion levels of 20 ppm The pH of the supporting electrolyte (seawater) was adjusted to 4.0 using HCl. Lead ion solutions from 4 to 100 ppm were prepared. These solutions were stable and no precipitation occurred.

The samples of Pb^{++} ion in seawater whose concentrations varied from 4.84×10^{-4} molar to 1.94×10^{-5} molar were then scanned polarographically from 0.00 to -1.2 volts versus S.C.E. A well defined wave appeared at -0.47 volts. The diffusion current (id) was proportional to the lead ion concentration. A plot of the data appears in figure 5.

These data indicate that lead ion concentrations in seawater can be accurately estimated at levels as low as 4 ppm. The lead ion concentrations in seawater at pH values above 8 would always be low and would not exceed 100 ppm. Direct current polarograph seems an excellent way to monitor lead ion concentrations with only minimal sample treatment.

F. Simultaneous Determination of Zinc, Lead, and Cadmium in Seawater.

In order to study the effect of multiple metal ion concentrations on the determination of individual ion concentration, the following solution was prepared. Using the stock solutions described earlier, sufficient lead, cadmium and zinc ions were added to one liter of seawater at pH value of 4.2 to cause lead, cadmium and zinc ion concentrations of 10.0, 11.2, and 6.54 ppm respectively. This solution was then scanned polarographically from -.1 volts to -1.9 volts versus S.C.E. Three well-defined and separated polarographic waves appeared which corresponded to the E 1/2 voltages of the lead, cadmium and zinc ions. The concentrations of the three ions were then determined by measuring the diffusion currents and reading their concentrations from the respective plots in appendix A. The data is summarized in the following table:

Ion of interest	E 1/2 volts	id μamps	Known concentration in ppm	Concentration determined in ppm	% Dev
Pb++	-0.35	0.322	10.0	9.50	-5
Cd	-0.57	0.650	11.2	11.2	0
Zn++	-0.98	0.630	6.70	6.54	-2.4

This data was obtained with a low cost Heath built polarograph.

These data indicate that lead, cadmium and zinc ion concentrations in seawater can be accurately estimated at levels above 1 ppm using direct current polarography.

CONCLUSIONS

This work shows that lead, cadmium and zinc ions can be qualitatively identified and their concentrations estimated in seawater at concentrations above 1 part per million. The method is fast and does not require prior sample concentration and only a minimum of sample treatment.

It should be practicable to use any direct current dropping mercury electrode polarograph for this analysis. Expensive sophisticated equipment is not required.

Interfering ions would be those whose half wave potentials (E 1/2) fall within .2 volts of the ions of interest and even these can be avoided in most circumstances.

RECOMMENDATIONS

Since this method of examining contaminated seawater samples has received so little attention, it is recommended that further work be accomplished to extend it to cover other ions for example; copper, nickel, cobalt, thallium and manganese.

Actual field samples should be examined and the analysis of these samples by other methods should be compared to the analyses by polarography.

This method may find application in monitoring the corrosion of stainless steel and may be helpful in determining the rate of corrosion in seawater.

SUPPORTING ELECTROLYTE SEAWATER pH = 8.2

Zn++ concentration PPM	Molar	Id μamps
653.7	10^{-2}	62.0
65.4	10^{-3}	6.25
6.54	10^{-4}	0.616
0.654	10^{-5}	0.056

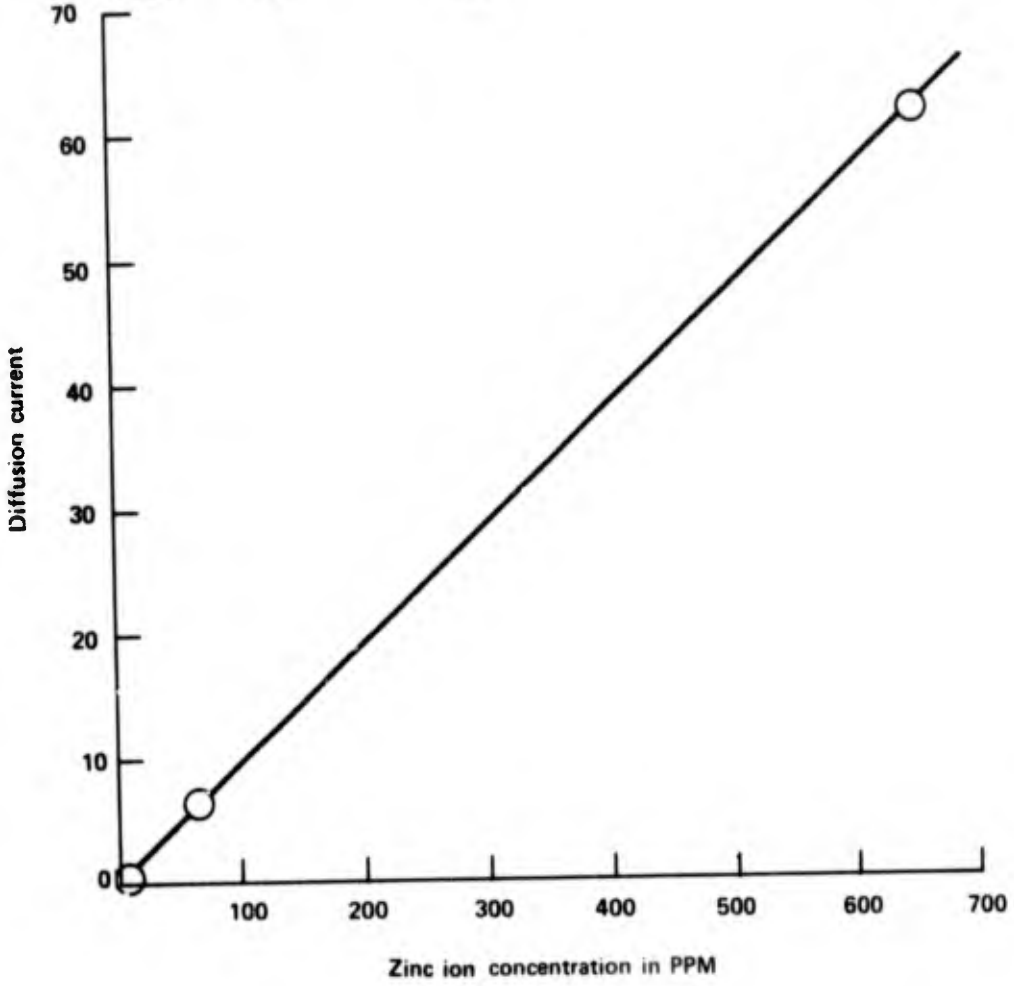

Figure 1. Data for Cadmium Ion, at Higher Concentration, in Seawater

SUPPORTING ELECTROLYTE SEAWATER pH = 8.2

[Cd++]		E 1/2	id
PPM	Molar		
1.124	1×10^{-5}	-0.560	0.045
2.248	2×10^{-5}	-0.545	0.103
4.556	4×10^{-5}	-0.573	0.248
5.620	5×10^{-5}	-0.560	0.313
9.112	8×10^{-5}	-0.578	0.504
11.24	1×10^{-4}	-0.583	0.653

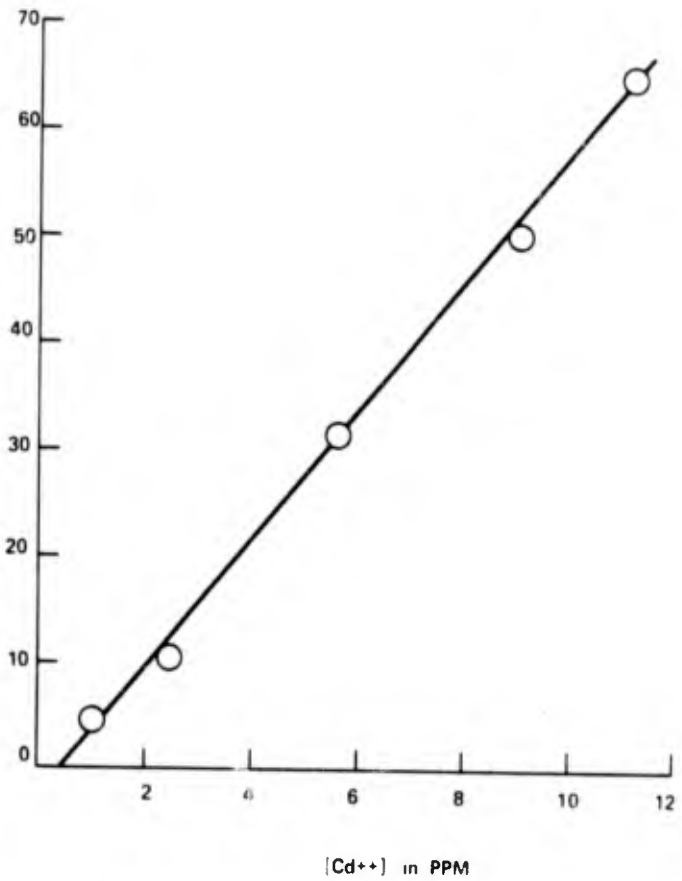

Figure 2. Data for Cadmium Ion, at Lower Concentration, in Seawater

SUPPORTING ELECTROLYTE SEAWATER pH = 8.2

[Cd++]		E 1/2	id
PPM	Molar		
1124	1×10^{-2}	-0.605	66.5
112.4	1×10^{-3}	-0.615	6.65
11.24	1×10^{-4}	-0.580	0.644

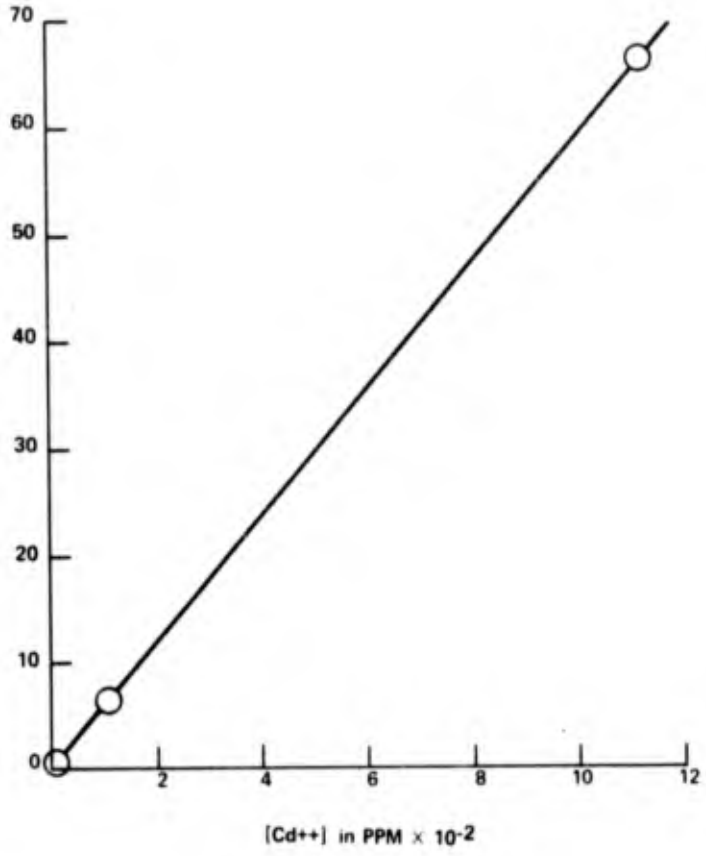

Figure 3. Data for Zinc Ion, at Higher Concentrations, in Seawater

SUPPORTING ELECTROLYTE SEAWATER pH = 8.2

Zn++ concentration		id μamps
PPM	Molar	
6.54	1×10^{-4}	0.616
5.23	8×10^{-5}	0.488
2.62	4×10^{-5}	0.236
1.31	2×10^{-5}	0.112
0.65	1×10^{-5}	0.056

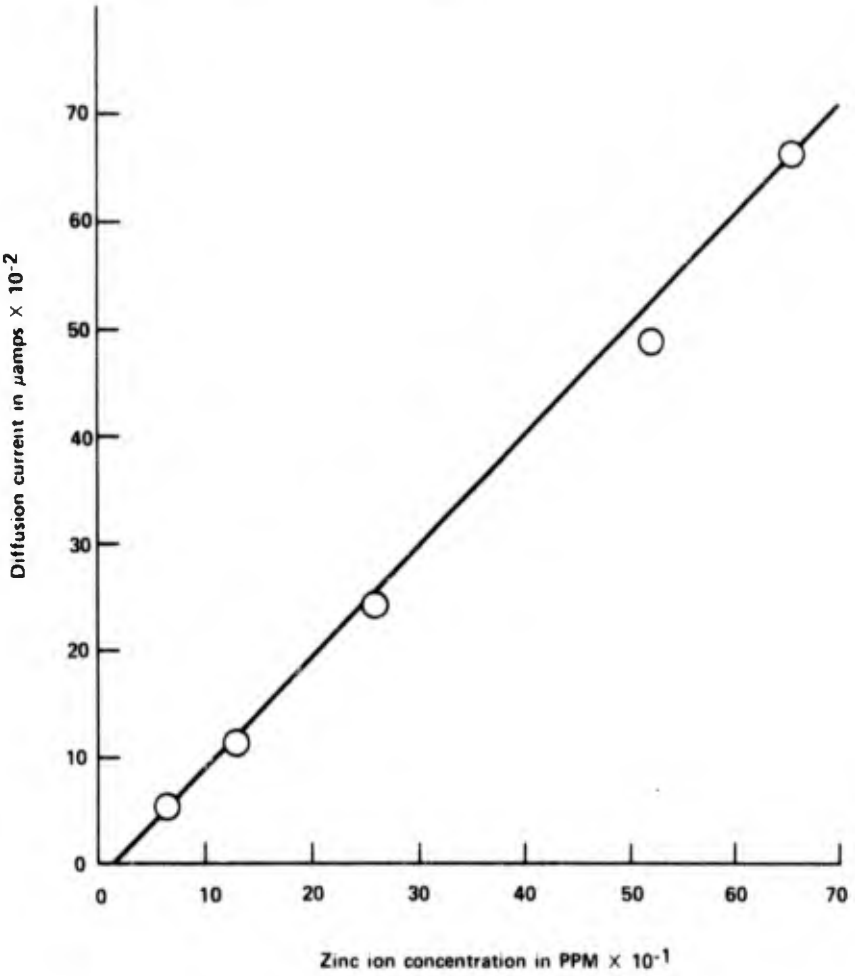

Figure 4. Data for Zinc Ion, at Lower Concentrations, in Seawater

SUPPORTING ELECTROLYTE SEAWATER
pH ADJUSTED WITH HCl TO 4.0

Pb++ PPM	concentration Molar	Current id μ amps
100	4.8×10^{-4}	3.57
40	1.94×10^{-4}	1.42
20	9.7×10^{-5}	0.666
8	3.9×10^{-5}	0.280
4	1.9×10^{-5}	0.133

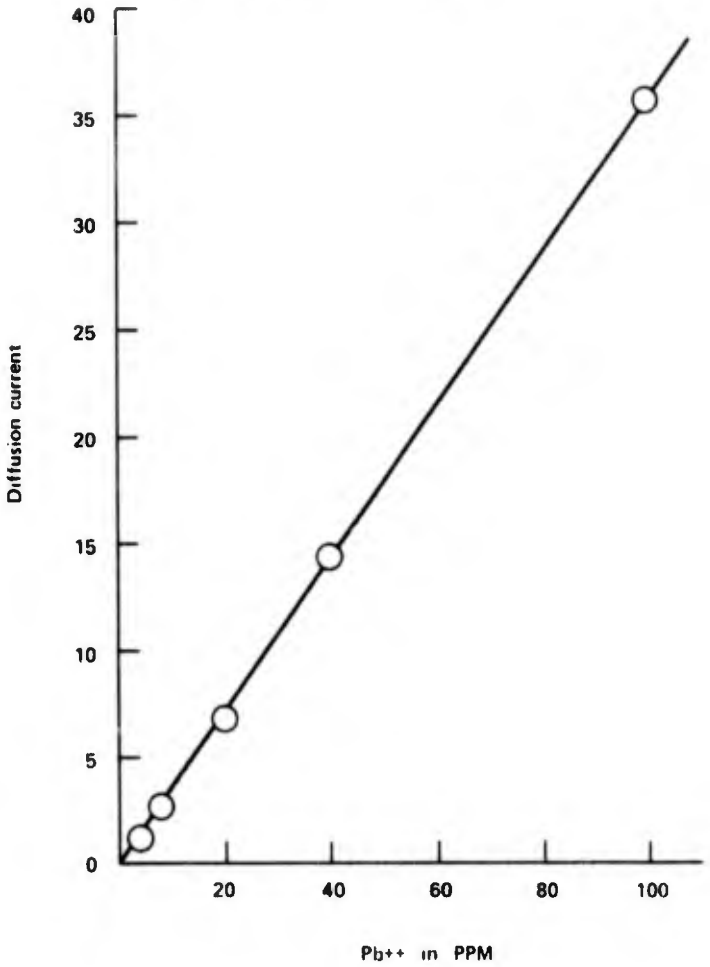

Figure 5. Data for Lead Ion in Seawater

BIBLIOGRAPHY

BOOKS

American Public Health Association. Standard Methods for the Examination of Water and Wastewater. 13th ed. Washington, DC, American Public Health Association, 1971.

Sargent-Welch Scientific Company. Bibliography of Polarographic Literature, 1922-1967. Skokie, Ill., Sargent-Welch Scientific Co., 1969.

GOVERNMENT PUBLICATIONS

Naval Facilities Engineering Command. General Catalog of Instruments and Techniques for Measuring and Monitoring Pollutants. MPS 2.4 and 3.2, Navy Environmental Protection Data Base. Port Hueneme, Calif., Naval Engineering Laboratory, June 1972.

PERIODICALS

Baric, A., and Branica, M. Polarography in Seawater. Ionic State of Cadmium and Zinc in Seawater. Journal of Polarographic Society. (Eng.) 13 (1), 4-8 (1967). C.A. 67-70045a. 1967).

Ishibashi, M., and Fuginaga,T. Studies in Polarographic Analysis in Determination of Aluminum in the Presence of Much Iron and Its Application to the Determination of Aluminum in Seawater. Journal of the Chemical Society of Japan. 73, 783-785 (1952).

Whitnack, Gerald C. Applications of Cathode Ray Polarography in the Field of Polarography. Journal of Electroanalytical Society, 2, 110-115 (1961).

A NEW HIGHLY SENSITIVE DETECTION TECHNIQUE BASED ON THE PHOTOELECTRIC PROPERTIES OF MATRIX ISOLATED DONOR AND ACCEPTOR COMPLEXES

by

A. Snelson
IIT Research Institute, 10 W. 35th St. Chicago, Illinois

ABSTRACT

The existence of a photoconductivity effect in matrix isolated donor and acceptor species has recently been demonstrated at IIT Research Institute. The phenomenon appears to have some very attractive possibilities in several areas, and in this paper, its potential in the field of chemical detection is presented. Although the approach needs further investigation in the laboratory, an ultimate level of detection of $\simeq 10^2$ molecules appears possible. In addition to this extremely high sensitivity, the approach could also have a marked degree of specificity.

I. INTRODUCTION.

The matrix isolation technique is now a well established method for obtaining spectroscopic data for atomic, molecular and radical species. More recently the method has been extended so that the spectra of trapped ionic species may also be obtained.[1-5] In this latter technique suitable electron donating and electron accepting species are isolated within the same inert gas matrix and electron transfer between the donors and acceptors is promoted by photoexcitation.[1,2] Electron spin resonance techniques have been used to characterize the isolated anionic and cationic species,[1-3] and the infrared spectra of a variety of matrix isolated negative ions have been reported.[4,5] The most commonly used electron donors have been alkali metal atoms. A variety of electron accepting species have been used, NO_2,[5] NO,[5] SO_2,[4] B_2H_6,[3] tetracyanoethylene[3] and furan.[3]

Recently in this laboratory some preliminary studies have been made on a possible photoconductivity effect which might be expected to exist for matrix isolated donor and acceptor species. A paper describing the results of these initial studies has been published.[5a] In addition the results of some further studies, not yet published will be mentioned.

Briefly, a photoconductivity effect was observed for matrix isolated sodium atoms (donors) and tetracyanoethylene, sym-trinitrotoluene, dibenzofuran, and 1:1:1-trichloro-2,2-bis-(p-chlorophenyl)ethane (DDT) (acceptors). This demonstration of a photoconductivity effect for matrix isolated species is of interest not only from a basic chemistry standpoint, but also from a potentially practical angle of providing new techniques for:

1. Measuring very low concentrations of atoms, molecules and radicals,

2. Measuring electron affinities for atoms, molecules, or radicals and,

3. Measuring light intensities in real time or after storage (i.e., an image storage effect).

Although the photoconductivity effect could find use in all three areas given above, in this paper the concern is largely with the possibilities of the phenomenon with respect to chemical detection. At the present time the possible harmful effects of small concentrations of a variety of chemical substances to human life have been well publicized; e.g., NO-NO_x levels at the fractional to low ppb(v) level; Freons at the 0.01 to 0.001 ppb(v) level capable of upsetting the upper atmosphere ozone balance; vinyl chloride and chlorodibenzofurans as possible carcinogens at low ppm(v) level, etc. The measurement of these and other materials at very low levels presents many analytical problems both in terms of inherent sensitivity and specificity of the detection method and new or improved methods of analysis are constantly being sought. As will be outlined shortly there is reason to believe that the photoconductivity effect under discussion here could provide a new, extremely sensitive, detection technique. Obviously, at the present time, the observed photoconductivity effect needs careful investigation to define its true potential in the area of chemical detection.

II. THE PHOTOCONDUCTIVITY EFFECT.

A schematic description of the new photoconductivity effect is most easily obtained from figure 1. Alternate matrix-isolated layers of sodium and tetracyanoethylene were deposited on a suitable cooled surface. Under illumination transfer of an electron from the sodium to the tetracyanoethylene is promoted and under the influence of an applied field conduction takes place. Experiments indicate that the charge transfer complex is only formed at the interface of the matrix-isolated layers. It may be estimated, based on the matrix dilution factors used in the experiments that a maximum of approximately 10^{13} complexes could be formed at the layer interfaces. The maximum current obtained with this arrangement was approximately 10^{-8} amp. Since the current measuring device used in the study (A Keithley electrometer) could detect currents as low as 10^{-11} amp, the minimum number of donor-acceptor complexes detectable with this experimental arrangement was of the order of 10^{10}. This level of detection is of course very good, rivaling many of today's best existing detection devices.

In order to improve the minimum detection level two approaches are possible.

1. The cryogenic sample is in a vacuum environment and thus it is possible to use an electron multiplier[6] as the primary current detector. These devices are easily able to detect 5-10 electron sec^{-1} and have gains of approximately 10^7. At 5-10 electrons sec^{-1}, currents of approximately 10^{-11} amp result which are suitably measured by conventional electrometers or electron-counting procedures. Extrapolating from the above experimental data, it may be calculated that on introducing an electron multiplier into the system as the primary current detector, approximately 10^4 donor-acceptor complexes could be detected.

2. The illumination of the matrix containing the donor-acceptor complexes in the IITRI experiments was from an ordinary 150-watt tungsten filament electric light bulb. The filament was about 10 cm from the surface on which the matrix was deposited and no attempt to focus the radiation on the matrix was made. It is reasonable to assume that the photo-current

depends both on the number of donor-acceptor complexes and the rate at which they are synthesized from the neutral molecules by the photon energy prior to being discharged. It would be an easy matter to increase the illumination at the matrix by at least two orders of magnitude and hence increase the sensitivity of the device by a similar order of magnitude.

It appears therefore, that by making the above modifications to the original experimental arrangement, as shown in figure 2, the detection of $\simeq 10^2$ donor-acceptor complexes is entirely possible. Practically there may be difficulties in attaining this limit due to the presence of impurities in a real experimental situation. The detection of $\simeq 10^2$ molecular species represents an extremely high level of sensitivity, some six orders of magnitude higher than obtained with the most commonly available systems.

The possibility that the photoconductivity effect could be used not only as a highly sensitive detector, but as a detector with specificity will now be considered. In order to do this it will be necessary to consider the energetics of the photoconductivity process. For this purpose a system consisting of matrix-isolated sodium and chlorine atoms will be discussed since some numerical values are available for the energetics involved. Reference will now be made to the diagram shown in figure 3. The figure shows how the potential energy changes as a function of the internuclear separation, R, for neutral and ionic sodium and chlorine species. The most stable configuration for Na^+ and Cl^- occurs at about 2.4Å, corresponding to a gaseous molecule NaCl (salt). This is taken as the zero energy reference state for the two systems. Although the Na^+ and Cl^- system has an energy minimum as the species approach each other from infinite separation, the neutral Na and Cl system does not. In the latter system as the atoms approach each other from infinity the potential energy remains essentially constant until at fairly small values of R, the energy starts increasing very rapidly.

The energetics of the photoconductivity process will now be considered in terms of the potential energy diagram. For the sake of simplicity the following is assumed:

1. The sole function of the host matrix in the present context is to keep the species (Na and Cl or Na^+ and Cl^-) rigidly fixed in their respective positions within the inert gas matrix.

2. The energy of interaction between the trapped species and the surrounding matrix is small, and for the present purpose may be ignored. There is a considerable body of evidence that this indeed is the case.[8]

3. Electrode tunneling phenomena can be ignored. With these assumptions, the energy E, required to transfer an electron from a sodium atom to a chlorine atom within the matrix is given by:

$$E = E_{ip}(Na) - E_{ea}(Cl) - e^2/ER \qquad (1)$$

where

$E_{ip}(Na)$ = Ionization potential of the sodium atom = 5.2 ev

$E_{ea}(Cl)$ = Ele ctron affinity of the chlorine atom = 3.8 ev

e^2/ER = Coulombic potential energy of the resulting ion pair and E is the dielectric constant of the matrix.

In the case of sodium atoms and chlorine atoms, reference to figure 1 shows that at internuclear separations greater than about 10Å (this is where the two potential energy curves intersect) electron transfer from a sodium atom to a chlorine atom requires a net input of energy while at R values <10Å the same process occurs with a net release of energy. Under matrix isolation conditions R values greater or less than 10Å may be obtained, depending on the dilution factor. Although energetically, for R<10Å, a spontaneous electron transfer from sodium to chlorine would be favored, practically the process has never been observed in the matrix.[3] It must therefore be assumed that in order to effect the ionization process an energy barrier not included in equation (1) must be involved, thus;

$$E = E_A + E_{ip}(Na) - E_{ea}(Cl) - e^2/ER \qquad (2)$$

where E_A, representing a quantity analogous to a chemical activation energy term is required. In practice the energy required to bring about the ionization process is provided by illumination and (2) may be rewritten as,

$$h\nu = E_A + E_{ip}(Na) - E_{ea}(Cl) - e^2/ER \qquad (3)$$

or more generally

$$h\nu = E_A + E_{ip}(D) - E_{ea}(A) - e^2/ER \qquad (4)$$

where

$E_{ip}(D)$ and $E_{ea}(A)$ are the ionization potentials and electron affinities of the donor and acceptor species respectively.

Thus in a given system E_A will presumably have a characteristic value. R can be fixed by the matrix dilution factor and the light energy required to bring about the ionization process will then depend on the energy difference $E_{ip}(D) - E_{ea}(A)$. Since the ionization potentials and the electron affinities have unique values for different elements and compounds, the wavelength of the exciting radiation may be used as a means of characterizing the donor-acceptor complex.

Assuming therefore the validity of the above equations and assumptions, it appears that the photoconductivity effect could be used in a mode to offer selective detection of different molecules and atoms. However, it is well appreciated by the writer that although the above equations appear to satisfy the few known facts concerning the matrix photoconductivity process, the validity of the relationship expressed in equation 4 between the photon energy, and the energy terms on the right hand side of the equation is very uncertain. Quantum mechanical selection rules for photoionization processes require only that $h\nu$ be $\geq$ the ionization potential of the material

under consideration. Practically the cross-section for a photoionization process may be quite small and result in an extremely long period of irradiation to effect significant ionization. In the experiments with Na and TCNE, the photoionization appeared to be instantaneous. However, the irradiation covered a wavelength interval from 3700Å to greater than 7000Å and included the wavelength of the sodium resonance line at 5890Å. It is entirely possible that the main photoionization process may have resulted from absorption of radiation by the sodium resonance line. If indeed this is the case equation 4 would require modification.

Finally a note with respect to the kinds of material which can be used in the matrix photoconductivity effect. The prime requirement is for electron donors and electron acceptors which may be isolated in suitable matrices and undergo photoionization on irradiation. In general, electron donors are considered as materials with low ionization potentials. Metals are typical of such materials with ionization potentials in the range 3.9 to ≈9ev. From a practical point of view the alkali metals will probably be most suitable since they have the lowest ionization potentials 5.36(Li) to 3.87(Cs) ev. A low ionization potential is desirable since it allows the photoionization process to take place with radiation in the visible region of the spectrum instead of the UV. If UV radiation were necessary to produce ionization, problems would probably be encountered with photoionization of of the bulk metals used in constructing the equipment, thus adding an undesirable photoelectron source to the detection system.

Electron acceptors cover a wide range of compounds; values range from 0 to as high as 3.8ev for atomic Cl. In the table some typical electron affinities are listed. It will be observed that O_2, N_2, CO_2, and H_2O, the major components of the air, have electron affinities of 0.48, 0, 0.48 and ≈1.3ev respectively, and purely from a detection point of view it appears entirely probable, based on equation 4, that any materials in air with electron affinities greater than that of O_2, N_2, CO_2, and H_2O could be detected directly using the air as the matrix material, i.e., direct air sampling is a possibility for materials with electron affinities greater than 1.3ev.

It is also worth noting that electron-induced reaction with matrix-isolated materials can occur as shown below:[5]

$$M + HI \xrightarrow{h\nu} M^+ + H + I^-$$

where X = halogen, NO_2 etc:

$$C_nH_{2n+1}X + M \xrightarrow{h\nu} M^+ + C_nH_{2n+1} + X^-$$

$$M + C_6H_5F \xrightarrow{h\nu} M^+ + C_6H_5 + F^-$$

$$M + C_5H_4NCl \xrightarrow{h\nu} M^+ + C_5H_4 + Cl^-$$

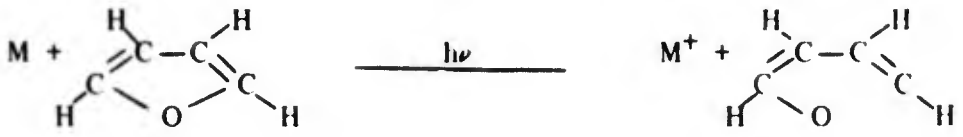

M = Electron donor

Obviously a very large group of compounds can act as electron acceptors, either directly or as indicated above via electron-induced reaction.

In the above discussion, it has been assumed that only inert gas matrices could be used for the host material containing the electron donor and acceptor. This situation obviously requires the use of low temperatures for the formation of the solid matrix. The possibility that suitable matrices can be found that would be solid at room temperature and still allow the photoconductivity effect to occur is likely. Finally, in figures 4 and 5 some typical photoconductivity curves are presented.

III. CONCLUSION.

A basis for a new, highly sensitive detection technique has been presented. Admittedly the approach needs careful laboratory study to determine its true potential at this time, but the high sensitivity of the device looks very promising. At a time when it is becoming to be realized that very small amounts of chemical substances can sometimes have unexpected effects on human life and the environment, the possibility of developing an extremely sensitive detection device is very attractive.

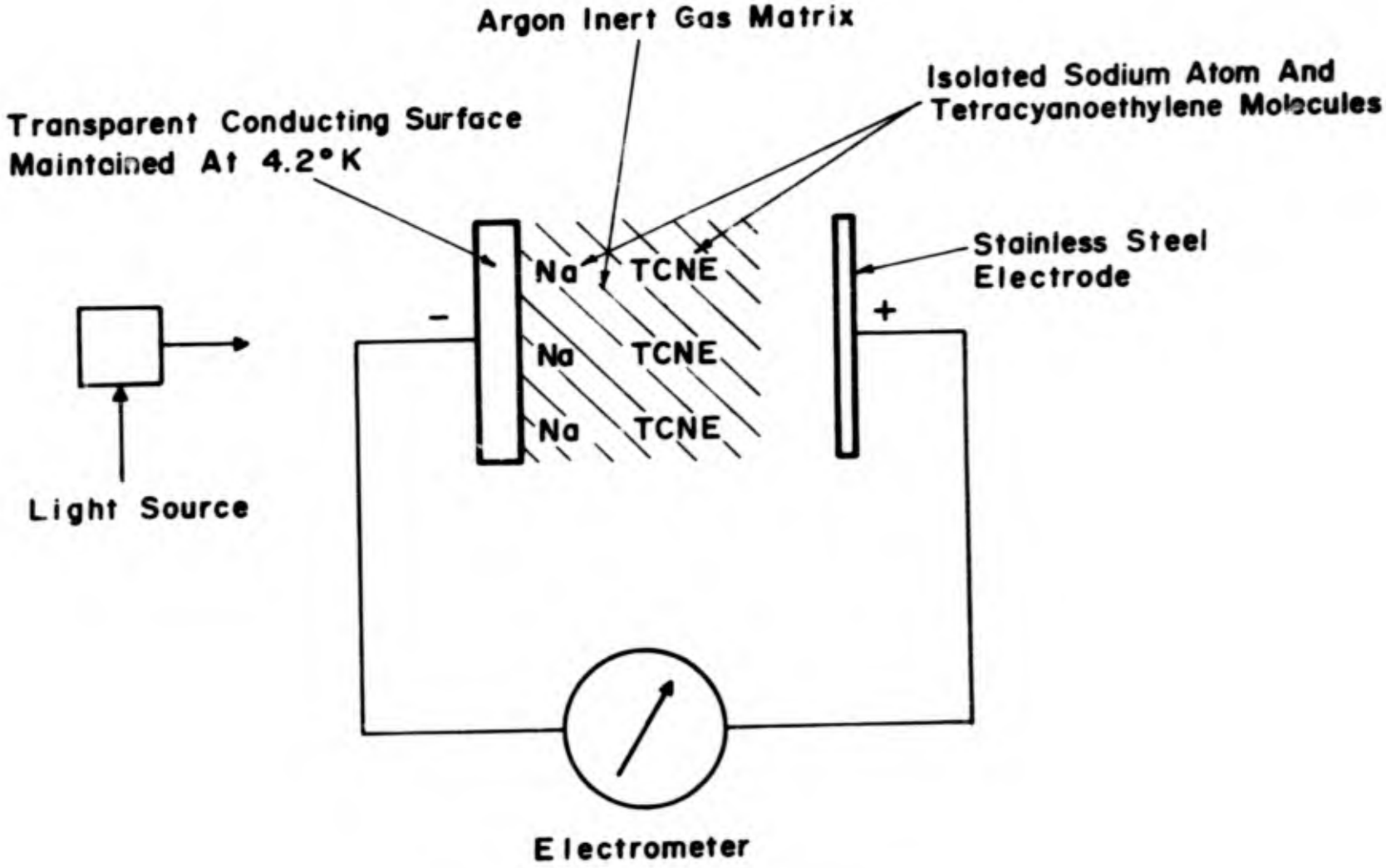

Figure 1. Schematic of the Experimental Arrangement for Observing the Cryogenic Photoconductivity Effect

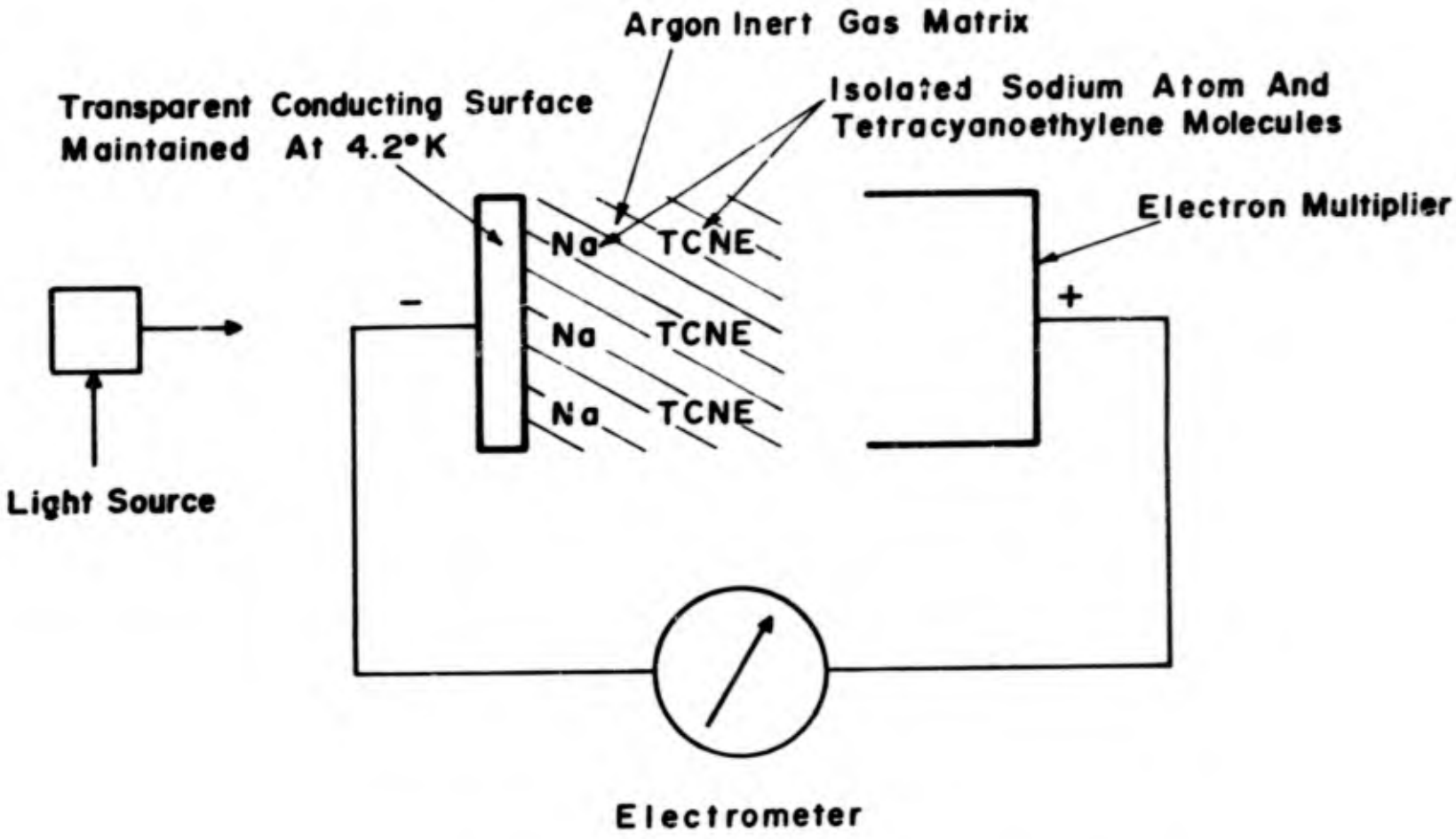

Figure 2. Schematic of the Proposed Experimental Arrangement for Observing the Cryogenic Photoconductivity Effect with Maximum Sensitivity

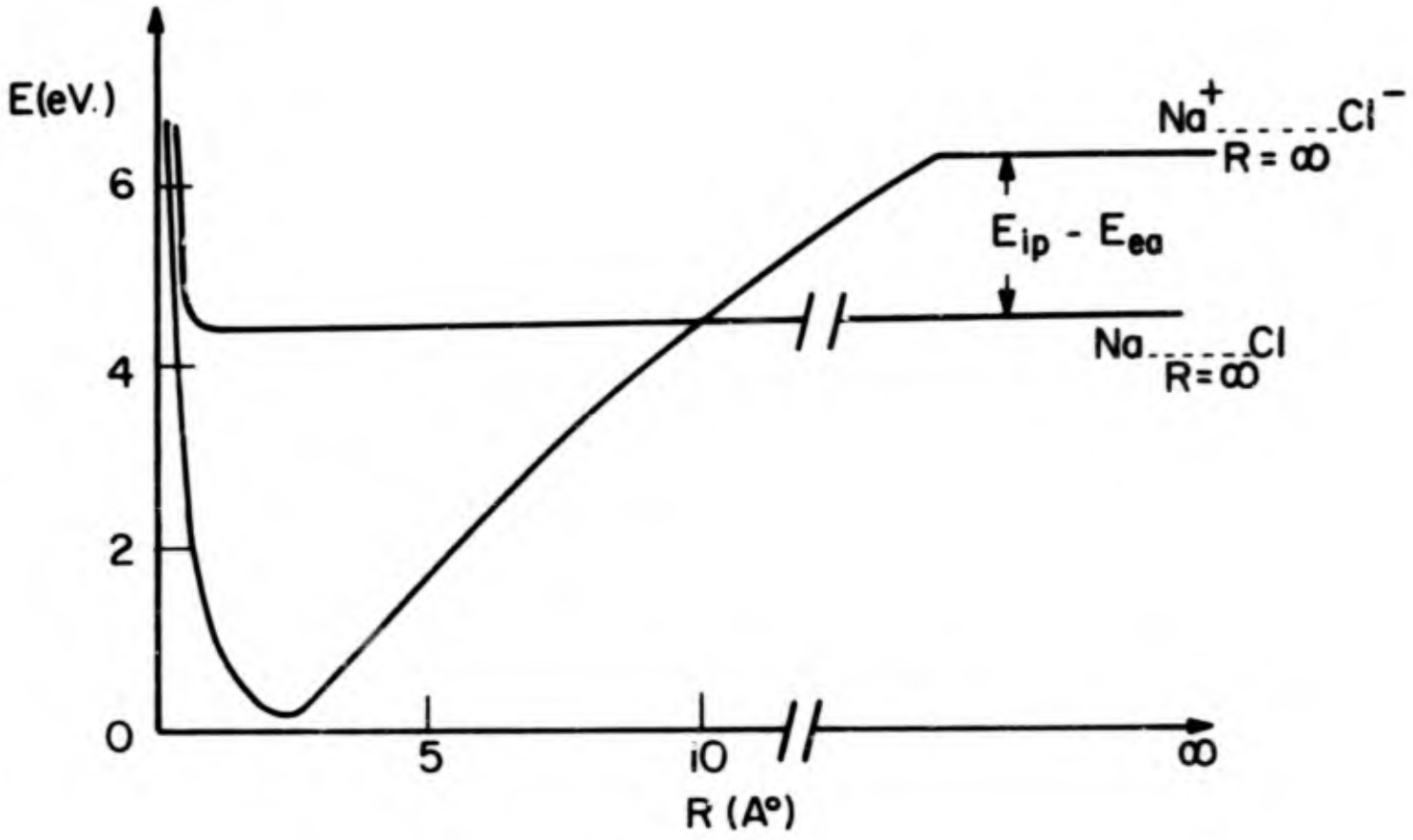

Figure 3. Potential Energy Diagram of Neutral and Ionic Na and Cl Atoms

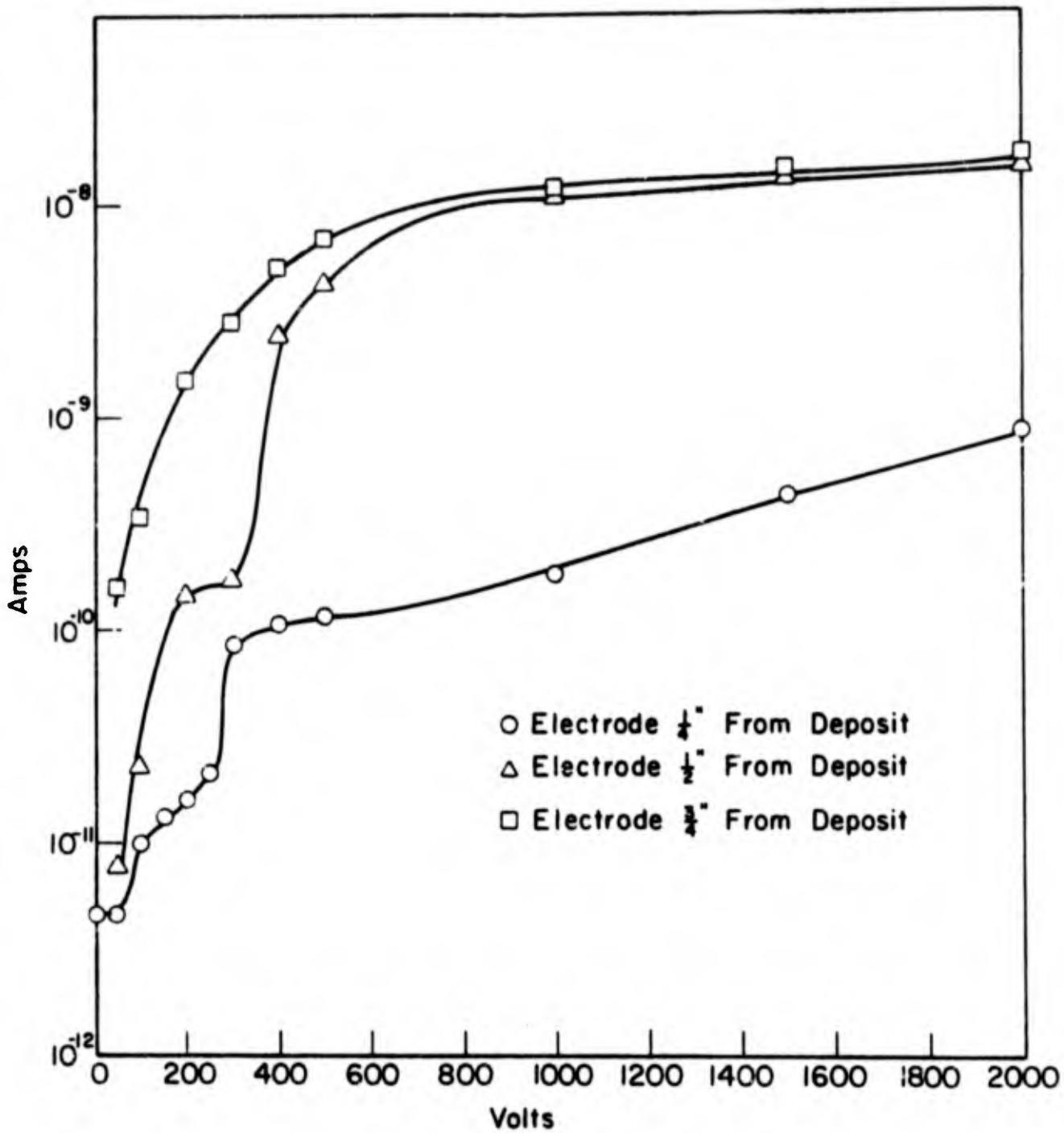

Figure 4. Photoconductivity Curves for Sodium and Tetracyanoethylene, in an Argon Matrix, 30 Layers of Each

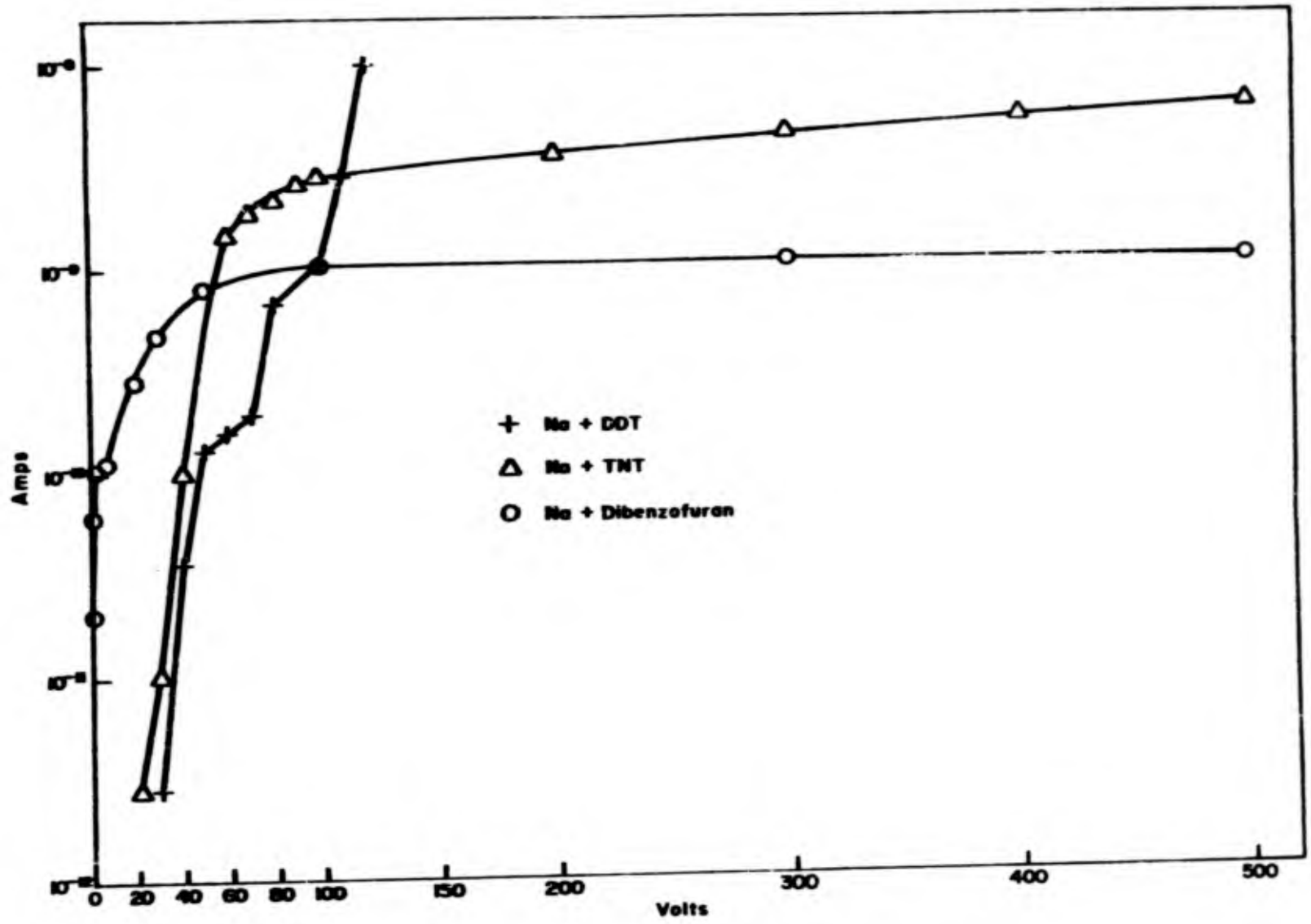

Figure 5. Photoconductivity Curves for Sodium with DDT(+), TNT(Δ), and Dibenzofuran(o) in an Argon Matrix, 10 Layers of Each Deposited

Table. Some Electron Affinities of Elements and Compounds*

Material	Electron affinity in ev	Material	Electron affinity in ev
F_2	3.08	S	2.07
Cl_2	2.38	SO_2	1.1
Cl	3.8	SF_6	>0.43 <1.47
Br_2	2.51	P	0.71
I_2	2.58	C	1.27
O_2	0.48	CH	2.6
N_2	≈0	C_2	3.3
O_3	1.96	C_2H	2.1
NO	0.09	$C_6H_3(NO_2)_3$ (sym)	1.86
NO_2	2.04	$C_6H_4(NO_2)_2$ (meta)	1.43
NO_3	2.48	$C_6H_5NO_2$	≈0.5
H_2O	1.31	CO_2	0.48
HO_2	≈3.5	CO	-1.8
CH_3O	0.39	$C_{20}H_{12}$ (1:2 benzopyrene)	≈0.48
HNO_3	1.99	$C_{20}H_{12}$ (3:4 benzopyrene)	≈0.82

* These values are taken from R. P. Blaunstein and L. G. Christophorou, "On Molecular Parameters of Physical Chemical and Biological Interest", Radiation Research Reviews, 3, 69 (1971).

REFERENCES

1. Kasai, P. H. Phys. Rev. Lett. 21, 67 (1968).

2. Kasai, P. H. and McLeod, D. Jr. J. Chem Phys., 51, 1250 (1969).

3. Kasai, P. H. Acc. of Chem Res. 4, 329 (1971).

4. Milligan, D. E. and Jacox, M. E. J. Chem Phys. 55, 3404 (1971).

5. Snelson, A. J. Phys. Chem 77, 2434 (1973).

6. Ramsay, N. F. Molecular Beams. Oxford Clarendon Press. Page 387 (1956).

7. Herzberg, G. Spectra of Diatomic Molecules, Van Nostrand Company. Inc., Princeton, NJ 1950.

8. Wahl, A. C. Sci. Am. 222, 54 (1970).

9. Pritchard, H. O. Chem Rev. 52, 529 (1953).

10. Field, H. F., and Franklin, J. L. Electron Impact Phenomena and the Properties of Gaseous Ions. Academic Press, New York, New York. 1957.

11. Branscomb, L. M., and Battes, D. R. Atomic and Molecular Processes. Academic Press, New York, New York. 1962.

12. Buchel'nickova, N. S. Usp. Fiz. Nauk. 65, 351 (1958).

13. Smirnov, B. M. High Temp. 3, 716 (1965).

14. Moiseiwitsch, B. L., Bates, D. R., and Estermann, I. Advances in Atomic and Molecular Physics. Academic Press. New York, New York, 1965.

15. Vedeneyer, V. I. Band Energies, Ionization Potentials and Electron Affinities. St. Martens Press, New York, New York, 1966.

16. Christophorou, L. G., and Compton, R. N. Health Phys. 13, 1277 (1967).

17. Page, F. M., and Goode, G. C. Negative Ions and the Magnetron. Wiley-Interscience, London, 1969.

18. Christophorou, L. G. Atomic and Molecular Radiation Physics. John Wiley and Sons, Inc. London. 1970.

19. Blaunstein, R. P., and Christophorou, L. G. Radiat. Res. Rev. 3, 69 (1971).

20. Mulliken, R. S. J. Am. Chem. Soc. 72, 600 (1950).

21. Mulliken, R. S. J. Chem. Phys. 19, 514 (1951).

22. Mulliken, R. S. J. Am. Chem. Soc. 56, 801 (1952).

23. Hastings, H. S., Franklin, J. L., Schiller, J. C., and Matsen, F. A. J. Am. Chem Soc. 75, 2900 (1953).

STUDIES ON THE FORMATION OF DYES FROM DIINDOLYLPYRIDYLMETHANES

by

David N. Kramer, Thaddeus J. Novak, Harold Klapper, and Lester Daasch

Chemical Laboratory
Edgewood Arsenal
Aberdeen Proving Ground, Maryland

Brown Murr

Chemistry Department
Johns Hopkins University
Baltimore, Maryland

There is a need for more sensitive and specific detection tests for alkylating agents, e.g., mustard gas.

The current test used most widely employs DB-3 [4-(p nitrobenzyl)pyridine] and requires a preheating step followed by the addition of alkali. The reaction is illustrated in figure 1.

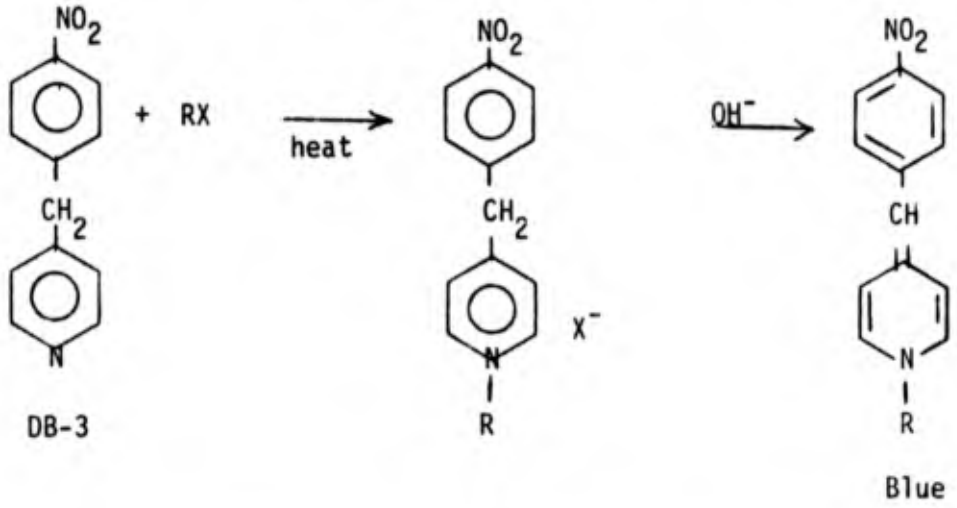

Figure 1. Reaction of the DB-3 Test (Sensitivity 0.1 μg on Silica Gel Tube)

In attempts to improve on the DB-3 reaction we have synthesized a series of diindolylpyridylmethanes by reacting two equivalents of indole and one equivalent of 4-pyridinecarboxaldehyde in the presence of alcoholic hydrochloric acid. Figure 2 and the table summarize the variously substituted analogues that were synthesized. We have also studied the kinetics of the alkylation and have illustrated the possible reaction mechanisms leading to dyes depicted in figure 3.

The sensitivity achieved with the new series of reagents is of the order of DB-3. It was also found that an increase in sensitivity can be achieved by coupling the reaction with a triaryltetrazolium salt (to form the colored formazan).

Table. Diindolylpyridylmethanes[a]

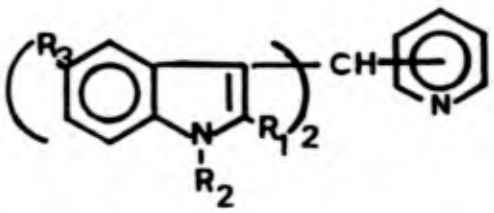

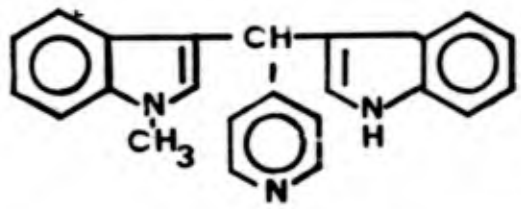

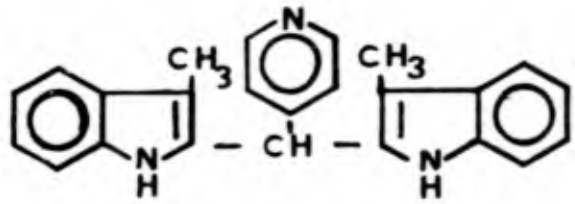

Compnd	Ar	R_1	R_2	R_3	mp, °C	Elemental Analyses %					
						Calcd			Found		
						C	H	N	C	H	N
1a	4-pyridyl	H	H	H	156-158 dec	81.7	5.3	13.0	81.9	5.5	13.0
1b	4-pyridyl	H	CH_3	H	184-185 dec	82.0	6.0	12.0	81.7	6.3	11.7
1c	4-pyridyl	CH_3	H	H	241-244 dec	78.0	6.3	11.4	78.0	6.0	11.5
1d	4-pyridyl	H	H	CH_3	256-260 dec	82.0	6.0	12.0	81.7	5.9	12.0
1f	4-pyridyl	H	H	Cl	261-263 dec	67.4	3.8	10.7	67.1	4.0	10.5
1g[b]	4-pyridyl	H	H	Br	277-279 dec	54.9	3.1	8.7	55.2	3.3	9.4
1h	4-pyridyl	H	H	CN	275-277 dec	77.2	4.1	18.8	77.0	4.2	18.8
1i	4-pyridyl	H	H	COOH	185-188 dec	70.1	4.2	10.2	69.6	4.3	10.3
1j[b]	4-pyridyl	H	H	CH_3O	181-185 dec	75.2	5.5	11.0	74.6	5.6	10.9
1l	2-pyridyl	H	H	H	211-212 dec	81.7	5.3	13.0	81.9	5.3	13.1
1m	3-pyridyl	H	H	H		81.7	5.3	13.0			
1e[b]					146-148 dec	81.9	5.7	12.5	80.1	5.7	12.0
1k					264-266 dec	82.0	6.0	12.0	81.9	6.2	12.2

[a] Substantial parent peaks were shown by these compounds.

[b] Analyses unsatisfactory; homogenous by tlc under conditions that separate 1a and 1b.

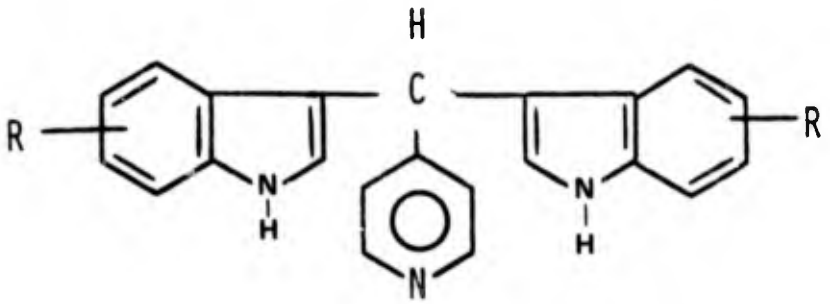

1. HAVE PREPARED MANY ANALOGUES.

   R = Cl, Me, MeO, Br, CN, CO_2H

2. STUDIED KINETICS AND THE MECHANISMS.

3. SENSITIVITY AND SENSITIZATION WITH TTZ.

Figure 2. Work Done on D[illegible]tolylpyridylmethanes

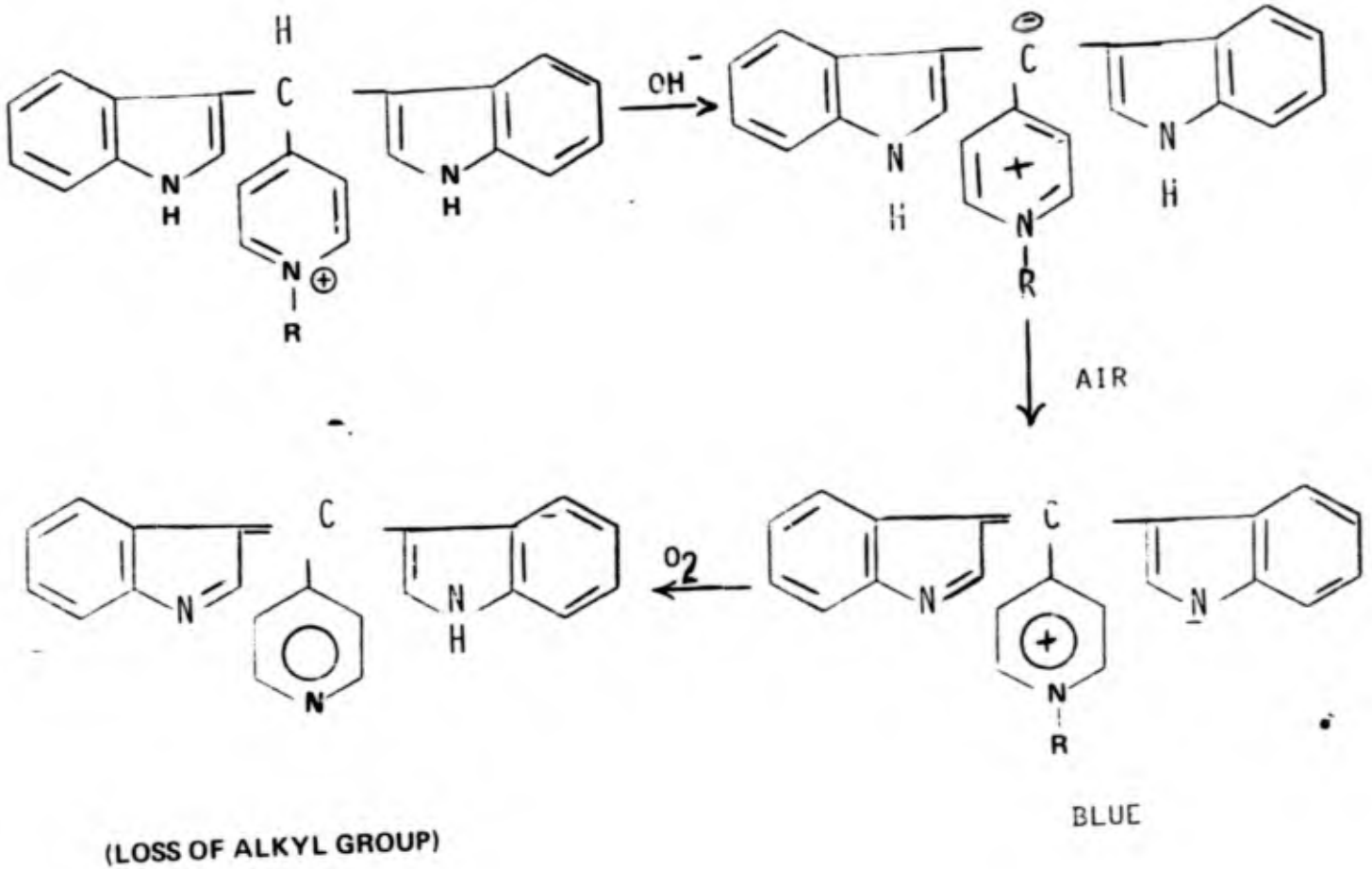

Figure 3. Color Production from Diindolylpyridylmethanes